Mechanisms and Consequences of GLO1 Attenuation in Obese Skeletal Muscle: Exploring a Potential Role for SIRT1-Mediated GLO1 Stability

by

Edwin R. Miranda Jr.

A dissertation submitted in partial fulfillment
of the requirements for the degree of
Doctor of Philosophy
(Movement Science)
in The University of Michigan
2022

Doctoral Committee:

Associate Professor Jacob M. Haus, Chair
Professor Gregory D. Cartee
Professor Jeffery F. Horowitz
Associate Professor David B. Lombard
Assistant Professor Andrew T. Ludlow

Edwin R. Miranda

edwinray@umich.edu

ORCID iD: 0000-0003-2370-4118

DEDICATION

This work is dedicated to my daughter Reya.

Reya, my dream is that you one day realize your dreams. My hope is that I can be an inspiration for you to fearlessly pursue your passions. My motivation is to make you proud in the pursuit of my dream.

ACKNOWLEDGEMENTS

To my committee: Thank you for your support and guidance throughout this process. Your collective feedback and expertise have been invaluable to this project, and I have learned so much throughout this process thanks to you all. I want to particularly thank Dr. Ludlow for allowing me to rotate in his lab to learn ddPCR, primer/probe design, and methods for studying splicing regulation. Thank you also for providing the cells for this project, teaching me tissue culture, and related techniques such as plasmid expansion, validation and transfection as well as siRNA transfection.

To Dr. Haus: Thanks for taking a chance on this wet ball of clay and helping mold me into a scientist. Thank you for letting me fail and learn from my mistakes and for inspiring me to push out beyond my scientific comfort zone to learn as much as possible.

To Dr. Mazzetti: I would not be here without you and for that I am so grateful. You introduced me to research and pushed me to discover my own potential because you truly believed in me. Thank you.

To my friends and colleagues: This has been a long, rewarding, and tough journey. Thank you to all my colleagues who became great lifelong friends along the way. From those that I met back at Salisbury University in the Laboratory for Human Performance, the University of Illinois at Chicago, and the University of Michigan. There are too many great people to list here that I have met over this time who I now consider life-long friends and each of you were instrumental for my success and ability to accomplish this feat. I love you all, thank you!

To my mom and dad: Thank you for the love and support you perpetually gave me throughout this process even when my goals took me far from home away from you. Thank you for believing in me and having the strength and selflessness to sacrifice your time with me in the interest of my pursuits. I love you.

To my brother Erick: Thank you for being a motivating force for me. I am so proud of you and impressed by your passion and work ethic. Thank you for being an example for me to look up to. I love you.

To my wife Tori: We did it! **WE** did it. This is as much of my accomplishment as it is yours because I could not have done this without you. This was the most difficult thing I have ever done and in your unwavering support of me throughout my 8-year graduate school career you have sacrificed so much. And while it has been difficult, and required sacrifices from both of us, having you with me through it all has also provided us with a lot of great opportunities that have enriched our lives. So, thank you so much for going on this journey with me and supporting me every step of the way, through the good times and the difficult times. I am so excited to continue this journey with you and Reya in Utah. I love you so much!

TABLE OF CONTENTS

LIST OF TABLES

LIST OF FIGURES

LIST OF APPENDICES

LIST OF ABBREVIATIONS

Abbreviated Term	Definition
CaMKII	Calcium/calmodulin-dependent Protein Kinase II
2-DG	2-Deoxy Glucose
2-ODH	2-Oxoaldehyde
3-DG	3-Deoxyglucosone
4-HNE	4-Hydroxynonenal
AAA	Amino Adipic Acid
ACL	ATP-Citrate Synthase
AGEs	Advanced Glycation End products
AGK2	2-Cyano-3-[5-(2,5-dichlorophenyl)-2-furanyl]-N-5-quinolinyl-2-propenamide
AKR	Aldoketo Reductase
ALDH	Aldehyde Dehydrogenase
AMPK	AMP-activated Protein Kinase
ANOVA	Analysis of Variance
APOE	Apolipoprotein E
Apy	Argpyrimidine
ARE	Antioxidant Response Element
AUC	Area Under the Curve
BCA	Bicinchoninic Acid
bFGF	Beta Fibroblast Growth Factor
BHAD	Beta-Hydroxyacid Dehydrogenase
BMDC	Bone Mineral-Derived Cells
BMI	Body Mass Index
BNIP3	BCL2 Interacting Protein 3
C2C12	Immortalized Mouse Myoblast Cell Line
cADP	Cyclic ADP
CASP7	Caspase 7
CCM	Curcumin
CD38	Cluster of Differentiation 38/Cyclic ADP-Ribose Hydrolase
CDK4	Cyclin Dependent Kinase 4
CEA	Carboxyethyl Arginine
CEL	Carboxyethyl Lysine
CR	Caloric Restriction
CrAT	Carnitine O-Acetyltransferase

cRNA	Circular RNA
Cull3	Cullin-3
CVD	Cardiovascular Disease
DAVID	Database for Annotation, Vissualization, and Integrated Discovery
ddPCR	Droplet Digital Polymerase Chain Reaction
DHAP	Dihydroxy Acetone Phosphate
DIO	Diabetic Induced Obese Rat Model
DMSO	Dimethyl Sulfoxide
dPBS	Dubelcco's Phosphate Buffered Saline
eNAMPT	Extracellular NAMPT
eNOS	Endthelial Nitric Oxide Synthase
ET-1	Endothelin-1
FAD	Flavin Adenine Dinucleotide (Oxidized)
$FADH_2$	Flavin Adenine Dinucleotide (Reduced)
FASN	Fatty Acid Synthetase
FBS	Fetal Bovine Serum
FSHD	Fascioscapulohumeral Muscle Dystrophy
G-H1	Glyoxal Hydroimidazolone
G3P	Glycerol-3-Phosphate
GALT	Galactose-1-Phosphate Uridylyltransferase
GAPDH	Glyceraldehyde Phosphat Dehydrogenase
GCN5	General Control Non-Depressible 5
GLO1	Glyoxalase-1
GLO2	Glyoxalase-2
GLP1	Glucagon-Like Peptide-1
GNPAT	Glyceronephosphate O-Acetyltransferase
GOF	Gain-of-Function
GRx1	Glutaredoxin-1
GSH	Reduced Glutathione
GSR	Glutathione Reductase
GSSG	Oxidized Glutathione
GTT	Glucose Tolerance Test
H3K9	Histone 3 Lysine 9
HAECS	Human Aortic Endothelial Cells
HAT	Histone Acetyl Transferase
HBFA	Heptofluorobutyric Acid
HCR	High Capacity Running Rats
HDAC	Histone Deacetylase
HEK293T	Human Embryonic Kidney Cells
HEPG2	Liver Hepatocellular Carcinoma Cell Line
Hesp	Hesparatine
HFD	High Fat Diet
HGF	Hepatocyte Growth Factor

HO-1	Hemeoxygenase-1
HOMA-IR	Homeostatic Model Assessment for Insulin Resistance
HS	Horse Serum
hTERT	Human Telomerase Reverse Transcriptase
IAA	Iodoacetamide
ICU	Intensive Care Unit
IGT	Impaired Glucose Tolerance
INS-1	Rat Insulinoma Cell line
I.P.	Intraperitoneally
IP	Immunoprecipitation
IR	Insulin Receptor
IRS1	Insulin Receptor Substrate-1
ITT	Insulin Tolerance Test
JCAD	Junctional Cadherin 5 Associated
KAT	Lysine Acetyltransferase
KD	Genetic Knock Down
KDAC	Lysine Deacetylase
KEAP1	Kelchlike-ECH-Associated-Protein 1
KO	Gene Knock Out
L6	Rat Myogenic Cell Line
LC-MS/MS	Liquid Chromatography Tandem Mass Spectrometry
LCR	Low Capacity Running Rats
LDH	Lactate Dehydrogenase
LH	Lean Healthy
LOF	Loss-of-Function
LoxP	Locus of X over P1
M/I	Glucose Metabolism Relative to Circulating Insulin
MB-3	Butyrolactone-3
MDA	Malondialdehyde
METSO	Methionine Sulfoxide
MG	Methylglyoxal
MG-H1	Methylglyoxal Hydroimidazolone-1
MGdG	Methylglyoxal Deoxyguanosine
MICA	Methylimidazole Arginine-Cysteine Crosslink
MMT	Mixed Meal Test
mNKO	Muscle Specific NAMPT Knock Out
MODIC	Methylglyoxal-Derived Imidazolium Crosslink
MOLD	Methylglyoxal-Derived Di-Lysine Imidazolium Crosslink
mRNA	Messenger RNA
MX	Media X
MYH3	Myosin Heavy Chain 3
NA	Nicotinic Acid
NAD	Nicotinamide Dinucleotide (Global)

NAD^+	Oxidized NAD (Free NAD)
NADH	Reduced NAD
NAFLD	Non-Alcoholic Fatty Liver Disease
NAM	Nicotinamide
NAMPT	Nicotinamide Phosphoribosyl Transferase
NF-κB	Nuclear Factor Kappa B
NGT	Normal Glucose Tolerance
NHS	Nurses' Health Study
NMNAT	Nicotinamide-Nucleotide Adenylyltransferase
NO	Nitric Oxide
NQO1	NADPH Quinone Oxidoreductase 1
NR	Nicotinamide Riboside
NRF2	Nuclear Factor Erythroid 2-related Factor 2
NRK	Nicotinamide Riboside Kinase
OB	Individuals with Obesity
OGTT	Oral Glucose Tolerance Test
P300	AKA EP300; E1A Binding Protein P300
PARP1	Poly ADP Ribose Polymerase 1
PBEF	Pre-B-Cell Colony Enhancing Factor (Alternate name for NAMPT)
PEPCK	Phosphoenol Pyruvate Carboxykinase
PGAM1	Phosphoglycerate Mutase-1
PGC1α	Peroxisome Proliferator-Activated Receptor Gamma Coactivator 1-Alpha
PGK	Phosphoglycerate Kinase
PIGT	Phosphatidylinositol Glycan Anchor Biosynthesis Class T
PK	Pyruvate Kinase
PK-LR	Pyruvate Kinase (Liver and Red Blood Cell Expressing)
PKB/Akt	Protein Kinase B
PRPP	Phosphoribosyl Pyrophosphate
PSMA3	Proteasome 20S Subunit Alpha 3
PSMA5	Proteasome 20S Subunit Alpha 5
PSMB1	Proteasome 20S Subunit Beta 1
PTM	Post-Translational Modification
RBC	Red Blood Cells
RBD	receptor binding domain
S6K	Ribosomal Protein S6 Kinase
scRNA	Scrambled (Non-specific) Small RNA
SDS PAGE	Sodium Dodecyl Sulfide Polyacrylamide Gel Electrophoresis
SEM	Standar Error of the Mean
SFN	Sulforophane
SH-SY5Y	Neuroblastoma Cell Line
siRNA	Small Interfering RNA
SIRT1	Sirtuin 1

SIRT2	Sirtuin 2
SIRT3	Sirtuin 3
SLC1A5	Solute Carrier Family 1 Member 5
SLG	S-d-Lactoylglutathione
SOD1	Superoxide Dismutase 1
STAC	Sirtuin Activating Compoud
STZ	Streptozotocin
T-Res	Trans-Resveratrol
T2D	Type 2 Diabetes
TAG	Triacylglyceride
TMT	Tandem Mass Tagging
TNFα	Tumor Necrosis Factor Alpha
TNNC2	Troponin C2, Fast Skeletal Type
TPI	Triose Phosphate Isomerase
TSA	Trichostatin A
TXNIP	Thioredoxin-Interacting Protein
TXNRD1	Thioredoxin reductase
UBQLN2	Ubiquilin-2
UPR	Unfolded Protein Response
VAT	Visceral Adipose Tissue
VO_{2Max}	Volume of Maximal Oxygen Consumption
WT	Wild Type
βME	Beta Mercaptoenthanol
γH2AX	Gamma Histone 2 A Family Member X (Phosphorylated form of H2AX)

Abstract

The obesity pandemic is persistent with global rates of obesity exceeding 13%. Obesity results in the development of insulin resistance which through a myriad of mechanisms increases the risk for secondary disease development such as type 2 diabetes (T2D). Glyoxalase I (GLO1) is the rate-limiting enzyme for detoxification of the reactive dicarbonyl methylglyoxal which is formed in proportion to glycolytic flux and rapidly modifies and damages proteins, and DNA. Loss of GLO1 drives the development of insulin resistance (IR) and T2D in preclinical models. Skeletal muscle is critical for whole body insulin stimulated glucose uptake and plays a major role in T2D development. We previously demonstrated that muscle from patients with T2D possess lower levels GLO1 protein which was correlated with BMI and clamp-derived insulin sensitivity. Our preliminary data demonstrated GLO1 is attenuated in muscle from individuals with obesity prior to T2D development. However, the mechanisms, and consequences of attenuated muscle GLO1 are unknown. Recent *in vitro* evidence suggests that GLO1 is acetylated under obesogenic conditions, marking it for ubiquitination and degradation although the factors regulating GLO1 acetylation were not identified. SIRT1 is an NAD^+-dependent deacetylase that promotes oxidative metabolism, is augmented by exercise, and is purported to be attenuated with obesity. Therefore, we tested the hypothesis that loss of SIRT1 would promote GLO1 acetylation thereby destabilizing and attenuating GLO1 protein. We also set out to determine if acute exercise could rescue GLO1 protein in individuals with obesity, potentially by promoting SIRT1 and GLO1 deacetylation. Lastly,

we employed human immortalized myotubes to directly test the proposed mechanisms of GLO1 acetylation and determine the proteomic consequences of GLO1 knock down in muscle. We collected muscle biopsies from 15 lean healthy (LH) individuals and 5 individuals with obesity (OB) before, 30 minutes, and 3 hours after treadmill exercise at 80% of participants' VO_{2Max}. Baseline GLO1 ($p < 0.01$) and SIRT1 ($p < 0.05$) proteins were lower in OB muscle and GLO1 protein was correlated to SIRT1 protein (Rho = 0.639, $p < 0.01$). Knock down of GLO1 in human immortalized myotubes upregulated ubiquitin proteasome, and apoptosis pathways while downregulating glycolytic proteins and proteins involved in sarcomere organization. Acute exercise provoked a trend in increased SIRT1 protein 30 minutes after exercise in the OB group (post-hoc pre – 30 min. $p = 0.13$) along with a trend for decreased GLO1 acetylation ($p = 0.09$). However, GLO1 protein abundance and activity were not affected by exercise in OB muscle. Studies in human immortalized myotubes aimed at depleting or rescuing SIRT1 activity by modulating cellular NAD^+ or by directly knocking down SIRT1 did not alter GLO1 acetylation, protein, mRNA or activity. Lastly, a screen of other factors that regulate protein acetylation revealed differential effects of specific deacetylases (SIRT2) and acetyltransferases (GCN5 and P300) on GLO1 protein and activity. Collectively these data are the first to demonstrate lower GLO1 protein abundance in muscle from individuals with obesity and to describe the proteomic consequences of GLO1 attenuation in human muscle. We also excluded SIRT1 as a regulator of GLO1 while demonstrating the potential for more nuanced regulation of GLO1 by acetylation. These data establish GLO1 as a novel target for the prevention and treatment of obesity-related maladaptive

phenotypes in muscle. Future work is still needed to uncover targetable mechanisms underpinning GLO1 attenuation with obesity in muscle.

Chapter 1

Introduction

As of 2016 more than 13% of adults world-wide were classified as obese or having a body mass index (BMI) ≥30 kg/m^2, which is nearly triple the prevalence since 1975 [1]. Women with a BMI greater than 30 kg/m^2 are 1.5 times more likely to develop heart disease and men of the same BMI range were at a 2-fold increased risk for heart disease compared to sex-matched individuals with BMI <25 kg/m^2 [2]. Men and women with obesity are also 10 – 23 times more likely to develop type 2 diabetes (T2D) depending on the severity of obesity [2]. Increased risk for disease is thought to be primarily driven by the development of insulin resistance. At its most basic level, obesity is a result of a sustained imbalance of energy intake and energy expenditure which results in surplus energy storage.

Mechanisms of insulin resistance development resulting from this sustained imbalance are multifactorial and involve several tissues. The onset of dicarbonyl stress is an understudied and potentially important mechanism which may be a critical driver of insulin resistance development with obesity. Methylglyoxal (MG) is the most abundant dicarbonyl and the primary contributor to dicarbonyl stress which promotes damage to DNA and proteins through direct and irreversible modification of these molecules. Accumulation of MG with obesity and diabetes has been previously shown in both animals [3, 4] and humans [5, 6]. MG accumulation is primarily the result of triosephosphate degradation [7, 8]. Triosephosphates are intermediary metabolites formed during

lipolysis, triglyceride synthesis, and glycolytic flux although the spontaneous degradation of the Triosephosphates glyceraldehyde-3-phosphate (G3P) and dihydroxyacetone phosphate (DHAP) from glycolytic flux are the primary pathway through which MG is formed.

However, attenuation of key MG detoxification mechanisms such as the primary MG detoxifying enzyme Glyoxalase I (GLO1) is likely necessary for MG accumulation [9]. Skeletal muscle is the primary site of insulin stimulated glucose disposal and is therefore not only relevant for the development of insulin resistance but also has a relatively high glycolytic flux compared to other tissues. Consequences of MG accumulation in muscle are poorly characterized but so far have been described to include modification of key insulin signaling pathways [10, 11], impaired 2-Deoxy-Glucose (2-DG) uptake [11] and increased fibrosis in muscle [12]. Our lab has recently shown that GLO1 protein abundance is attenuated in muscle from patients with T2D and is negatively correlated with clamp-derived insulin sensitivity and BMI.

To follow up on these data, we set out to test the hypothesis that GLO1 protein in muscle is attenuated in individuals with obesity prior to the onset of T2D. Our rationale was that if this were the case, it may be partially driving an increase in dicarbonyl stress to promote the development of insulin resistance in skeletal muscle. We also set out to determine the potential role for hyperacetylation of GLO1 to attenuate its protein abundance in skeletal muscle as has been demonstrated previously in HEPG2 cells under obesogenic (fatty acid treatment) conditions [13]. However, whether GLO1 acetylation plays a role in human muscle and the molecular mechanisms contributing to this purported hyperacetylation of GLO1 with obesity has not been explored. This

potential mechanism would therefore present a novel and promising target for the prevention and treatment of obesity related metabolic dysfunction.

Our central hypothesis was that GLO1 would be attenuated in OB muscle and related impaired protein abundances of SIRT1, P300, NAMPT and CD38 to promote hyperacetylation and subsequent attenuation of GLO1 abundance and activity. We further hypothesized that the obesity phenotype would be rescued to represent the molecular milieu of muscle from lean healthy individuals following a bout of exercise. A graphical depiction of our central hypothesis is given in Figure 1.1. To test this central hypothesis, we developed and executed the following specific aims:

Aim 1: Determine if GLO1 abundance is attenuated and related to mechanisms regulating protein acetylation in muscle from individuals with obesity. We also aimed to determine if acute treadmill exercise was able to promote a molecular phenotype in muscle from individuals with obesity which resembles that found in muscle from lean healthy individuals. Finally, we set out to determine the proteomic consequences of muscle lacking GLO1 protein.

Aim 1a. *Our hypotheses for Aim 1a* are OB muscle will have higher levels of the NADase CD38, increased levels of the acetyltransferase P300, lower levels of the NAD^+-scavenging enzyme NAMPT, lower abundance of the NAD^+-dependent deacetylase SIRT1 and lower GLO1 abundance and activity. *We further hypothesize acute aerobic* exercise will promote GLO1 deacetylation and increase GLO1 activity.

Aim 1b. *Our hypotheses for Aim 1b* are that muscle from individuals with obesity will have elevated MG-modified proteins and increased circulating AGE-free adducts. In addition,

proteomic analysis from human immortalized myotubes following GLO1 KD will reveal enrichment of pathways related to inflammation, and oxidative stress.

Aim 2: Determine the role of NAD^+ bioavailability and enzymes mediating protein acetylation to regulate GLO1 protein abundance and activity in human myotubes.

Aim 2a. *Our hypotheses for Aim 2a* are that FK866 treatment will promote hyperacetylation of GLO1, promoting its subsequent ubiquitination and degradation and impair GLO1 activity. *We further hypothesize* that, co-treatment with NR to restore NAD in FK866 treated cells, will prevent GLO1 hyperacetylation and preserve its abundance and activity.

Aim 2b. *Our hypothesis for Aim 2b* is that SIRT1 KD will promote hyperacetylation of GLO1, and attenuate GLO1 abundance and activity.

Aim 2c. *Our hypotheses for Aim 2c* are that inhibitors targeted against non-SIRT1 deacetylases will inhibit GLO1 abundance and activity whereas inhibitors targeted against acetyltransferases will promote GLO1 abundance and activity.

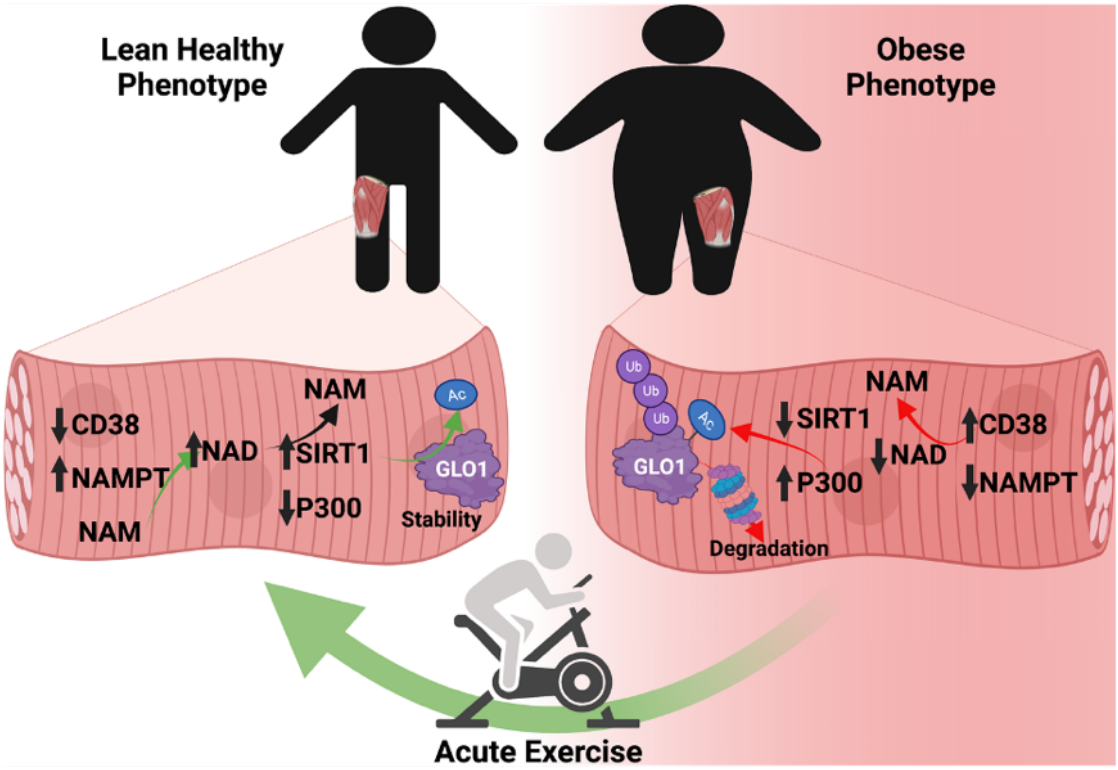

Figure 1.1 Graphical Depiction of Central Hypothesis. In the lean healthy condition, we hypothesize that low levels of CD38 and relatively higher levels of NAMPT maintain optimal levels of cellular NAD to support SIRT1 mediated deacetylation and stabilization of GLO1. In addition, low levels of P300 may also promote a deacetylation of GLO1. Conversely, we hypothesize that obesity will possess elevated levels of CD38 and low levels of NAMPT along with low levels of SIRT1 and high levels of P300, favoring GLO1 acetylation and degradation. Lastly we hypothesize that acute exercise will promote deacetylation of GLO1 via augmenting SIRT1 and NAMPT thus stabilizing GLO1 and restoring the lean healthy phenotype.

Chapter 2

Literature Review

2.1 The Obesity Pandemic

2.1.1 The Persistence of the Obesity Pandemic

The obesity pandemic persists and there are no indications of its deceleration or cessation in the near future. As of 2016 more than 13% of adults world-wide were

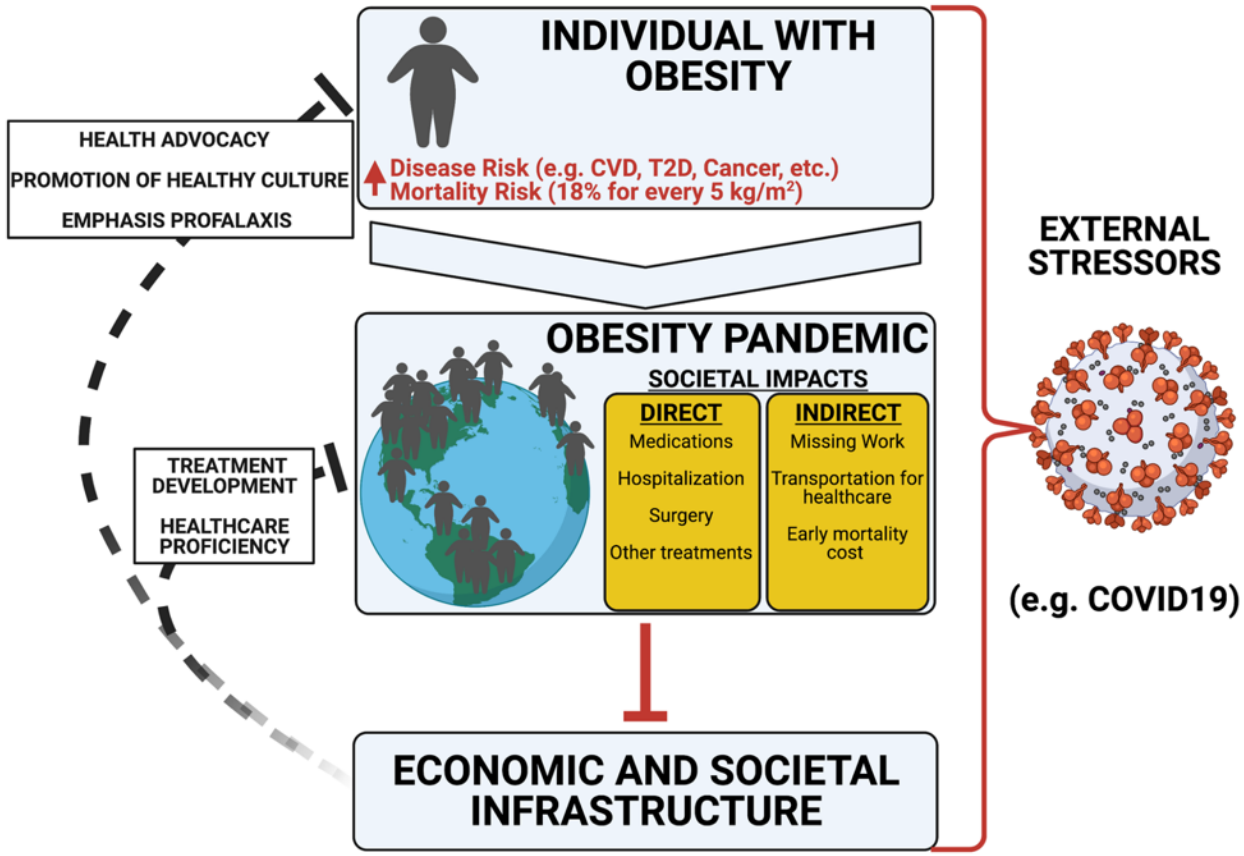

Figure 2.1 The Individual and Global Impacts of Obesity. Individuals with obesity possess increased risk of disease and mortality. This compromised state of health on a large scale can leave individuals susceptible to external stressors (e.g. COVID19) to enhance the economic, public health care and societal infrastructures. Bolstering the economy and public health infrastructure plays a critical role in preventing obesity and subsequent global impacts.

classified as obese or having a body mass index (BMI) ≥30 kg/m^2, which is nearly triple the prevalence since 1975 [1]. The persistence of this problem into the next generation and beyond is evidenced by the fact that the prevalence of childhood obesity also continues to rise. In 2019 an estimated 38.2 million children under the age of 5 years were classified as overweight or obese and in 2016, 340 million children and adolescents between the ages of 5 and 19 years were also classified as overweight or obese [1]. These data suggest that the end to increased global prevalence of obesity is nowhere in sight. In fact, if this rate of prevalence continues nearly half of the global adult population will be overweight or obese by 2030 [14].

2.1.2 Societal and Individual Burdens of Obesity

The obesity pandemic confers a myriad of deleterious consequences on both the societal and individual levels (Figure 2.1). On the societal level, obesity is a serious public health issue which contributes significant economic burden that can be attributed to direct costs (e.g., medications, surgical interventions, hospitalizations and other treatments) and indirect costs (e.g. transportation to health care providers, early mortality costs, loss of work productivity etc.) [14]. According to a recent systematic review, the annual direct costs of obesity in the US have increased from $2,741 per person in 2005 to $6,899 per person in 2011 [14]. One study attempted to estimate the annual productivity loss as a result of obesity and reported this indirect cost to be approximately $8.65 billion per year. Given the prevalence of adult obesity in the US in 2011 was 34.9% [15] these estimates would suggest that the economic burden of obesity in 2011 was at least $680 billion with approximately 84% attributed to direct costs. Considering the proportion of individuals with obesity in the US is now nearly 40% [1], the direct and indirect costs today have

certainly risen in parallel. Not to mention the societal impact that obesity has had on exacerbating the burden of the current COVID-19 pandemic. Recent meta-analyses found that higher BMI is associated with increased risk of hospital admission, ICU admission, need for mechanically assisted ventilation and death as a result of COVID-19 [16-18]. Steinberg and colleagues found that in the US alone, individuals with obesity were more than twice as likely to be hospitalized and more than six times more likely to need mechanically assisted breathing and die after contracting the novel sars-cov2 virus [19]. With the International Monetary Fund estimating in October 2020 that the gross economic losses as a result of the COVID-19 pandemic would reach 4.7% of the world's GDP by the end of 2021 (~$11 trillion) [20], the convergence of the obesity and COVID-19 pandemic has provided a grim example of how individual consequences of a disease can have large scale repercussions on the global economy and our societies.

In addition to the increased risks associated with communicable diseases such as COVID-19, the approximately 650 million adults and 124 million children and adolescents afflicted with obesity world-wide are also burdened with significant increased risk for the development of a number of non-communicable diseases including cardiovascular disease (CVD), hypertension, dyslipidemia, non-alcoholic fatty liver disease (NAFLD), certain types of cancer, and type two diabetes (T2D) to name a few. In a study that analyzed 10 year follow-up data of women from the Nurses' Health Study (NHS) and men from the Health Professionals Study, women with a BMI greater than 30 kg/m^2 were 1.5 times more likely to develop heart disease and men of the same BMI range were at a 2-fold increased risk for heart disease compared to sex-matched individuals with BMI <25 kg/m^2 [2]. In the same analysis men and women with obesity had a 30 – 80% increased

risk to develop colon cancer and were 10 – 23 times more likely to develop T2D depending on the severity of obesity [2]. In a more recent trial, 30-year follow-up data of the NHS demonstrated that women with obesity alone were at nearly 40% greater risk of CVD and those who had obesity along with hypertension, diabetes and hypercholesterolemia had a greater than 3-fold risk of CVD and nearly 4-fold increased risk of heart attack [21]. Finally, and perhaps most importantly, obesity contributes to an increased risk of all-cause mortality in individuals with obesity compared to those without obesity [22, 23]. A recent meta-analysis which included data from over 30 million individuals over follow-up times of up to 20 or more years, demonstrated an 18% increased relative risk of all-cause mortality for every 5 kg/m^2 increase in BMI [23]. From a humanitarian perspective, these dramatic health consequences on the individual level certainly are enough to warrant large amounts of attention, energy, and resources go into investigating the pathogenesis of obesity and the ensuing secondary complications the obese state provokes. However, considering the existential economic burden obesity places on our economy and society as a whole, it is made even more obvious that there is a need to invest substantial resources on the prevention and treatment of obesity and the subsequent pathogenesis of secondary diseases.

2.2 Development of Obesity

2.2.1 Chronic Positive Energy Imbalance Drives Obesogenesis

At its core, the development of obesity is a result of energy imbalance such that energy intake exceeds energy expenditure. However, the factors that drive and sustain this energy imbalance in an organism are unfathomably complex and poorly understood. As is true with all emergent phenomenon of our physiology, an understanding of human

evolution is crucial to the understanding of several potential drivers of obesity. Although human evolution is outside the scope of this review (for a comprehensive review the reader is directed to [24]) it suffices to say that the way in which humans have evolved has set in motion the genetic and molecular underpinnings that influence crucial factors related to the development of obesity such as what we choose to eat, how we metabolize and store what we eat, how we interact with our environment, how we respond to fluctuations in our body weight, and how much we move.

2.2.2 Thrifty Genotype Hypothesis for Obesity Development

We humans who evolved to hunt and forage for food sources while prioritizing energy efficiency so as to be robust against starvation in the event of failures in pursuit of these endeavors, now find ourselves in the modern world where energy dense foods are readily acquired at little to no energy cost. The number of fast-food restaurants in the US doubled from 1972-1997 [25] and in 2004 Americans spent $100 billion on fast food (~50% of their monetary food expenditure) [26]. In addition, not only is there no longer an energy cost of acquiring food for most of modernity, but everyday life also has an extremely low energy requirement with the frequency of sedentary jobs, the advent of machines and appliances to carry out energy-intensive tasks, and the popularization of motorized vehicles for transportation. The paradigm described above is the framework for a hypothesis known as the “Thrifty Genotype” hypothesis of obesity [24].

However, this is an oversimplified view of a more complex problem that manifests not only as a result of our evolution but also of our epigenetics as a result of our contemporary environment spanning from pre-conception, through development, and continuing across our lifespan. Hints of these effects were first exemplified by studying

the effects of overfeeding in twins which demonstrated variability in the hypothalamic response to regulate energy expenditure and thus resulting in differential weight gain in twins despite similar increases in energy intake [27]. Recent work has followed up on these observations to identify specific genes that may be differentially regulated by epigenetics in an attempt to explain this variability in obesogenesis (for comprehensive reviews on this topic the reader is directed to [28] and [29]). However much of the variability in obesogenesis is left unexplained, and the precise molecular mechanisms that drive obesity and emerge from the complex interactions of our genetics, epigenetics, behavior and environment remain incomprehensively understood.

2.3 Obesity-Related Diseases are Driven by Insulin Resistance

As mentioned previously, obesity dramatically increases the risk for a number of diseases including CVD, cancer, non-alcoholic fatty liver disease and T2D. Given the complex machinations underlying the development of obesity, it follows that the molecular and physiologic consequences of this milieu are equally if not exceedingly complex. However, the development of insulin resistance has been identified as common factor and one of the most important drivers of the development of these and other obesity-related diseases. This is in part due to the fact that obesity results in the development of insulin resistance in every tissue in the body resulting in metabolic, cellular and molecular consequences that promote disease development [30].

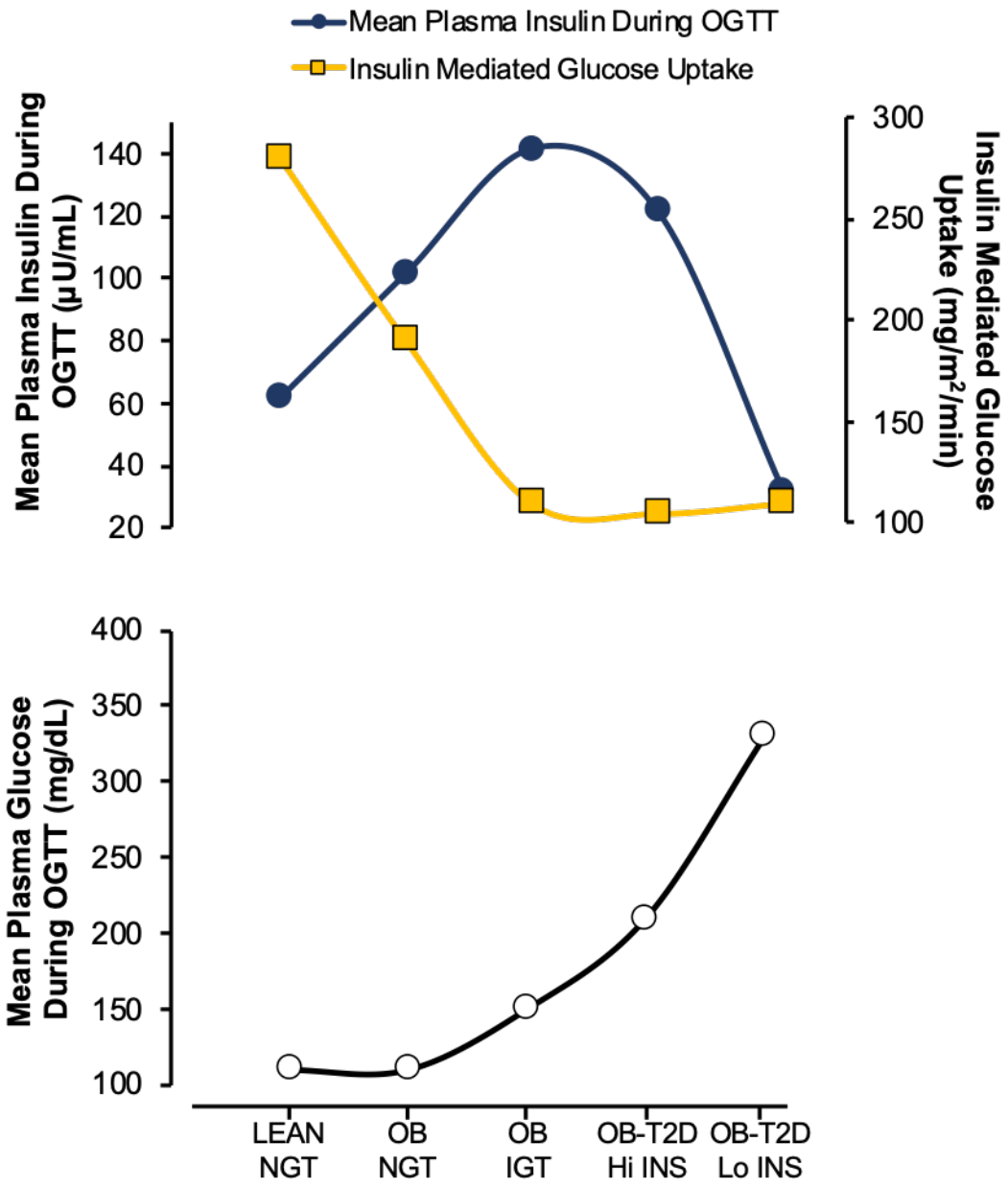

Figure 2.2 Natural History of Insulin Resistance and Diabetes (Adapted from DeFronzo et al). Early pathology of obesity is characterized by normal glucose tolerance (NGT) via compensatory hyperinsulinemia allowing for maintenance of glucose uptake. As pathology progresses, hyperinsulinemia can no longer compensate for the underlying insulin resistance resulting in impaired glucose tolerance (IGT) and eventually type 2 diabetes (T2D). Uncontrolled T2D eventually results in beta cell failure and an inability to produce insulin in response to glucose consumption.

Like all of physiology, the severity of insulin resistance exists on a continuum and as this continuum progresses so too does the severity of the resultant phenotype of glucose intolerance. Figure 2 (adapted from [30]) depicts the natural history of T2D by superimposing the progression of insulin resistance over the physiologic response to an oral glucose tolerance test (OGTT). Note that in this data set, individuals with obesity and normal glucose tolerance (OB NGT) there already exists an approximately 33% reduction in insulin mediated glucose uptake. Despite this reduction in insulin sensitivity, individuals with the OB NGT phenotype maintain normal plasma glucose levels due to a compensatory hyperinsulinemia during the OGTT. As this obesity phenotype persists, a myriad of mechanisms promotes the progression of insulin resistance at a rate that eventually outpaces the ability of hyperinsulinemia to compensate resulting in hyperglycemia and T2D. In prolonged states of uncontrolled T2D, the pancreatic beta cells begin to fail in their ability to produce insulin at which point plasma glucose values in response to OGTT become exceedingly elevated. This etiology of disease clearly implicates the manifestation of insulin resistance as the primary driver of T2D in individuals with obesity. In addition, the pathogenesis appears to begin early with even apparently metabolically healthy individuals with obesity (OB NGT) presenting with the beginnings of insulin resistance. The development of insulin resistance in this context is an aggregate manifestation of insulin resistance in several tissues including adipose, liver, pancreatic beta cells, skeletal muscle and others [30]. However, skeletal muscle is the primary contributor of this effect given that it is responsible for >85% of insulin stimulated glucose uptake [31]. Therefore, uncovering the mechanisms promoting insulin resistance in skeletal muscle, especially in the early stages of the pathogenesis (i.e., OB

NGT phenotype) should be a primary focus for the prevention of obesity-related diseases. However, there are seemingly innumerable mechanisms at play and as such we still do not possess a comprehensive understanding of the development of insulin resistance in skeletal muscle as a result of obesity. One mechanism that has been understudied in this context is the accumulation of reactive dicarbonyls in skeletal muscle as a result of obesity.

2.4 Role of Dicarbonyl Stress in the Development of Obesity-Related Diseases

2.4.1 Formation and Consequences of Dicarbonyls

Dicarbonyls are a large group of reactive metabolites produced *in vivo* as byproducts of several metabolic processes. For example, methylglyoxal (MG) and 3-deoxyglucosone (3DG) are the primary dicarbonyls formed as byproducts of glucose metabolism whereas 4-hydroxynonenol (4-HNE) and malondialdehyde (MDA) are formed as byproducts of lipid peroxidation [32]. Due to their relationship with metabolic flux, accumulation of these reactive dicarbonyls (termed dicarbonyl stress) are implicated as cause and consequence of several disease states characterized by metabolic dysfunction such as obesity [5, 33], diabetes [5, 34, 35], and aging [36]. Due to their highly reactive nature, dicarbonyls are able to rapidly modify and damage proteins, lipids and DNA when they accumulate. Overtime, these modifications undergo non-enzymatic structural rearrangement to form irreversible advanced glycation end products (AGEs). Formation of AGEs promotes cellular oxidative stress [37-40] , inflammation [4, 38, 41-48], and has been implicated in the development of insulin resistance [4, 35, 43, 49-57] and several diabetic complications such as retinopathy [58-62] , neuropathy [34, 37, 63], nephropathy [60-62, 64-73], and vascular dysfunction [42, 74-82].

Of the aforementioned dicarbonyls, MG is the primary source of AGEs *in vivo* and is the most well studied in the context of obesity, insulin resistance and diabetes. Plasma concentrations of MG in humans range from 50 – 250 nM and intracellular concentrations are maintained at 2 – 10 μM depending on the physiological context and cell type [33].

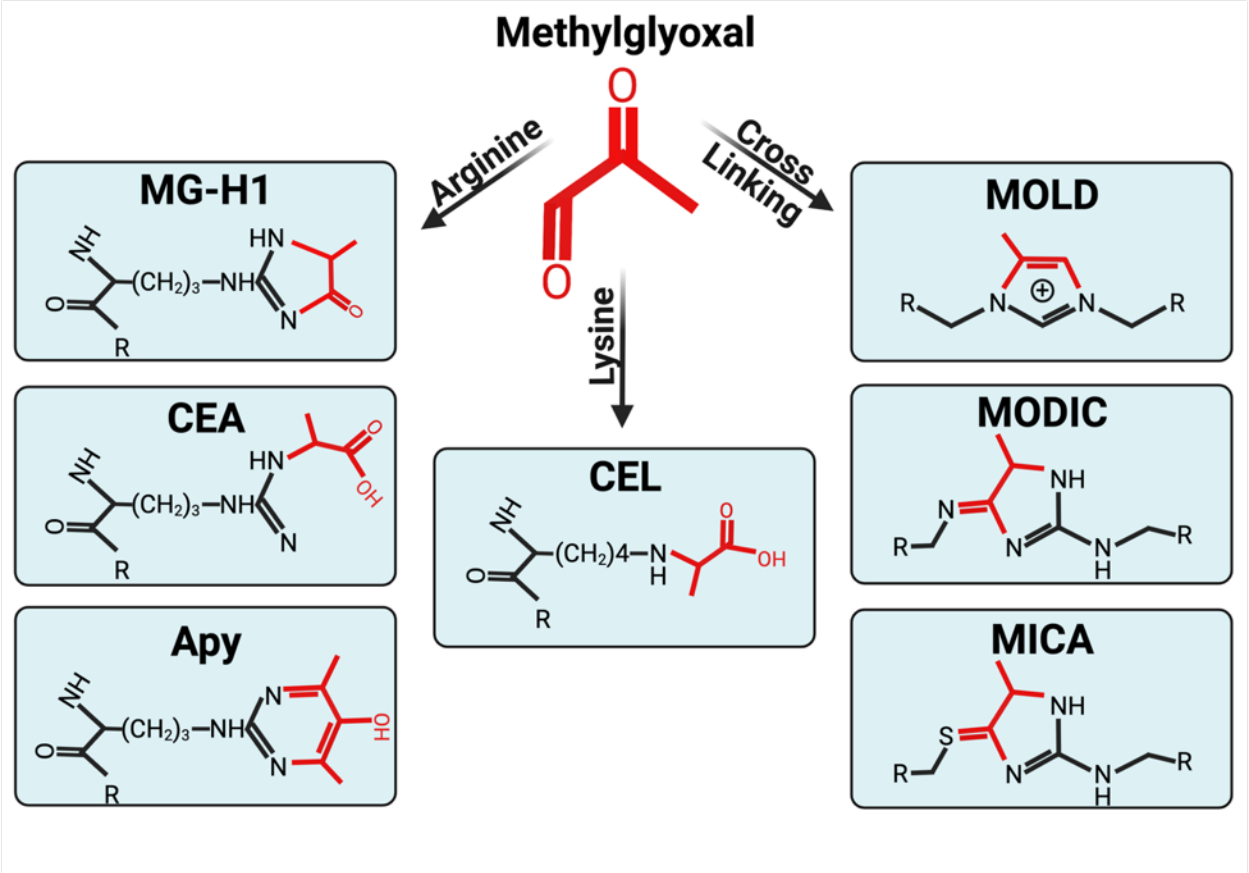

Figure 2.3 Methylglyoxal and MG Derivative Advanced Glycation End Products. Methylglyoxal is the primary source of AGEs *in vivo.* MG derived AGEs include those resulting from MG-modification of arginine (MG-H1 – methylglyoxal hydroimidazolone, CEA – carboxyethyl arginine and Apy - argpyrimidine), Lysine (CEL – carboxyethyl lysine) or by crosslinking of amino acids across or within proteins (MOLD, MODIC, and MICA).

Early studies demonstrated increased MG formation in red blood cells incubated in hyperglycemia and increased MG in plasma from patients with diabetes [8]. Although small amounts of MG seem to be necessary for proper organismal function (e.g. hormetic response to acute stress [83], and anti-microbial action [84]), excessive MG accumulation is a strong driver of cellular dysfunction [85]. This is due primarily to the fact that MG is

approximately 20,000-fold more reactive than glucose to non-enzymatically modify proteins and DNA. MG modifies DNA by attacking deoxyguanosine residues to form imidazopurinone 3-(2'-deoxyribosyl)-6,7-dihydro-6,7-dihydroxy-6/7-methylimidazo-[2,3-b]purin-9(8)one (MGdG) [86] (Figure 3). This results in DNA damage such as frame shift mutations and DNA strand breaks which is linked to cell death as well as oncogenesis [87, 88]. Free MG primarily promotes glycative damage of proteins by rapidly reacting with thiols, lysine residues, and arginine residues. Modification of lysine residues by MG generates several irreversible AGEs including carboxyethyl lysine (CEL) as well as lysine-lysine (MOLD), and lysine-arginine protein crosslinks (MODIC). However, arginine is the primary amino acid target for MG to irreversibly modify with the primary AGE produces being MG-H1 [89-93]. The most susceptible arginine residues are those exposed on protein surfaces and "activated" by nearby lysine or arginine residues which act to lower the microscopic pKa of the target arginine residue [94]. In addition, proximal glutamine or asparagine residues also increase the rate of MG-modification on arginines by providing a proximal conjugate base to catalyze the dehydration step involved in producing MG-H1 [95, 96]. MG-modification of arginine residues can result in the non-enzymatic formation of several irreversible AGE species including carboxyethyl arginine (CEA), Argpyrimidine (APY), and methylglyoxal-hydroimidazolone 1 (MG-H1). MG-H1 is the primary product of arginine modification by MG and it is also the most abundant AGE *in vivo* [97] (Figure 3).

Formation of MG-H1 on arginine residues damages proteins by robbing the arginine of its structure and charge. Specifically, MG-H1 increases the molecular volume of the arginine residue by 18% and reduces the arginine residue's transfer energy by approximately 32% indicating an increase in the hydrophobicity of the residue [97].

Importantly, arginine residues are commonly found in catalytic domains of enzymes and therefore MG modification arginine is likely to alter protein function [93, 98]. Interestingly, MG-modification of some enzymes may induce impaired activity (e.g. IRS1 [11], and SOD1 [40]) whereas some MG-modified proteins actually have been shown to possess enhance protein activity (e.g. fatty acid synthase [FASN] [99]). A recent screening of the cytosolic dicarbonyl proteome (i.e. the cytosolic proteins most susceptible to modification) in human endothelial cells, in which cells were treated with exogenous MG (500 μM, 24h) to enrich the MG-modified proteins, found that of the 220 MG-modified proteins identified, 47% of all MG modification events occurred in RBD sites of proteins [91]. Interestingly, many of the most highly modified proteins were involved with glycolysis (PKM, α-enolase, G6P, GAPDH, LDH and PGK-1 all in the top 25). However, the cellular process with the most MG-susceptible proteins identified was protein folding [91], which is linked to oxidative stress and inflammation [97]. Polar residues such as arginine are often found on protein surfaces to promote the solubility of proteins. As previously mentioned, MG-H1 formation increases the hydrophobicity of the arginine residue. Hydrophobic residues are often shielded from the aqueous cellular matrix by other polar amino acid residues. In this way the interactions between an amino acid's charge and their environment partially informs secondary structure. As a result, the increased hydrophobicity of arginine residues on the surface of proteins via formation of MG-H1 is recognized by the cell as misfolded or damaged proteins and activate the unfolded protein response (UPR) [91].

In addition, another study using a similar model to enrich MG-modified proteins identified 28 site specific modifications by MG (MG-H1 and/or CEA) on arginine (R) or lysine (K) residues were found on histones H3 (8 R), H2A (1 R), H2Ax (1 R), H2B (4 R, 3

K), H4 (4 R, 1 K) [100]. Another group treated HEK293T cells with 250, 500 or 1000 μM of MG for 12 hours [101]. The increasing concentrations of MG resulted increased crosslinking of histones H3 and H4, as well as decreased acetylation and ubiquitination of both proteins and concomitant ubiquitination [101]. Much like ablation of a residue's charge, protein crosslinking is also recognized by UPR machinery as damaged or misfolded protein and marked for degradation. Over activation of the UPR by MG mediated dicarbonyl stress has been linked to oxidative stress, inflammation and cell damage and may play a mechanistic role in pathogenesis [91].

Activation of the UPR results in ubiquitination and degradation of MG-modified proteins via the 20S proteasome. However, given the MG-modification on the amino acid is irreversible, the MG-modified amino acids remain in their modified state following protein degradation (termed AGE free-adducts) which are then cleared from the cell, appear in the circulation, and are eventually cleared by the kidney [6, 67, 102, 103]. Indeed, circulating concentrations of MG-H1 free adducts accumulate in individuals with diabetes [6, 104] and the extent to which they accumulate have proven to be good markers of diabetic complications such as kidney disease [61, 67, 68], and cardiovascular dysfunction [105, 106].

2.4.2 Evidence for MG Accumulation in Obesity

Although it is well established that MG and MG-H1 accumulate in diabetes and drive diabetic complications, less work has been done to link MG accumulation with obesity. MG is primarily formed in proportion to glycolytic flux via spontaneous degradation of the triosephosphates dihydroxyacetone phosphate (DHAP) and glyceraldehyde 3-phosphate (G3P) at a rate of circa (c.a.) 0.05% of glucotriose flux

(Figure 2.4) [7, 8]. This flux may very well be exacerbated during the development of obesity and insulin resistance. Consider for example the OB NGT phenotype described in the previous section. These individuals possess underlying insulin resistance which is being overcome by fasting and post-prandial hyperinsulinemia.

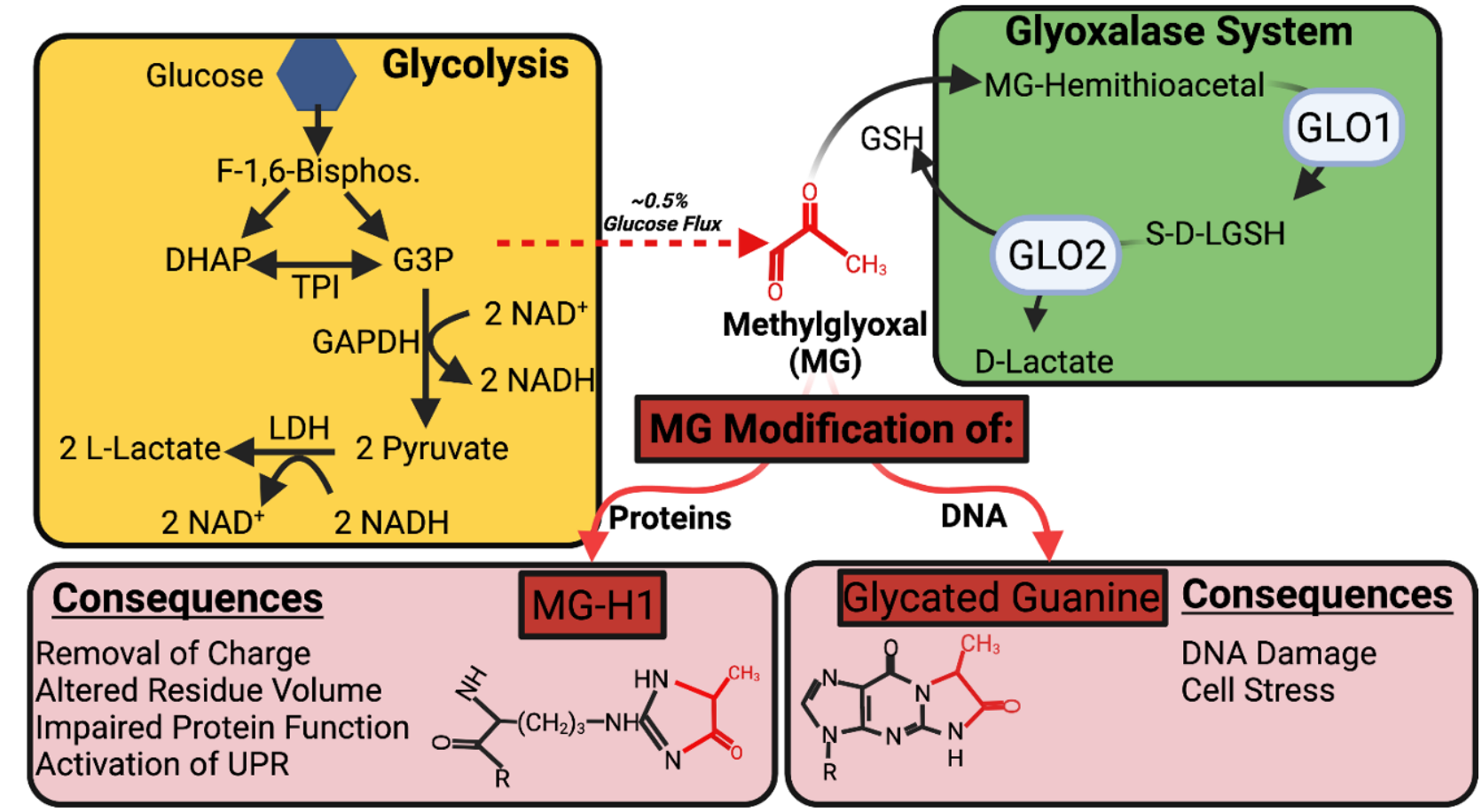

Figure 2.4 MG Formation, Detoxification and Consequences. MG is formed in proportion to glycolytic flux at a rate of approximately 0.5% of all triosephosphates formed. MG is rapidly detoxified by the glyoxalase system where the rate-limiting enzyme GLO1 uses a catalytic amount of glutathione (GSH) to convert MG-hemithioacetal to s-D-lactoylglutathione which is then converted back to GSH and D-lactate by GLO1. Failure of the glyoxalase system or increased production of MG results in modification of proteins and DNA by MG to promote cellular stress termed dicarbonyl stress.

This phenotype has been characterized as having similar whole-body glucose disposal rates as lean age-matched individuals under hyperinsulinemic states [107]. In addition, muscle from OB NGT individuals incubated *ex vivo* in 5 mM glucose, exhibits an approximately two-fold greater basal non-oxidative glycolysis compared to muscle from lean individuals [108]. This has recently been partially corroborated by *in vivo* data demonstrating that women with obesity have higher circulating concentrations of L-lactate, indicative of greater production via anaerobic glycolysis and/or impaired clearance via oxidative phosphorylation compared to age matched lean healthy (LH) individuals [109]. Taken together, the body of evidence suggests that the state of obesity is characterized by a combination of constant hyperinsulinemia, and increased glucose partitioning in the skeletal muscle toward non-oxidative glucose disposal, which may exacerbate muscle glucotriose flux and MG production.

In addition, triosephosphate flux is also increased during glyceroneogenesis which occurs during adipose expansion. During obesogenesis, adipocyte expansion is chronically occurring in order to meet the storage demand of metabolic substrates which are accumulating as a result of energy intake exceeding energy expenditure. In this context, the increased adipose tissue mass results in increased fasted whole-body glycerol and free-fatty acid release [110, 111]. This increase in glycerol flux requires increased triosephosphate flux which may increase the proportion of triosephosphates that degrade into MG. Therefore, in the context of obesogenesis both increased adipose expansion and glycolytic glucose disposal in muscle likely contribute to increased MG formation.

Unfortunately, the data on *in vivo* levels of MG in the context of obesity are relatively scarce owing to a lack of a reliable commercially available assay for MG, the technical nature of the gold standard LC-MS/MS methodology, and the lack of a commercially available MG standard of adequate purity [33]. Regardless, the limited data that exists examining MG in preclinical models as well as observations in humans have shown elevations in circulating and tissue levels of methylglyoxal with obesity. Young (6 week old) male mice fed a high fat diet (HFD) (60% kcal from fat) for 16 weeks developed obesity and saw a 20% increase in circulating MG [3]. In another HFD mouse model of obesity, 12 week old male mice were fed a HFD (45% kcal from fat) for 18 weeks which resulted in a nearly 3-fold increase in visceral adipose tissue MG concentration compared to their low fat diet fed littermates [4]. In both of these mouse models, the onset of obesity coincided with glucose intolerance which, along with the increases in MG, were rescued by co-treating the HFD-fed mice with molecules purported to have MG scavenging actions (Genistein in ref [3] and pyridoxamine in ref [4]). Similar to these preclinical models of obesity, the onset of overweight and obesity in humans also results in MG accumulation. In lean healthy humans, plasma MG levels assessed via the gold-standard LC-MS/MS method were found to be 132 $\pm$ 63 nM [112] which is increased by ~37% to 181 $\pm$ 61 nM in overweight individuals and even further by ~85% in participants with obesity to 245 $\pm$ 123 nM [5]. Several studies now have also demonstrated that plasma MG area under the curve (AUC) is exacerbated following an oral glucose tolerance test in individuals with obesity or diabetes [104, 113]. In a recent randomized controlled clinical trial, an 8 week very low calorie diet intervention eliciting c.a. 10 kg weight-loss in individuals with obesity reduced fasting MG levels by approximately 8% and post-prandial MG levels by

approximately 57% whereas the control group saw no changes in fasting or post-prandial MG [114]. Collectively the preclinical and clinical data implicate the accumulation of MG in both the fasted and post-prandial state as consequences of the development of obesity. However, several questions remain to be elucidated including: 1) what potential role MG accumulation may have in the progression of obesity and obesity-related metabolic dysfunction? and 2) what is the primary tissue contributing to and affected by the increase in circulating MG?

Publication	Model	Treatments/Conditions	Outcome
Fiory, F et al.	INS-1E (Rat Beta Cells)	500 µM MG, 30 minutes	Impaired IRS1 and AKT phosphorylation Impaired insulin gene expression and secretion in response to 20 mM glucose
Nigro, C et al.	MAEC (Mouse Aortic Endothelial Cells)	500 µM MG, 16 hours GLO1 Inhibitor for 48h	MG and GLO1 inhibition Impaired IRS1 and AKT phosphorylation MG and GLO1 Inhibition attenuated P-eNOS^{S117} and release of NO
Riboulet-Chavey, A et al.	L6 Myotubes (Rat Skeletal Muscle Cells)	2.5 mM MG (2-^{14}C, radiolabel) + AG 2.5 mM MG (2-14C, radiolabel) - AG	MG treatment modified IRS1, and impaired P-AKT and 2-DG uptake by ~60% 2-DG uptake and P-AKT rescued by co-treatment with AG
Moraru, A et al.	Drosophila	GLO1 KO	Increased MG and fasting TAGs and Glucose in GLO1 KO flies Decreased insulin-stimulated PS6K in GLO1 KO flies
Lodd, E et al.	Zebrafish	CRISPR/Cas9-Glo1 KO	Increased MG in GLO1 KO fish 2-fold increase in 1 hour post-prandial glucose in GLO1 KO fish
Nigro, C et al.	12 week-old C57BL/6 Male Mice	50 mg/kg/day MG IP, Ramp to 75 mg/kg/day over 7weeks	IP MG attenuated insulin sensitvity via insulin tolerance test IP MG impared IRS1, AKT and eNOS phosphoryation in response to insulin
Matafome, P et al.	6 and 14 month-old Wistar and Goto-Kakizaki (non-obese T2D) rats	50 mg/kg/day MG in drinking water in Wistar rats Ramp to 75 mg/kg/day from 14 weeks to 6 months	No effect of age or MG on fasted glucose or 2hr post IPGTT.
Rodrigues, T et al.	Male Wistar and Goto-Kakizaki rats	8 weeks of standard diet, HFD alone or with 50 mg/kg/day MG in drinking water in Wistar rats only Ramp to 75 mg/kg/day from 14 weeks to 6 months	Elevated glucose AUC in HFD, HFD+MG, and Goto-Kakizaki rats during IPGTT. Elevated glucose AUC in HFD+MG vs HFD Wistar rats.
Neves, C et al.	Male Wistar rats	18 weeks (8 - 12 months old) of standard diet (CON) alone or with 75 mg/kg/day MG and HFD alone, or with 75 mg/kg/day MG	Elevated glucose AUC with IPGTT in HFD and HFD+MG vs CON and MG Elevated glucose AUC with IPGTT in HFD+MG vs HFD
Cai, W et al.	C57BL/6	Fourth generation of mice fed isocaloric diets with or without elevated MG-derivatives (heat-treated chow)	Elevated glucose and insulin AUCs with OGTT in MG fed mice Decreased insulin-stimulated 2-DG uptake in muscle from MG fed mice Decreased P-IR, P-IRS1, and P-AKT in muscle from MG fed mice Decreased SIRT1 and NAMPT protein muscle from MG fed mice
Schumacher, D et al.	C57BL/6N	CRISPR/Cas9-Glo1 KO	40% increase in circulating MG in GLO1 KO mice 55% increase in glucose AUC in GLO1 KO mice
Egawa, T et. al.	9 week-old C57BL/6NC	4 Weeks Sedentary (Sed), Running Wheel Access (EX), Sed + 1% MG in drinking water, EX + 1% MG in drinking water	EX enhanced insulin-stimulated AKT Ser473 phosphorylation in plantaris No enhancement of instulin-stimulated AKT Ser473 phosphorylation with EX+MG

Table 1 Data Demonstrating the Potential for GLO1 Attenuation to Drive Metabolic Dysfunction.

2.4.3 MG Drives Systemic Metabolic Dysfunction

MG accumulation has long been appreciated as a primary driver of the development of diabetic complications including neuropathy [37, 63, 115, 116], nephropathy [68, 88, 117], retinopathy [118], and microvascular dysfunction [41, 50, 75, 91, 118-120]. However, recent cell culture and animal models have also implicated MG as a driver of systemic metabolic dysfunction and subsequent development of diabetes itself (Table 1). For instance, *in vitro* experiments treating beta cells [121] and endothelial cells [122] with exogenous MG demonstrate a direct ability of MG to impair insulin sensitivity in these cells. Incubation of the pancreatic beta cell line INS-1E with 500 μM MG for 30 minutes impaired insulin signaling as determined by IRS and AKT phosphorylation [121]. In addition, MG treated INS-1E cells had diminished insulin gene expression and insulin secretion in response to incubation in 20 mM glucose media. Another study treated mouse aortic endothelial cells with 500 μM MG for 16h and found similar attenuations in IRS1 and AKT phosphorylation, as well as a reduction in the release of the vasodilator nitric oxide [122]. These authors followed up the *in vitro* experiments *in vivo* by treating mice intraperitoneally (I.P.) with 50 mg/kg per day of MG for 5 days increasing to 75 mg/kg over 7 weeks. Mice treated with I.P. MG had impaired whole body insulin sensitivity as assessed by an insulin tolerance test [122]. This impairment was coincident with impaired concentration of circulating vasoactive factors. Specifically, MG treated mice had elevated serum concentrations of the vasoconstrictive endothelin-1 (ET-1) and did not experience an increase in NO or aortic endothelial nitric oxide synthase (eNOS) after insulin administration. Importantly, endothelial NO release

in response to insulin in the microvasculature of skeletal muscle is necessary for increased perfusion of the skeletal muscle to promote insulin stimulated glucose uptake in muscle [123]. In addition, individuals with diabetes have elevated ET-1 along with impaired dilation of skeletal muscle arterioles in response to insulin stimulation which is related to the degree of insulin resistance [124]. However, MG may also be directly attenuating insulin action in the muscle itself. One study treated L6 muscle cells with 2.5 mM of radiolabeled (2-^{14}C) methylglyoxal (of which only ~100 uM was incorporated into the cells) for 30 minutes [11]. Insulin stimulated 2-Deoxyglucose (2-DG) uptake in L6 myotubes treated with MG was impaired by ~60% which was rescued by co-incubation with the MG scavenger aminoguanidine. The authors went on to demonstrate that MG impaired the insulin signaling cascade by directly modifying IRS1. A series of manuscripts using another experimental model of dicarbonyl stress corroborated the aforementioned evidence by demonstrating the ability of MG to promote the development of insulin resistance in rats. In particular they fed rats MG 50 mg/kg ramping to 75 mg/kg for 14 weeks by adding it to their drinking water and demonstrated the ability of MG to promote adipose tissue inflammation and hypoxia [125]. The same group using a similar approach found MG impaired adipose microvasculature and perfusion, liver lipid saturation, insulin signaling in the adipose and liver, as well as whole body insulin resistance [49, 50]. Moreover, another study in mice found that mice fed heat-treated chow possessing over 3-fold greater MG than non-heat-treated chow resulted in a 2-fold elevation in circulating MG-modified proteins [54]. These mice possessed impaired muscle, liver and adipose insulin signaling and impaired glucose and insulin AUC during an OGTT. Further mice fed the high MG diet also had impaired insulin stimulated 2-DG uptake in adipose, muscle

and liver arguably the three most important tissues for glucose regulation. Interestingly, the NAD-dependent deacetylase sirtuin 1 (SIRT1), the NAD scavenging protein nicotinamide phosphoribosyltransferase (NAMPT) and NAD/NADH ratio were all attenuated in all three of those tissues implicating redox imbalance and SIRT1 dysfunction as a potential underlying mechanism.

Collectively, although the current evidence is limited, the data strongly point towards MG accumulation as a driver of obesity-related metabolic dysfunction. However, the precise mechanism for the accumulation of MG with obesity and the primary tissues affected and responsible for this increase are unknown. Given the dominant role skeletal muscle plays in glucose disposal, it is reasonable to suspect that skeletal muscle MG may be a primary contributor to the systemic accumulation of MG and may also be dramatically negatively affected by MG's accumulation resulting in skeletal muscle insulin resistance with obesity. Interestingly, one analysis of 14 mouse tissues from wild type C57BL6 mice showed that skeletal muscle possessed approximately 8 nmol/g tissue of MG, second only to the brain (c.a. 13 nmol/g tissue) and the third highest being the duodenum (c.a. 6 nmol/g tissue) [100]. In another similar analysis of wild type C57BL6 mice, of the 5 tissues analyzed muscle possessed the second highest MG concentration (c.a. 3.8 uM) whereas liver (c.a. 4.3 uM) had the highest MG concentration.

These data clearly support the hypothesis that the skeletal muscle may be a significant producer of MG and may also be relevant in the MG-mediated pathogenesis of obesity-related metabolic dysfunction. As previously discussed, this may be due to an increase in glycolytic flux in skeletal muscle resulting in increased MG production. However, another important factor to consider as a potential contributor of MG

accumulation is a potential impairment of mechanisms responsible for the detoxification of MG.

2.5 Role of Glyoxalase I in Obesity and Metabolic Disease

2.5.1 Cellular and Molecular Physiology of GLO1

As mentioned previously, MG is highly cytotoxic and as such intracellular levels are kept in the low micromolar concentrations. This is primarily achieved by the glyoxalase enzymatic defense system which is responsible for majority of MG detoxification by catalyzing its conversion to D-Lactate [8]. Other redundant mechanisms exist for MG detoxification although these enzymes play a minor role in MG detoxification under normal circumstances. Such enzymes include aldoketoreductases (AKRs, specifically AKR1b1), betaine aldehyde dehydrogenase (ALDH9), and 2-Oxoaldehyde dehydrogenase (2-ODH) [126]. Together, the glyoxalase system and AKR isozymes account for >99% of MG detoxification. However, the rate limiting enzyme of the glyoxalase system glyoxalase 1 (GLO1) is a highly abundant protein (in the top 13% of protein abundance [127]) that is ubiquitously expressed across all tissues and is highly efficient. Based on this disparity in expression between GLO1 and AKRs, as well as GLO1's enzymatic efficiency compared to that of AKR isozymes [128, 129], it has been estimated that GLO1 activity for MG is approximately 30-fold greater than AKRs in most contexts [130].

The glyoxalase system consists of two enzymes, GLO1 and glyoxalase 2 (GLO2), and a catalytic amount of reduced glutathione (GSH). Majority of intracellular MG (>99%) is reversibly bound to GSH [97] forming a MG-hemithioacetal which is the substrate for GLO1 (Figure 2.4). In humans the *GLO1* gene is located on Chromosome 6 and encodes

a functional transcript of 2,016 base pairs and a non-functional splice variant which lacks 3 of the 6 coding exons resulting in a transcript of 1,939 base pairs. GLO1 is located primarily in the cytosol but has been also described in the nucleus. Transcription of GLO1 is regulated by nuclear factor erythroid 2-related factor 2 (NRF2) [131]. NRF2 is a transcription factor that regulates the transcription of several genes involved in cellular redox and oxidative stress, such as those involved in glutathione metabolism (e.g. glutathione reductase [GSR]), thioredoxin metabolism (e.g. thioredoxin reductase [TXNRD1]), iron metabolism (e.g. heme oxidase [HO-1]) and NADPH production (e.g. NAD(P)H quinone oxidoreductase 1 [NQO1]) [132].

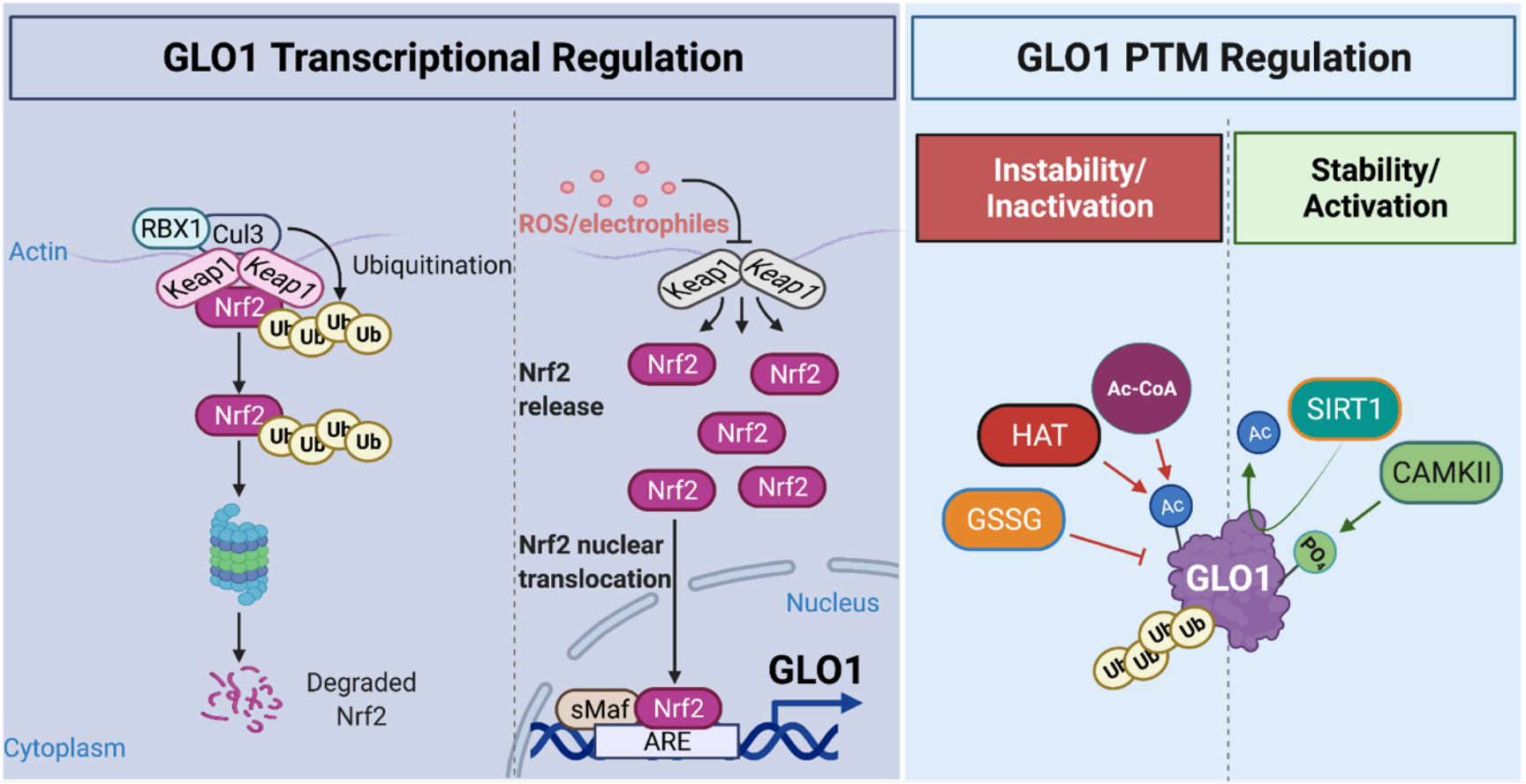

Figure 2.5 GLO1 Transcriptional and Post-Translational Regulation of GLO1. GLO1 is transcriptionally regulated by NRF2 which is negatively regulated by KEAP1 through ubiquitin ligation and degradation of NRF2 protein under conditions resulting in reduced presentation of key cysteine residues of NRF2. Oxidation of these cysteine residues stabilize NRF2 allowing for NRF2 transcriptional activity including GLO1 transcription. Several post translational modifications have been documented to affect GLO1 stability and activity both positively and negatively. (Ac – Acetyl group, Ac-CoA – Acetyl-CoA, HAT – histone acetyl transferase, GSSG – oxidized glutathione, PO_4 – phosphate group, Ub – Ubiquitin protein).

Perhaps unsurprisingly given its critical role in regulating stress response genes [133], NRF2 is critical for organismal health and longevity. In fact, NRF2 is overexpressed in the long-lived naked mole rat [134] and NRF2 activation has been shown extend lifespan in mice [135] and drosophila [136], and prevent diabetes in db/db mice [137]. The transcriptional activity of NRF2 is tightly regulated by the redox state of the cell through its interaction with Kelch-like-ECH-associated-protein 1 (KEAP1) which is an adaptor for the ubiquitin ligase cullin-3 (Cull3). Under cellular conditions which favor the reduction of protein thiols, homodimers of KEAP1 interact with NRF2 through key cysteine residues sequestering NRF2 in the cytosol and allowing it to be ubiquitinated by Cull3, thus promoting NRF2's degradation. In response to an electrophile or oxidant, these key cysteine residues are oxidized thus liberating NRF2 and allowing it to translocate to the nucleus [138]. Once in the nucleus, NRF2 regulates the transcription of its target genes, including GLO1 by binding to antioxidant response element (AREs) enhancer regions on the target genes [131]. Once the *GLO1* gene is transcribed the full-length transcript is translated into a functional protein 184 amino acids in length. Active GLO1 exists as a homodimer with a molecular weight of 42 kDa [139]. This GLO1 homodimer catalyzes the first step of MG detoxification by converting the MG-hemithioacetal to S-D-Lactoylglutathione. S-D-Lactoylglutathione is then acted on by GLO2 which completes the reaction, generating D-Lactate and replenishing the GSH. D-Lactate (the radio isomer of L-Lactate produced in glycolysis) is therefore often used as a marker of glyoxalase flux. In fact, individuals with obesity in addition to having higher levels of circulating MG also have been reported to have >2-fold higher levels of circulating D-Lactate [33].

Given its predominant role in detoxifying MG, it should be no surprise that GLO1 is highly evolutionarily conserved across bacteria [140], and eukarya including plants [141], and animals ranging from C. elegans [142] to humans [9].

2.5.2 GLO1 Loss of Function Drives Obesity-Related Metabolic Dysfunction

The generation of loss of function models *in vitro* (via genetic deletion, mutation, silencing etc.) is crucial for establishing the roles of a given molecule in regulating cellular physiology and investigating the mechanisms by which it carries out its function. However, few *in vitro* investigations, primarily focused on endothelial cells, have demonstrated the importance of GLO1 for the prevention of MG accumulation and subsequent MG-modified proteins, oxidative stress and dysfunction [47, 91, 100, 143]. For instance, Yao and Brownlee demonstrated that silencing of GLO1 in human aortic endothelial cells (HAECs) increased MG-modified proteins by 2-fold in cells kept in 5 mM glucose (low glucose) and 2.5-fold when they were kept in 30 mM glucose (high glucose) for 5 days [47]. They also demonstrated that GLO1 silencing increased inflammatory signaling. In another study, GLO1 knockdown in HAECs was again employed to more comprehensively examine “functional estimates of endothelial cells lacking GLO1” [143]. Herein, HAECs lacking GLO1 and incubated in 25 mM glucose had a ~30% increase in cellular MG and a similar increase in MG appearance in the media compared to GLO1-expressing cells in the same condition. Using the gold-standard LC-MS/MS method, kinetic rates for MG-H1 free adduct release into the media in these models were determined. HAECs kept at 5 mM glucose release c.a. 0.4 pmol/day/1x10^6 cells, which was increased approximately 3-fold when incubated at 25 mM glucose (c.a. 1.0 pmol/day/1x10^6 cells). Importantly, this rate was further exacerbated at nearly 10-fold above normal HAECs kept at 5 mM glucose in

cells incubated at 25 mM glucose lacking GLO1 (c.a. 3.2 pmol/day/1x10^6 cells). Similar to the investigation by Brownlee and Yao, HAECs lacking GLO1 also experienced exacerbated inflammation and in addition displayed elevated markers of apoptosis such as cleaved caspase-3 and poly ADP ribose polymerization (PARP1). HAECs lacking GLO1 also increased protein expression of the vasoconstrictor ET-1, and markers of vascular fibrosis suggesting loss of GLO1 may promote mechanisms of vascular dysfunction. In a follow up investigation, induction of dicarbonyl stress either by incubation of HAECs in 20 mM glucose or GLO1 KD also activated the UPR promoting inflammation, mitochondrial dysfunction, and metabolic dysfunction [91]. Another group recently employed CRISPR/Cas9 to delete GLO1 from HEK293T cells and co-incubated them with vehicle, 50 μM MG or 500 μM MG for 6 hours to promote dicarbonyl stress and assay potential histone MG modifications and corresponding transcriptomic changes [100]. As described in the previous sections, MG is an abundant histone modification and as such the authors found a dose response of MG-modified histones which promoted transcriptomic changes and toxicity with exacerbated dicarbonyl stress. Finally, to date only one peer reviewed manuscript has investigated the effect of GLO1 deletion in muscle cells [12]. Deletion of GLO1 in rat L6 myoblasts incubated in 25 mM glucose resulted in increased MG, MG-H1 proteins and promoted expression of collagen 1, 3, 4 and 5 compared to wild type myoblasts incubated in 25mM glucose. Although in their infancy, these *in vitro* loss of function data clearly establish GLO1 as a critical enzyme for the prevention of dicarbonyl stress and proper cellular function.

Because genetic deletion of GLO1 was previously reported to be embryonically lethal [144], generation of *in vivo* models proved difficult and slow to develop. Therefore,

earlier loss of function studies targeting GLO1 *in vivo* relied on partial GLO1 knock down (KD) via viral transfection of a GLO1 siRNA [145]. This viral KD of GLO1 ($GLO1^{KD}$) in mice resulted in a 50% reduction in GLO1 activity in the kidney which was sufficient to promote accumulation of MG-H1 adducts, and recapitulate hallmarks of diabetic kidney failure [145]. Another group later acquired these $GLO1^{KD}$ mice and crossed them with apolipoprotein E (APOE) null ($APOE^{-/-}$) mice to determine if attenuated GLO1 exacerbates atherosclerotic development [146]. Interestingly, GLO1 protein was only reduced in the kidney and not in the liver or heart which may explain why this model did not experience accelerated atherosclerotic development with HFD [146]. These data suggest that this loss of function model for GLO1 lacks utility for the elucidation of its role in disease progression and prevention.

In an attempt to create a superior loss of function animal model, the International Mouse Knockout Consortium created a GLO1 knockout ($GLO1^{KO}$) mouse using a gene trapping mutation [144]. Surprisingly, the genetic deletion of GLO1 was not embryonically lethal and the mice possessed a healthy phenotype. However, reappraisal by an independent group found that the knockout was unsuccessful due to *Glo1* gene duplication in the animals which allowed GLO1 protein expression to be conserved at normal levels [144]. Fortunately, a recent viable $GLO1^{KO}$ mouse has been developed using a similar gene cassette trapping strategy [147]. While only liver, kidney, and brain were assessed in this model, all three tissues lacked detectable GLO1 protein, and transcripts in the homozygous $Glo1^{-/-}$ mice. In addition, brain and liver were assayed for GLO1 activity in $Glo1^{-/-}$ mice which was undetectable. However, MG-H1 modified proteins increased by 2-fold in the liver but did not increase in the brain. The authors speculate

that this may be to the fact that AKR expression is c.a. 20-fold higher in brain compared to other tissues which may be able to compensate for the loss of GLO1 in that tissue.

In the only other *Glo1*$^{-/-}$ mouse model that has been published to date, this idea of other redundant MG detoxifying mechanisms being able to compensate for loss of GLO1 is corroborated [148]. In this model, two strains of *Glo1*$^{-/-}$ mice were generated using CRISPR-Cas9 gene editing which targeted exon 1 of the *Glo1* gene to delete 8 (Δ8) or 7 (Δ7) base pairs of exon 1. Both strains resulted in a read frame shift and the loss of *Glo1* transcript and protein, but majority of the studies were performed in the *Glo1*$^{\Delta 8/\Delta 8}$ which will be referred to as *Glo1*$^{-/-}$ from here on. Muscle, brain, heart, kidney, and liver from *Glo1*$^{\Delta 7/\Delta 7}$ mice were void of GLO1 activity although expression levels were not reported in this strain. Brain, heart, kidney, and liver from *Glo1*$^{-/-}$ mice all lacked GLO1 protein and activity but did not accumulate tissue MG or MG-H1 modified proteins compared to WT mice. MG measured in the circulation did increase about 40% suggesting that GLO1 expression in a tissue other than kidney and liver were likely responsible. The primary physiological outcomes reported by this manuscript were related to kidney function and found no effect of the *Glo1*$^{-/-}$ genotype. The authors go on to characterize the expression and kinetic profiles of AKR1b3 and ALDH1a3 in the liver and kidneys and demonstrate that in the WT mice AKR is likely responsible for about 40% and 60% of MG detoxification in the kidney and liver respectively and GLO1 is responsible for majority of the remainder. They go on to estimate that AKR accounts for approximately 90% and 75% of MG detoxification in the kidney and liver respectively in the *Glo1*$^{-/-}$ genotype mice due to enhanced expression and activity of this enzyme in this context. Thus, the authors conclude that the upregulation of the redundant detoxification mechanisms (AKR and

ALDH) in these tissues explain the lack of these mice developing diabetes-related renal dysfunction.

However, while the primary outcome of kidney function in this model was unremarkable, the supplementary data demonstrated that *Glo1*$^{-/-}$ mice did possess a 55% increase in glucose area under the curve (AUC) during a glucose tolerance test (GTT) and only a 3.6% reduction in plasma glucose AUC during an insulin tolerance test (ITT) compared to the WT mice. These data indicate the onset of glucose intolerance and insulin resistance respectively in GLO1$^{-/-}$ mice. The latter result was even 42% lower than their litter mates made diabetic via streptozotocin (STZ) injections. Importantly, these *Glo1*$^{-/-}$ mice were also approximately 40% larger than the WT mice but possessed a similar fasting plasma glucose compared to the WT mice. This phenotype is similar to that observed in the early pathogenesis of obesity in humans described in earlier sections of this review whereby subclinical insulin resistance manifests but is not evident by fasting plasma glucose level due to compensatory hyperinsulinemia. These data along with the comprehensive profiling of the liver's ability to adequately accommodate a loss of genetic *Glo1* deletion positions skeletal muscle as the prime suspect responsible for the dysregulation in glucose tolerance and insulin resistance that manifests with a loss of GLO1.

In addition to genetic deletion of *Glo1* in mice, other KO models in lower organisms have also been developed [99, 149]. These models have clearly implicated GLO1 as a driver of obesity and diabetes. For example, *Glo1*$^{-/-}$ drosophila generated by deletion of exons 1-3 of the *Glo1* gene develop an approximately 50% increase in MG and MG-H1 proteins as well as hyperglycemia and reduced phosphorylation of S6K with insulin

stimulation [99]. The authors also describe an increased adiposity of the animals as measured by an increase in triacylglycerides (TAGs, ~60%). The authors implicate an increase in fatty acid synthase (FASN) for this observation and go on to describe an ability of MG modification to enhance FASN activity *in vitro.* Using a click chemistry approach, they are also able to demonstrate that FASN isolated from drosophila void of GLO1 is more heavily modified by MG than that isolated from WT animals. In another preclinical model loss of function model, viable *Glo1*$^{-/-}$ zebrafish were successfully generated by using a similar CRISPR/Cas9 strategy as [148] but targeted exon 3 rather than exon 1 [149]. This approach resulted in undetectable GLO1 activity and protein expression in zebrafish lysates with a concomitant 50% increase in MG. Remarkably in line with the previous observations made in *Glo1*$^{-/-}$ mice, *Glo1*$^{-/-}$ zebrafish do not possess increased fasting blood glucose but do have an approximately 2-fold increase in one hour post prandial blood glucose compare the WT fish. Unlike the mouse and drosophila models, genetic deletion of *Glo1* in zebrafish does not result in weight gain. In addition, after overfeeding *Glo1*$^{-/-}$ zebrafish for 8 weeks they experience similar weight gain compared to WT zebrafish. However, whereas overfeeding produced similar steatosis and impairments in liver and skeletal muscle insulin signaling in both genotypes, only the *Glo1*$^{-/-}$ fish developed fasting hyperglycemia. Together, these preclinical data suggest that the lack of GLO1 promotes glucose intolerance which, when compounded with an obesogenic diet, promotes the development of diabetes. These data again implicate skeletal muscle as a potentially important tissue involved in this early pathogenesis.

2.5.3 GLO Attenuation in Models of Obesity and Diabetes

Unfortunately, the current preclinical and clinical models examining the effect of models of obesity and diabetes on GLO1 expression and subsequent metabolic consequences are extremely lacking. In particular, there is very little focus on tissues of metabolic significance such as skeletal muscle in this context. Instead, once again the *in vitro* models examining the effect of obesity or metabolic dysfunction have taken place primarily in endothelial cells with only recent work turning to examine more metabolically relevant cells such as hepatocytes. For example, HAECs treated with 20 mM glucose have reduced GLO1 protein abundance and enzymatic activity compared to those treated with 5 mM glucose [91]. In addition, the GLO1 protein was more ubiquitinated in the high glucose condition suggesting that scenarios resulting in exposure of endothelial cells to high glucose such as metabolic dysfunction may promote the ubiquitination of degradation of GLO1 protein. A separate study used exogenous MG treatment (400 μM, 72 hours) of HAECs to mimic the dicarbonyl stress experienced with obesity and metabolic dysfunction and found GLO1 activity was reduced [150]. Interestingly, another study treated liver (HEPG2) cells with high levels of fatty acid (400 μM palmitic acid or 500 μM oleic acid for 24 hours) to model obesity related non-alcoholic fatty liver disease (NAFLD) and demonstrated that both treatments resulted in ubiquitination and subsequent diminished GLO protein abundance (~30 and 50% of control respectively).

Similar to the literature *in vitro,* little work has been done to examine the effects of models of obesity or metabolic dysfunction on GLO1 in animals or humans. Seminal work by Paul Thornalley and colleagues demonstrated that the obesity and diabetic milieus could have an effect on the glyoxalase system [151]. In that study, Thornalley et al found

that GLO1 activity in red blood cells (RBCs) from OB/OB or STZ treated mice was severely reduced [151]. More recently, a similar study found that GLO1 protein was reduced by nearly 50% in bone marrow derived progenitor cells (BMDCs) isolated from db/db compared to WT mice [152]. This loss of GLO1 impaired BMDC proliferation, and tissue regeneration in wounded db/db mice. While these examples demonstrate the ability of GLO1 to be attenuated in the context of obesity and metabolic dysfunction, very few studies have examined the effect of obesity *per se* in more metabolically relevant tissues such as adipose, liver, and skeletal muscle. In addition, the data collected so far in this area is largely inconclusive. For example, one study found no change in GLO1 protein in epididymal adipose tissue in mice fed MG, HFD, or HFD+MG despite impaired adipose angiogenesis, increased adipose inflammation and IR [50]. Conversely, a similar study found that GLO1 activity was reduced in visceral adipose tissue (VAT) of HFD fed mice [4]. Similar conflicting observations have been made in liver as well where one study found no change in GLO1 protein in mice fed MG, HFD or HFD + MG despite the onset of obesity, steatosis and increased liver MG-H1 [49]. On the other hand, another study found GLO1 protein to be reduced in the livers and kidneys of HFD-fed mice [3]. Importantly, other work (although limited in scope) in humans with obesity have demonstrated attenuated GLO1 protein in liver biopsy samples from NAFLD patients [13], and reduced GLO1 activity in white blood cells from individuals with overweight or obesity [153]. Each of these observations also coincided with evidence of dicarbonyl stress in the respective tissues studied. Given these inconsistent results, the remarkable negative metabolic effects that dicarbonyl stress has on skeletal muscle [10, 11, 54, 154] and the dominant role of muscle on insulin mediated glucose disposal, it is surprising that to our

knowledge there are limited investigations on the effect of obesity on GLO1 abundance or activity in muscle in pre-clinical models (Table 2).

In fact, to our knowledge there have only been three studies that have partially addressed if GLO1 protein is altered in the skeletal muscle with obesity. One investigation by Hwang et al utilizing tandem mass spectrometry (MS/MS) to compare the proteomic profile of skeletal muscle biopsies from individuals who were lean, obese and T2D (n=8 per group) and found no difference in GLO1 protein expression [155]. Similarly, another proteomic profiling using MS/MS found no difference in skeletal muscle GLO1 protein abundance in T2D compared to age and BMI-matched individuals (n=6 each) [156]. However, in our own study, we probed muscle biopsies from patients with obesity and T2D (n=5) for GLO1 and compared that expression to the GLO1 expression measured in young, lean healthy individuals (n=10) using western blotting [35]. We observed an approximately 70% reduction in skeletal muscle GLO1 in the individuals with obesity and diabetes which was positively correlated to insulin sensitivity (M/I) and negatively correlated with BMI. Interestingly, the individuals with obesity and T2D also had lower muscle NRF2 and higher Keap1 protein abundance. Our data suggested that skeletal muscle GLO1 may be diminished with increasing degrees of insulin resistance and obesity however, that study design did not allow us to tease out the potential independent effect of obesity on GLO1 from other potential confounding variables. In addition, all of the aforementioned samples including our own are limited by the small sample sizes leaving a gap in the literature for more work to be done examining the effects of obesity on GLO1 abundance in skeletal muscle.

2.5.4 GLO1 Gain of Function Prevents Obesity-Related Metabolic Dysfunction

While limited, the GLO1 loss-of-function models to date clearly and convincingly demonstrate the importance of GLO1 for the prevention of MG-mediated inflammation, oxidative stress and metabolic derangement. Similarly, the limited data that has accumulated to date clearly depict dicarbonyl stress resulting from both an accelerated MG flux as well as a loss of GLO1 abundance and activity in several tissues is a common phenotype of obesity and may in fact contribute to the development of metabolic disease. On the other hand, GLO1 gain-of-function models clearly demonstrate an attenuation of these maladies and even promotion of lifespan extension in lower organisms. For example, C. elegans overexpressing GLO1 have increased mean and maximal life spans (c.a. 30% and 20% respectively) [142]. However, majority of GLO1 gain-of-function studies so far have focused primarily on microvascular consequences associated with the development of diabetic complications rather than the ability of GLO1 gain-of-function to prevent the development of metabolic dysfunction and T2D itself. For example, HAECs incubated in 30 mM glucose for 16 hours have elevated NF-κB transcription and promotor activity compared to those incubated in 5 mM glucose which is completely prevented by GLO1 overexpression [157]. In line with these *in* vitro findings, GLO1 transgenic rats are protected from endothelial dysfunction and subsequent renal dysfunction as a result of STZ induced diabetes which appeared to be driven at least in part to the accumulation of microvascular and glomerular MG-modified proteins [158]. These researchers went on to demonstrate that in the same model of diabetes, rats overexpressing GLO1 were better able to promote angiogenesis following hindlimb ligation [159]. In STZ treated mice, ligation of the femoral artery increased the abundance of CML and decreased gene

expression of GLO1 in the skeletal muscle of the affected compared to the unaffected [160]. Importantly these phenotypes were exacerbated in the STZ treated mice and attenuated in mice overexpressing GLO1 which also demonstrated enhanced arterial blood flow and increased skeletal muscle capillary density in both non-diabetic and diabetic mice [160]. Another group corroborated these findings showing STZ treated mice have improved tissue perfusion and blood flow following critical limb ischemia when overexpressing GLO1 [161]. While these overexpression models strongly implicate GLO1 as a viable therapeutic target for the prevention of diabetes related complications, there is still a need for more translatable methods of GLO1 augmentation and for determining if targeting GLO1 can be a viable target in the prevention of metabolic disturbances that precede and promote diabetes development.

GLO1 is tightly regulated by a myriad of mechanisms at both the transcriptional and post-transcriptional levels. GLO1 transcription is thought to be primarily induced by activation of the transcription factor NRF2 in response to acute oxidative stress as described earlier. Regardless, several investigations have demonstrated the efficacy of targeting NRF2 to promote GLO1 abundance and the subsequent prevention of MG accumulation in disease. For example, sulforaphane (SFN) (a natural electrophile that exists in green vegetables such as broccoli) has been explored as a potential GLO1 inducer given its purported ability to activate NRF2 by oxidizing key cysteine residues on KEAP1 thus liberating NRF2 from KEAP1 and disinhibiting its activity [131]. *In vitro* studies in liver (HepG2) [131], neuronal (SH-SY5Y) [162, 163], and rat cardiomyocytes [164] have demonstrated the ability of SFN to promote GLO1 expression and activity thus enhancing MG detoxification. However, a study examining the effect of SFN on PBMCs

isolated from young healthy individuals found that SFN treatment resulted in only a modest (~3%) yet significant increase in GLO1 gene expression without any effect on GLO1 activity [165]. Interestingly, SFN severely reduced the concentration of reduced GSH in isolated PBMCs. GLO1 activity is directly proportional to GSH concentration *in situ [5]* as the GSH is a necessary coenzyme for GLO1's MG detoxification activity. Because SFN is an electrophile, the scavenging of GSH may be an off-target effect of SFN treatment which may limit its utility as a GLO1 inducer.

To address the need to identify effective GLO1 inducers, a recent screen was conducted to examine other compounds targeting NRF2 activation [153]. This screen identified resveratrol (a polyphenolic compound found in the skin of dark grapes) and hesperetin (an electrophilic compound found in the skin of orange peels) to synergistically promote NRF2 and subsequently induce GLO1. In agreement with this effect of resveratrol, HUVECs cultured in high glucose media are protected from cell death and accumulation of the MG-derived AGE, arg-pyrimidine, when treated with resveratrol by promoting GLO1 activity [166]. Interestingly, these protective effects were abolished with concomitant inhibition of the NAD-dependent deacetylase Sirtuin1 (SIRT1). One potential explanation for this observation is SIRT1's ability to deacetylate NRF2 which promotes its cellular translocation to the nucleus [65, 167, 168].

Unfortunately, the efficacy of targeting NRF2 to promote GLO1 *in vivo* are extremely limited. One study in rats found that attenuated GLO1 protein as a result of STZ-induced diabetes was reversed by adding 1% glycine to the rats' drinking water for 12 weeks [150]. Similar to SFN and trans-resveratrol and hesperetin (T-Res/Hesp), glycine improved kidney Nrf2 expression, nuclear translocation and in turn GLO1 mRNA,

protein and activity. In a small double-blind, placebo-controlled clinical trial, administration T-Res/Hesp for eight weeks in adults with overweight or obesity resulted in modest increases in GLO1 mRNA (~6%) and GLO1 activity (~5%) in PBMCs compared to placebo in which GLO1 activity was reduced by approximately 11% [153]. However, these modest changes to GLO1 were accompanied with decreased circulating MG (-20%) in the treatment group whereas the placebo group increased their plasma MG levels (37%). Importantly, the treatment group also saw reductions in fasted insulin (-16%) and insulin at the 90-minute time point of an OGTT (-21%) along with increased insulin sensitivity derived from the OGTT [153]. While these data are extremely limited, they suggest that targeting NRF2 to promote GLO1 transcription may be an effective strategy for alleviating dicarbonyl stress with obesity to promote metabolic health. However, as previously mentioned GLO1 regulation is layered with complexity involving mechanisms at the post-transcriptional and post-translational levels.

2.5.5 Post-Transcriptional Regulation of GLO1 Stability and Activity

New evidence has found that GLO1 can be post-transcriptionally processed into non-functional circular RNAs [169]. Furthermore, this investigation found the abundance of GLO1 circular RNAs to increase by over 2-fold muscle from older compared to younger individuals suggesting an aging effect. To date, a number of post-translational modifications (PTMs) of GLO1 have also been described to regulate GLO1's enzymatic activity as well as its stability including glutathionylation [170], MG modification [171], modification by nitric oxide (NO) [172, 173], phosphorylation [172-174], acetylation [13, 175], and ubiquitination [13, 91].

Transcriptional regulation of GLO1 via NRF2 is not the only way in which GLO1 is related to the redox status of the cell. The redox status of the cell is a balance between the reduction and oxidation of several molecular entities including methionine and cysteine residues on proteins, oxidation of lipids, the ratio of NAD(P):NAD(P)H, the ratio of FAD:$FADH_2$, and GSH:GSSG. GSH:GSSG is particularly relevant to GLO1 for a number of reasons. For one, majority of cellular MG is bound to GSH, which forms the MG-hemithioacetal substrate for GLO1. It is for this reason that GLO1 activity *in situ* is directly proportional to the abundance of GSH [5]. However, reduction of GLO1 also has independent effects on its activity, exemplified by studies that have shown GLO1 specific activity to be augmented by incubating GLO1 with increasing concentrations of the reducing agent β-mercaptoethanol [170]. Conversely, incubation of GLO1 with increasing GSSG resulted in GLO1 inhibition which Birkenmeier et al. determined was due to glutathionlyation of GLO1 at Cysteine 139 (Cys^{139}) [170]. The authors went on to provide evidence that glutathionylation at Cys^{139} perturbs GLO1 activity by closing the substrate binding domain. Although it is unclear how exactly this glutathionylation occurs previous evidence has demonstrated that formation of reactive sulfhydryl intermediates of protein thiols and GSH such as *S*-nitrosylation are likely to precede protein glutathionylation. Interestingly, nitrosylation of GLO1 has been previously described on cysteines 18, 19 and 138 which [172]. Nitrosylation of GLO1 on these residues may not only promote subsequent glutathionylation and enzyme inhibition but it was also shown to promote the increase in TNFα-mediated activation of NF-κB transcription [172]. GLO1 has repeatedly been shown to have an inverse relationship with NF-κB [47, 157, 160]. In fact, treatment of a HFD mouse model of obesity with the B6 derivative pyridoxamine increased GLO1

activity, reduced adipose MG levels and lowered adipose inflammation, including TNFα mRNA [4]. These data suggest that the inverse relationship of GLO1 with inflammatory signaling may be related to redox balance and in turn its MG-detoxification activity. Other potential mechanisms to promote protein glutathionylation such as glutathione-*S*-transferase and GRx1 [176] have not been explored in the context of GLO1 regulation or in models of metabolic dysfunction such as obesity or diabetes. However, glutathionylation has been described to occur in and attenuate almost every glycolytic enzyme including glyceraldehyde-3-phosphate dehydrogenase (GAPDH), aldolase, phosphoglycerate kinase (PGK), pyruvate kinase (PK), triose phosphate isomerase (TPI), and lactate dehydrogenase (LDH) [177-180]. Importantly, perturbation of GAPDH activity may increase the accumulation of the triosephosphates glycerol-3-phosphate (G3P) and dihydroxyacetone (DHAP) phosphate which are major sources of MG.

This scenario of oxidative stress mediated GLO1 and GAPDH inhibition may promote a feed forward loop of exacerbated MG accumulation given GLO1 has been shown to be modified by MG itself, resulting in GLO1 protein degradation [171]. This may explain why treating cells or whole organisms under pathologic dicarbonyl stress with compounds that scavenge MG tend to increase GLO1 protein. For example, genistein which is a dietary flavonoid found in soybeans, was shown to sequester MG and increase GLO1 protein in mice fed a high fat diet [3]. One example of a drug with this MG-scavenging effect is metformin. Metformin has been demonstrated to have the ability to sequester MG which interestingly also tends to promote upregulation of GLO1 activity which has been shown in animals [181-183] and humans [184, 185]. Also interesting is the recently reported independent ability of the MG-metformin adduct to promote

microvascular function [182]. It is tempting to hypothesize if a similar mechanism could at least partially explain the effects of another diabetes drug Liraglutide. A recent study found that treatment of genetically diabetic rats (Goto-Kakizaki) with sleeve gastrectomy or the GLP1 receptor agonist Liraglutide had improvements in insulin sensitivity, circulating AGEs, as well as GLO1 protein and activity compared to sham surgery or placebo [186].

Conversely to MG-modification of GLO1 which promotes its degradation, a recent study found phosphorylation of GLO1 on Threonine 107 (Thr^{107}) by CaMKIIδ to directly enhances GLO1 MG detoxifying activity and promote GLO1 stability *in vitro* [174]. They went on to show that CaMKIIδ KO mice had reduced GLO1 protein and activity in the liver, kidney, heart, and brain with a concomitant decrease in GLO1 phosphorylation and increase in the MG-modified DNA adduct MG-dG in nuclear extracts of the liver. Lastly, they also demonstrated that two models of diabetic mouse (STZ and db/db) also exhibited attenuated CaMKII protein, GLO1 phosphorylation, and GLO1 activity in liver although GLO1 protein was not affected in these models. CaMKII is an interesting target which through its dependence on calcium flux is closely linked to hormonal influences such as epinephrine, and insulin and in turn to the metabolic state of the cell and organism. Importantly, calcium flux and subsequent activation of CaMKII are thought to be largely responsible for skeletal muscle's contraction-mediated, insulin independent glucose uptake during exercise [187-189].

Another potential mechanism for the regulation of GLO1 stability and activity which is closely tied to both redox regulation and metabolism is GLO1 acetylation. Recently, acetylation has been demonstrated to result in its subsequent ubiquitination and

degradation [13]. Importantly, hyperacetylation, ubiquitination and subsequent degradation of GLO1 was able to be provoked by treatment of HepG2 cells with high levels of palmitate and oleate to mimic obesogenic conditions experienced by the liver [13]. This group went on to show that GLO1 protein was severely reduced in human liver biopsy samples from adolescents with NAFLD which resulted in exacerbated MG-H1 levels in the liver. However, this manuscript failed to elucidate the mechanism whereby this obesity model in HepG2 cells and obesity *per se, in vivo* may be able to promote GLO1 hyperacetylation and its subsequent ubiquitination and degradation.

Mouse models of obesity have previously observed that GLO1 and the NAD-dependent deacetylase SIRT1 are downregulated in parallel [54]. In addition, as previously mentioned several studies *in vitro* [91, 166] and one small study in humans [153] have demonstrated the ability of resveratrol, a putative SIRT1 activator, to promote GLO1 expression and activity. Santini et al. demonstrated that the GLO1 enhancing effects of resveratrol were abolished by co-treating cells with the SIRT1 inhibitor EX527 [166]. In another recent study, treatment of endothelial cells with pterostilbene, a naturally occurring derivative of resveratrol, increased GLO1 protein expression, NRF nuclear translocation, GSH levels and reduced MG levels when cells were directly incubated with MG [190]. However, none of these studies have examined the possibility of GLO1 acetylation to be altered by these pathogenic models or if these treatments are mediating their effects through GLO1 deacetylation. Lastly, but most importantly only one of these studies have employed a translational approach to determine if this is an effective strategy in humans. There is clearly lots of work left to be done to determine if augmenting GLO1 expression in the context of obesity is an effective strategy for the prevention and

treatment of associated metabolic dysfunction. This is especially true for translational studies in humans and investigations involving tissues that are highly relevant to the pathogenesis of insulin resistance and T2D with obesity such as skeletal muscle. In addition, it is unclear if targeting one or several of the aforementioned GLO1 regulatory mechanisms will be effective and if so, which tissues are of primary relevance for the observed effects and how best to promote the mechanisms governing these effects. The prospect of GLO1 acetylation being a key regulatory PTM is particularly interesting due to the relationship of protein acetylation to both the energy and redox status. It follows that energy and redox status, as well as the protein acetylome are all dramatically perturbed in the context of obesity and may drive the metabolic consequences of obesity. Conversely, exercise training is well known to have a myriad of beneficial effects on obesity, metabolism and health which are driven by altering the redox status, gene transcription, protein acetylation, and protein phosphorylation. Given the breadth of mechanisms involved in adaptation to exercise, many studies are continuing to examine which are most important, the extent of their effects and how they may be targeted for treatment of obesity and metabolic disease.

2.5.6 Exercise as a Potential Regulating Stimulus of GLO1

Exercise is well known to reduce the risk of cardiovascular disease and all-cause mortality [191]. These beneficial effects of exercise training stem from adaptations which occur in essentially every tissue in the body. However, the skeletal muscle is the source of locomotor force, the largest consumer of energy [192], and has the largest increase in perfusion during exercise [193, 194]. As such, muscle is perhaps the most important and most affected tissue by acute exercise demands and the cite of many adaptations to

training. Adaptations of skeletal muscle in response to acute exercise and exercise training include, improved insulin sensitivity [195-205] (for review see [206]), improved body composition [207-209] (for review see [210]), improved mitochondrial biogenesis [211-213] (for review see [214]), improved antioxidant [215-219] (for review see[220]) and anti-inflammatory defenses [221, 222] (for reviews see ([222] and [223]). These beneficial effects have been repeatedly demonstrated to successfully prevent and treat obesity as well as the metabolic and cardiovascular dysfunctions that result from obesity [224].

Given the complex interactions of mechanisms that underly the benefits that exercise confer to the organism, much work is continuing to be done to expand our understanding of such mechanisms and how they contribute to the emergent benefits of exercise. This is to suggest that exercise may be a useful tool in the examination of how GLO1 may be regulated in the muscle, and it follows to also wonder if exercise-mediated augmentation of GLO1 activity or protein may play some role in the metabolic benefits demonstrated that are repeatedly demonstrated with exercise. Given the importance of GLO1 in the prevention of dicarbonyl stress, it is certainly reasonable to ask the questions, “Does exercise augment GLO1 and if so, what is the mechanism by which this may occur?”. So far, the literature is extremely sparse in this area (Table 2).

Publication	Measurement	Model	Intervention	Sampling Timepoints/Conditions	Outcome
Kar and Pearson	GLO1 activity	Individuals with Muscle Dystrophy (n = 24) Healthy Control Individuals (n = 6)	N/A	Basal	GLO1 activity reduced in muscle dystrophy
Haralambi and Mossinger	GLO1 activity	Trained Cyclists (n = 7) Healthy Control Individuals (n = 7)	N/A	Basal	Trend for 21% higher GLO1 activity in cyclists
Radom Aizik et al.	Gene Microarray	Elderly, Sedentary Men (n = 6)	12-Weeks Aerobic Exercise Training	Pre and Post Training	GLO1 gene expression increased after exercise training
Hwang et al.	HPLC MS/MS	Healthy Control Individuals (n = 8) Individuals with Obesity (n = 8) Individuals with T2D (n = 8)	N/A	Basal	No difference in GLO1 protein between groups
Hussey et al.	HPLC MS/MS	Individuals with T2D (n = 6) Healthy Control Individuals (n = 6)	4-Weeks Aerobic Exercise or HIIT Training (T2D only)	Pre and Post Training	No difference in GLO1 protein between groups. Decrease in GLO1 protein aftere exercise training.
Hoffman et al.	TMT MS/MS	Healthy Control Individuals (n = 4)	Acute High Intensity Cycling Exercise	Pre and Post Acute Exercise	Non-sig. 21% increase in GLO1 protein
Mey et al.	GLO1 Protein Immunoblot	Healthy Control Individuals (n = 10) Individuals with T2D (n = 5)	Hyperinsulinemic-Euglycemic Clamp	Basal and 120 minutes of insulin stimulation	75% lower GLO1 protein in T2D No effect of insulin on GLO1 protein
Guo et al.	RNA Seq (Circular RNAs)	Young (3 month old) C57BL/6J mice (n = 6) Old (18 month old) C57BL/6J mice (n = 12)	8-Weeks Treadmill Training (Old Mice Only)	Pre and Post Training	3-fold increase in GLO1 cRNA in Old Mice No effect of Training on GLO1 cRNA
Egawa, T et. al.	GLO1 Protein Immunoblot	9 week-old C57BL/6NC	4 Weeks Sedentary (Sed), Running Wheel (EX), Sed + 1% MG in water, EX + 1% MG in water	Pre and Post Training	GLO1 protein increased by ~50% in plantaris No change in soleus muscle in EX No change in GLO1 in SED+MG or EX+MG

Table 2 Effect of Disease and Exercise on Skeletal Muscle GLO1.

Many studies now have demonstrated the ability of exercise to increase NRF2 expression and nuclear translocation (for review see [220]). Only four studies have directly examined the effect of exercise on skeletal muscle NRF2 in humans [225, 226]. Ballman et al., showed a trend toward increased NRF2 protein in the vasus lateralis muscle from young lean, physically active men 6 hours after a 90 minute cycling exercise bout [225]. In a similar study population, Gallego-Selles et al. found a nearly two-fold increase in total NRF2 protein and phosphorylated NRF2 in muscle at 10 seconds and 60 seconds following a graded cycling bout to exhaustion [226]. In another study of young men, NRF2 nuclear translocation was increased by 30% with no change in total NRF2 protein after an acute exercise bout at 70% VO_{2Max} for 30 mins [227]. Interestingly, Done et al. found that while both young (23 y) and older (mean age 63 y) increased total NRF2 following a similar acute exercise bout, only the young participants increased the nuclear translocation of NRF2 [228]. These latter data suggest that aging perturbs the acute exercise redox response. This finding provokes the question of whether other disease phenotypes such as obesity may also alter the exercise response. However, the effect of exercise on NRF2 in obesity has not yet been explored. In addition, none of these studies directly measured or reported changes in GLO1 with exercise.

To date, only three manuscripts have examined the effect of exercise on skeletal muscle GLO1 expression or activity in humans [229-231]. In a study of older men, gene microarray assays revealed that 12 weeks of aerobic exercise training increased GLO1 gene expression in muscle [229]. In another study, tandem mass tagging (TMT) mass spectrometry demonstrated that a single bout of high intensity cycling exercise elicited a non-significant 21% increase in GLO1 protein in muscle [230]. It is worth noting that the

sample size of this study was very low, only including four participants which likely contributed to lack of significant findings. Interestingly, a study examining the effect of 4 weeks of high intensity interval training and traditional aerobic exercise training in participants with T2D found GLO1 protein was decreased following the trainings [156]. This study was also limited by its sample size (n = 6) however, it is clear much more work is warranted to explore the effect of obesity and exercise on GLO1 regulation.

Both exercise and obesity have significant effects on metabolism, regulation of protein acetylation, and redox status which converge on a myriad of mechanisms including NRF2. In addition, these metabolic and redox changes provoke changes in gene transcription, and protein regulation via PTMs such as acetylation. However, in kind with the ambiguity of the effects of obesity on GLO1, the effects of exercise on GLO1 *per se* are also poorly studied and understood especially in the skeletal muscle. These gaps in the literature provide the rationale for the remainder of this review and dissertation to focus on the potential for perturbations in skeletal muscle redox and metabolism to augment GLO1 acetylation in the contexts of obesity and exercise. Further, we will explore the potential for acetylation to alter GLO1's stability and function and the consequences that may result.

2.6 Regulation of Skeletal Muscle Protein Acetylation in the Context of Obesity and Exercise

2.6.1 Role of Acetylation in Cellular Physiology

Protein acetylation is the most common covalent protein modification which occurs both co- and post-translationally [232]. Amino-terminal acetylation, which occurs on 85% of eukaryotic proteins, occurs co-translationally on most proteins apart from ribosomal

proteins which occurs post translationally [232]. The importance of amino-terminal acetylation is unclear and may not be necessary for most proteins but is required for protein stability of some proteins [233]. Conversely, acetylation of proteins on the ε-amino group of lysines occurs post-translationally and is known to have numerous effects on a variety of proteins functions including enzymatic activity, stability, DNA binding, protein-protein interaction, and protein-ligand interaction. Interestingly, lysine acetylation dramatically alters the form and function of lysine in many of the same ways in which arginine is altered when modified by MG. Specifically, acetylation of lysine removes the positive charge of the ε-amino group. It is also a relatively bulky structure and therefore introduces the potential for steric hinderance of protein-protein, protein-ligand or protein-substrate interactions.

Acetylation of ε-amino groups on lysine residues of proteins was first described to occur on histones by Vincent Allfrey and colleagues nearly 60 years ago [234]. It is now well appreciated that these acetylation events on histones are important epigenetic modifications that primarily alter gene transcription via promoting the formation of euchromatin through the steric hinderance provided to the lysine by the addition of the acetyl group. In turn, the more loosely packed region of DNA is now accessible to transcription factors to promote the transcription of genes in that DNA locus. Several specific lysine residues are now being studied and have been linked to cellular processes implicated in disease. For example, endothelial cells treated with high glucose produced a TXNIP-dependent increase in histone 3, lysine 9 (H3K9) acetylation which promoted the transcriptional activity of NF-κB and subsequent inflammation [235]. However, many

of these underlying epigenetic mechanisms are just beginning to be uncovered and understood in a translational way.

More than 20 years after Allfrey's discovery of histone acetylation, tubulin was described as the first non-histone protein to be acetylated [236]. It wouldn't be until over a decade later until the next two acetylation targets (p53 [237] and Tat [238]) would be discovered. Now, with the help of advancing mass spectrometry methods, thousands of lysine acetylation events on proteins have been identified through unbiased proteomics analyses [239, 240]. With these developments, efforts to determine the regulation and potential functional consequences have dramatically increased to rival similar investigations exploring phosphorylation [241].

Importantly for its relevance in the context of metabolic perturbations such as obesity and exercise, lysine acetylation of histones and non-histone proteins is closely linked with cellular metabolism in several fundamental ways (Figure 2.6). Firstly, the substrate for protein acetylation is the metabolic bi-product acetyl-CoA. acetyl-CoA is broken down into three pools: mitochondrial, cytosolic, and nuclear. In the mitochondria, acetyl-CoA is the main carbon donor and substrate for the Krebs cycle thus acting as a conduit of both carbohydrate and lipid metabolism to produce cellular ATP. Carbohydrates contribute to the mitochondrial acetyl-CoA pool via glycolytic flux to produce pyruvate which is converted into acetyl-CoA in the inter-mitochondrial membrane. Lipids contribute to this pool of acetyl-CoA through the process of beta-oxidation whereby long chain fatty acyl-CoAs progressively catabolized to generate several 2-carbon acetyl-CoA molecules.

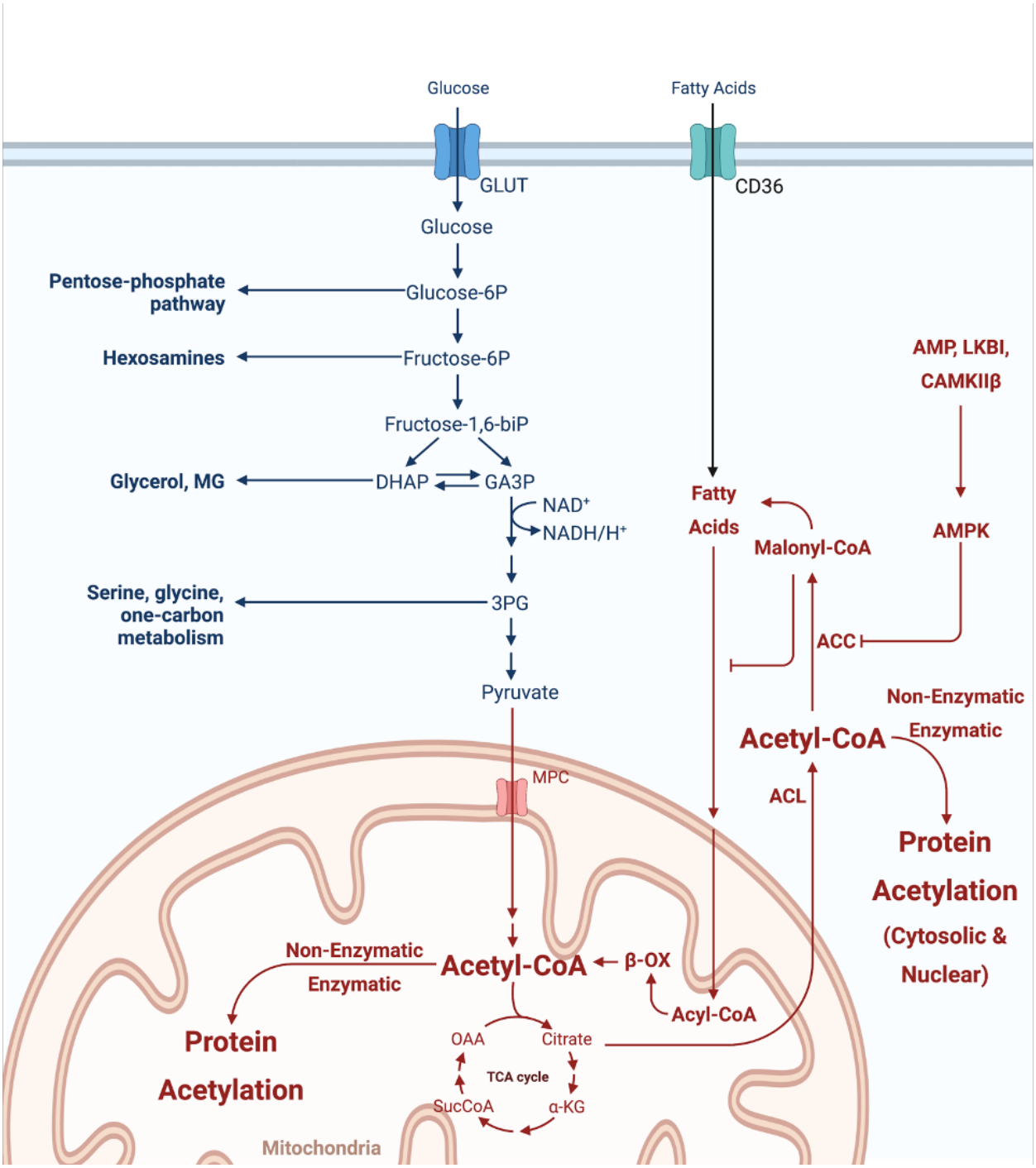

Figure 2.6 Integration of Metabolism and Protein Acetylation. Metabolism of both glucose and fatty acids contribute to acetyl-CoA pools in the mitochondria and cytosol. Accumulation of acetyl-CoA results in non-enzymatic and enzymatic protein acetylation in these cellular compartments.

Interestingly, although both lipid and carbohydrate substrates contribute to this paradigm, recent work has shown that glucose is the primary driver of acetyl-CoA abundance and histone acetylation in muscle stem cells [242]. Secondly, acetyl-CoA abundance and subsequent protein acetylation is also regulated by AMP-activated protein kinase (AMPK) [243]. AMPK is considered the master sensor and regulator of metabolism. Seminal work by D. Grahame Hardie and colleagues demonstrated that the activity of AMPK is enhanced by ~100-fold when phosphorylated by upstream kinases such as CaMKIIβ and LKB1 and another 10-fold by the allosteric binding of its two gamma subunits to AMP which also prevents its dephosphorylation [244]. Because AMPK activity is allosterically activated by AMP, its activity is highly dependent on the energy state of the cell. Importantly for protein acetylation, the primary target for AMPK is acetyl-CoA carboxylase (ACC). ACC is responsible for the conversion of cytosolic acetyl-CoA to malonyl-CoA which inhibits fatty acid oxidation as well as mitochondrial fatty acid uptake, thereby limiting both the cytosolic and mitochondrial acetyl-CoA pools [243]. Sensing and coordination of the energy state of the cell between the mitochondrial and cytosolic/nuclear pools is also achieved through the anaplerotic metabolite citrate being shuttled out of the mitochondria and into the cytosol where cytosolic ATP citrate lyse (ACL) converts citrate into acetyl-CoA and oxaloacetate. Cytosolic acetyl-CoA is used for several functions including fatty acid and synthesis when ACC is disinhibited as previously mentioned. However, cytosolic acetyl-CoA is used as the substrate for lysine acetylation of cytosolic proteins, and it can also be indirectly transported to the nucleus by citrate entering the nucleus and being converted to acetyl-CoA by ACL as well. This nuclear acetyl-CoA then serves as the substrate for histone acetylation. AMPK also has

other effects on protein acetylation by attenuating histone acetyl transferases (HATs, aka “writers”) while also promoting the activity of histone deacetylases (HDACs, aka “erasers”).

Collectively, these mechanisms tightly link the energy availability of the cell to acetyl-CoA abundance and protein acetylation. In general, high-energy states where energy substrates such as glucose, fatty acids and ATP are abundant (which is often the case in the context of obesity for example) results in increased acetyl-CoA and favors protein acetylation. On the other hand, low energy states or states of increased energy utilization characterized by relatively low levels of glucose, fatty acids, and high AMP (such as in the context of caloric restriction (CR) or exercise) are characterized by lower acetyl-CoA and generally favor lower protein acetylation.

As previously alluded to, acetylation of proteins has a wide range of effects including alterations to enzymatic function, protein-protein interaction, and protein stability. For example, acetylation of the glycolytic enzyme phosphoglycerate mutase (PGAM1) increases its activity under high glucose conditions [245]. Similarly, the activity of GAPDH is also enhanced by acetylation in response to increased glucose availability [246]. Conversely, acetylation of lysine 305 of pyruvate kinase (PK) (the last step in glycolysis), inhibits its activity and targets this protein for degradation via lysosomal degradation [247]. In another example of acetylation affecting protein stability, acetylation of the gluconeogenic enzyme phosphoenol pyruvate kinase (PEPCK) also targets it for ubiquitination by E3 ligases resulting in proteasomal degradation [247]. These observations of PEPCK are similar to those made of GLO1 by Spanos et al. who demonstrated increased acetylation, ubiquitination, and degradation of GLO1 following

an obesogenic environment [13]. Acetylation also regulates mitochondrial enzymes which can be influenced by metabolic flux. For instance, rats that were selectively bred for intrinsic running capacity (High Capacity Running rats; HCR rats) over several generations have a generally lower abundance of acetylated mitochondrial proteins. Lower abundance of acetylated proteins in the mitochondria were demonstrated to be related to improved reliance on oxidative metabolism and the ETS to produce ATP at rest and during exercise compared to low capacity running rats (LCR) [248]. Conversely, muscles from HFD mice were found to have a 2.5-fold increase in acetylated mitochondrial proteins compared to WT mice which corresponded to impaired mitochondrial respiration, insulin sensitivity and muscle glucose uptake [249]. The authors then went on to determine if exacerbation of the mitochondrial acetylome would further promote this phenotype. To do this they employed a muscle-specific, inducible KOs of carnitine acetyl transferase (CrAT), which uses Acetyl-CoA to import long fatty acyl chains into the mitochondrial, SIRT3 which is the primary enzyme responsible for mitochondrial protein deacetylation [250], or both. Paradoxically, exacerbation of the mitochondrial protein acetylome rescued the mitochondrial dysfunction characterized in the HFD mice and did not worsen insulin resistance in these animals. In interpreting these findings, the authors offer the possibility that the importance my lie in altering the turnover of specific lysine residues on specific proteins, which may not necessarily be realized or appreciated by dramatically altering the stoichiometry of all possible acetylation events.

Consider that acetylation of lysines only occurs at an occupancy rate of ~1% *in vivo*. This makes it difficult to measure low abundant proteins or proteins that may be minimally modified yet extremely important to the emergent phenotype of the cell, tissues,

and organism. When approaching this problem, researchers typically take the approach to alter the acetylome globally and massively in hopes to increase sensitivity and likelihood of finding an effect. However, given some lysine acetylation events occur non-enzymatically especially in the mitochondria for example, with high amounts of substrate and relatively low pH, a 40-fold increase in acetylation of mitochondrial proteins successfully side steps the abundance problem but creates a new problem by potentially causing acetylation of proteins that are inconsequential or would never be acetylated under physiologic circumstances creating an unpredictable phenotype. Therefore, there is a clear need for investigations to examine the regulation of enzyme acetylation in physiologic contexts such as exercise and obesity to determine the consequences of these events and the potential for these PTMs to serve as therapeutic targets.

2.6.2 Enzymatic Regulation of Protein Acetylation

The abundance of existing data clearly demonstrates the importance of protein acetylation in regulating metabolic enzymes in response to perturbations such as increased substrate abundance (e.g., obesity) and energetic demand (e.g., exercise). Given its critical role in titrating metabolic activity, protein acetylation is tightly regulated primarily by the counterbalance of lysine acetyl transferases (KATs) and HDACs. KATs utilize cellular Acetyl-CoA to move acetyl groups on to the epsilon amine of lysine residues. The product of this reaction is acetyl-lysine and a free CoA-SH (Coenzyme-A). KAT activity is largely driven by the abundance of Acetyl-CoA available and is inhibited by CoA-SH [251]. There are four families of KATs: GNAT, p300/CBP, MYST, and an unclassified family (Table 3). Similarly, there are four classes of HDACs: class I, IIa/b, and IV are Zn^{2+}-dependent deacetylases, whereas the class III Sirtuins are NAD^{+}-

dependent deacetylases (Table 3). While KATs and HDACs are in constant push and pull to regulate the protein acetylome, there is evidence to suggest that HDACs may have the

Enzyme	Family	Cellular Localization	Primary Activity	Co-Factor
HDAC 1	Class I HDAC	Nucleus	Deacetylase	Zn^{2+}
HDAC 2	Class I HDAC	Nucleus	Deacetylase	Zn^{2+}
HDAC 3	Class I HDAC	Nucleus	Deacetylase	Zn^{2+}
HDAC 8	Class I HDAC	Nucleus	Deacetylase	Zn^{2+}
HDAC 4	Class IIa HDAC	Nucleus	Deacetylase	Zn^{2+}
HDAC 5	Class IIa HDAC	Nucleus	Deacetylase	Zn^{2+}
HDAC 7	Class IIa HDAC	Nucleus	Deacetylase	Zn^{2+}
HDAC 9	Class IIa HDAC	Nucleus	Deacetylase	Zn^{2+}
HDAC 6	Class IIb HDAC	Cytosol	Deacetylase	Zn^{2+}
HDAC 10	Class IIb HDAC	Cytosol	Deacetylase	Zn^{2+}
SIRT1	Class III HDAC	Cytosol/Nucleus	Deacetylase	NAD^{+}
SIRT2	Class III HDAC	Cytosol	Deacetylase	NAD^{+}
SIRT3	Class III HDAC	Mitochondria	Deacetylase	NAD^{+}
SIRT4	Class III HDAC	Mitochondria	Deacetylase, ADP-ribosyl transfer	NAD^{+}
SIRT5	Class III HDAC	Mitochondria	Demalonylase, Desuccinylase, Deglutarylase	NAD^{+}
SIRT6	Class III HDAC	Nucleus	Deacetylase, Demyristoylase	NAD^{+}
SIRT7	Class III HDAC	Nucleus	Deacetylase	NAD^{+}
HDAC 11	Class IV HDAC	Nucleus	Deacetylase	Zn^{2+}
GCN5 (KAT2A)	GCN5	Nucleus	Acetyltransferase	Ac-CoA
PCAF (KAT2B)	GCN5	Nucleus	Acetyltransferase	Ac-CoA
CBP (KAT3A)	P300	Nucleus	Acetyltransferase	Ac-CoA
P300 (KAT3B)	P300	Nucleus	Acetyltransferase	Ac-CoA
TIP60 (KAT5)	MYST	Nucleus	Acetyltransferase	Ac-CoA
MOZ (KAT6A)	MYST	Nucleus	Acetyltransferase	Ac-CoA
MORF (KAT6B)	MYST	Nucleus	Acetyltransferase	Ac-CoA
HBO (KAT7)	MYST	Nucleus	Acetyltransferase	Ac-CoA
MOF (KAT8)	MYST	Nucleus	Acetyltransferase	Ac-CoA

Table 3 Description of Deacetylases and Acetyltransferases.

prevailing influence. This notion is supported by evidence demonstrating the ability of SIRT1 to target KATs in the MYST and p300/CBP families for de-acetylation and negatively regulate their activity [239].

SIRT1 is one of the seven class III HDACs called Sirtuins. Sirtuins (Sir-2-ins) are mammalian homologs of the silent information regulator 2 (*Sir2)* which is a member of the *Sir* family of genes first discovered in budding yeast [252]. The *Sir* genes (*Sir1*, *Sir2*, *Sir3*, and *Sir4*) were first described as a protein complex localized on the mating type locus of yeast DNA [253] and telomeres [254] and were described to silence the genes in the

mating type locus via histone deacetylation, and extend yeast lifespan [255, 256]. However, of the four *Sir* genes identified in yeast, only *Sir2* was found to be highly conserved across species including eukaryotes [257]. Importantly, Sir2 overexpression alone is sufficient to extended lifespan in yeast [258, 259]. Since these seminal discoveries, a large amount of effort has been placed on determining if similar benefits of Sir2 could be realized in mammals by targeting the mammalian Sir2 homologs, the Sirtuins.

Mammals express seven Sirtuins (SIRT 1-7) each with different cellular compartmentalization (Table 3). SIRT1, 6, and 7 are located in the nucleus where they primarily target histones and transcription factors for deacetylation. However, SIRT1 is also found in the cytosol as it can shuttle in-between the two compartments where it has been shown to deacetylate several cytosolic substrates. SIRT2 is also located in the cytosol although there is recent evidence for SIRT2 to exists in the inner mitochondria membrane as well where it regulates autophagy and mitophagy [260]. The canonical mitochondrial Sirtuins are SIRT3, 4, and 5 where SIRT3 is the primary regulator of lysine deacetylation in the mitochondria [250]. As previously mentioned, acetylation of mitochondrial proteins can regulate enzyme activity including those involved in oxidative phosphorylation [248, 249] and scavenging of ROS production [261]. This exclusive influence of SIRT3 on mitochondrial protein acetylation is likely in part due to the absence of strong deacetylase activity of the other mitochondrial Sirtuins, SIRT4 and SIRT5. In fact, although majority of the Sirtuins are characterized as deacetylases, a more accurate description is to refer to them as deacylases as deacetylation is not the primary activity of all deacetylases. For example, SIRT4 may act exclusively as a deacylase and in doing

so regulate leucine oxidation and beta cell insulin secretion [262]. Similarly, the enzymatic activity of SIRT5 is primarily deacylation of negatively charged lysine acyl modifications including succinyl, malonyl, and glutaryl moieties [263].

As previously mentioned, Sirtuins like their yeast homologs are NAD^+ dependent [258]. Deacetylation of a lysine residue by Sirtuins transfers the acetyl moiety from the lysine to the ribose of NAD^+ to generate 2'-O-acetyl-ADP-ribose while simultaneously displacing the nicotinamide (NAM) moiety from NAD^+. Thus, NAD^+ is effectively consumed in the process of lysine deacetylation. In fact, SIRT1 and SIRT2 are responsible for nearly one third of cellular NAD^+ consumption [264]. The reliance of Sirtuins on NAD^+ as a cofactor crucially links these deacetylases to the redox state (balance of reduced and oxidized molecules and metabolites) as well as the metabolic state of the cells to integrate important downstream, signaling events, enzyme regulation, transcriptional activity, and gene regulation.

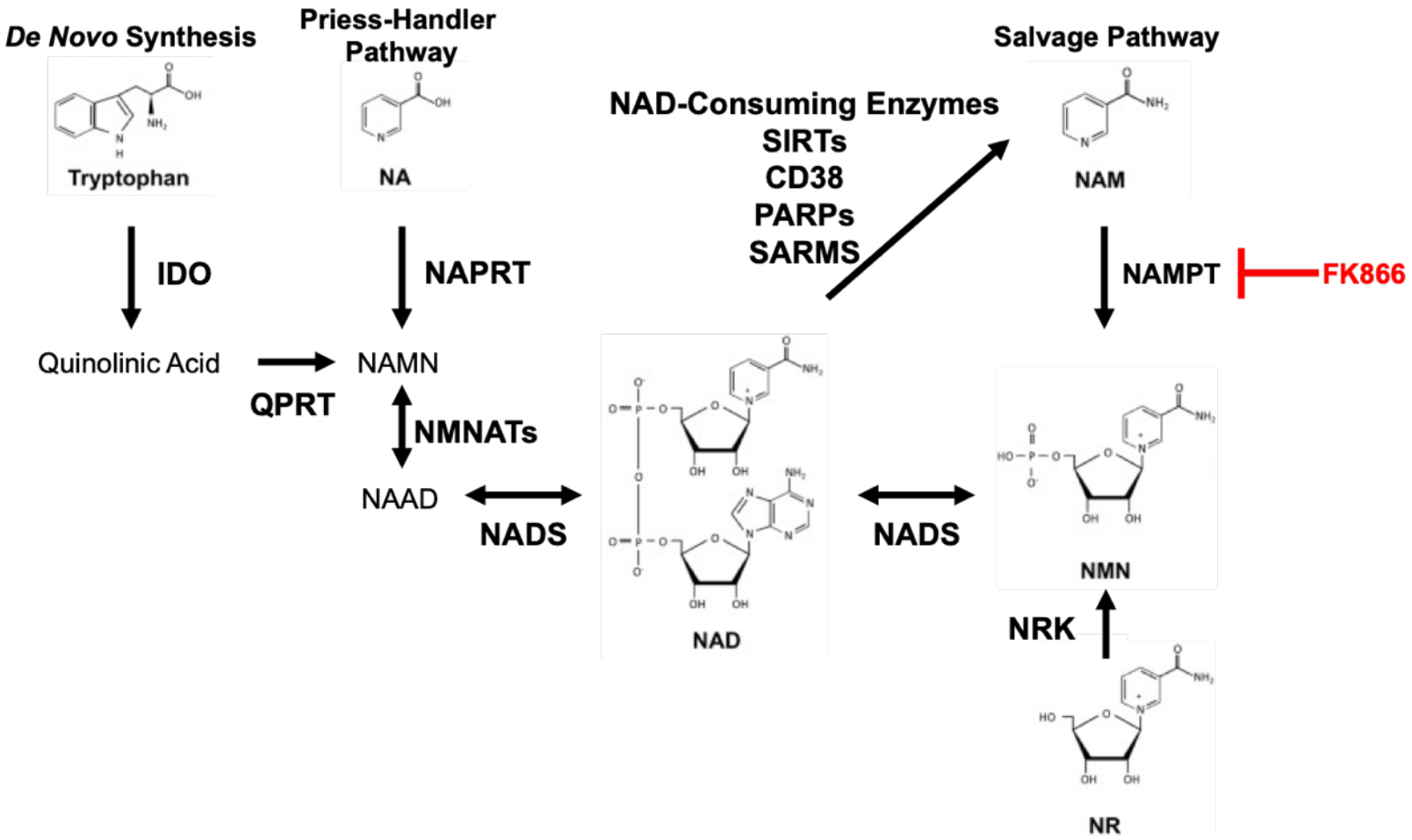

Figure 2.7 NAD Synthesis, and Salvage Pathways (Adapted from Okabe et al). NAD synthesis is achieved via the *de novo* synthesis from tryptophan or via the Priess-Handler pathway from nicotinic acid (NA). The primary pathway to maintain cellular NAD is via the salvage pathway where nicotinamide (NAM) produced from NAD consumption by various enzymes is reconverted back to NAD through a series of reactions. Blocking of NAMPT, a key enzyme in the salvage pathway, with a potent inhibitor such as FK866 is thereby able to deplete cellular NAD.

NAD is a nucleotide-based coenzyme that is ubiquitously present in all tissues and is required for life as it has several critical roles in facilitating metabolism, energy regeneration, and cell signaling. NAD is *de novo* synthesized from the essential amino acid tryptophan through the Kyneurine pathway Figure 2.7 (adapted from [265]). Niacin (vitamin B3) is an intermediate product of the Kyneurine pathway and is also now appreciated as an important dietary vitamin. Pellagra, is a condition that manifests from a lack of niacin which leads to lack of NAD^+ synthesis and is characterized by the "three D's": diarrhea, dementia, and death [266]. Widespread Pellagra in the early 20^{th} century, is the reason why almost all wheat flour is now supplemented with niacin and it also sparked many of the classic investigations into NAD's critical role in cell function.

The totality of cellular NAD exists as mixture of the reduced form (NADH) and the oxidized form (NAD^+) which like acetyl-CoA exists in two compartments: the nuclear/cytosolic compartment and the mitochondrial compartment. Recently however, this view has been complicated by the discovery of a mitochondrial transporter (SLC25A51) that functions to import NAD+ into the mitochondria [267]. In general however, cytosolic NAD(H) is a primary conduit for the transfer of electrons in the cell between other metabolites such as GSH as well as proteins containing sulfhydryl containing amino acids such as cystine and methionine. In the mitochondria, NADH is also the primary proton donor (along with $FADH_2$) for the generation of the proton gradient in the electron transport chain for the goal of generating a proton motor force for ATPase activity. In both compartments, NAD(H) is also used as a cofactor for dehydrogenase enzymes. For example, in the cytosol, GAPDH and LDH both require NAD^+ to act as a proton acceptor for their dehydrogenase activity. In the mitochondria, β-hydroxybutyrate

dehydrogenase (BHAD) also uses NAD^+ as a cofactor in the same manner. In fact, since LDH and BHAD are such large users of NAD^+ Hans Krebs and colleagues demonstrated that the lactate:pyruvate and the β-hydroxybutyrate:acetoacetate ratios reflect the free NAD:NADH ratio in the cytosol and mitochondria respectively [268]. This method for estimating the free concentrations of NAD^+ and NADH was developed due to the methodological difficulties of measuring the quantities of these labile metabolites directly. However, it also exemplifies the tight relationship between the redox state of NAD(H) and cell metabolism. The NAD:NADH ratio is also reflective of the energy state of the cell whereby a high energy state is characterized by a more reduced state (i.e. low NAD/NADH ratio). This is generated by the abundance of metabolic substrates producing increased NADH primarily through Krebs cycle to eventually be used for ATP generation via the ETC. Under chronic states of over-nutrition, this sustained high energy state is purported to generate an “over reduced” state which can eventually promote cell stress through inhibition of SIRT1 and other cytoprotective enzymes requiring NAD^+ as well as promoting increased proton leak in the mitochondria to generate ROS [269]. Conversely, seminal work by Imai et al. demonstrated that calorie/nutrient restriction increases mitochondrial respiration along with NAD^+ abundance and Sir2 activity leading to lifespan extension in yeast [255, 256].

In addition to Sirtuins, NAD^+ is also an important cofactor for other key cytoprotective enzymes. NAD^+ declines with age and as mentioned previously is also diminished by conditions such as obesity which create an over reduced state. Recent evidence supports that the primary cause of NAD^+ depletion in these conditions is through upregulation of NAD^+ consumption by several enzymes [270]. Poly ADP-ribose

polymerases (PARPs) for example are critical enzymes for DNA-damage repair. In response to DNA breaks, PARPs add ADP-ribose chains to the DNA at the site of the break to recruit DNA repair enzymes. Like Sirtuins, PARPs 1 and 2 account for approximately one third of NAD^+ consumption under basal conditions but this can be increased over 100% with DNA damage [264]. Recently muscle from individuals with obesity was found to have increased γH2AX indicating exacerbated DNA damage suggesting that increased PARP activity may promote exacerbated NAD^+ consumption in muscle [271].

CD38 is a cyclic ADP-Ribose hydrolase which is ubiquitously expressed on the cell surface. CD38 generates ADP-Ribose and cyclic ADP-ribose from NAD^+ to regulate cellular calcium signaling. In muscle cells where calcium is integral to excitation contraction coupling, CD38 has been demonstrated to play a role in regulating force of muscle contraction [272]. However, increased CD38 expression has also been implicated in NAD^+ depletion in the context of both aging [273] and Obesogenesis [274]. In addition, inhibiting or deletion of CD38 in these contexts can rescue NAD^+ and improve cell function and outcomes [274-276].

Given the presence of these vast number of NAD consuming enzymes that are of immense importance to the cell, biology has evolved a well conserved NAD recycling pathway which is the primary mechanism by which NAD levels are maintained in the cell. While tryptophan is essential for *de novo* NAD synthesis, recent tracer studies have shown that tryptophan is only used to large extent by the liver [264]. The liver appears to preferentially utilize tryptophan to synthesize NAD and subsequently release the NAD intermediates Nicotinic Acid (NA) and NAM into the circulation to be used as NAD

precursors by other tissues to synthesize NAD from the Priess Handler pathway or the NAD salvage pathway respectively (Figure 2.7).

The primary route for NAD resynthesis is the NAD salvage pathway using NAM produced from NAD consuming enzymes such as Sirtuins (Figure 2.7). NAMPT is the rate limiting enzyme of NAD salvage pathway. NAMPT was first known as a circulating cytokine and early on was referred to as pre-B-cell colony-enhancing factor (PBEF) or Visfatin because of the observation that it was primarily secreted by visceral adipose tissue [277]. It is now more commonly referred to as extracellular NAMPT (eNAMPT). The role of eNAMPT as a signaling molecule is complex and still under investigation. Investigations regarding eNAMPT have been mixed in regards to the effect of obesity and T2D on eNAMPT (reviewed in [278]). For example, one subsequent investigation by an independent research group showed increased eNAMPT in patients with T2D compared to lean healthy controls, but no difference when comparing to individuals with obesity and subclinical impaired glucose tolerance [279]. In a larger cross-sectional study (n=124) serum eNAMPT concentrations were no different in individuals with obesity compared to lean individuals [280]. In addition, others have also demonstrated that eNAMPT is increased in women with obesity following bariatric surgery [281]. Conversely, Haus et al. demonstrated that eNAMPT is reduced following a 12-week intervention lifestyle intervention which included diet and exercise in individuals with obesity [282]. In addition, reductions in eNAMPT correlated with the reduction in visceral adipose tissue and glucose and insulin AUC during a 75g, 2-hour OGTT [282]. In addition, relatively recent data also demonstrates a potential for eNAMPT to be taken up by the hypothalamus and alter the hypothalamic NAD^+ concentration [283]. In doing so, eNAMPT is purported to

act as a whole-body energy sensor that can influence physical activity behavior through augmenting NAD^+ levels in areas of the hypothalamus. These data clearly demonstrate an important and unique role of eNAMPT and certainly there is much more work to be done. However, for the purpose of providing relevant rationale for this dissertation work, the remainder of this review will focus on the role of intracellular NAMPT in the context of NAD^+ regeneration, specifically in skeletal muscle.

NAMPT expressed intracellularly regenerates NAD^+ by catalyzing the rate limiting reaction of converting NAM into NMN by transferring a phosphoribosyl moiety to NAM from 5-phosphoribosyl-1-pyrophosphate (PRPP). The phosphorylated state of NMN that results from this first step is important because it effectively "locks" NMN in the cell, much like the conversion of glucose to glucose-6-phosphate by action of hexokinase. NMN is then converted to NAD by Nicotinamide Mononucleotide Adenylyltransferase (NMNAT) which hydrolyzes an ATP molecule into AMP which is ligated to NMN to form NAD. In a relatively newly discovered parallel pathway, nicotinamide riboside (NR) is phosphorylated by NR kinase (NRK) to form NMN [284] (Figure 2.7). This route of NAD^+ production, unlike the canonical salvage pathway, does not require NAMPT, but the capacity of intrinsic NR is not sufficient to meet the demands for NAD^+ salvage. However, NR may be a viable target for supplementation to bolster NAD^+ levels in certain tissues. Interestingly, muscle in particular appears to prefer NR rather than NA, NMN, or NAM for NAD resynthesis as it does not take up and use NA or NAM as well as other tissues [264].

2.6.3 Targeting SIRT1 and NAD for the Treatment of Obesity

While much work is being done on all Sirtuins and their roles in cellular physiology and their potential efficacy for targeting for prevention and curing of disease, the most

highly studied and well described Sirtuin to date is SIRT1. This is likely due in part to SIRT1 being the mammalian ortholog to the yeast Sir2 which was demonstrated early on to extend lifespan in yeast [255, 256, 258, 259]. From this point on research regarding SIRT1 in the context of aging and age-related diseases exploded. In 2000, there were 6 manuscripts published studying SIRT1. One of which was the seminal work of Imai et al. demonstrating the lifespan extension of yeast with CR in a Sir2 and NAD^+-dependent manner [258]. Four years later, 25 manuscripts studying SIRT1 were published with one being the work by Cohen et al. which demonstrated that CR induced SIRT1 expression in rats resulting in amelioration of apoptosis in mammalian [285]. In 2021 over 1,500 manuscripts investigating SIRT1 were published, a pace that has been sustained for over 5 years now. These studies range from investigations of cellular mechanisms exploring how SIRT1 activity promotes its beneficial effects, to different ways in which SIRT1 could be targeted, to determining what age-related diseases and symptoms could be ameliorated by increased SIRT1 activity. The first confirmed SIRT1 targets included Histone H3 [286], the tumor suppressor P53 [287], the master regulator of mitochondrial biogenesis PGC1α [288], and the inflammatory transcription factor NF-κB [289]. The consensus of data investigating SIRT1's role in regulating these signaling pathways suggests that SIRT1's deacetylase activity on these and other targets promote an anti-inflammatory cellular milieu, and promote cellular metabolic function through driving mitochondrial biogenesis and increasing fat oxidation [290]. SIRT1 has also been purported to promote longevity in some preclinical models such as yeast [258, 259, 291] and drosophila [292, 293] although the data is mixed with some work finding no effect of SIRT1 overexpression on longevity of drosophila and C. [294]. In addition, global

overexpression of SIRT1 has not been shown to extend lifespan of higher organisms such as mice but does appear to promote healthy aging [295]. Interestingly overexpression of SIRT1 in the brain does however modestly extend mouse lifespan [296]. Given the purported roles for SIRT1 on metabolism and its potential responsiveness to CR and exercise, it is intuitive that SIRT1 has been extensively investigated as a potential target for the prevention and treatment of obesity and insulin resistance.

The potential SIRT1-targeting treatments under investigation for the treatment of obesity and metabolic dysfunction include pharmacologic interventions such as SIRT1 agonists (for review see [297]), administration of NAD^+ precursors (e.g. NR, NMN. For review see [298]), and lifestyle interventions such as CR and exercise (for review see [299]). Resveratrol is a naturally occurring polyphenol found in the skin of red grapes and other plants. Resveratrol was one of the first discovered sirtuin activating compounds (STACs) identified by a large screen [300]. Follow up studies from this screen found resveratrol to extend yeast lifespan through activation of SIRT1 [300].

One of the first studies examining resveratrol's potential relevance in the context of obesity found that HFD mice treated with resveratrol had improved VO_{2Max}, mitochondrial biogenesis in skeletal muscle, and glucose disposal during a hyperinsulinemic euglycemic clamp [301]. Deacetylation of PGC1α was exacerbated in gastrocnemius muscle from HFD mice treated with resveratrol compared to those only fed HFD alone. In C2C12 myotubes, the authors demonstrated that expression of SIRT1 was necessary for the deacetylation of PGC1α in response to resveratrol. These data suggest that augmenting SIRT1 activity may promote deacetylation of PGC1α and subsequent mitochondrial biogenesis to prevent the impaired insulin sensitivity of muscle

that manifests with obesity. In a very similar investigation, mice made obese by HFD were found to have poorer survival compared to chow fed mice or mice fed a HFD with concomitant treatment with resveratrol [302]. Baur et al. also demonstrated that the findings made by Lagouge et al. in the muscle were in line with observations in the liver. For example, similar to the muscle, Baur et al. demonstrated that livers from mice fed HFD and treated with resveratrol had superior mitochondria number and enhanced deacetylation of PGC1α [302]. In addition, they found similar effects on glucose handling whereby glucose and insulin AUCs were lower in the HFD mice co-treated with resveratrol compared to HFD mice alone during an OGTT.

However, data from an RCT conducted in humans demonstrated more subtle and heterogeneous effects of resveratrol. In one study, administration of 150mg/day of resveratrol for 30 days in middle aged adults with obesity did not improve glucose tolerance but did improve muscle mitochondria respiration [303]. In another study, individuals with T2D were given either placebo or increasing doses of resveratrol up to 3g per day for 12 weeks [304]. The resveratrol group saw increased muscle SIRT1 activity and increased energy expenditure, but no effects on HbA1c compared to placebo. As previously mentioned, a screen for GLO1 inducers recently identified resveratrol to activate GLO1 transcription [153]. In addition, oral administration of resveratrol and hesperitin to individuals with overweight or obesity increased GLO1 activity and improved glucose tolerance, although the potential mechanistic role for SIRT1 in this study was not examined [153]. In addition, several other studies in preclinical models have demonstrated the ability of resveratrol to resist dicarbonyl stress and AGE accumulation perhaps through activation of SIRT1 [65, 166, 305, 306].

Similar to the findings with resveratrol, diabetic, obese (DIO) zucker rats [307] and HFD fed mice treated with another STAC (SRT1720) saw similar improvements in glucose tolerance, mitochondrial biogenesis and exercise endurance [308]. However, it has come into question whether resveratrol and other STACs exert their actions primarily via SIRT1 *per se*. Several issues have been raised including the lack of translatability of the *in vitro* deacetylase activity assay substrate used to screen for these compounds, and the potential that activation of AMPK rather than SIRT1 is the main target of these compounds [309-311].

Regardless of the mechanism, these compounds do appear to exert beneficial effects on muscle and whole-body metabolism in the context of obesity. However, this could potentially explain the discrepancy between studies using STACs and other studies over-expressing SIRT1 in specific tissues such as muscle which have largely demonstrated no protective effect during obesogenesis [312-316]. Another possibility is the dramatic overexpression of SIRT1 in muscle results in limited NAD^+ because of increased consumption. As previously mentioned, SIRT1 and SIRT2 are responsible for approximately one third of basal NAD^+ use which may increase linearly with increased SIRT1 expression. If overconsumption of NAD^+ by SIRT1 were to explain this effect, it would suggest that SIRT1 is necessary but not sufficient for the beneficial metabolic effects seen with STAC treatment which would be consistent with the state of that literature. Unfortunately, NAD^+ was not assessed in these studies and so this interpretation remains speculative and untested.

2.6.4 Strategies for Augmenting NAD

As discussed earlier, increased NAD^+ consumption occurs in aging for several reasons including increased expression of other NAD^+ consuming enzymes such as PARP1/2 and CD38 [270, 275, 276]. The obesogenic environment has the potential to limit NAD^+ bioavailability through this mechanism as obese muscle has been demonstrated to possess increased DNA damage that would likely require increased PARP1/2 activity. Obesity is also characterized as a state of chronic low-grade inflammation (ref). This inflammatory milieu may recruit macrophages expressing CD38 to the muscle or upregulate CD38 intrinsically [317] to promote NAD^+ degradation. Indeed, some investigations have demonstrated reduced skeletal muscle NAD^+ in mouse models of obesity [318, 319]. However, the data are mixed, lack human evidence, and are limited in the context of obesity in general as majority of effort has been placed on this system in the context of aging thus far. As a result, the mechanism of how this may occur in obesity is not clear.

Another potential mechanism in addition to increased NAD^+ consumption in muscle is reduced expression of NAMPT. Muscle NAMPT protein expression has been found to be reduced approximately 2-fold in sedentary individuals with obesity compared to lean endurance athletes [320]. However, no difference in muscle NAMPT protein was observed when comparing the individuals with obesity to lean, sedentary individuals suggesting that exercise may be a more potent modulator of NAMPT expression. Indeed, these authors found that NAMPT protein expression was rescued in individuals with obesity following a 3-week aerobic exercise training protocol [320]. Similar increases in skeletal muscle NAMPT expression were also found in studies utilizing resistance

exercise training in populations of middle-aged, overweight adults [321, 322]. Reduced NAMPT expression limits NAD^+ from being salvaged once consumed resulting in a number of metabolic and functional consequences [323]. Interestingly, one of the primary consequences of inhibiting NAMPT and depleting NAD^+ in skeletal muscle cells (C2C12 and human myotubes) is inhibition of GAPDH and accumulation of triosephosphates (DHAP and G3P) [323]. DHAP and G3P are liable to spontaneously degrade into MG, suggesting that limited NAD^+ bioavailability is likely to exacerbate dicarbonyl stress in muscle via increased MG formation. Studies in mice corroborate and expand on the *in vitro* NAMPT inhibitor findings showing that muscle specific NAMPT deletion (mNKO) results in NAD^+ depletion, DHAP accumulation, and impaired mitochondrial respiration [324]. Importantly, this and other work has demonstrated that these metabolic effects have important functional consequences including muscle atrophy, reduced muscle strength, impaired exercise capacity, and premature death [324, 325].

To address these issues, NAD precursors such as NR, NAM, NMN and niacin (vitamin B3) have begun to be studied extensively for their potential therapeutic effect on obesity and metabolic dysfunction. As previously discussed, NR may be attractive therapy for specifically targeting the muscle under states of metabolic stress since muscle appears to take up and use NR more readily compared to other NAD precursors [264]. Another benefit of NR is its ability for NAMPT-independent NAD resynthesis [326, 327]. This latter point is important considering NAMPT expression and activity may be attenuated with obesity [320, 328]. Inhibition of NAMPT activity via FK866 in cultured myotubes has several metabolic consequences including depletion of NAD, inhibition of GAPDH leading to accumulation of G3P and DHAP as well as impaired mitochondrial

respiration [323, 326, 327]. These effects of FK866 are rescued with co-treatment of NR through restoration of NAD concentration [323, 326, 327].

The consequences of NAMPT loss of function in muscle have been further exemplified in two independent studies which developed mNKO mice [324, 325]. Both models found dramatic myopathies in these mouse models with one study demonstrating reduced survival of mice lacking skeletal muscle NAMPT [325]. Both models also described the ability of oral NR supplementation to partially rescue the reduction in NAD as well as improve exercise capacity, muscle mass, strength and mitochondria function.

Given severe consequences of NAD depletion in muscle, and the potential for this to manifest in obese muscle via numerous mechanisms, the effects of NR on skeletal muscle metabolism is currently under intense investigation for its potential to treat metabolic derangements as a result of obesity. Early studies in HFD fed mice demonstrated the ability of oral NR supplementation to improve glucose tolerance, exercise capacity and muscle mitochondrial biogenesis [319, 329]. In addition, Trammell et al. demonstrated an ability of NR to protect diabetic mice from motor and sensory neuron dysfunction [319]. However, one recent study did not find any effect of addition of NR to drinking water HFD-fed mice on glucose tolerance or muscle mitochondria [330]. One potential caveat to this study is the HFD fed mice significantly reduced their intake of water leaving open the possibility that they did not receive an optimal dose of NR. Unfortunately, blood and tissue NR and NAD metabolites were not measured to confirm or rule out this possibility. Another similar study fed NR to HFD with or without muscle specific CrAT KO [331]. NR had no effect on muscle NAD regardless of CrAT expression although NR supplementation did lower insulin AUC during an OGTT and increased area

above the curve during ITT indicating improved insulin sensitivity [331]. Another recent study administered NR intraveneously to mice fed a western died and found that NR was able to augment muscle NAD but found no effect on mitochondrial respiration or insulin sensitivity [332].

Several studies have now demonstrated the safety of orally administering NR in humans [333-335]. In addition, several studies have shown NR is effective at improving circulating NAD levels in both healthy individuals and individuals with overweight or obesity [333-336]. However, none of these studies in humans have observed increased NAD in skeletal muscle when assessed [335, 337, 338]. Instead, the consensus effect on the NAD metabolome in muscle following NR administration is a dramatic elevation in MeNAM, a break down product of NAD indicating accelerated NAD clearance from the muscle. In addition, NR administration across these various investigations has failed to improve glucose tolerance and insulin resistance as assess by HbA1c [334], HOMA-IR [335], or glucose disposal rate (GDR) determined via hyperinsulinemic-euglycemic clamp [336]. However, in older, overweight individuals 21 days of 1g NR supplementation per day did improve circulating inflammatory markers in the absence of remarkable changes in skeletal muscle [335].

Although much less work has been done utilizing other NAD precursors such as NMN, early investigations in rodent models provided promising effects on HFD fed mice such as augmented NAD concentration in liver, adipose and skeletal muscle along with improvements in glucose tolerance [328]. So far only one clinical investigation has been conducted using NMN [339]. This placebo controlled RCT like those performed showed no effect of NMN on muscle NAD but instead large elevations of MeNAM. However, unlike

the NR clinical trials, administration of 250 mg/day of NMN in women with obesity significantly improved their GDR and improved insulin stimulated insulin signaling including p-AKT and p-mTOR in muscle during the clamp [339]. There is contention surrounding these findings due to questions of whether exogenous NMN can be taken up by cells given its phosphorylated status. In addition, concern has been raised regarding the placebo and treatment group not being matched for intrahepatic lipid content at baseline [340]. Regardless, more work is warranted to further investigate the potential for NMN as a viable treatment for obesity-related insulin resistance.

NAM is another NAD precursor that has been understudied due to its complicated biology. Given the relationship between NAD and SIRT1 activity, it has been assumed that the primary mechanism for increased NAD to promote beneficial metabolic effects is in large part due to SIRT1 activation. While NAM is a precursor of NAD, it is also a potent inhibitor of sirtuins. This complexity has limited the work done to determine if NAM is a viable treatment for metabolic disorders that manifest in reduced NAD. Given the lack of data, and complexity of NAM's biology it is unsurprising that the data are mixed with some investigations demonstrating beneficial metabolic effects of oral NAM supplementation in HFD fed rats and mice such as improved glucose tolerance, increased liver NAD, and reduced liver lipid [341, 342]. Conversely, another study found mice given IP injections of NAM for 8 weeks to have impaired glucose tolerance and increase muscle TAGs while simultaneously increasing NAD/NADH ratio [343].

Clearly there are still several issues to address regarding the potential of using NAD precursors to augment metabolism. One of the biggest questions is if it is possible to deliver these NAD precursors to metabolically relevant tissues such as liver, adipose

and muscle without these tissues rapidly discarding them as MeNAM. Another novel strategy may be to enhance NAD^+ by targeting NAMPT instead. Earlier this year a novel compound was synthesized and described to be orally bioavailable and activated NAMPT [344]. Chronic treatment of DIO mice with this compound significantly increases muscle and liver NAD^+ concentrations. These mice also experienced significant weight loss (~8% over 20 days) compared to the vehicle control, although other metabolic effects are not yet known. However, the most effective tools we currently have to augment metabolism and prevent metabolic disease are CR and exercise. Both of which appear to exert their positive health effects at least in part through altering NAD metabolism and related signaling.

2.6.5 Effect of Caloric Restriction and Exercise on SIRT1 in Muscle

CR is a first-line prevention and treatment strategy for obesity and related metabolic complications. CR that results in just 5% of body weight-loss in individuals with obesity has been repeatedly demonstrated to improve glucose tolerance, circulating lipids, blood pressure and reduce risk of developing diabetes and cardiovascular disease. Following the seminal paper by Imai et al. in 2000 demonstrating that NAD^+ and Sir2 were augmented by calorie restriction in yeast, many more investigations have set out to determine if this mechanism is underlying the beneficial effects of CR in aging [258]. However, fewer studies have investigated the potential role of skeletal muscle SIRT1 in promoting positive metabolic effects. Instead, many investigations have focused on the role of SIRT1 in the liver in response to CR where it appears to play a critical role. However, skeletal muscle is also an important tissue for regulating glucose tolerance as it is the primary site of insulin mediated glucose disposal. One of the first investigations

in humans was conducted as a part of the Comprehensive Assessment of Long-term Effects of Reducing Intake of Energy (CALERIE) study. In this investigation, 36 individuals with overweight were randomized to either control, CR (25% caloric deficit), or CR and aerobic exercise (25% deficit driven by 12.5% reduced intake and 12.5% exercise-mediated energy expenditure [345]. This was the first study in humans to demonstrate that CR or CR with exercise could increase skeletal muscle SIRT1 protein along with its downstream targets PGC1α and eNOS.

Like caloric restriction, exercise promotes a low-energy state in the skeletal muscle. Increased demand of ATP during prolonged exercise promotes utilization of intrinsic energy stores (i.e. fat and glycogen) which results in increased AMP [244] and NAD^+ [346] concentrations. In addition, during contraction large concentrations of calcium (Ca^{2+}) are released from the sarcoplasmic reticulum which activates calcium sensitive kinases such as CaMKIIβ [187, 188, 244]. These metabolic events during exercise collectively promote activation of SIRT1 via phosphorylation of SIRT1 by AMPK [288, 346] as well as increased activity due to increased NAD^+ abundance [346]. In addition, several studies have demonstrated exercise to induce NAMPT expression, leading to increased NAD^+ in exercising muscle to support SIRT1 activity [320, 321, 346, 347]. Lastly, SIRT1 may also be induced in muscle as a result of mechanical signaling from contraction and stretching [348]. A recent cross-sectional study demonstrated that master athletes, have higher SIRT1 skeletal muscle gene expression than their age-matched non-exercising counterparts suggesting exercise training may augment SIRT1 expression [349]. Indeed, several studies in rodents [350-354] and humans [354-359] have demonstrated the ability of acute and chronic exercise to promote SIRT1 activity

and expression (Table 4). These studies have collectively shown exercise to promote deacetylation of PGC1α to promote fat oxidation, and mitochondrial biogenesis via SIRT1.

Publication	Model/Participants	Treatment/Intervention	Outcome
Cantô, C et al. (a)	C2C12 Myotubes C57BL6 Mice	Myotubes: AICAR 0.5 mM 2-8 hours or NAM 5mM 12h Treadmill exercised mice AICAR treated mice	AICAR-treated myotubes induce SIRT1-dependent PGC1α deacetylation Mucles from AICAR-treated mice decreased acetylation of PGC1α
Koltai, E et al.	Masters Athletes (n = 10) Age-matched Sedentary Controls (n = 13)	N/A	Muscle SIRT1 mRNA higher in Masters Athletes
Koltai, E et al.	3 month-old and 26 month-old Wistar Rats	6-weeks progressive treadmill exercise training	Exercise decreased SIRT1 protein in gastrocs from young and old rats Exercise increased SIRT1 activity in gastrocs from young and old rats
Pardo, P.S. et al.	C2C12 Myotubes C57BL/6J Mice	Myotube stretching grown on flexible cell culture plates Ex vivo diaphragm stretching from C57BL/6J Mice	Increased SIRT1 mRNA and Protein in stretched myotubes Increased SIRT1 mRNA and Protein in ex vivo stretched diaphragm muscle
Liao, Z.Y. et al.	6 month-old and 25 month-old Wistar Rats	6-weeks progressive treadmill training 150 mg/kg/d Resveratrol Exercise with resveratrol	Decreased SIRT1 protein in old rats Additive increase in SIRT1 protein in old rats following exercise with resveratrol
Quinn, L.S. et al.	4 month-old C57BL/6 Male Mice WT vs. IL-15 KO	Acute exhaustive treadmill exercise	SIRT1 mRNA increased 30 mins post-exercise in muscle from WT and IL15 KO SIRT1 protein increased 3h post-exercise ~4-fold in muscle from WT No change in SIRT1 protein with exercise in IL15 KO
Li, L. et al.	2.5 - 3 month-old C57BL/6 Mice WT vs. IL6 KO	12-weeks of progressive treadmill exercise training	Increase in SIRT1 protein with exercise training in muscle from WT and IL6 KO
Suwa, M. et al.	7 week-old Wistar Rats	Treadmill exercise (45 min, 20 m/min, 18.5% incline) Endurance exercise training (Low or High Intensity) 14-day CR to match energy deficit of High Intensity training	SIRT1 protein similarly increased in soleus with both Low and High Intensity training SIRT1 protein increased in plataris with High Intensity training only
Gurd, B.J. et al. (a)	3 - 6 month-old Female Sprague-Dawley Rats 3 male, 4 female recreationally active humans	Rats: Treadmill exercise (2 h, 15 m/min then increase by 5 m/min every 5 min until volitional fatigue) Humans: 7 cycling HIIT sessions over 2 weeks	No effect of acute exercise on nuclear SIRT1 protein in rat muscle ~43% increase in nuclear SIRT1 activity in rat muscle 3h post-acute exercise No effect of HIIT cycling on whole muscle or nuclear SIRT1 protein in human muscle
Edgett, B.A. et al.	Young, lean, healthy men (n = 8)	Acute cycling HIIE (77%, 100%, 133% work rates)	SIRT1 mNRA increased simiarly with all work rates
Guerra, B et al.	Young, lean, healthy men (n = 15)	Wingate test with or without prior glucose ingestion (75g)	~60% increase in SIRT1 protein 2h post exercise No effect of exercise in glucose group
Radak, Z et al.	Young sedentary men (n = 12) Young active men (n = 12) Old sedentary men (n = 12) Old active men (n = 12)	Exhaustive treadmill exercise (45 min @ 70-75% VO2max, then 90% VO2max until volitional fatigue)	33% increase in SIRT1 mRNA in young sedentary men No effect of exercise in active men or old sedentary men
Little, J.P. et al.	Young, lean, healthy men (n = 7)	2-weeks cycling HIIT 3d/week	~2-fold increase in SIRT1 protein following training
Gurd, B.J. et al. (b)	Young, lean, healty men (n = 6) and women (n = 3)	6-weeks cycling HIIT 3d/week	31% increase in SIRT1 activity, 20% decrease in SIRT1 protein

Table 4 Effect of Exercise on SIRT1 in Skeletal Muscle.

However, it is still unclear if skeletal muscle SIRT1 expression or activity is affected by obesity or if it is necessary for the metabolic benefits provided by exercise. Currently the data investigations in skeletal muscle are limited and mixed with several studies finding no change in skeletal muscle SIRT1 expression following exercise in rodent models of obesity [360-362] as well as in humans with obesity [363], whereas others have found the opposite [364, 365]. Interestingly, recent investigations in skeletal muscle specific SIRT1 KO mice demonstrated that SIRT1 was not required for mitochondria biogenesis following exercise training [366], contraction-stimulated glucose uptake [367], or have an effect on glucose homeostasis or exercise performance [312, 313]. This strong line of evidence rules out the possibility of SIRT1 being necessary for these adaptations. However, mammalian physiology is robust because of redundancies that exist to preserve important cellular functions. Therefore, these data do not indicate that skeletal muscle SIRT1 is unimportant but instead that it is not the only factor playing a role in regulating skeletal muscle adaptations to exercise.

The metabolic adaptations that occur in skeletal muscle from exercise are critically important for the metabolic health benefits that are conferred with exercise. However, the totality of molecular adaptations in skeletal muscle to promote metabolic health as a result of exercise is unclear. Interestingly, our previous data demonstrate that GLO1 protein is reduced by approximately 75% in skeletal muscle from individuals with T2D compared to lean, age-matched control participants and was negatively correlated with BMI. Recent evidence in the literature suggests GLO1 protein to be negatively influenced by hyperacetylation under obesogenic conditions [13]. However, the effect of obesity alone

on skeletal muscle GLO1 abundance and the mechanisms by which obesity may promote GLO1 acetylation and subsequent degradation are not known. Therefore, the overarching goal of this dissertation was to determine if there is a regulatory role of acetylation on GLO1 protein abundance or activity via SIRT1. In addition, given the exercise responsiveness of SIRT1 and the gap of knowledge surrounding GLO1 in this area, we also set out to determine the effect of acute exercise on GLO1 protein expression and acetylation in muscle from individuals with obesity and lean healthy individuals.

Chapter 3

Methods

3.1 Methods for Aim 1a

3.1.1 Study Design

The current investigation is a retrospective analysis of a larger study that consisted of four sequential visits as previously described [368]. Prior to enrollment, all participants provided verbal and written informed consent. Baseline measures including height, weight, body fat percentage via dual x-ray absorptiometry (DXA), and maximal aerobic capacity (VO_{2Max}) were collected on the first visit of the study. Apart from these demographic data, all other data in this current reporting were collected on the final visit of the study which consisted of 30 minutes of treadmill exercise performed at 80% of the participants' VO_{2Max}. Three days before each visit participants completed diet and physical activity logs, which they were asked to replicate in the days leading up to their subsequent visits. Participants were also instructed to abstain from vigorous exercise, and alcohol consumption 48 hours prior to each visit, and caffeine consumption 24 hours prior to each visit. Participants were asked to arrive at each visit by sedentary means (i.e. car, public transportation etc.) and having fasted for at least 12 hours. Testing of all participants was done in the early morning (0700 – 0900 hours) to account for any diurnal variations in outcome measures and to minimize the participants' burden of having to be fasted for the study. All experimental protocols were approved by the Institutional Review Board at the University of Illinois of Chicago (IRB Approval #: 2015-0127). A timeline for

the clinical procedures relevant to these data is presented in Figure 3.1.

3.1.2 Participants

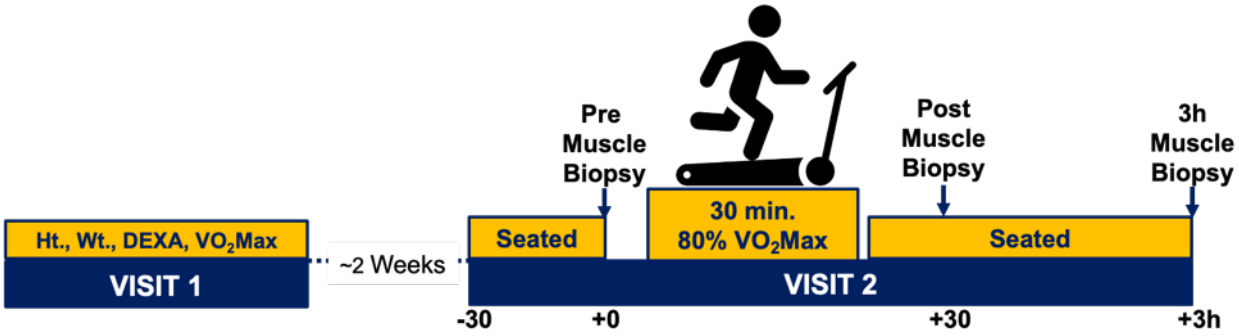

Figure 3.1 Schematic for the Acute Exercise Study Design. Participants came to the lab on two occasions for baseline and acute exercise testing. Visit one consisted of baseline measures including determination of VO_2Max via treadmill test. On visit two participants returned to the lab to perform acute treadmill exercise at 80% of their VO_2Max where muscle biopsies were taken from the vastus lateralis immediately before, 30 minutes after and 3 hours after the cessation of exercise.

Fifteen lean, healthy (LH) adults (8 M, 7 F, Age: 26 ± 1 years, BMI: 22.4 ± 0.7 kg/m^2) and five healthy adults with obesity (OB) (3 M, 2 F, Age: 28 ± 2 years, BMI: 32.4 ± 1.3 kg/m^2) volunteered to participate in the study. Participants were screened for eligibility using the following criteria: 18-35 years of age, BMI between 18-26 kg/m^2 (LH) or >29.9 kg/m^2 (OB), and absence of any chronic disease. Participants were excluded if they were a current smoker, quit smoking within the past year, and if they were previously diagnosed with any major disease such as diabetes, cardiovascular disease, kidney disease, major depression, high blood pressure, or high blood cholesterol. Fasting plasma glucose was measured via glucose oxidase reaction using a YSI STAT 2300 (YSI Life Sciences, Yellow Springs, OH) for the LH samples and a Bayer Contour Next Link glucometer (Bayer, Whippany, NJ) for the OB samples. Fasting plasma insulin was determined via ELISA in both groups (90095, Crystal Chem, Elk Grove Village, IL).

Baseline characteristics for all participants are presented in Table 5.

Variable, Units	LH, n = 15	OB, n = 5	*p*
Age, years	26 ± 1.0	28 ± 1.9	0.338
Sex, %F	47%	40%	-
Weight, kg	68.3 ± 2.4	93.9 ± 7.2	**0.020**
BMI, kg/m²	22.4 ± 0.7	32.4 ± 1.3	**0.0004**
Body Fat, %	23.1 ± 1.5	40.0 ± 2.8	**0.001**
VO_{2Max}, ml/kg/min	47.7 ± 1.9	37.2 ± 3.0	**<0.05**
Glucose, mg/dL	91.5 ± 2.1	89.1 ± 4.2	0.585
Insulin, mU/L	4.9 ± 0.5	11.6 ± 3.4	**0.005**
HOMA-IR	1.1 ± 0.1	2.5 ± 0.7	**0.006**

Table 5 Participant Baseline Characteristics. 15 lean, healthy (LH) and 5 age-matched obese (OB) participants were studied. By design the OB participants had higher body weight, BMI, and body fat. There was no difference between groups on fasting glucose. OB group possessed higher fasting insulin and HOMA-IR. All data are presented as Mean ± SEM and were analyzed via unpaired T-Test.

3.1.3 VO_{2Max} and Treadmill Exercise

VO_{2Max} was determined using a treadmill ramp protocol during which the participants ran at a self-selected speed while the treadmill grade increased two percent after every two-minutes, until volitional fatigue was reached. Participants were consulted on the selection of the speed with the goal of reaching their max at 8 – 12 minutes. Expired air was collected for the duration of the test and was analyzed via the PARVO Medics metabolic cart (Salt Lake City, UT). As a further validation of exercise intensity, heart rate was monitored via Polar heart rate monitors fitted to the participants' chest prior to testing. Rating of perceived exertion (RPE) on the Borg scale (6-20) was also assessed at the end of each two-minute interval. VO_{2Max} was achieved if the subjects met 3 of the 4

criteria: a plateau in VO_2 despite an increase in workload, an RPE >17, RER >1.1, and a HR >85% age-predicted maximal heart rate. ACSM metabolic equations were used to derive the estimated treadmill settings (speed and grade) to attain the appropriate intensity for the acute exercise bout (80% VO_{2Max}). Participants' expired air was collected throughout the acute exercise test as described above to monitor and confirm solicitation of the appropriate VO_2 during the test. Adjustments to speed and incline were made as necessary throughout the test to achieve the goal VO_2.

3.1.4 Skeletal Muscle Biopsy

Skeletal muscle biopsies were taken from the vastus lateralis before (Pre), 30 minutes after (Post), and three hours after completion of exercise (3h) as previously described [368]. Briefly, local anesthetic (1% lidocaine HCl) was administered followed by a small incision (~0.5 cm) at the biopsy site. Through this incision, a Bergstrom needle was inserted with suction extracting ~200 mg of muscle tissue. Muscle tissue was cleared of all visible connective tissue and fat, blotted with gauze to remove blood, and immediately flash frozen in liquid nitrogen or preserved in RNAlater and then stored at -80°C until further analysis was performed.

3.1.5 Tissue Homogenization and Protein Concentration Determination

Approximately 10 mg of muscle tissue was weighed and homogenized with ceramic beads (Lysing Matrix D; FastPrep®-24; MP Bio, Santa Ana, CA) in 20 volumes of ice cold 1X Cell Lysis Buffer (#9803, Cell Signaling Technology, Danvers, MA) supplemented with 1X Protease/Phosphatase Inhibitor Cocktail (#5872, Cell Signaling Technology, Danvers, MA). Protein concentration for each sample homogenate was determined by a commercially available bicinchoninic acid (BCA) protein assay kit

(Pierce, Rockford, IL).

3.1.6 GLO1 Activity

To determine GLO1 activity, 10 µL aliquots of muscle homogenate were analyzed in triplicate via a colorimetric enzymatic activity assay (K591, BioVision, Milpitas, CA). This assay was performed according to the manufacturer protocol except for the homogenates being made in the cell lysis buffer as previously described rather than the GLO1 activity buffer provided with the kit to avoid the need for using more precious sample for a separate homogenization. This activity kit uses the same principle for determination of GLO1 activity as described by Thornalley et al. [8]. Briefly, solutions containing methylglyoxal and glutathione were incubated for 10 minutes, protected from light at room temperature to create the MG-hemithioacetal which is the substrate for GLO1. Samples along with a blank (water) and a positive control (recombinant GLO1) were then incubated with equal volumes of the resultant substrate solution and the formation of S-D-lactoylglutathione (SLG) is monitored by immediately measuring the absorbance of light at 240 nm and subsequently measuring its absorbance every 5 minutes for a total of 20 minutes. The change in absorbance is calculated from two timepoints during which the slope of the line is linear and GLO1 activity is calculated from the following equation:

$$\frac{Units}{mg\ protein} = \frac{\left(\frac{\Delta Abs_{240nm}}{\Delta t}\ sample\right) - \left(\frac{\Delta Abs_{240nm}}{\Delta t}\ Blank\right) x(0.1)\ x\ D}{3.37\ x\ 0.29\ x\ V\ x\ P}$$

Where 0.1 is the reaction volume (mL), D is the sample dilution factor (1), 3.37 is the millimolar extinction coefficient of SLG ($mM^{-1}cm^{-1}$), 0.29 is the light path (cm), V is the sample volume added (mL) and P is the protein concentration of the sample (mg/mL).

One unit is defined as the activity to convert 1 μmol of SLG in 1 minute under the assay conditions at 25 C.

3.1.7 RNA Extraction and Reverse Transcription

At the time of collection, a portion of the biopsy sample (~20 mg) was fixed in RNAlater (AM7021, Thermo Fisher, Waltham, MA) and immediately frozen in liquid nitrogen. Samples were then stored at -20°C until RNA extraction. RNA extraction was performed using Qiagen's RNeasy kit as per kit protocol with modifications to increase yield for fibrous tissue. Briefly, RNAlater-fixed samples were homogenized in RLT buffer with BME via bead homogenization as described above. Samples were treated with 10 μL Proteinase K (Qiagen), incubated at 55°C for 10 min and then centrifuged at 10,000 X G for 3 minutes at room temp. Supernatants were transferred to a sterile microfuge tube and 450 μL of ethanol was then added to each sample which were then transferred on to the RNeasy spin columns. Ethanol extracts were collected via centrifugation at 9,000 X G for 30 seconds at room temperature and the protocol provided by Qiagen was then followed thereafter. 2 μL of each extraction was analyzed for RNA concentration via Nanodrop (ThermoFisher). Average RNA concentration was 128 ± 9.9 ng/uL (Mean ± SEM) for LH and 118 ± 17.7 ng/uL for OB samples. Reverse transcription was performed with iScript Advanced reverse transcriptase kit (BioRad) via manufacturer protocols to generate 150 ng of cDNA which was then diluted 1:4 with nuclease-free water.

3.1.8 Plasma Oxidative Damage Markers and AGE-Free Adducts via LC-MS/MS

Antecubital venipuncture was performed, and blood samples were collected in EDTA-treated vacutainers immediately prior to each muscle biopsy sampling time point. Plasma was isolated from whole blood via centrifugation at 3,000 rpms for 10 minutes at

4°C. Pre- and post-exercise plasma samples were collected after 30 minutes of quiet sitting to account for plasma volume shifts due to postural changes and exercise. Participants also remained seated until the final blood draw at the 3h time point. Circulating oxidative damage products methionine sulfoxide (METSO), 2-Amino adipic acid (AAA), and AGE-free adducts MG-H1, G-H1, CML, CEL, and 3DG-H were measured via isotope dilution analysis liquid chromatography-tandem mass spectrometry (LC-MS/MS) with an Agilent model 6410 triple quadrupole MS system with 1200 Rapid Resolution 1200 LC system as described previously [67]. Briefly, oxidative damage markers and AGE-free adducts were quantified in plasma filtrates prepared via centrifugation through 10 kDa cut-off Amicon® filters and separated by liquid chromatography with a methanol/H_2O gradient mobile phase with 0.29% heptafluorobutyric acid (HBFA).

3.1.9 Statistical Analysis

All data are presented as mean ± standard error of the mean (SEM). Statistical analyses for clinical, anthropometric, acetylation, protein, activity, transcript and plasma data were performed using Prism 4.0 software (GraphPad Software, Inc., La Jolla, CA). Baseline differences were assessed via unpaired T-Test. Change scores were calculated for outcomes at the 30-minute post (Post-Pre) and 3-hour (3h-Pre) time points and change scores were compared via 2-way (Group by time) mixed effect model to account for missing data. Group by time differences in protein and transcript targets at each individual time point were also analyzed via two-way mixed effects model with repeated measures (Data representation in Supplemental Figure 1 and Supplemental Figure 2). Spearman's Rho was performed to analyze the relationship between dependent

variables. Data were investigated for outliers, defined as being two standard deviations outside of the mean. One outlier was identified in the immunoprecipitation data, which was excluded from analysis and replaced with an imputation of the mean. These data were analyzed for an effect of time via one-way repeated measures ANOVA. Bonferonni post-hoc tests were used for all ANOVA analyses. Significance was set at $p < 0.05$.

3.2 Methods Pertaining to Aim 1b

3.2.1 Description of Human Immortalized Myotube Model

The cells used for this dissertation were human immortalized myotubes developed at the University of Texas Southwestern in the lab of Dr. Woodring Wright as previously described [369]. To develop this immortal cell line a muscle biopsies were taken from patients with facioscapulohumeral muscle dystrophy (FSHD) and unaffected control participants from either the biceps or the deltoid. Biopsy explants were then cultured, and eventually myoblasts were isolated and expanded. Myoblasts were then infected with pBabe vectors containing cyclin-dependent kinase 4 (CDK4) and human telomerase (hTERT) as well as flanking LoxP sites to allow for excision of either or both expression cassettes. An aliquot of one of the immortalized clones developed from a deltoid biopsy of an unaffected control participant was a kind gift from Dr. Ludlow and were the cells used for the purposes of this dissertation. These immortalized cells were chosen to avoid issues with myoblast senescence that occurs rapidly in human primary myoblasts (~8-10 passages). Conversely, these cells have been previously passaged over 80 times without senescing and grow more rapidly compared to their primary cell counter parts making them a valuable and convenient biotechnology tool. In addition, until recently, a human immortalized myoblast cell line has not been commercially available. In addition, a recent

transcriptomic investigation of this model demonstrated that the immortalized myoblasts and myotubes do not possess dramatically different expression profiles from their primary parents [370]. However, given the known interactions between sirtuins and telomeres, we repeated FK866 experiments in cells from the same donor in which the hTERT floxed cDNA was previously removed by CRE excision and therefore were only expressing the CDK4 exogenous cDNA to determine if our outcomes were affected by the exogenous expresson of hTERT (Supplemental Figure 6).

3.3 Tissue Culture Procedures

In attempt to closely mimic the physiologic environment and limit the oxidative stress of canonical tissue culture conditions of growing cells under physiological

Figure 3.2 Low Oxygen Incubator Set-Up. Low O_2 gas being pumped into an air-tight chamber containing a plate of cells to displace atmospheric air. Chambers are gassed for 4 minutes prior to sealing with rubber stoppers. After gassing, cells are placed in a standard tissue culture incubator maintaining at temperature of 37 C.

hyperoxic conditions (~20% O_2), we cultured the human immortalized myoblasts and differentiated myotubes at oxygen tensions more closely mimicking those experienced by skeletal muscle *in vivo* (~5%). To accomplish this, cells were placed in air-tight low-oxygen chambers and the air was displaced by injecting low oxygen gas (5% CO_2, 2% O_2, N_2 balance) for 4 minutes at ~5 psi into the chambers through re-sealable inlets before sealing and placing the chambers in a humidified tissue culture incubator similar to previous published descriptions [371]. A picture of this set-up is provided in Figure 3.2. We also determined that there was no effect of performing tissue culture at 5% O_2 on NAD concentration, GLO1 protein or NAMPT protein (**Supplemental Figure 8**).

Cells were cultured in custom growth media designed to accommodate optimum, healthy growth of these immortalized myoblast. The growth media was made in batches of 500 mL and consisted of 4:1 DMEM (SH30021FS, Hyclone) : M199 (SH3025301, Hyclone) (reffered to as Media X or MX), 15% fetal bovine serum (FBS) (10437028, Fisher), 50 mM HEPES buffer (15630-080, Invitrogen), 0.03 µg/mL Zing Sulfate (Zn_2SO_4) (S68-500, Fisher Scientific), 1.4 µg/mL Vitamin B12 (V2786, Sigma), and 55 ng/mL Dexamethasone (72092, Stem Cell Technology). Media was brough up to a final glucose concentration of 25 mM by adding D-glucose and was then sterile filtered through a 0.22 µm vacuum driven filtration system into 50 mL aliquots (Steriflips, SCGP00525, Sigma). Hepatocyte growth factor (HGF) (GF116, Chemicon International) and basic fibroblast growth factor (bFGF) (HRP-0011, BioPioneer) were added to 50 mL aliquots of sterile media at final concentrations of 2.5 ng/mL and 10 ng/mL respectively on a weekly basis to avoid the degradation of the growth factors in media.

Prior to initiating the tissue culture, tissue culture plates were coated with 0.1% pigskin gelatin. Plates were coated by incubating plates in sterile 0.1% pigskin gelatin solution at 37^{o}C in a sterile incubator for at least 30 minutes. Coated plates were not kept for more than one week without use. Immediately prior to use, the liquid in the plate was aspirated and 8 mL of warm growth media was added to the plate. To initiate tissue culture, cells cryopreserved in 10% DMSO, 90% FBS were thawed in a 37^{o}C hot water bath before adding 1 mL of warmed growth media to the cryovial containing the cell suspension resulting in a final volume of 2 mL. This 2 mL cell suspension was then distributed across coated plate(s) containing warm growth media. When plating cells following cryopreservation, seeding density for a 10 cm^2 plate was at least 1.5 x 10^6 cells per 100 mm plate. In anticipation of ~70% attrition following cryopreservation, this would result in a seeding density of ~1.0 x 10^6 live cells per 100 mm plate (1x10^4 live cells per mm) which was the seeding density used when passaging cells into subsequent 100 mm plates. The plate(s) containing the cell suspension was gently rocked to make sure the cells were in a position to evenly adhere to the plate. The tissue culture plate containing the cell suspension was then placed into a low O_2 chamber, gassed as previously described, sealed and placed into a humidified (95%) cell culture incubator. The next day (approximately 24 hours after seeding), the growth media was replaced with 10 mL of fresh, warmed growth media. Growth media was changed every 48 hours from then on until cells reached at least 80% confluence at which point they were either passaged, cryopreserved, or differentiated depending on the need.

Differentiation of myoblasts into myotubes was performed by removing growth media from the cells at ~80% confluency and rinsing the cells twice with warm dPBS (14-

190-136, Fisher) before placing the cells in pre-warmed MX with 2% Horse Serum (26050088, Fisher) and 25 mM glucose. Cells were left in differentiation media for 5 days and replaced with fresh media every 48 hours during that period. Given that the differentiation process is a low serum condition, the cells were not placed in an addition serum starved condition prior to treatments. Example images of myoblasts prior to differentiation, after 5 days of differentiation and after various treatments used are in (Supplemental Figure 16).

3.3.1 GLO1 siRNA Experiments

Transfection of small interfering RNAs (siRNAs) were performed in MX + 10% FBS with 25 mM Glucose supplemented with scrambled control siRNAs (scRNAs) or siRNAs against the target gene and RNAiMax (13778150, Fisher) diluted in OptiMEM (31985062, Fisher). First, 2 aliquots RNAiMax and 2 separate aliquots of scRNA or siRNA were diluted in OptiMEM. Next, equal volumes of the diluted scRNA or siRNA were added to one of the 2 aliquots of diluted RNAiMax. Then, these solutions incubated for 5 minutes at room temperature. During this time, differentiation media was removed from 6-well plates containing fully differentiated myotubes and cells were rinsed twice with pre-warmed dPBS. Lastly, 1.75 mL of pre-warmed MX + 10% FBS and 25 mM Glucose was added to each of the wells and 0.25 mL of diluted scRNA or siRNA with RNAiMax were added dropwise onto appropriate wells. Cells were then incubated for 48 or 72 hours as indicated before being harvested as described previously.

3.3.2 TMT

3.3.2.1 Protein Digestion and TMT Labeling

Frozen cell pellets were lysed in ice-cold 1X RIPA buffer (CST), supplemented with 1X protease/phosphatase inhibitor cocktail (CST), as well as 10 mM nicotinamide (NAM, N06336-100G, Sigma Aldrich), and 1 μM Trichostatin A (TSA, T8552-1MG, Sigma Aldrich) to inhibit sirtuin and HDAC activity respectively to preserve the acetylation state of proteins at the time of sample collection. Following resuspension of pellets in lysis buffer, samples were frozen in liquid N2 and then thawed on ice for cryo-lysis. Next, samples were sonicated on ice two times for 30 seconds. Lastly, samples were centrifuged at 14,000 X G for 10 minutes at 4^{o} C. The supernatant was transferred to a new tube to be used for downstream western blotting (WB), and TMT-LC-MS/MS applications. An aliquot of the supernatant was diluted and assayed for protein concentration via BCA (Pierce) (Figure 3.3). Lysates were adjusted to 2 mg/mL concentration. Samples (75 μg/condition) were lysed and labeled with TMT 6-plex essentially by following manufacturer's protocol (ThermoFisher) Figure 3.4. Briefly, upon reduction (5 mM DTT, for 30 min at 45 C) and alkylation (15 mM 2-chloroacetamide, for

30 min at room temperature) of cysteines, the proteins were precipitated by adding 6 volumes of ice cold acetone followed by overnight incubation at -20° C. The precipitate was spun down, and the pellet was allowed to air dry. The pellet was re-suspended in 0.1M TEAB and overnight (~16 h) digestion with trypsin/Lys-C mix (1:25 protease:protein; Promega) at 37° C was performed with constant mixing using a thermomixer. The TMT 6-plex reagents were dissolved in 41 µl of anhydrous acetonitrile and labeling was performed by transferring the entire digest to TMT reagent vial and incubating at room temperature for 1 h. Reaction was quenched by adding 8 µl of 5% hydroxyl amine and

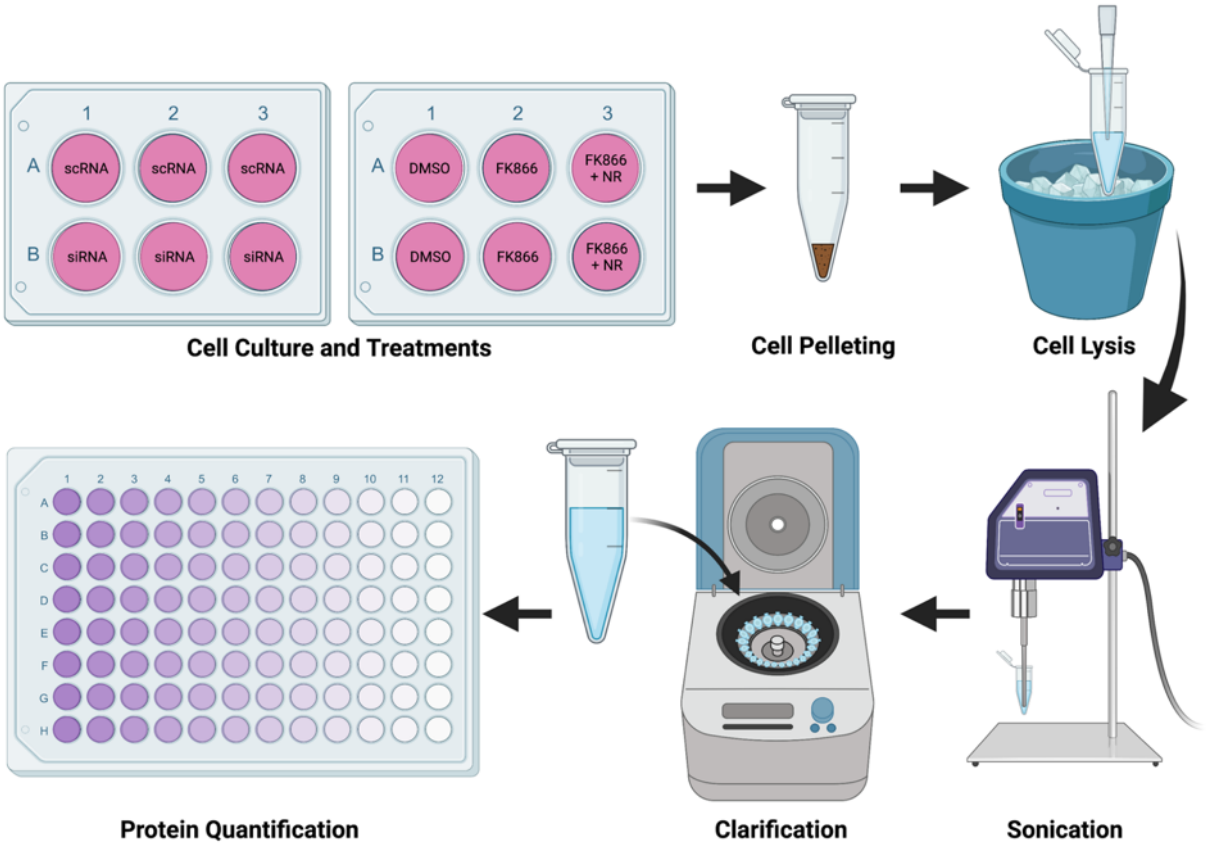

Figure 3.3 Workflow for Cell Lysis. This workflow (described in methods) was used for all protein-based outcomes in cell culture models (i.e. western blotting, TMT LC-MS/MS, GLO1 activity and ELISA). For western blotting cell lysis buffer from CST was used. RIPA buffer was used for lysates prepared for TMT analysis and GLO1 assay buffer provided with the activity kit was used for GLO1 activity and ELISA.

further 15 min incubation. Labeled samples were mixed together, and dried using a vacufuge. An offline fractionation of the combined sample (~200 µg) into 8 fractions was performed using high pH reversed-phase peptide fractionation kit according to the manufacturer's protocol (Pierce; Cat #84868) (Figure 3.4). Fractions were dried and reconstituted in 9 µl of 0.1% formic acid/2% acetonitrile in preparation for LC-MS/MS analysis. Table 6 depicts the isobaric channel assigned to each sample.

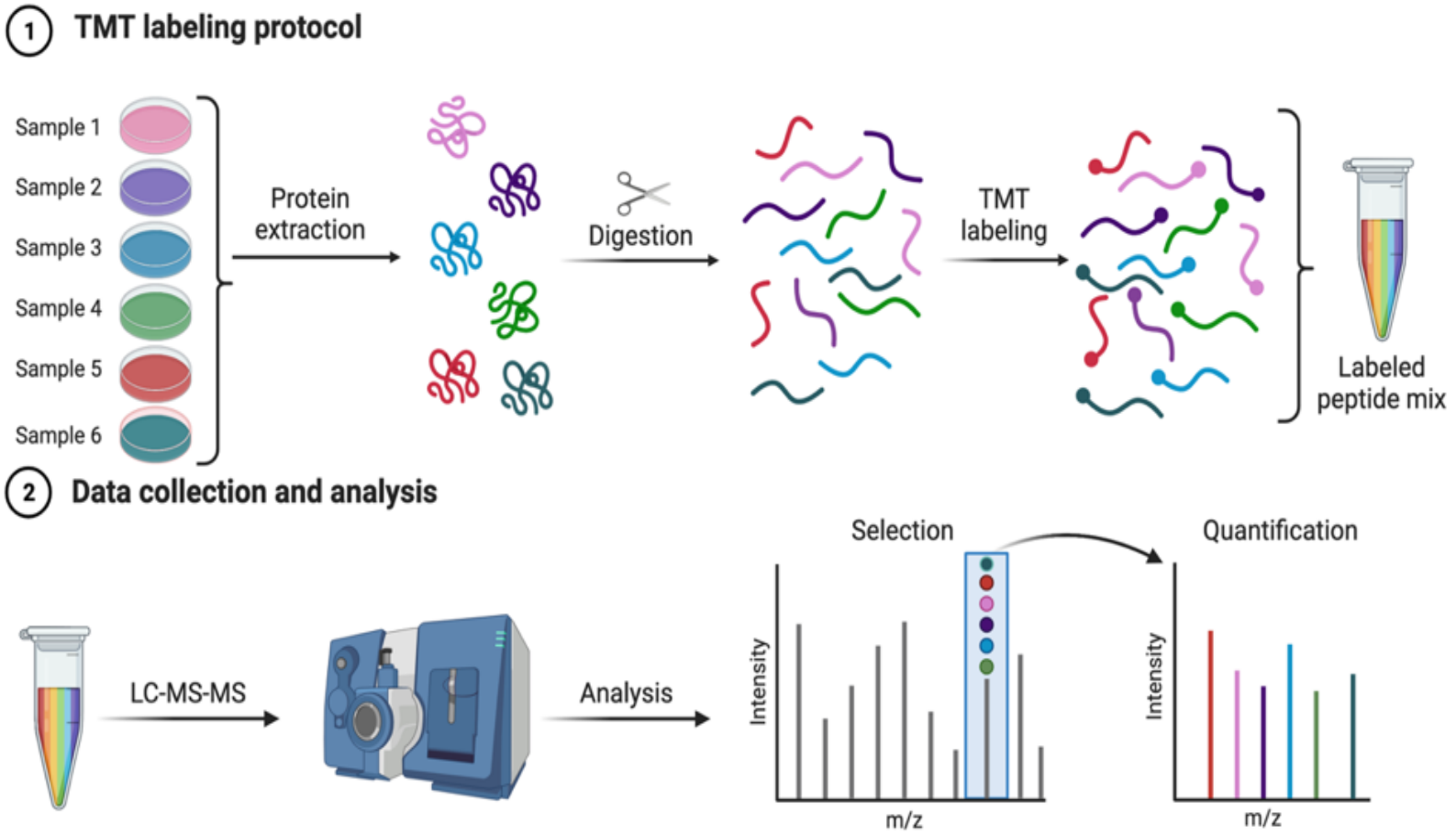

Figure 3.4 TMT LC-MS/MS Workflow. Overview of workflow for TMT analysis used for cell culture samples. Lysates containing 75 µg of protein were brought to a common protein concentration prior to digestion labeling and analysis as described in detail in the methods.

3.3.2.2 Liquid Chromatography-Mass Spectrometry Analysis (LC-multinotch MS3)

In order to obtain superior quantitation accuracy, we employed multinotch-MS3 (McAlister GC) which minimizes the reporter ion ratio distortion resulting from fragmentation of co-isolated peptides during MS analysis. Orbitrap Fusion (Thermo Fisher Scientific) and RSLC Ultimate 3000 nano-UPLC (Dionex) was used to acquire the

Sample ID	TMT Mass Tag
72h GLO1 scRNA 1	126
72h GLO1 scRNA 2	127
72h GLO1 scRNA 3	128
72h GLO1 siRNA 1	129
72h GLO1 siRNA 2	130
72h GLO1 siRNA 3	131

Table 6 Isobaric Tagging Scheme for GLO1 KD Experiment.

data. Two µl of the sample was resolved on a PepMap RSLC C18 column (75 µm i.d. x 50 cm; Thermo Scientific) at the flow-rate of 300 nl/min using 0.1% formic acid/acetonitrile gradient system (2-22% acetonitrile in 150 min;22-32% acetonitrile in 40 min; 20 min wash at 90% followed by 50 min re-equilibration) and directly spray onto the mass spectrometer using EasySpray source (Thermo Fisher Scientific). Mass spectrometer was set to collect one MS1 scan (Orbitrap; 120K resolution; AGC target $2x10^5$; max IT 100 ms) followed by data-dependent, “Top Speed” (3 seconds) MS2 scans (collision induced dissociation; ion trap; NCE 35; AGC $5x10^3$; max IT 100 ms). For multinotch-MS3, top 10 precursors from each MS2 were fragmented by HCD followed by Orbitrap analysis (NCE 55; 60K resolution; AGC $5x10^4$; max IT 120 ms, 100-500 m/z scan range) [372].

3.3.2.3 Data Analysis

Proteome Discoverer (v2.4; Thermo Fisher) was used for data analysis. MS2 spectra were searched against SwissProt human protein database (20,353 entries; download date: 6/17/2020) using the following search parameters: MS1 and MS2 tolerance were set to 10 ppm and 0.6 Da, respectively; carbamidomethylation of cysteines (57.02146 Da) and TMT labeling of lysine and N-termini of peptides (229.16293 Da) were considered static modifications; oxidation of methionine (15.9949 Da) and deamidation of asparagine and glutamine (0.98401 Da) were considered variable. Identified proteins and peptides were filtered to retain only those that passed ≤1% FDR threshold. Quantitation was performed using high-quality MS3 spectra (Average signal-to-noise [S/N] ratio of 6 and <50% isolation interference).

Normalized factors were calculated using the Gygi method for TMT quantification. Briefly, S/N of all proteins in each channel were summed to quantify total protein and then divided by the channel with the largest total protein value. The unique channel normalization factor was then added to each protein identified to create normalized abundance of protein. These normalized abundances were then used to calculate Log2 fold change scores using GLO1 scRNA as the reference.

3.3.3 Statistical Analysis

T Test was used to compare protein expression differences between groups. Resultant p values were the adjusted via Benjamini-Hochberg correction method. For data analysis and representation (volcano plots and heat maps), adjusted p values were converted to -log10 p. For gene ontology enrichment analyses, only proteins that significantly changed with GLO1 siRNA (-Log10 $p < 1.3$) were used for analysis. Uniprot

accessions of significantly up regulated proteins and down regulated proteins were entered into DAVID independently. Proteins were searched against the human gene ontology biological process annotations. Pathway fold enrichments were generated by DAVID based on the number of highly associated proteins identified determined by Fisher's exact test.

3.4 Methods Pertaining to Aim 2

3.4.1 FK866/NR Treatments

Lyophilized FK866 (APO866, ApexBio, Houston, TX) was dissolved in warm DMSO to create a stock concentration which was then diluted in MX + 10% FBS with 25 mM Glucose to achieve a final concentration of 50 nM. IC50 values for FK866 range from 0.9 nM to 27.2 nM [373]. Following 5 days of differentiation, myotubes in 6-well plates were treated with conditioned media containing either 50 nM FK866 (4 wells) or media containing equal volume of DMSO (2 wells) for 48 hours. At 44 hours, lyophilized nicotinamide riboside (NR, NC1627048, Cayman Chemical, Ann Arbor, MI) was reconstituted in sterile ultrapure water (W3500-1L, Sigma) and then diluted into freshly prepared conditioned media containing 50 nM FK866 to a final concentration of 0.5 mM. For co-treatment rescue experiments with NR, conditioned media was removed from two of the wells containing FK866 media, rinsed twice with pre-warmed dPBS and replaced with freshly prepared media containing 50 nM FK866 and 0.5 mM NR at 44 hours. Doses and timing of FK866 and NR co-treatments were based on previous experiments performed in C2C12 myotubes and primary mouse skeletal muscle which confirmed NAD depletion and rescue respectively in the two conditions [323]. Surplus stocks of NR and FK866 were aliquoted and stored at -20^{o} C. Timing of NR treatment was also limited by

its instability in water. Stocks of FK866 were only used within the storage stability indicated by the vendor and only if they have not previously undergone freeze-thaw. Fresh NR stock solutions were exclusively used and not stored to avoid concerns with stability in aqueous solutions. Final volume of DMSO for all cell culture treatments were less than 0.1% of the total media volume.

After 48 hours, cells were harvested by trypsinization. Briefly, condition media was removed, cells were rinsed twice with pre-warmed dPBS before being placed in 200 uL per well (6-well plate) of TrypLE Express (50-591-419, Fisher) for 3 minutes to lift cells off the plate. Cells were then resuspended by adding 800 uL of MX + 10% FBS and equally aliquoted into two, labeled microcentrifuge tubes. Cell suspensions were then centrifuged for 5 minutes at 1,000 X G to pellet cells before removing the media and flash freezing the cell pellets in liquid nitrogen. Cells were then stored at -80^{o} C until analysis.

3.4.2 SIRT1 and NAMPT siRNA Treatments

Transfection of siRNAs were performed in MX + 10% FBS with 25 mM Glucose supplemented with scRNAs or siRNAs and RNAiMax diluted in OptiMEM. Treatments were performed as previously described for GLO1 KD Cells were then incubated for 48 or 72 hours as indicated before being harvested as described previously.

3.4.3 KDAC and KAT Inhibitor Treatments

Human immortalized myoblasts were seeded at 1x10^{5} cells per well in 12-well plates and allowed to grow to approximately 80% prior to differentiation. Following 5 days of differentiation, myotubes were either treated with inhibitors against SIRT2 (25 or 100 μM AGK2, S7577, SelleckChem, Houston, TX), all sirtuins (25 or 100 μM NAM), all HDACs (2.5 or 10 nM TSA), P300 (10 or 40 μM Curcumin, S1848, SelleckChem), and

GCN5 (10 or 40 μM Butyrolactone-3, sc-358657) or DMSO for 24 hours. After the treatment period, cells were pelleted and flash frozen as previously described.

3.4.4 Cell Lysis for Protein Extraction

Frozen cell pellets were lysed in ice-cold 1X Cell Lysis Buffer (CST), supplemented with 1X protease/phosphatase inhibitor cocktail (CST), as well as 10 mM nicotinamide (NAM, N06336-100G, Sigma Aldrich), and 1 μM Trichostatin A (TSA, T8552-1MG, Sigma Aldrich) to inhibit sirtuin and HDAC activity respectively to preserve the acetylation state of proteins at the time of sample collection. Following resuspension of pellets in lysis buffer, samples were frozen in liquid N2 and then thawed on ice for cryo-lysis. Next, samples were sonicated on ice two times for 30 seconds. Lastly, samples were centrifuged at 14,000 X G for 10 minutes at 4^{o} C. The supernatant was transferred to a new tube to be used for downstream western blotting (WB), immunoprecipitation (IP) applications. An aliquot of the supernatant was diluted and assayed for protein concentration via BCA (Pierce). This cell lysis procedure was also used for samples analyzed for GLO1 content via ELISA and GLO1 activity except for the buffer used. For these applications the GLO1 activity assay buffer provided with the purchased kit supplemented with protease/phosphatase inhibitors, 10 mM NAM and 1 μM TSA was used instead. A workflow of the cell lysis procedure is provided in Figure 3.3

3.4.5 GLO1 Immunoprecipitation

To determine the effect of FK866/NR on GLO1 ubiquitination status, human immortalized myotubes were treated with 10 μM of the proteasome inhibitor MG-132 (501126889, Ubpbio, Dallas, TX) alone or with 50 nM FK866 or 50 nM FK866 + 0.5 mM NR for 24 hours as previously described to enrich the samples with polyubiquitinated

proteins. Protein was extracted from these samples as previously described except for the addition of 100 mM of the deubiquitinase inhibitor iodoacetamide (IAA) (205-630-1, Arcos Organics) to the cell lysis buffer to preserve the ubiquitination status of the proteins in the samples. GLO1 was immunoprecipitated from these 500 µg of protein from these samples using a column-based immunoprecipitation platform (Catch and Release, 17-500, Millipore Sigma). This system consists of spin-columns prepackaged with a proprietary resin in a microcentrifuge-compatible tube with a screw cap and break away seal on the bottom. Rather than being directly conjugated to a ligand such as protein A or G, the system provides and antibody capture affinity ligand to be used to tether the antibody to the resin.

To immunoprecipitate GLO1 from samples using this system, sample aliquots containing 500 µg of protein were first brought up to a final volume of 230 µL with lysis buffer. Samples were then incubated for 1 hour at room temperature with rotation with washed, unconjugated catch and release columns to preclear the samples. After preclearing, the spin columns were placed in a capture tube with the bottom of the spin column unsealed. The spin column was then centrifuged at 2,000 X G for 30 s to collect the pre-cleared samples. The original spin column was then discarded, and a new column was washed. Samples, 4 µg of GLO1 antibody (sc133144, Santa Cruz), and 10 µL of the affinity ligand were then combined and placed in the new spin column. The final volume was then brought up to 500 µL with wash buffer supplemented with 100 mM IAA. As a negative control, 500 µg of protein from one of the samples was also incubated in a column with an isotype control (4 µg mouse IgG2a antibody, sc-3878, Santa Cruz) instead of the GLO1 antibody. Samples were incubated at room temp for one hour with slow

rotation. After incubation the spin columns were placed in a collection tube with their bottoms unsealed and were centrifuged at 2,000 X G for 30 seconds to collect the supernatant. The columns were then washed once with 400 µL of wash buffer before placing the spin column in a new capture tube for elution with 70 µL of denaturing elution buffer with 5% βME. 35 µL of supernatant was combined with equal volume of 2X Laemmeli Buffer with βME and heated at 95^{o} C for 5 minutes. 30 µL of the eluates and supernatants were then loaded onto a 10% polyacrylamide gel, separated by SDS-PAGE, and transferred to a nitrocellulose membrane via semi-dry transfer for 11 minutes with a Transblot Turbo (BioRad). Membranes were blocked in PFBB for 1 h followed by incubation with an anti-ubiquitin antibody solution (1:1000) (A0126, ABclonal) in PFBB with 0.1% Tween-20 overnight at 4^{o}C with gentle rocking. After primary incubation, membranes were washed as previously described and then placed in an anti-rabbit secondary antibody conjugated to IRDye 800CW (1:20,000) (926-32213, LiCor) in PFBB with 0.1% Tween-20 for 1 hour at room temperature with gentle rocking. Membranes were then washed and imaged on the Odyssey CLx as previously described and then incubated in anti-GLO1 antibody solution (1:1300) (SAB4200193, Sigma Aldrich) in PFBB with 0.1% Tween-20 overnight at 4^{o}C with gentle rocking. After incubation, membranes were washed as previously described and then placed in an anti-rat secondary antibody conjugated to IRDye 680RD (1:20,000) (926-68076) for 1 hour at room temperature with gentle rocking. Membranes were washed again as described and imaged on the Odyssey CLx. For quantitation, the Ubiquitin signal in the eluate corresponding with GLO1's molecular weight was quantified as the ubiquitinated version of GLO1 and was normalized to the corresponding GLO1 signal in the eluate on the opposite channel.

3.4.6 RNA Extraction and Reverse Transcription

RNA was extracted from pellets collected and designated for RNA analysis with a commercial RNA isolation kit (RNeasy Plus Universal, 1062832, Qiagen) according to the manufacturer's instructions with minor modifications. Cells were lysed in 900 uL of Qiazol (1023537, Qiagen) by pipetting up and down. Lysates were then added to QiaShredder (79654, Qiagen) columns and centrifuged at 8,000 X G for 1 minute at room temperature to ensure complete cell lysis. Lysates were then transferred to a new tube where they incubated at room temperature for 5 minutes. Next, 100 µL of gDNA eliminator solution (provided with the kit) and 180 µL of chloroform (C2432-25ML, Sigma Aldrich) was added to the sample and mixed via briefly vortexing. Homogenates were then incubated for 3 minutes at room temperature before centrifuging at 12,000 X G for 15 minutes at 4^{o} C to bring the aqueous phase to the top of the mixture. The aqueous phase (~600 µL) was then transferred to a new tube to which equal volume of 70% ethanol was added and mixed by pipetting. This mixture was then added to the RNeasy spin column fitted with a collection tube 700 µL at a time followed by centrifuging at 8,000 X G for 30 seconds at RT after each addition. The flow through following each centrifugation was discarded. The remainder of the RNA extraction procedure was carried out according to the manufacturer's instructions. 2 µL of each extract was used for RNA quantification via nanodrop. Reverse transcription was performed with iScript Advanced reverse transcriptase kit (BioRad) via manufacturer protocols to generate 300 ng of cDNA which was then diluted 1:4 with nuclease-free water.

3.4.7 NAD Assay

Cell pellets collected and designated for NAD quantification were assayed for NAD using a modified cycling assay originally developed to quantify cADP-ribose (Graeff R 2002). Briefly, alcohol dehydrogenase reduces the sample NAD^+ to NADH which is then cycled back to NAD^+ by the action of diaphorase using the NADH to reduce resazurin into a fluorescent resorufin molecule. The fluorescence is then monitored in samples and a standard curve of NAD^+ over time where the change in fluoresence is proportional to the NAD^+ concentration in the curve and samples.

For this assay, acidic NAD^+ extracts were prepared by lysing cell pellets in 200 µL of ice-cold 0.6 M perchloric acid (A2296-1LB, Fisher) by pipetting. Acid extracts were then centrifuged at 21,000 X G for 15 minutes at 4^o C. The supernatant was transferred to a new tube and the protein pellet was resuspended in 10 µL of 1M NaOH and then 50 uL of 0.1 M sodium phosphate buffer (Na-PO4) (pH 8) and subsequently used for protein determination via BCA. Immediately prior to the assay, aliquots of the supernatants were diluted 1:10 in ice-cold 0.1 M NA-PO4 (pH8). Diluted samples were then assayed in triplicate for NAD^+ alongside a standard curve of NAD (10127965001, Roche, Basel, Switzerland) serially diluted in 0.1 M Na-PO4 (pH8) from 1 µM to 0.0625 µM by loading 5 µL of the samples or standards on to a black 96-well flat bottom plate (CLS3915, Sigma Aldrich) followed by the rapid addition of 95 µL of the cycling mix. 10 mL of cycling mix per plate was prepared fresh on the day of the assay and was composed of 8.4 mL of ultrapure water, 1 mL of 1M Na-PO4 (pH 8), 20 µL BSA (50 µg/µL) (03117405001, Roche), 0.1 mL of 1 M NAM (N06336-100G, Sigma Aldrich), 0.2 mL ethanol (100%) (BP2818500, Fisher Scientific), 10 µL of 10 mM FMN (F6750, Sigma Aldrich), 10 µL 20

mM resazurin (75005, Stem Cell Tech.), 110 µL alcohol dehydrogenase (10 mg/mL) (A3263, Sigma Aldrich), 110 µL diaphorase (1 mg/mL) (5540, Sigma Aldrich). The fluorescence of the samples and standards is then immediately determined at 530 nm excitation and 590 nm emission and subsequently determined at 10 and 20 minutes following the initiation of the reaction. The nM NAD concentration of the sample was then determined by creating a standard curve plotting the change in fluorescence in the standards over 20 minutes against their known NAD concentrations and fitting the change in fluorescence in the samples over the same time to this curve and applying the dilution factor. The NAD concentration was then corrected for protein using the protein concentration determined from the protein pellet to express the NAD concentration in nmol/mg protein.

3.4.8 GLO1 Specific Activity

To determine GLO1 activity, 10 µL aliquots of muscle homogenates and cell lysates prepared in GLO1 activity assay buffer supplemented with 10 mM NAM and 1 uM TSA were analyzed in duplicate via a colorimetric enzymatic activity assay (K591, BioVision, Milpitas, CA). This assay was performed according to the manufacturer protocol as described in the methods for Aim 1.

To determine GLO1 specific activity, the activity data from the GLO1 activity assay was made relative to the amount of GLO1 in the sample. GLO1 input was determined by performing a GLO1 ELISA (MBS2021816, MyBioSource, San Diego, CA) on another aliquot of same samples analyzed for GLO1 activity. Samples were assayed according to the manufacturer protocol. Briefly, aliquots of cell lysates containing 20 µg of protein were diluted to 200 µL in PBS and run in duplicate (10 µg/100 µL per replicate) alongside

a standard curve of known GLO1 concentrations run in triplicate. After capture and detection of GLO1, color development of the enzyme linked antibody was allowed to proceed for 15 minutes prior to quenching the reaction. Absorbance was determined at 450 nm and the absorbance of the unknowns was fit to the standard curve to determine sample GLO1 concentrations. The dilution factors for each sample were calculated and applied before using this value to calculate specific activity (Units/mg GLO1 protein).

3.4.9 Statistical Analysis

Given that several of these experiments were done in several different batches all data that is semi-quantitative (e.g. western blot signal intensities) was made into a fold change score by dividing the resultant value of individual replicates with the average value of the respective control conditions in a given experiment. Quantitative data (e.g. ddPCR and NAD) are presented as their quantifications and not made into fold change values. All data were checked for normality prior to running statistical analyses. For FK866/NR experiments a one-way ANOVA was performed to compare the three conditions and Bonferroni post-hocs were performed to determine where potential differences may exist. For SIRT1 siRNA experiments, unpaired T Tests were used to compare scRNA and siRNA-treated samples. Due to limited n size in KDAC/KAT inhibitor studies T Tests were used to compare independent treatments to DMSO. All individual data are presented in the figures with the columns representing the mean values and the error bars representing standard error of the mean (SEM). All figures were made using GraphPad Prism. Significance was set at $p < 0.05$

3.5 Methods Pertaining to All Aims

3.5.1 Western Blotting

Aliquots of muscle homogenate or cell lysates containing 20 and 10 µg of total protein respectively were diluted in equal volumes of 2x Laemmli Buffer (BioRad, 1610737, Hercules, CA) with 5% β-mercaptoethanol (βME) (BioRad, 1610710) prior to heating at 90°C for 10 min. Denatured samples were brought to room temperature, loaded onto 10% pre-cast Criterion TGX gels (5671033, BioRad) and separated by SDS-PAGE at 200 V for 50 minutes. Separated proteins were then transferred to nitrocellulose membranes via Transblot Turbo semi-dry transfer system for 11 minutes (BioRad). Membranes were then blocked with Protein-Free Blocking Buffer (PFBB, 92780003, Li-Cor, Lincoln, NE) for 1 hour at room temperature with gentle rocking. After blocking, membranes were cut at 38 kD, and 90 kD to create three membrane strips (260 – 90 kD, 90 – 38 kD and <38 kD) which were incubated with primary antibodies against SIRT1 (1:500, #9475, Cell Signaling Technology), NAMPT (1:1000, A0256, ABclonal), and GLO1 (1:1000, SC-133144, Santa Cruz Biotechnology, Dallas, TX), respectively diluted in PFBB with 0.1% Tween-20 overnight at 4^{o} C with gentle rocking. The next day, membranes were removed from primary antibody solutions and washed 3 times 5 minutes each with Tris-Buffered Saline + 0.1% Tween-20 (TBST) with gentle rocking. After washing, membranes were incubated with an anti-rabbit or anti-mouse fluorophore-conjugated secondary antibody (1:20,000, Li-Cor, Lincoln, NE) diluted in PFBB + 0.1% Tween-20 for 1 hour at room temperature with gentle rocking while protected from light. The secondary antibody solution was subsequently removed the membranes were washed 3 times 5 minutes each with Tris-Buffered Saline + 0.1% Tween-20 (TBST) with

gentle rocking followed by a 5-minute wash with TBS. The membrane strips were then placed on the scanning glass surface of the Odyssey CLx Imaging System (Li-Cor) in their original (pre-cut) orientation and then imaged. After imaging was completed for the proteins of interest, membrane strips were returned to their individual boxes and rinsed in ultrapure water prior to incubating in 5 mL of REVERT total protein stain for 5 minutes at room temperature with gentle rocking. Membranes were then rinsed for 30 seconds in 5 mL of REVERT wash solution before returning the membranes to the Odyssey CLx for imaging where they were again scanned in their original orientation to capture a signal for total protein. All proteins of interest were probed with secondary antibodies conjugated to Alexa Fluor 800 whereas the REVERT total protein stain produces fluorescent signal on the 680 nm channel. This western blotting and imaging procedure was repeated using another 10 ug aliquot of the sample where available to probe for secondary outcome targets NRF2 (1:500, AB-62352, ABCAM, Cambridge, UK), and KEAP1 (1:1000, A1820, ABclonal, Woburn, MA). Protein fluorescent signal was quantified on Image Studio software (V4.0.21; Li-Cor) using the western blot quantification function. Quantification boxes were drawn manually around the bands of interest and were adjusted according to the fluorescence histogram provided by the software to ensure complete capture of the protein signal. Total protein was quantified using EmpiriaStudio software's total protein quantification function (V2.0.0.131; Li-Cor) which automatically traces the total protein signal in each lane. The signal obtained from the protein of interest was then made relative to the total protein signal quantified in the entire respective lane. Representative western blot images include a shrunk image of the total protein stain for the sake of space.

In addition, membranes that were cut prior to incubation are depicted as individual image boxes.

3.5.2 Acetyl-Lysine Immunoprecipitation

Due to limitations in sample, immunoprecipitation of acetylated GLO1 in human samples was performed in the OB samples only to investigate the potential effect of exercise on GLO1 acetylation in these samples. For human samples, 10 mg of skeletal muscle was weighed out and homogenized as described above with the addition of 10 μM NAM and 1 μM TSA to the lysis buffer. For human immortalized myotubes, cells were lysed as previously described. 500 ug of skeletal muscle homogenates or 125 ug of cell lysates were incubated with unconjugated protein A agarose beads (Santa Cruz Biotechnology, Dallas, TX) for 1 hour at 4° C with rotation to preclear the lysates of any potential interfering or non-specific interacting substances from the lysates.

Following incubation with unconjugated beads, samples were centrifuged at 21,000 X G for 1 minute and the pre-cleared lysates were retrieved and the unconjugated beads were discarded. The pre-cleared lysates were then incubated with a 50 uL suspension of agarose beads conjugated with anti-Acetyl Lysine antibody (ICP03880, ImmuneChem, Burnaby, BC) overnight while rotating at 4° C. After incubation, the samples were centrifuged at 21,000 x G for 1 minute. The supernatant was then removed and saved in a new microcentrifuge tube. The beads containing the antigen-antibody complex were washed three times with ice cold 1X PBST and two times with 1X PBS before the suspension was moved to a new tube. Following the last wash, the beads were resuspended in 60 μL 1X Laemmeli Buffer (BioRad, Hercules, CA) with without βME and heated at 90°C for 5 min to elute the proteins from the beads. 35 μL of supernatant was

combined with equal volume of 2X Laemmeli Buffer with βME and heated at 95^{o} C for 5 minutes. 30 µL of the eluates and supernatants were then loaded onto a 10% polyacrylamide gel, separated by SDS-PAGE, and transferred to a nitrocellulose membrane via semi-dry transfer for 11 minutes with a Transblot Turbo (BioRad). Membranes were blocked in PFBB for 1 h followed by incubation with anti-GLO1 antibody (1:1000) (sc-133144, Santa Cruz Biotechnology) overnight at 4°C. Membranes were washed with TBST and were incubated with an anti-mouse secondary antibody conjugated to IRDye 800CW (1:20,000) (926-32212, LiCor) in PFBB supplemented with 0.1% Tween-20 for 1 hour. The membranes were then washed 3 times, 5 minutes each with TBST followed by one 5-minute washe with TBS prior to being scanned and quantified on the Odyssey CLx Imaging System (Li-Cor). Next, membranes were probed for acetylated proteins by incubating them with an anti-acetyl lysine antibody (1:1000) (Ab21623, Abcam) overnight at 4^{o} C with gentle rocking. Following primary incubation, the membranes were washed as described above and incubated with an anti-rabbit secondary antibody conjugated to IRDye 680RD (1:20,000) (926-68071, LiCor) in PFBB with 0.1% Tween-20 for 1 hour. Following this incubation, the membranes were washed, imaged, and analyzed as previously described. In a subset of samples from the FK866/NR experiments, remaining eluates and supernatants from these IPs were probed for p53 (1:1,000) (sc-126, Santa Cruz) followed by total acetylated proteins using the same procedures to gauge the potential impact of the treatments on p53 acetylation as a surrogate marker of SIRT1 activity. For quantitation, the GLO1 or p53 signal in the eluate was quantified as the acetylated versions of these proteins and was normalized to the total acetyl lysine signal in the eluate.

3.5.3 Droplet Digital PCR (ddPCR)

Droplet digital PCR (BioRad) was used to quantify transcripts of GLO1, NRF2, KEAP1, SIRT1, and NAMPT as previously described [374]. Primers were designed for each target using Roche's universal probe library (UPL) assay design center (lifescience.roche.com). Primers and probes used for each of the targets are provided in Appendix Table 7. In brief, ddPCR assay was performed by combining 2 µL of cDNA (3.75 ng) with ddPCR mix for probes (BioRad), along with appropriate probes, primers and nuclease free water yielding a 20 µL reaction. A triplicate of no-template negative controls in which the cDNA was substituted for nuclease-free water was performed alongside each of the assays and subtracted from the final signal. The 20 µL reaction was then combined with 70 µL of droplet oil for probes (BioRad) and droplets were generated using a droplet generator (BioRad). 40 µL of the resultant droplet suspension was then carefully pipetted onto a 96 well plate which was then sealed and placed in a thermocycler where 40 cycles of PCR were performed. The droplets were then analyzed using a QX200 Droplet Digital PCR system (BioRad) by counting the droplets positive for FAM fluorescent probes. Transcript copy number was corrected for non-specific signal by subtracting the number of copies detected in the NTC samples. All transcript data are presented as copy number per ng cDNA input. This method is superior to gel based PCR given its quantitative nature and the high specificity of the probe-primer interactions.

Chapter 4

Results

4.1 Specific Aims

Aim 1. Determine if GLO1 abundance is attenuated and related to mechanisms regulating protein acetylation in muscle from individuals with obesity. We also aimed to determine if acute treadmill exercise was able to promote a molecular phenotype in muscle from individuals with obesity which resembles that found in muscle from lean healthy individuals. Finally, we set out to determine the proteomic consequences of muscle lacking GLO1 protein.

Aim 2. Determine the role of NAD^+ bioavailability and enzymes mediating protein acetylation to regulate GLO1 protein abundance and activity in human myotubes

4.1.1 Results Pertaining to Aim 1

We analyzed muscle biopsy samples from 15 lean, healthy individuals (LH) and 5 age-matched individuals with obesity (OB). Individuals with obesity presented with moderate obesity as their BMI was only 2 kg/m^2 above the obesity cut off on average and their average fitness was still in acceptable range for their age-group (Table 5). In addition, OB individuals possessed normal fasting glucose although fasting insulin was elevated over 5-fold above the LH controls driving significantly elevated HOMA-IR values (Table 7). Despite the mild clinical phenotype, muscle from OB individuals was found to possess approximately 50% GLO1 protein abundance ($p < 0.01$) compared to that of LH individuals (Figure 4.1 B). In addition, GLO1 protein was negatively correlated with BMI and fasting insulin (Figure 4.1 E and F). In line with the protein data, we also found a trend for a reduction in GLO1 activity the OB muscle ($p = 0.1$, Figure 4.1 D). Like GLO1 protein, there were trends for GLO1 activity to be negatively correlated with BMI (Rho = -0.404, $p = 0.109$) and body fat percentage (Rho = -0.418, $p = 0.098$) (Table 7). However, GLO1 activity was not correlated with fasting glucose, insulin, or HOMA-IR (Table 7).

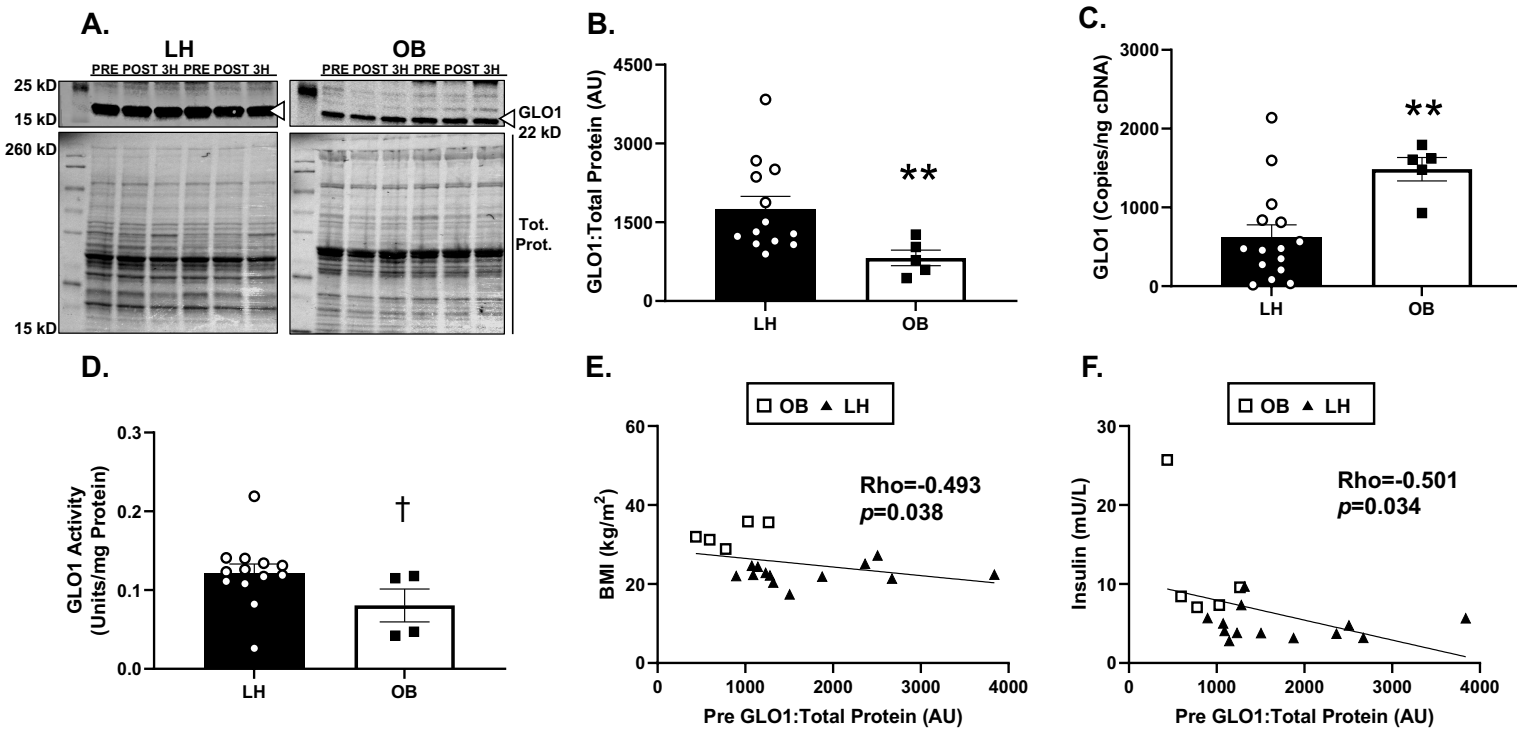

Figure 4.1 Effect of Obesity on Skeletal Muscle GLO1. A) Representative blots for GLO1 protein. B) Skeletal muscle homogenate from individuals with obesity has approximately 50% less GLO1 protein compared to LH individuals. C) ddPCR reveals an increase in GLO1 transcripts in OB muscle. D). GLO1 activity is not significantly altered in OB muscle. E) GLO1 protein is negatively correlated to BMI and F) fasting insulin. Data in B-D were analyzed by T-test and are expressed as mean ± SEM. Correlations in E and F were analyzed by Spearman's Rho. ** p <0.01. † p = 0.1.

	GLO1 Protein	GLO1 Transcript	GLO1 Activity	SIRT1 Protein	SIRT1 Transcript	NAMPT Protein	NAMPT Transcript
BMI, kg/m^2	**Rho = -0.492 *p* = 0.038**	Rho = 0.206 *p* = 0.384	Rho = -0.404 *p* = 0.109	**Rho = -0.524 *p* = 0.033**	Rho = -0.072 *p* = 0.762	Rho = -0.325 *p* = 0.237	**Rho = 0.450 *p* = 0.047**
Body Fat, %	Rho = -0.388 *p* = 0.111	**Rho = 0.454 *p* = 0.045**	Rho = -0.418 *p* = 0.096	Rho = -0.458 *p* = 0.066	Rho = 0.129 *p* = 0.589	Rho = -0.465 *p* = 0.082	**Rho = 0.471 *p* = 0.036**
Lean Mass, %	Rho = 0.298 *p* = 0.229	**Rho = -0.490 *p* = 0.028**	Rho = 0.304 *p* = 0.235	Rho = 0.470 *p* = 0.059	Rho = -0.269 *p* = 0.251	Rho = 0.275 *p* = 0.320	**Rho = -0.531 *p* = 0.015**
VO_{2Max}, mL/kg/min	Rho = 0.139 *p* = 0.581	Rho = -0.304 *p* = 0.193	Rho = 0.305 *p* = 0.232	Rho = 0.184 *p* = 0.476	Rho = 0.007 *p* = 0.977	**Rho = 0.618 *p* = 0.016**	Rho = -0.300 *p* = 0.199
Glucose, mg/dL	Rho = 0.367 *p* = 0.135	Rho = -0.417 *p* = 0.067	Rho = 0.034 *p* = 0.896	Rho = 0.192 *p* = 0.458	Rho = -0.325 *p* = 0.162	Rho = 0.248 *p* = 0.369	Rho = -0.058 *p* = 0.808
Insulin, mU/L	**Rho = -0.501 *p* = 0.034**	**Rho = 0.481 *p* = 0.032**	Rho = -0.255 *p* = 0.322	Rho = -0.269 *p* = 0.295	Rho = 0.296 *p* = 0.205	Rho = -0.104 *p* = 0.714	Rho = 0.420 *p* = 0.066
HOMA-IR, AU	Rho = -0.404 *p* = 0.097	Rho = 0.324 *p* = 0.163	Rho = -0.257 *p* = 0.316	Rho = -0.214 *p* = 0.407	Rho = 0.137 *p* = 0.565	Rho = -0.193 *p* = 0.490	Rho = 0.384 *p* = 0.095

Table 7 Baseline Correlations Between Clinical and Molecular Outcomes. A spearman correlation matrix was constructed to determine potential relationships between baseline GLO1, SIRT1, NAMPT and clinical outcomes. Bolded correlations reached statistical significance ($p < 0.05$).

Given these findings, we next attempted to probe for potential mechanisms in these tissues that may explain this attenuation. To do this we probed the NRF2/KEAP1 axis which we had previously found to be dysregulated in muscle from individuals with T2D. However, in contrast with the T2D cohort, NRF2 protein was not attenuated and KEAP1 protein was not elevated in OB muscle suggesting that GLO1 transcriptional machinery should be operating at similar capacity in the OB as in the LH muscle (Supplemental Figure 4). In fact, GLO1 transcripts were significantly elevated in OB compared to LH muscle (Figure 4.1 C).

These data led us to the hypothesize that there may be some post-transcriptional event that may explain the diminished GLO1 protein abundance in OB muscle for which an elevation in GLO1 transcripts was trying to compensate for. Upon searching the literature, a recent manuscript had described a mechanism for GLO1 degradation under obesogenic conditions (fatty acid treatment) in HEPG2 cells whereby GLO1 becomes hyperacetylated leading to its subsequent ubiquitination and degradation [13]. We next asked 1) if this mechanism could be playing a role in muscle, 2) if dysregulation of the NAD^+-dependent deacetylase SIRT1 could be a regulator of GLO1 via deacetylation, and 3) if acute exercise could modulate GLO1 acetylation thereby rescuing GLO1 protein expression. Our rationale for investigating SIRT1 as a potential role player in regulating GLO1 acetylation include its purported responsiveness to exercise [346, 347, 353, 354, 356, 359, 364, 375, 376] and its reliance on NAD^+ [287] which ties its activity not only to the redox status of the cell but also the energy status of the cell.

Interestingly, SIRT1 protein abundance was found to be significantly lower in OB compared to LH muscle which was positively correlated with GLO1 protein (Figure 4.2 A

and C). Lastly, there was a weak trend for GLO1 activity to be correlated with SIRT1 protein (Rho = 0.353, $p = 0.179$) which is in line with our observation of GLO1 and SIRT1 protein being positively correlated (Figure 4.2 C).

Given the relationships we observed between SIRT1 and GLO1, we next set out to determine if factors that regulate cellular NAD^+ and therefore have an indirect effect on the activity of NAD^+-dependent enzymes such as SIRT1 are altered with obesity. NAMPT is a critical enzyme in NAD^+ scavenging pathway. When enzymes such as SIRT1 utilize NAD^+ as a cofactor for its action, NAD^+ is consumed and NAM is produced as its byproduct. It is the role of NAMPT and the NAD^+ scavenging pathway to convert NAM back into NAD^+ to maintain cellular NAD^+ levels. However, there was no difference NAMPT protein abundance in OB muscle ($p = 0.25$, Figure 4.2 D). CD38 is another

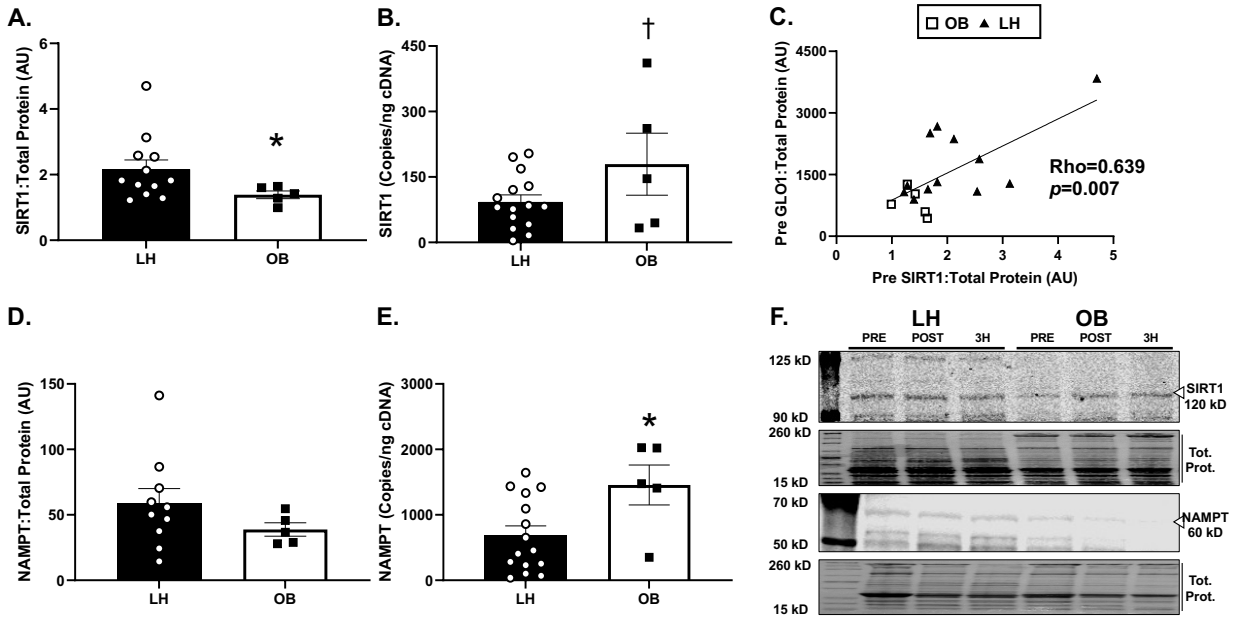

Figure 4.2 Effect of Obesity on Regulators of Acetylation and NAD^+ in Skeletal muscle. A) Obesity reduces NAD^+-dependent deacetylase SIRT1 protein but not B) transcripts. C) GLO1 and SIRT1 protein are positively correlated. D) Trend for lower NAMPT protein in OB muscle. E) NAMPT transcripts are elevated by obesity. F) Representative blots for SIRT1 and NAMPT proteins. Data in A, B, D and E were analyzed via T-Tests and are expressed as mean ± SEM. Correlation in C was analyzed by Spearman's Rho * $p < 0.05$. † $p = 0.09$.

regulator of cellular NAD^+. CD38 is a glycoprotein that plays roles in calcium signaling and cell adhesion. Importantly, CD38 also catalyzes the synthesis of ADP ribose and cADP ribose and in doing so consumes NAD^+. Elevations in immune cell CD38 has been implicated in promoting NAD^+ depletion in aging [317]. Therefore, we probed our samples for CD38 to determine if elevated CD38 could be affecting muscle NAD^+. However, there was no effect of OB on CD38 protein expression in these samples (Figure 4.3 A).

Acetylation is a balance between the rate of adding and removing acetyl-groups to targets. Acetyl groups can be added spontaneously under states of high cellular energy status during which the acetyl donor acetyl-CoA is likely to build up or enzymatically through action of acetyltransferases. P300 is an acetyltransferase that is relatively highly expressed in muscle and is necessary for muscle glucose uptake [377]. However, there was no difference in P300 protein in OB compared to LH muscle (Figure 4.3 B). Collectively these data implicate SIRT1 as a potential regulator of GLO1 acetylation in muscle while NAMPT, CD38 and P300 may not be implicated although a larger sample size is required to be confident in these observations

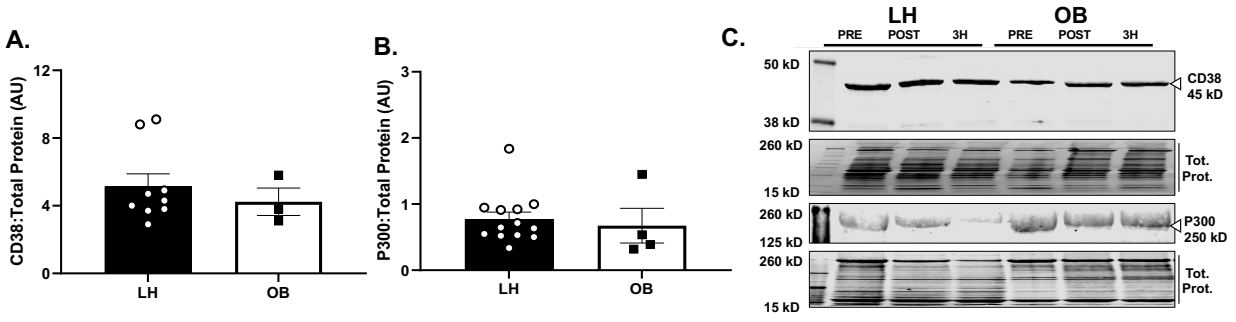

Figure 4.3 Effect of Obesity on CD38 and P300 in Skeletal muscle. A) NADase CD38 and B) Acetyltransferase P300 proteins are unaffected by obesity. G) Representative blots for proteins. Data were analyzed via T-Test and are expressed as mean ± SEM.

Exercise has many beneficial effects on whole body and skeletal muscle metabolism. However, the mechanisms by which the beneficial effects of exercise are instigated are not comprehensively understood although several lines of work have implicated SIRT1 to be involved in exercise-mediated metabolic adaptations. Our preliminary data corroborate this notion, demonstrating trend for an increase in SIRT1 protein following acute exercise in muscle from the OB cohort (Figure 4.4 A, Supplemental Figure 2).

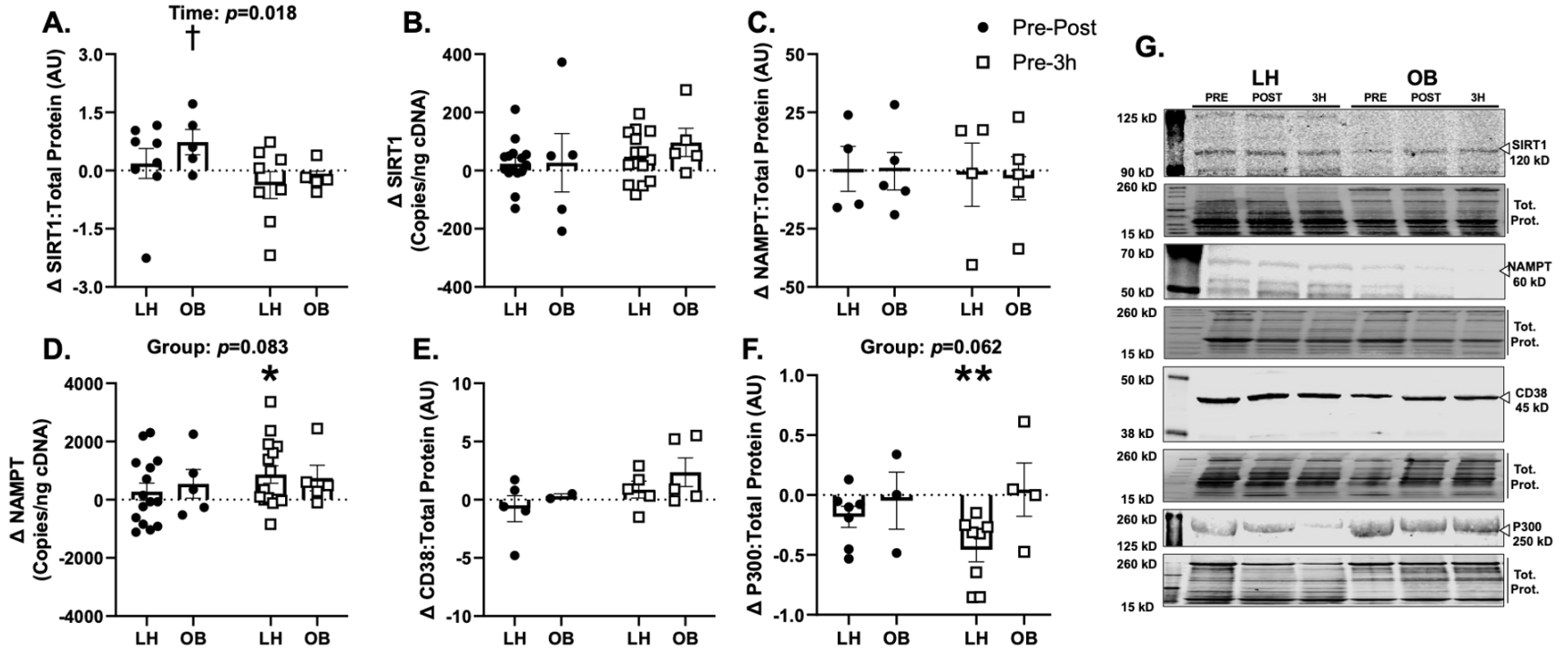

Figure 4.4 Effect of Acute Exercise on Regulators of Acetylation and NAD in LH and OB Participants. A) SIRT1 protein trended to increase 30 mins post exercise in the OB group (p = 0.103). There were no effects of acute exercise on B) SIRT1 transcripts, C) NAMPT protein, D) NAMPT transcripts, E) CD38 protein, or F) P300 Protein. G) Representative blots for protein outcomes. Data are represented as mean ± SEM. Delta data (represented) were analyzed by a 2x2 mixed model and data of individual timepoints (not shown) were analyzed by 3x2 mixed model with Bonferroni post hoc analysis.

However, despite the increase in SIRT1 protein we did not see a parallel increase in GLO1 protein or transcripts with acute exercise (Figure 4.5 A and B). In addition, NRF2 and KEAP1 protein and transcripts were unaltered by acute exercise (Supplemental Figure 1, Supplemental Figure 3). However, changes in abundance of some proteins following acute exercise may take longer than 3 hours following exercise. Post-translational modifications such as phosphorylation and acetylation on the other hand are likely to take place rapidly which may also affect GLO1 activity on a more rapid time scale. Therefore, we next set out to determine the effect of acute exercise on GLO1 activity, and acetylation status. In addition, we also aimed to determine if any of the other NAD^+ and acetylation regulating proteins we measured were altered by acute exercise as well.

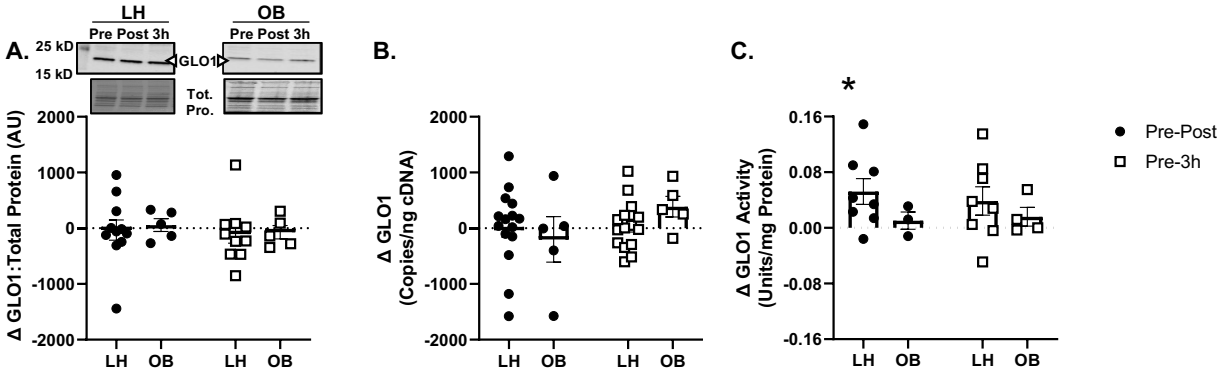

Figure 4.5 Effect of Acute Exercise on GLO1 in LH and OB Participants. A) GLO1 protein, B) Transcripts and C) Activity are unaffected by acute exercise within the 3 hours following the exercise bout in both the LH and OB groups. Data are represented as mean ± SEM. Delta data (represented) were analyzed by a 2x2 mixed model and data of individual timepoints (not shown) were analyzed by 3x2 mixed model with Bonferroni post hoc analysis.

Immunoprecipitation of acetylated proteins revealed a strong trend for deacetylation of GLO1 in OB muscle with acute exercise whereby acetylated GLO1 signal decreased by approximately 80% in the 30 minute and 3h post-exercise period (Figure 4.6 B, $p = 0.0889$). However, similar to GLO1 protein (Figure 4.5 A) and transcripts (Figure 4.5 B), there was no effect of the acute exercise on GLO1 activity in the OB muscle

(Figure 4.5 C). Interestingly, GLO1 activity was significantly increased 30 minutes post, acute exercise in the LH group only (Supplemental Figure 1F, $p = 0.0494$, Figure 4.5 C). Exercise had no effect of NAMPT protein in either group (Figure 4.4 C). However, NAMPT transcripts significantly increased in the LH group by 3h post exercise (Figure 4.4 D, $p = 0.037$). P300 was also reduced by 3h post exercise in the LH group only (Figure 4.4 F, $p = 0.0035$). Together these data suggest that attenuated SIRT1 may be related to diminished GLO1 protein expression in OB muscle. In addition, muscle from OB individuals seem to possess an impaired response to acute exercise compared to the LH group in regard to eliciting changes in GLO1 activity, P300 protein, and NAMPT transcripts. However, acute exercise was not able to rescue GLO1 protein within 3 hours post exercise despite a trend for the ability of GLO1 to be deacetylated in the OB muscle within that same time following exercise (Figure 4.6).

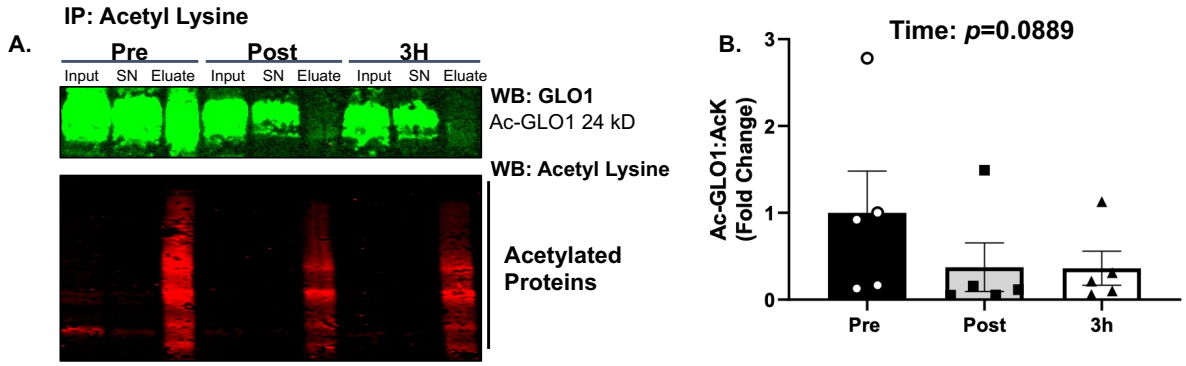

Figure 4.6 Effect of Exercise on GLO1 Acetylation. A) Representative image of immunoprecipitation of acetylated proteins and western blot for GLO1. B) Trend for reduced GLO1 acetylation in muscle from individuals with obesity. Data were analyzed via One-Way ANOVA with Repeated Measures and are expressed as mean ± SEM.

Regardless of the mechanisms and the potential effect of exercise, loss of GLO1 has been described to be detrimental to a number of cells and tissues. However, the consequences of muscle lacking GLO1 such as what these current data depict in obesity have not been well described. Therefore, given that loss of GLO1 protein was evident in

human muscle with obesity, we next aimed to determine if there was evidence for MG stress in the muscle and circulation with obesity. In addition, to gain an appreciation of the global proteomic consequences of GLO1 protein attenuation in human muscle, we also performed untargeted proteomic analyses on human immortalized skeletal muscles which had been treated with siRNAs against GLO1 to recapitulate the OB phenotype.

To examine the level of MG stress in muscle, we probed the LH and OB muscle for MG-modified proteins at baseline using a polyclonal antibody that we have previously validated [35]. Contrary to our hypothesis, there was a trend for MG-modified proteins to be lower in the OB compared to the LH muscle (Figure 4.7, $p = 0.09$). In addition, there

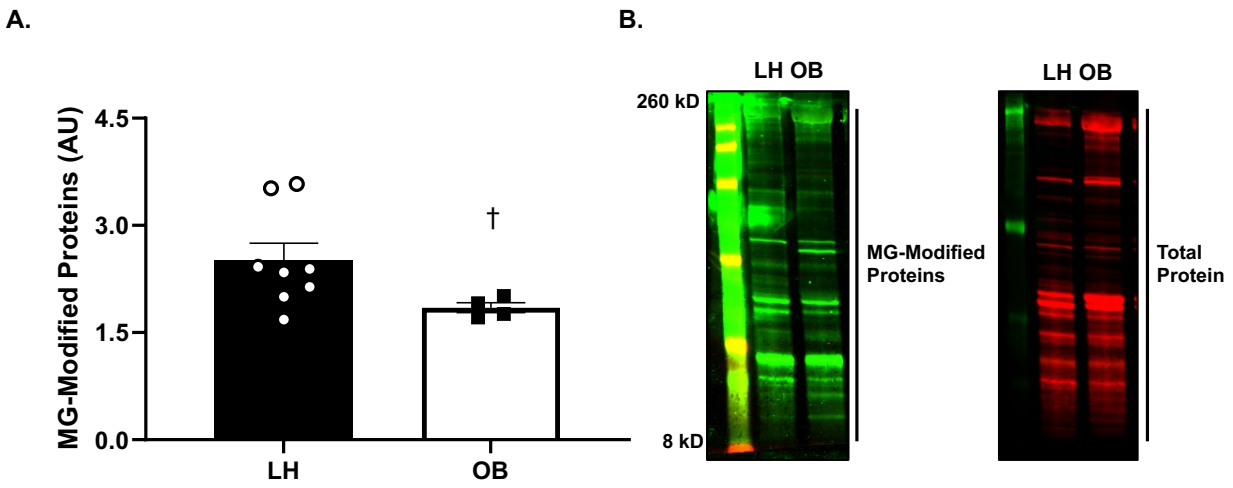

Figure 4.7 Effect of Obesity on Dicarbonyl Stress. A) No effect of obesity on MG-Modified proteins in skeletal muscle. B) Representative image of MG-Modified proteins in muscle. Entire lanes were quantified using EmpiriaStudio Software. Data were analyzed by T-Test and are expressed as mean ± SEM. † $p = 0.09$.

was no significant effect of obesity when we examined the plasma from LH and OB individuals for dicarbonyl derived AGE free-adducts such as G-H1, MG-H1, 3DG-H1, CML and CEL via LC-MS/MS (Table 8). We also measured circulating oxidative stress markers methionine sulfoxide (METSO) and aminoadipic acid (AAA) to assess if there was any evidence of increased oxidative stress in these individuals with obesity. Only

AAA was elevated with obesity (Table 8) which has been previously described in other investigations of obesity [378, 379]. Interestingly AAA is a product of lysine degradation, the primary target for acetylation and ubiquitination, and is also a target of MG-modification. Perhaps this may be interfering with quantifying MG modified proteins and AGE-free adducts involving lysines (CML) and can partially explain why we saw no difference in circulating or muscle derived evidence of MG stress.

	AGE FREE-ADDUCTS					OXIDATIVE STRESS MARKERS	
GROUP	**G-H1 (nM)**	**MG-H1 (nM)**	**3DG-H (nM)**	**CML (nM)**	**CEL (nM)**	**METSO (nM)**	**AAA (nM)**
LH	9.4 ± 0.7	189 ± 44.7	307 ± 42.0	86.9 ± 10.3	55.8 ± 6.7	671 ± 33.6	749 ± 58.1
OB	9.9 ± 1.3	143 ± 39.3	333 ± 24.4	96.0 ± 13.7	60.0 ± 11.4	1253 ± 488.4	1248 ± 123.8**

Table 8 Circulating AGE Free-Adducts and oxidative stress markers are largely unaffected by obesity. Data were analyzed via T-Test and are expressed as mean ± SEM. ** $p < 0.01$.

While the consequences of dicarbonyl stress as a result of cells, or animals lacking GLO1 has been well described, little is known about the global proteomic consequence of GLO1 attenuation in muscle and there is no data on this topic in human muscle. To fill this gap, we cultured human immortalized myoblasts which we differentiated into myotubes before treating them with siRNAs against GLO1 or non-specific scRNAs for 72 hours. KD was confirmed via western blot demonstrating a 50% reduction in GLO1 protein was achieved (a similar attenuation to what we observed in muscle from individuals with obesity) (Figure 4.8 A). Unsupervised hierarchical clustering was performed to demonstrate proteomic variability between technical replicates (Figure 4.8 B). In a similar investigation in rat L6 myotubes [12], several collagen proteins were significantly elevated in the GLO1 KD indicating increased fibrosis of the tissue. Gene ontology enrichment analysis demonstrated significant upregulation in pathways involved in NF-kappa B signaling apoptosis and cell death (Figure 4.8 D, Table 9). Pathways down regulated with GLO1 KD included those involved in muscle structure, development and contraction (Figure 4.8 D, Table 9).

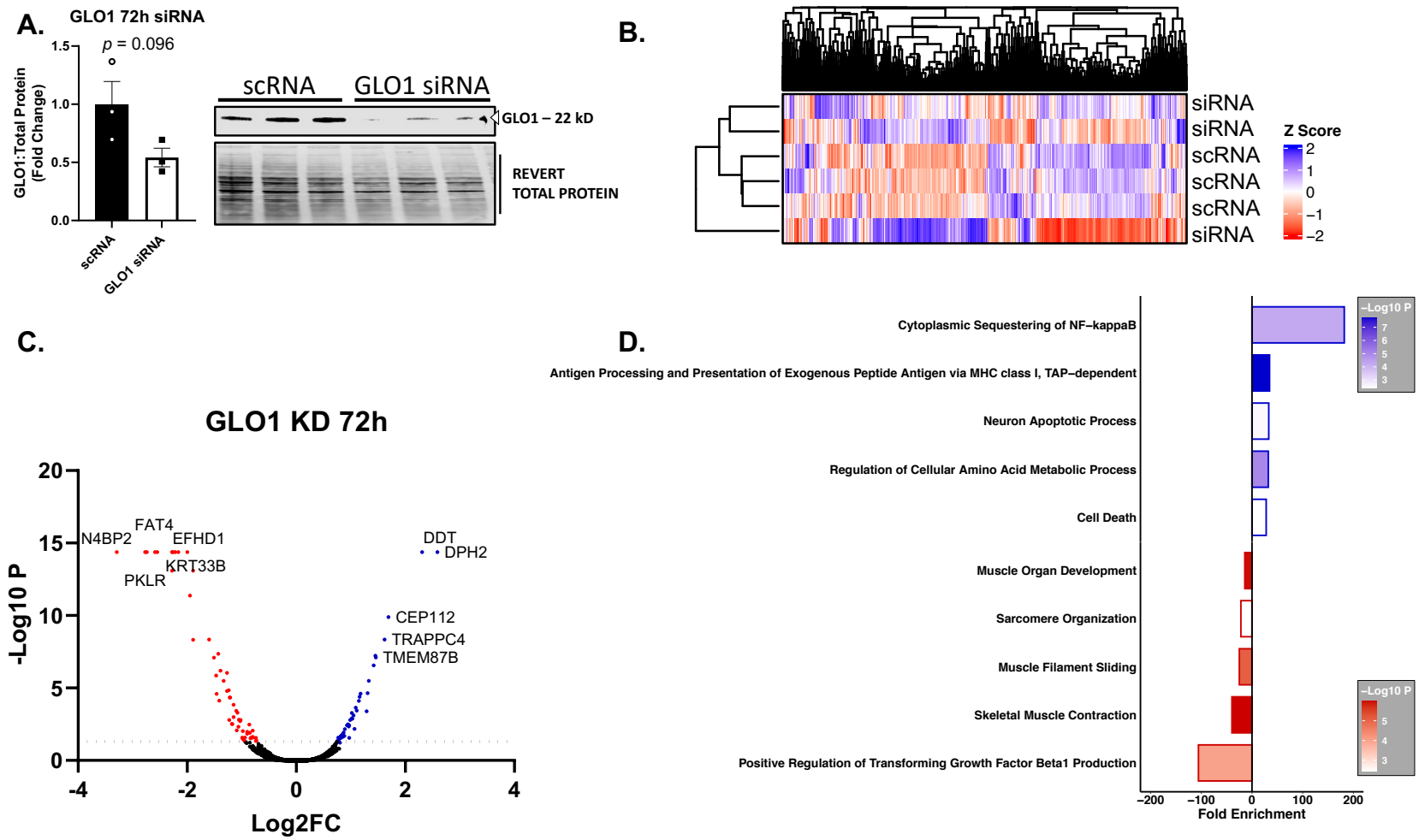

Figure 4.8 Proteomic consequences of 72h GLO1 siRNA in Human Immortalized Myotubes. A) Western blotting confirmation of GLO1 protein knock down with siRNA. B) Unguided hierarchical clustering on all proteins identified in each experimental replicate. C) Volcano plot of proteins. Dotted line cut of set to $p = 0.05$, red dots indicate significantly changed proteins. Gene ontology enrichment analysis of top 10 upregulated and top 10 down regulated pathways.

Term	Fold Enrichment	P-Value	Benjamini	Direction	Proteins
Cytoplasmic Sequestering of NF-kappaB	136.5	1.4E-02	3.6E-01	Up	FAF1, G3BP2
Positive Regulation of Transforming Growth Factor Beta1 Production	105.6	1.8E-02	1.0E+00	Down	ATP6AP2, SERPINB7
Skeletal Muscle Contraction	39.6	2.5E-03	4.7E-01	Down	CHUK, MYH3, TNNC2
Antigen Processing and Presentation of Exogenous Peptide Antigen via MHC class I, TAP-dependent	26	4.5E-04	9.7E-02	Up	B2M, PSMA3, PSMA5, PSMB1
Muscle Filament Sliding	25	6.2E-03	7.4E-01	Down	MYH3, NEB, TNNC2
Neuron Apoptotic Process	24.8	7.6E-02	9.1E-01	Up	BNIP3, CASP7
Regulation of Cellular Amino Acid Metabolic Process	24.1	6.6E-03	3.6E-01	Up	PSMA3, PSMA5, PSMB1
Sarcomere Organization	21.9	8.6E-02	1.0E+00	Down	LMOD2, MYH3
Cell Death	21	8.9E-02	1.0E+00	Up	BNIP3, FAF1
NIK/NF-kappaB Signaling	18.6	1.1E-02	3.6E-01	Up	PSMA3, PSMA5, PSMB1

Table 9 Top 10 Enriched Gene Ontology Pathways. Significantly altered proteins were entered into DAVID for gene ontology enrichment analysis. The top ten most enriched pathways and the proteins in those pathways that changed are presented.

Collectively the in vivo data demonstrate evidence for lower GLO1 protein and activity in skeletal muscle with obesity which may be related to attenuated SIRT1 expression. In addition, there was a trend for acute exercise was to promote deacetylation of GLO1 in OB muscle although acute exercise was unable to increase GLO1 protein or activity in OB muscle. However, acute exercise increased GLO1 activity in LH muscle suggesting a discrepancy in exercise response with obesity. Lastly, MG-modified proteins were not exacerbated in OB muscle however, human immortalized myotubes suggest that lack of GLO1 is damaging to muscle, promoting impaired structural proteins and evoking proteins involved in the NF-κB inflammatory pathway and proteasomal degradation pathway.

4.1.2 Results Pertaining to Aim 2

Given the implications of our human data suggesting SIRT1 to potentially regulate GLO1 and the importance of GLO1 for muscle function, we next aimed to test the hypothesis that NAD^+ and SIRT1 are necessary for GLO1 stability and activity in muscle. To address this aim we employed the use of our human immortalized myotube culture to perform loss of function and gain of function experiments. To test the effect of NAD^+ on GLO1 abundance and activity we treated cells with a potent and selective inhibitor of NAMPT, FK866. Inhibition of NAMPT via FK866 treatment has been previously demonstrated to reliably deplete NAD^+ in several tissues and cell lines including mouse primary muscle cells and C2C12 myotubes [323]. However, this has not yet been exemplified in human muscle cells. As a gain of function experiment, we attempted to rescue the FK866 treatment by co-treating cells with the NAD^+ precursor NR which is converted into NAD^+ via a parallel mechanism that does not rely on NAMPT activity.

Contrary to our hypothesis, FK866 treatment had no effect on GLO1 protein expression (Figure 4.9 A) or activity (Figure 4.9 G) in human immortalized myotubes. However, co-treatment of myotubes with NR elevated GLO1 protein approximately 50% above control suggesting that augmenting NAD^+ in the cell may enhance GLO1 protein while FK866 does not seem to have an effect ($p < 0.05$, Figure 4.9 A). Interestingly treating the cells with FK866 alone (~2.5-fold) and in combination with NR (~4.5-fold) resulted in a trend or significant increases in NAMPT protein respectively (Figure 4.9 B) without increasing NAMPT transcripts (Figure 4.10 B). These data suggest that these immortalized myotubes may stabilize NAMPT protein to compensate for NAMPT inhibition and protect NAD^+ concentration and that NR may also augment NAMPT stability. Similarly, SIRT1 protein was increased in cells co-treated with FK866 and NR (Figure 4.9 C) despite having no effect on SIRT1 transcripts (Figure 4.10 C). This may have only been observed in the NR co-treated cells since they trended to experience the largest increase in NAMPT protein which has been previously described to augment SIRT1 through a mechanism that has not yet been fully elucidated [380].

SIRT1 has been shown to deacetylate NRF2 and enhance its transcriptional activity by promoting its translocation to the nucleus [65, 167, 168]. Therefore, we next sought to determine if NRF2/KEAP1 protein or mRNA levels were altered with FK866 or co-treatment with NR. FK866 and co-treatment with NR also did not have any effects on NRF2 and KEAP1 protein (Figure 4.9 D and E) or GLO1 transcripts (Figure 4.10 A). NRF2 and KEAP1 transcripts were also unaltered (Figure 4.10 D and E) although FK866 and co-treatment with NR increased the ratio of NRF2:KEAP1 transcripts (Figure 4.10 F) likely primarily a result from slight decreases in KEAP1 transcripts.

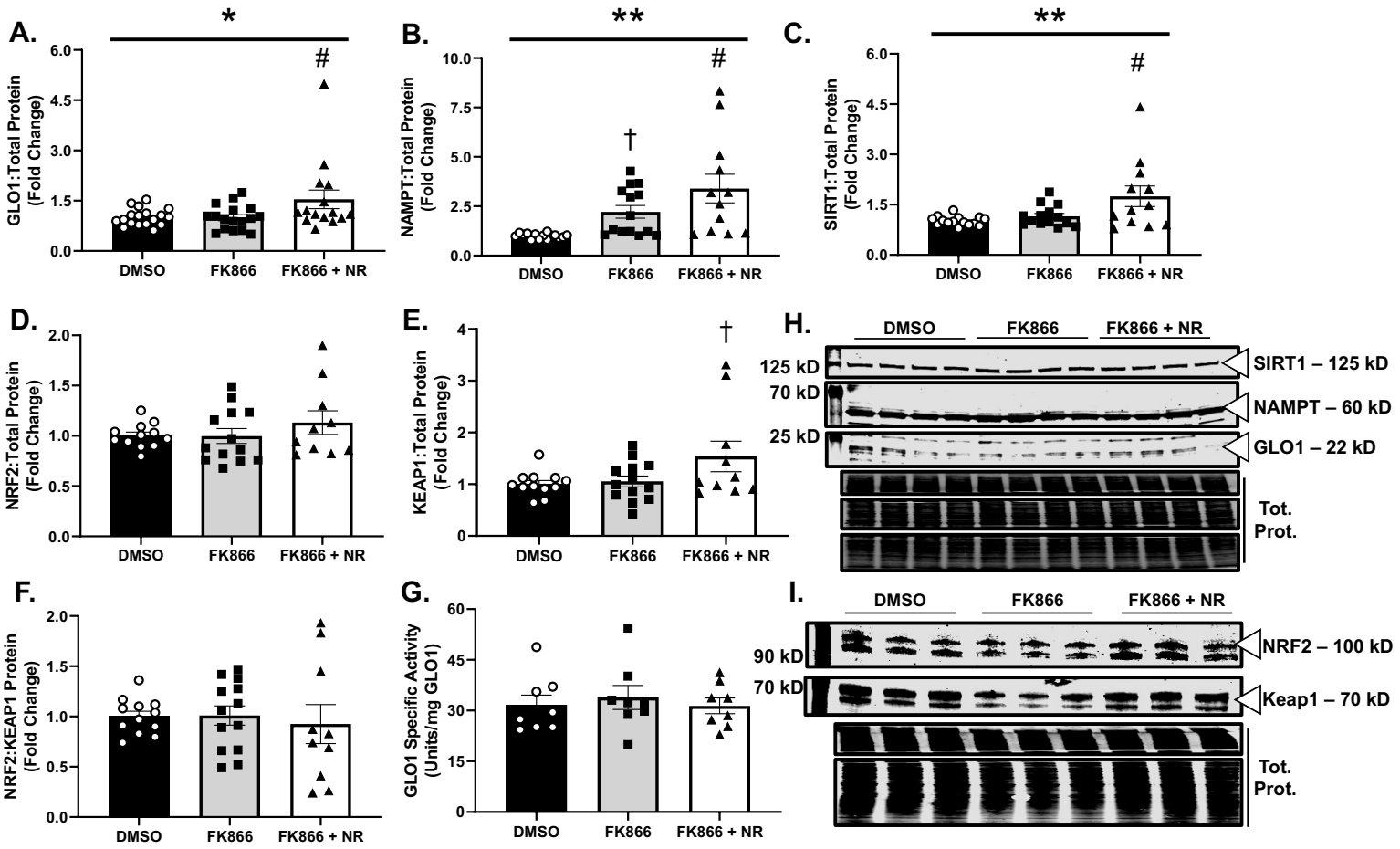

Figure 4.9 Effect of NAMPT Inhibition and NR on GLO1 Protein in Human Immortalized Myotubes. Human immortalized myotubes were treated for 48 hours with DMSO, 50 nM FK866, or 50 nM FK866 + 0.5 mM NR. A) GLO1 protein expression. B) NAMPT protein expression. C) SIRT1 protein expression. D) NRF2 protein expression. E) Keap1 protein expression. F) Ratio of NRF2:Keap1 protein. G) GLO1 specific activity. H) Representative western blot for proteins quantified in A – C. I) Representative western blot for proteins quantified in D and E. All western blot data are expressed as average fold change from DMSO ± SEM. Data analyzed via ANOVA: ** Significant main effect ($p < 0.01$), * Significant main effect ($p < 0.05$), # Significant difference vs. DMSO ($p < 0.05$), † Trend for significant difference vs. DMSO ($p = 0.07$).

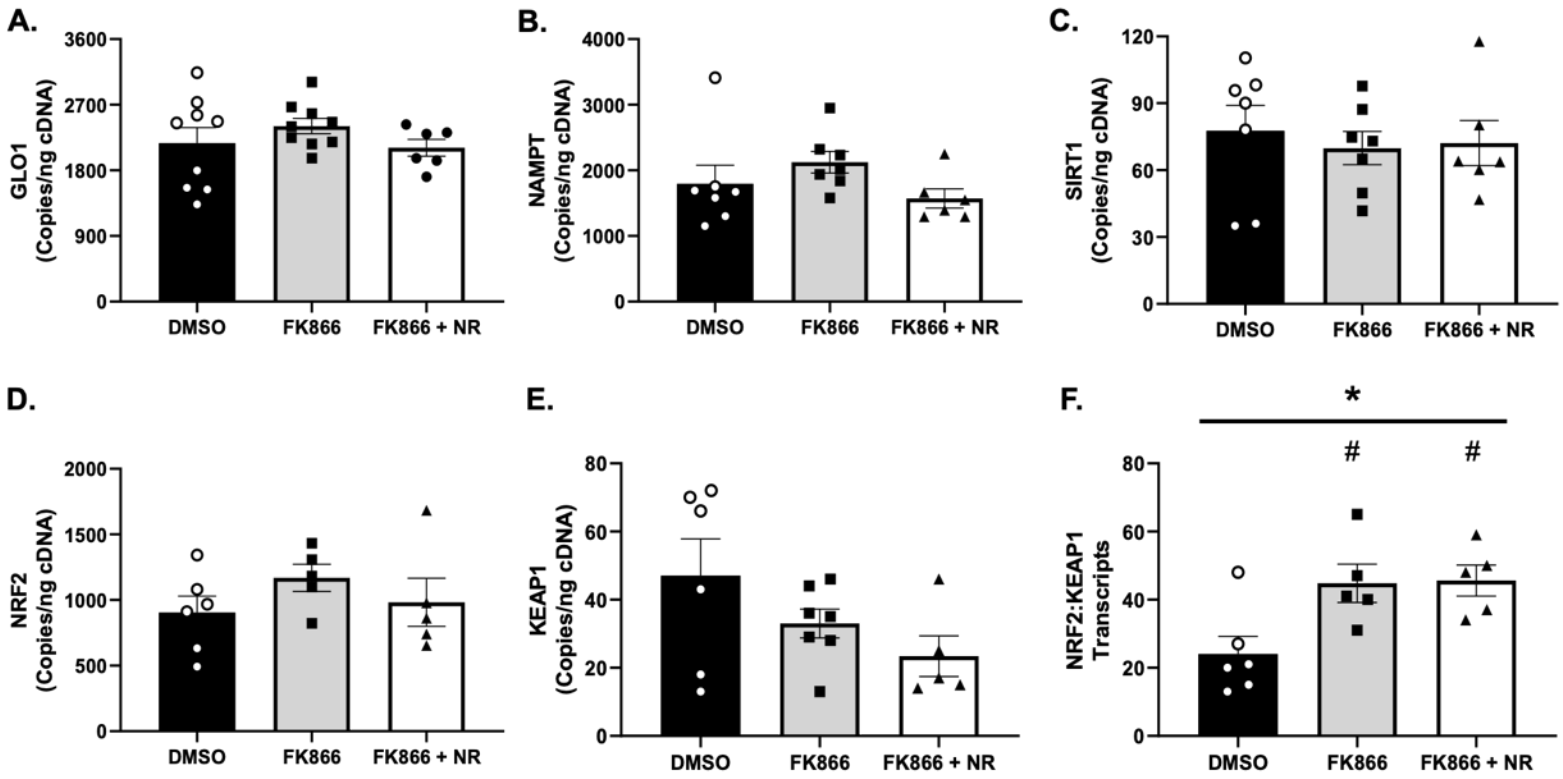

Figure 4.10 Effect of NAMPT Inhibition and NR on GLO1 Transcripts in Human Immortalized Myotubes. Human immortalized myotubes were treated for 48 hours with DMSO, 50 nM FK866, or 50 nM FK866 + 0.5 mM NR. Transcripts were quantified via droplet digital PCR with 6 ng cDNA input per reaction. A. GLO1 transcripts. B. NAMPT transcripts. C. SIRT1 transcripts. D. NRF2 transcripts. E. KEAP1 transcripts. F. Ratio of NRF2:KEAP1 transcripts. All data are expressed as average copies/ng cDNA input ± SEM. Data analyzed via ANOVA: * Significant main effect ($p < 0.05$), # Significant difference vs. DMSO ($p < 0.05$).

Using a similar immunoprecipitation strategy that was employed in the human samples demonstrated no effect of FK866 or co-treatment with NR to alter GLO1 acetylation (Figure 4.11). To examine the effect of FK866 and co-treatment with NR on GLO1 ubiquitination, we also immunoprecipitated GLO1 from human immortalized myotubes after treating cells with the proteasome inhibitor MG132 along with DMSO, FK866 or FK866 with NR. Neither FK866 nor co-treatment with NR had any effect on GLO1 ubiquitination (Figure 4.12). This is in agreement with the lack of change in GLO1 acetylation, protein abundance and specific activity. These western blot data were further confirmed via untargeted proteomic analysis where GLO1 protein was unchanged in FK866 treated myotubes, myotubes cotreated with FK866 and NR and NAMPT KD myotubes (Supplemental Figure 10, Supplemental Figure 11, Supplemental Figure 12, Supplemental Figure 13, Supplemental Figure 15). Together these data do not implicate NAMPT in the regulation of GLO1 protein, activity, acetylation or ubiquitination.

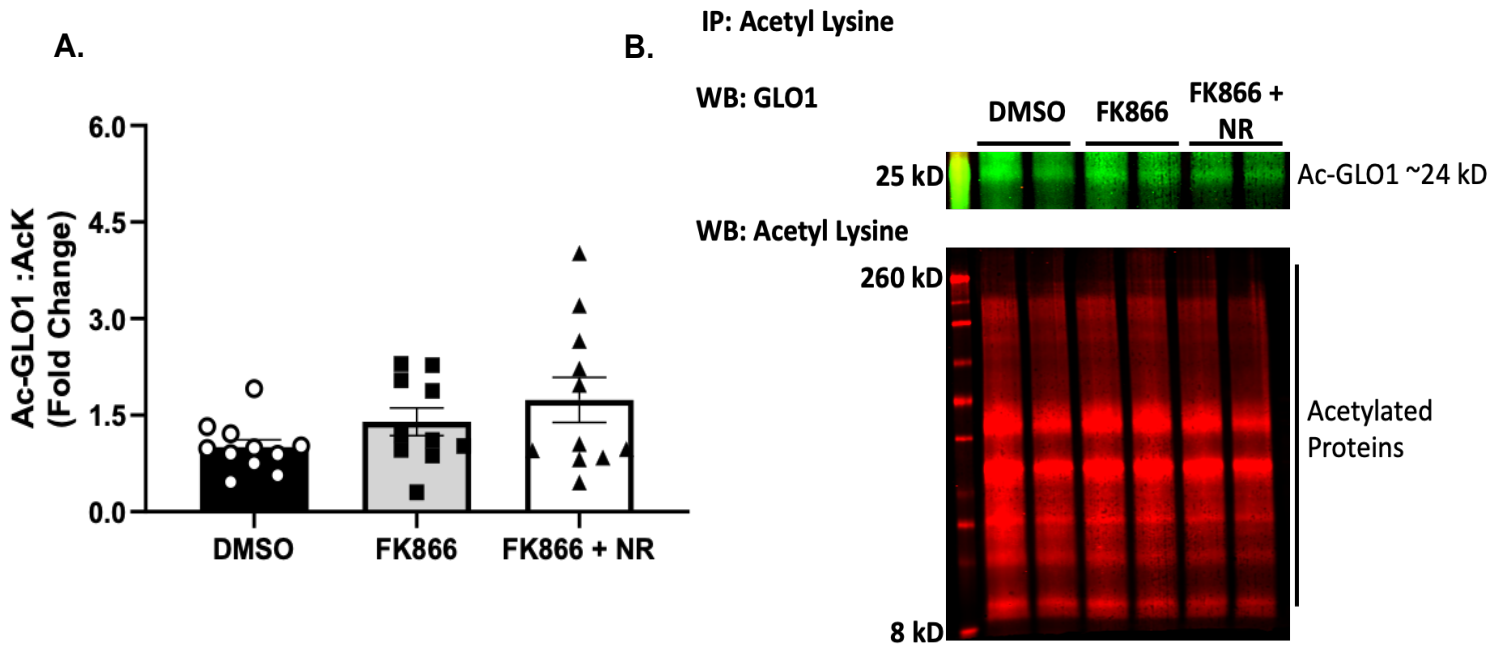

Figure 4.11 Effect of NAMPT Inhibition and NR on GLO1 Acetylation in Human Immortalized Myotubes. A) Acetylated GLO1 from acetyl lysine (AcK) immunoprecipitation (IP). B) Representative western blot of GLO1 and AcK in AcK IP eluates. All data are expressed as average fold change from DMSO ± SEM. Data analyzed via ANOVA.

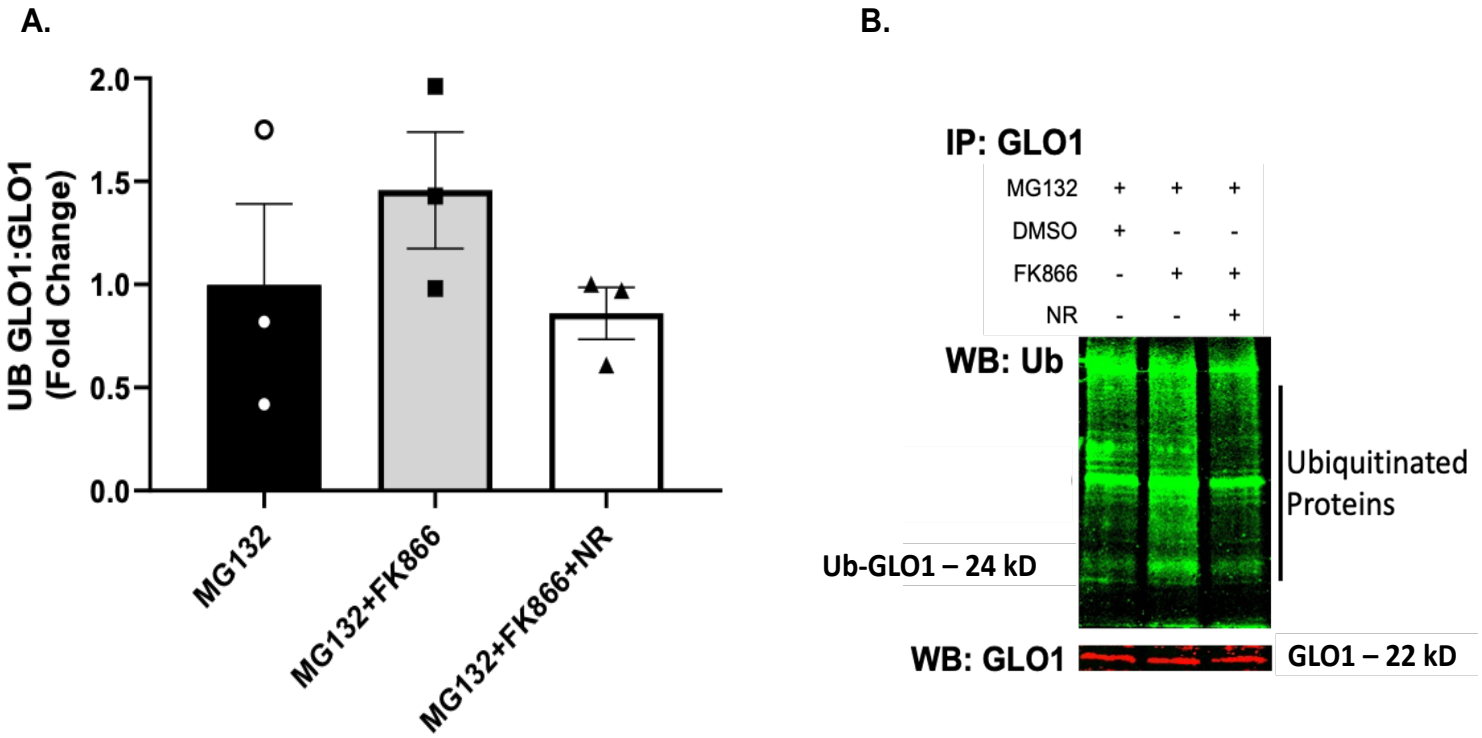

Figure 4.12 Effect of NAMPT Inhibition and NR on GLO1 Ubiquitination in Human Immortalized Myotubes. A) Ubiquitinated (UB) GLO1 from GLO1 IP from human immortalized myotubes treated with the proteasome inhibitor MG132. B) Representative western blot of GLO1 and ubiquitin in GLO1 IP eluates. All data are expressed as average fold change from DMSO ± SEM. Data analyzed via ANOVA.

To determine if SIRT1 is necessary for GLO1 abundance, activity, or acetylation we next performed SIRT1 KD experiments in human immortalized myotubes. SIRT1 KD successfully depleted cells of SIRT1 protein and transcripts by over 90% (Figure 4.13 C). However, SIRT1 KD did not have any effect on GLO1 protein (Figure 4.13 A), transcripts (Figure 4.14 A), or specific activity (Figure 4.13 G). In addition, SIRT1 KD did not have an effect on NAMPT, NRF2, or KEAP1 protein (Figure 4.13) or transcripts (Figure 4.14). Lastly, we again employed acetyl lysine IP to determine if SIRT1 KD promoted GLO1 acetylation. Similar to FK866-treated cells, SIRT1 KD did not affect GLO1 acetylation (Figure 4.15).

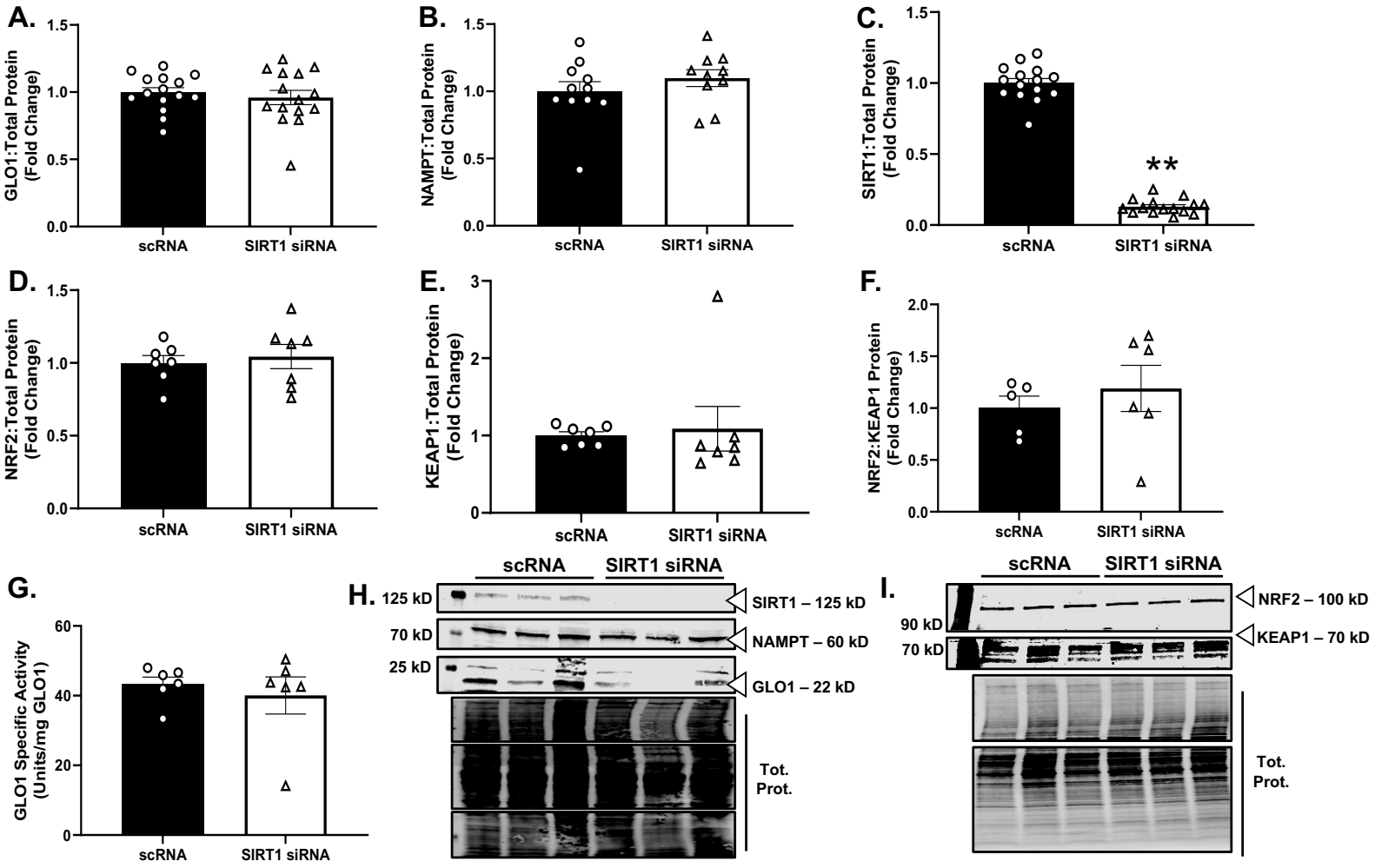

Figure 4.13 Effect of SIRT1 KD on GLO1 in Human Immortalized Myotubes. Human immortalized myotubes were treated with scRNA or SIRT1 siRNA for 48 hours. A. GLO1 protein expression. B. NAMPT protein expression. C. SIRT1 protein expression. D. NRF2 protein expression. E. KEAP1 expression. F. Ratio of NRF2:KEAP1 protein. G. GLO1 specific activity. H. Representative western blot for proteins quantified in A – C. I. Representative western blot for D and E. All data are expressed as average fold change from DMSO ± SEM. Data analyzed via T-TEST ** $p < 0.01$.

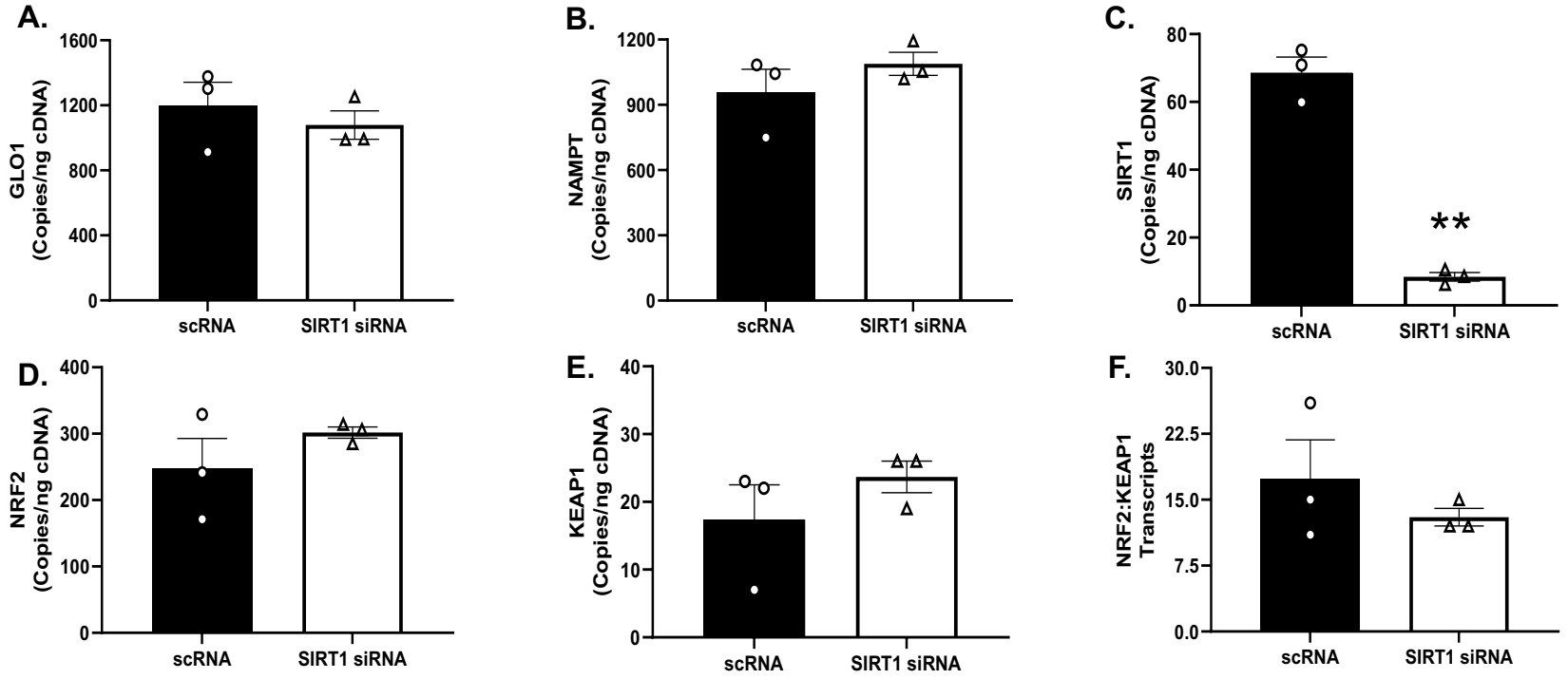

Figure 4.14 SIRT1 KD on GLO1 Transcripts in Human Immortalized Myotubes. Human immortalized myotubes were treated with scRNA or SIRT1 siRNA for 48 hours. Transcripts were quantified via droplet digital PCR with 6 ng cDNA input per reaction. A. GLO1 transcripts. B. NAMPT transcripts. C. SIRT1 transcripts. D. NRF2 Transcripts. E. KEAP1 Transcripts. F. Ratio of NRF2:Keap1 transcripts. All data are expressed as average copies/ng cDNA input ± SEM. Data analyzed via ANOVA: ** Significant effect ($p < 0.01$).

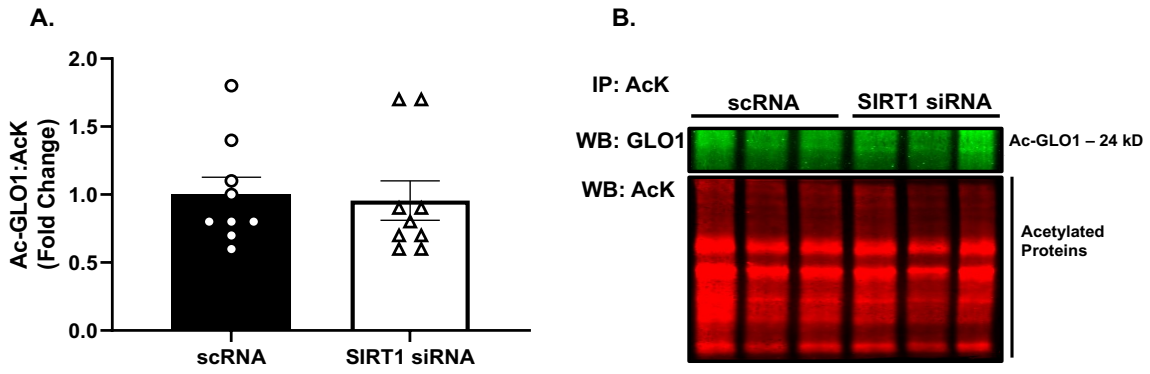

Figure 4.15 Effect of SIRT1 KD on GLO1 Acetylation in Human Immortalized Myotubes. A) Acetylated GLO1 from acetyl lysine (AcK) immunoprecipitation (IP). B) Representative western blot of GLO1 and AcK in AcK IP eluates. All data are expressed as average fold change from DMSO ± SEM. Data analyzed via ANOVA.

Collectively, these data do not support NAMPT inhibition or SIRT1 as regulators of GLO1 acetylation, stability, or activity. However, augmenting NAD via NR positively influenced GLO1 stability suggesting that some NAD^+ sensitive factor may be regulating this effect.

To explore other potential factors that may be regulating GLO1 acetylation we next employed a mini-screen of inhibitors against selective deacetylases and acetyltransferases in human immortalized myotubes. Human immortalized myotubes were treated with an inhibitor against the primary cytosolic sirtuin SIRT2, NAM which in relatively high doses acts as a sirtuin inhibitor, an HDAC inhibitor, and inhibitors against the acetyltransferases GCN5 and P300 (Figure 4.16). Although none of these treatments resulted in effects that reached significance (likely due to low sample size) some interesting trends did emerge. Inhibition of SIRT2 trended to increase GLO1 protein by approximately two-fold (Figure 4.16 A). However, GLO1 specific activity was reduced by approximately half in these samples (Figure 4.16 B). Conversely, global inhibition of sirtuins via treatment with NAM did not significantly alter GLO1 abundance (Figure 4.16 A) but appeared to double GLO1 specific activity (Figure 4.16 B). Inhibition of the

acetyltransferases P300 and GCN5 had opposite effects on GLO1 protein whereby P300 inhibition increased GLO1 protein by nearly 3-fold and GCN5 did not appear to appreciably alter GLO1 protein (Figure 4.16 A). However, inhibition of P300 had no effect

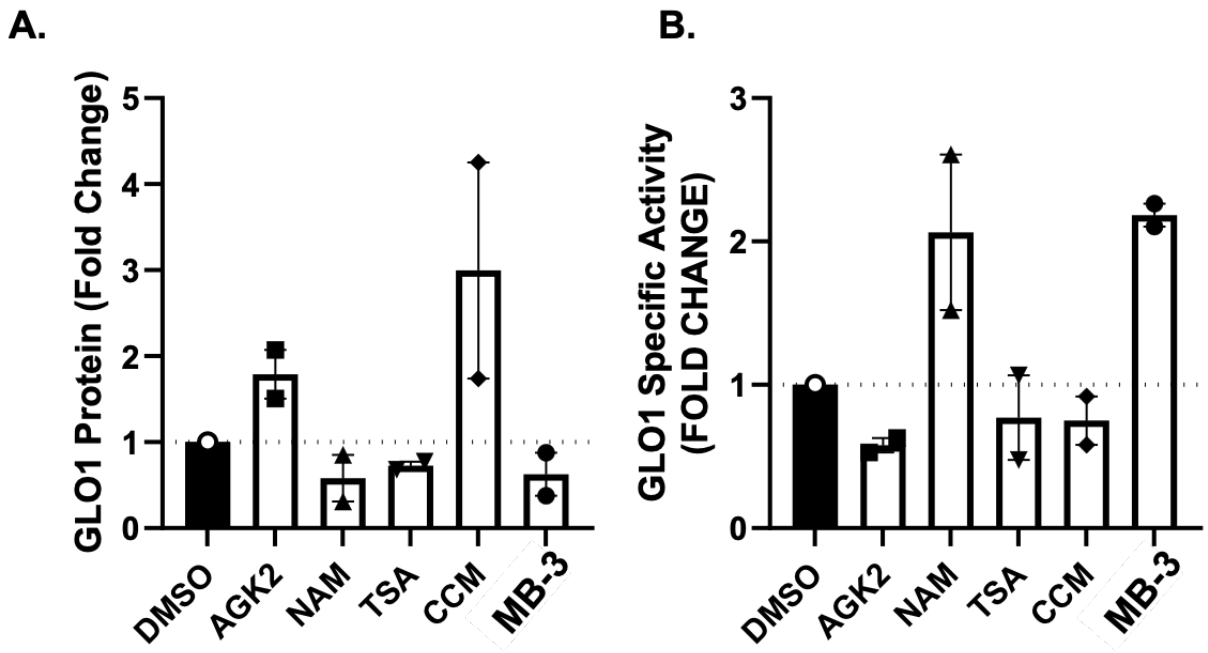

Figure 4.16 Lysine Deacetylase and Acetyltransferase Inhibitor Screen. Human Immortalized Myotubes were treated for 24 hours with inhibitors against A) SIRT2 (AGK2: 25 μM), B) All Sirtuins (NAM: 25μM), C) All HDACs (TSA: 0.25 μM), D) P300 (CCM: 10 μM), and E) GCN5 (MB-3: 10 μM). All samples were assayed for protein (A) and specific activity (B). Data analyzed via independent T-Tests and are represented as mean ± SEM.

on specific activity whereas inhibition of GCN5 improved GLO1 specific activity by approximately 2-fold (Figure 4.16 B). These data provide some insight into potential acetylation regulatory mechanism but also serve to further demonstrate how complex even a common PTM such as acetylation can be for this protein.

Chapter 5

Discussion

5.1 Overview

As of 2020 more than 40% of US adults are obese and recent predictions project that by 2030 the prevalence in the US will reach approximately 50% with 25% of those cases being classified as severe obesity (BMI $\geq$ 35 kg/m^2) [381]. Obesity increases the risk to develop T2D by up to 23% [2, 382] and increases the risk of all-cause mortality by up to 18% [22]. Muscle is a significant tissue in the regulation of plasma glucose, accounting for >80% of insulin stimulated glucose uptake [383]. In addition, being the source of locomotion, the metabolic demand of muscle scales with intensity of exercise, promoting non-insulin mediated glucose uptake and increased sensitization of the muscle to insulin with acute exercise [31]. Lastly, repeated acute exercise bouts over time promote numerous important training adaptations to augment skeletal muscle metabolism and improve insulin sensitivity. In general, these beneficial metabolic adaptations include increased oxidative phosphorylation, increased metabolic efficiency via reliance on lipid substrates, increased muscle perfusion, and increased muscle hypertrophy (reviewed in [384]). These molecular adaptations converge to promote numerous health benefits including improved insulin sensitivity and for this reason is the first line-therapy for the prevention and treatment of metabolic disease. However, while great strides have been made of late to uncover the molecular underpinnings of obesity-mediated metabolic dysfunction as well as the mechanisms that may prevent or reverse

these maladaptive events, our current knowledge still falls short of comprehensively understanding these processes.

For example, the role of the glyoxalase enzymatic system and dicarbonyl stress in muscle is an understudied potential contributor to the pathogenesis of metabolic dysfunction in the context of obesity. Increasing pre-clinical evidence suggests that loss of GLO1 may be a causal factor involved in the development of insulin resistance and T2D [99, 149]. Previously, our lab demonstrated that muscle from individuals with T2D had lower GLO1 protein and increased MG-mediated dicarbonyl stress which was correlated to BMI and insulin resistance [35]. To expand on our previous report, the current investigation aimed to determine if GLO1 protein was attenuated in individuals with obesity prior to the onset of T2D. In addition, we tested if GLO1 protein, transcripts or activity are augmented by an acute aerobic exercise bout and lastly, we sought to test the potential role of NAD-bioavailability, SIRT1 and GLO1-acetylation for the regulation of GLO1 protein abundance and activity.

5.2 Discussion Regarding Findings Pertaining to Aim 1

5.2.1 GLO1 Attenuation with Obesity

Here we present the first evidence of a ~50% reduction in GLO1 protein expression in skeletal muscle from normo-glycemic individuals with obesity compared to age-matched, lean, healthy individuals. We also found a trend for reduced GLO1 activity in muscle from individuals with obesity although these data normalize if made relative to GLO1 protein expression suggesting that the lack of GLO1 protein is driving attenuated GLO1 protein activity in muscle. Similar to our previous findings, we also found GLO1 protein expression to be negatively correlated with BMI and fasting insulin suggesting that

attenuation of GLO1 is related to degree of obesity and insulin sensitivity. Trends for similar correlations were also observed for GLO1 activity (GLO1 activity:. BMI: Rho = -0.404, p = 0.109; GLO1 activity:. BF%: Rho = -0.458, p = 0.096) The participants studied here-in are likely in a precarious stage of obesity characterized by elevated fasting hyperinsulinemia which serves to compensate for the subclinical peripheral insulin resistance to maintain normal fasting blood glucose levels. It is therefore not unreasonable to hypothesize that this fasting and post-prandial hyperinsulinemia is able to maintain or exacerbate glycolytic flux in muscle resulting in dicarbonyl stress due to the lack of GLO1 observed here. In support of this hypothesis, recent work has shown that MG AUC during an OGTT or mixed-meal test is exacerbated with obesity and T2D compared to lean healthy individuals and that this increase in MG production can be rescued with weight loss [113, 114].

5.2.2 Consequences of Attenuated GLO1 in Muscle

5.2.2.1 Dicarbonyl Stress

While, the source(s) of this exacerbated MG production has not been identified, the muscle may be a primary contributor due to its large contribution in post-prandial glucose disposal and the attenuation of GLO1 that we have observed. In addition to contributing to circulating dicarbonyl stress, the attenuation of GLO1 protein in the muscle has the potential to promote dicarbonyl stress in the muscle itself, which may manifest as increased modification of proteins by MG. However, when we measured plasma AGE-free adducts including those derived from MG we found no difference between the groups. AGE-free adducts are amino acids that have been modified and appear in circulation or interstitial spaces largely as a result of turnover of damaged proteins [6].

AGE-free adducts have been demonstrated to be indicative of fasting and post-prandial glycemia in patients with diabetes [104]. However, our group has recently shown that individuals with obesity maintain the capacity to clear AGE-free adducts in the urine [103]. In addition, during a hyperglycemic challenge we found that clearance of AGE-free adducts was increased to maintain stable circulating values of these metabolites which may explain why we observed no difference in fasting AGE-free adducts between groups in this cohort [103]. Similarly, when we probed the muscle for MG-modified proteins there was no significant difference in muscle from OB compared to LH individuals. As previously mentioned, these MG-modified proteins are targeted for proteolysis so that they can be cleared and replaced by new undamaged proteins. Interestingly, while not significant the MG-modified proteins was trending to be lower (p = 0.09) in the OB compared to LH muscle which may indicate and increase in proteolysis and clearance of these proteins. Another caveat to consider is that MG modifies other metabolites as well such as DNA, lipids and glutathione which are not captured with the assay we used. Lastly, GLO1 KO models in mice have demonstrated the ability to compensate for a loss of GLO1 by upregulating other detoxification mechanisms such as ALDH or AKR enzymes [148]. A similar phenomenon could be happening in these samples however we did not measure these targets. In the future, measurements of the dicarbonyl MG in muscle will be more informative especially in the context of time course during a metabolic challenge (e.g. OGTT, MMT etc.) than our static measurement of MG-modified proteins to gain insight on the potential dicarbonyl stress consequences of the observed reduction in GLO1.

5.2.2.2 Proteomic Consequences

To gain insight into the potential proteomic consequences of muscle lacking GLO1 we performed siRNA GLO1 KD experiments in human immortalized myotubes for 72 hours which were then analyzed by TMT LC-MS/MS. Conveniently, our siRNA experiments promoted an attenuation of GLO1 to a similar extent as that observed in the OB muscle (~50%). GLO1 KD most profoundly promoted increases in several proteasomal subunits (PSMA3, PSMA5, PSMB1) as well as factors associated with cell death and apoptosis such as BNIP3 and CASP7. Increased proteasomal assembly could be a result of increased dicarbonyl stress necessitating turnover of MG-modified proteins. In addition, one of the most significantly and dramatically reduced protein was PK-LR which are isoenzymes of pyruvate kinase canonically found in the liver (L-isozyme) and red blood cells (R-isozyme). The PKLR is the gene for these isozymes from which the L- or R-isozyme emerges from alternative splicing. PKM is the more abundant pyruvate kinase isozyme found in muscle and while PKM's abundance was approximately 167-fold higher than that of PKLR in our scRNA we did not observe a significant change in PKM with the GLO1 KD. While the relevance of PK-LR in muscle is not yet appreciated, a decrease of this protein could indicate a shift away from glycolytic metabolism which could limit MG flux. This was paralleled by downregulations of TNNC2 and MYH3 which are isoforms of troponin and myosin heavy chain typically found in glycolytic type II muscle fibers. Collectively, these proteomic data suggest that lack of GLO1 in muscle may promote a switch away from glycolytic metabolism and fast twitch muscle fiber programing to prevent MG flux. However, these data also demonstrate that lack of GLO1 rapidly (within 72 hours) also promotes apoptotic signaling mechanisms suggesting that

at least *in vitro* these compensatory mechanisms are not sufficient. Interestingly, we did not observe any increase in other MG detoxifying enzymes such as ALDH or AKR isoforms that have previously been described to occur in mouse muscle. To our knowledge these are the first data examining the proteomic consequences of GLO1 KD in human muscle. Previous reports have examined the effect of GLO1 KD in rat L6 myotubes and found increased fibrosis and collagen proteins which were not apparent in our human myotubes. Together these data demonstrate that loss of GLO1 protein appears to occur with obesity prior to onset of overt metabolic dysfunction and that while there is no apparent increase in MG-modification, *in vitro* models demonstrate the potential for loss of GLO1 to promote dramatic disruptions to the skeletal muscle metabolism and health.

5.2.3 Potential Mechanisms of Regulating GLO1 in Muscle

Given this evidence of GLO1 attenuation occurring in individuals with obesity who are otherwise relatively healthy and the purported negative proteomic consequences of this event, uncovering the mechanism of GLO1 attenuation in muscle may be important for developing novel strategies for the prevention of disease progression with obesity. Our group previously found that evidence that transcriptional regulation of GLO1 may drive decreased GLO1 protein observed in patients with T2D. In our previous investigation, muscle from patients with T2D had lower protein expression of GLO1's transcription factor NRF2 and increased protein expression of NRF2's negative regulator KEAP1 dysregulation. However, in the present investigation muscle from individuals with obesity showed no evidence of impaired NRF2/KEAP1-mediated transcriptional regulation of GLO1. In fact, individuals with obesity possessed significantly increased

GLO1 mRNA compared to the LH group. This could indicate that in the context of attenuated GLO1 protein, GLO1 transcription is being up regulated in the muscle in attempt to correct this deficiency. Another potential explanation for this observation is the presence of increased production of circular GLO1 RNA (cRNA). Generation of cRNA is a product of a specific form of alternative splicing called back splicing and was originally thought of as the result of splicing errors. However, recently, cRNAs have become more well studied and appreciated to have several roles independent of the original gene's roles. However, cRNAs do not result in appropriate translation of the target protein (for review on cRNAs the reader is directed to [385]). Interestingly, increased GLO1 cRNA has recently been found to be elevated in muscles from old mice [169]. The method used in the current study is unable to differentiate between cRNA and functional RNA of GLO1 and therefore, elevations observed in muscle from individuals with obesity may in part be contributed by an increase in cRNA which may also explain why this increase in gene transcripts does not appear to correct the differences in protein expression observed. Future work should determine if the production of cRNAs is indeed increased with obesity and contributing to the observed decrease in GLO1 protein abundance in muscle.

Certainly, other post-transcriptional events are implicated as well given the mismatch between GLO1 mRNA and protein abundance. Several post-translational modifications have been described for GLO1 which have been described to affect activity or protein stability. A recent study found GLO1 to be ubiquitinated in endothelial cells in response to incubation in high glucose media [91]. Another investigation in HEPG2 cells demonstrated the ability of an obesogenic environment to promote acetylation of GLO1 which subsequently promoted its ubiquitination and degradation [13]. The potential for

GLO1 to be regulated by acetylation is particularly interesting given that non-enzymatic acetylation of proteins is so tightly related to metabolism and in muscle appears to be reflective largely of glycolytic flux [242]. It follows that the enzymatic regulation of protein acetylation by deacetylases and acetyltransferases are also tightly regulated and reflective of cellular metabolism. Acetylation may therefore be an intuitive PTM for the regulation of an enzyme such as GLO1 which is also tightly related to metabolism and glycolytic flux in particular. However, the mechanisms by which acetylation may regulate GLO1 are not clear.

Our data demonstrates an attenuation in the NAD^+-dependent deacetylase SIRT1 protein with obesity but no difference in the expression of the acetyltransferase P300. SIRT1 protein also negatively correlated with BMI (Rho = -0.524, $p = 0.033$) and trended for a negative correlation with BF% (Rho = -0.458, $p = 0.059$). Interestingly, SIRT1 was also correlated with GLO1 protein (Rho = 0.639, $p = 0.007$). Other work has demonstrated a similar positive relationship between GLO1 and SIRT1 [166, 167] whereas dicarbonyl stress appears to have negative effects on SIRT1 protein [38, 54, 55, 64, 65]. Given the reliance of SIRT1 on NAD^+ we also probed the muscle for regulators of cellular NAD. CD38 is a NADase that has been implicated in NAD^+ depletion in the context of obesity and aging [274, 317]. However, protein levels of NAMPT and CD38 were not different between groups. However, NAMPT protein was correlated with VO_{2Max} (Rho = 0.618, $p = 0.016$) and trended to be negatively correlated with BF% (Rho = -0.465, $p = 0.082$). Inhibition of NAMPT has been shown to deplete mouse muscle cells [323] and tissues [324, 325] of NAD^+ thus limiting the activity of NAD^+-dependent enzymes such as SIRT1. In addition, previous work demonstrated that obesity results in the attenuation of NAMPT

protein abundance in the liver resulting in decreased cellular NAD^+, lower SIRT1 expression and activity, and metabolic consequences such as development of steatosis [380]. Metabolic tracing studies have shown that inhibition of NAMPT in skeletal muscle attenuates the activity of GAPDH which is also a NAD-dependent enzyme. Oakey et al. demonstrate NAMPT inhibition to promote the build-up of triosephosphates which are the primary precursors for MG formation [323]. Therefore, loss of NAMPT may promote dicarbonyl stress by attenuating cellular NAD^+, SIRT1 activity and subsequently acetylation and loss of GLO1. However, by attenuating GAPDH activity lack of cellular NAMPT may also promote a build-up of triosephosphates which are the primary source of MG production. Conversely, exercise has been repeatedly shown to augment both SIRT1 [346, 347, 350, 353, 354, 356, 359, 362, 364, 375, 386] and NAMPT [320, 322, 347] and therefore may be able to prevent or reverse this unfavorable metabolic milieu from developing perhaps in part through the deacetylation of GLO1.

To this end we were able to detect and quantify acetylated GLO1 via immunoprecipitation in OB muscle. Interestingly, we did see a trend for the AE to promote deacetylation of GLO1 in OB muscle which likely did not reach significance due to our relatively small *n* size. This observation may have been influenced by the increase in SIRT1 protein 30 minutes post exercise in muscle from individuals with obesity. However, despite these observations, GLO1 protein did not change within the 3 hours following acute exercise in either group. Perhaps the 3-hour window is too short after the exercise to observe changes in GLO1 protein. We have previously seen that skeletal muscle GLO1 protein is increased in response to exercise after a 12-week intervention in individuals with insulin resistance and obesity (unpublished observation). However, this trial

consisted of a dietary and exercise intervention and resulted in significant weight-loss (~7.6 kg) which may have affected GLO1 as well [387]. Importantly, the consensus of data in the literature suggests that weight loss is required for an insulin sensitizing effect of exercise training that lasts beyond 72 hours of the final exercise bout [196, 198, 199, 203, 388]. A recent study in mice has shown that 8 weeks of exercise training is able to augment muscle GLO1 protein [389]. However, Egawa et al. only saw increases in GLO1 in mouse plantaris muscle which is composed exclusively of type II glycolytic fibers (~60% Type IIb, ~40% Type IIa/x) whereas GLO1 protein was not significantly altered in soleus muscle, which is composed of more type I, oxidative fibers (~45% Type I, ~45% Type IIa/x, ~10% Type IIb). Notably, all of our muscle biopsies were performed in the vastus lateralis muscle which has a mixed fiber phenotype containing ~50% Type I fibers [390]. This fiber type specific effect reported by Egawa et al. could also potentially explain the lack of effect of acute exercise in our study on GLO1 protein although more work is needed to disseminate potential fiber type specific effects as well as the potential effect of training vs acute stimuli.

Interestingly GLO1 activity was significantly increased 30 minutes post exercise and trended toward significance at the 3-hour post time point in the LH group. It would have been interesting to see if GLO1 acetylation changed with exercise in the LH group as well. Unfortunately, we were not able to perform this assay in the LH samples to determine the effect of obesity on GLO1 acetylation due to limitations in sample. The LH group also demonstrate significant decreases in P300 and increases in SIRT1 and NAMPT transcripts which were not experienced by the OB group. This could be due to low *n* of the OB group although recent evidence has suggested that metabolic dysfunction

and dicarbonyl stress may blunt molecular responses to exercise [389, 391]. For example, mice that were supplemented with MG in their water failed to increase GLO1 protein with exercise training. Future work should be done to determine if obesity can modulate exercise effects on factors regulating skeletal muscle NAD, acetylation, and detoxification mechanisms such as GLO1.

5.3 Discussion in Regarding Findings in Relation to Aim 2

5.3.1 Effect of NAD^+ Bioavailability on Muscle GLO1

5.3.1.1 Effect of NAMPT Inhibition and NR on Muscle GLO1

To test the potential causality of NAMPT and SIRT1 on GLO1 abundance and activity, we next performed *in vitro* LOF and GOF models targeting NAMPT and SIRT1. Our first approach was to examine the effect of the NAMPT inhibitor FK866 with and without co-treatment with NR on GLO1 protein, acetylation, ubiquitination and specific activity. We found no effect of the FK866 or NR on GLO1 protein abundance, acetylation, ubiquitination, or specific activity. We performed several additional experiments to verify this finding including TMT LC-MS/MS analyses of cells treated in the same way which corroborated our findings that these treatments were not altering GLO1 protein (Supplemental Figure 10, Supplemental Figure 11, and Supplemental Figure 12).

5.3.1.2 Effect of NAMPT KD on Muscle GLO1

In addition, we also performed NAMPT KD experiments for 48h and 72h which also did not significantly affect GLO1 protein levels when analyzed via WB (Supplemental Figure 7) or TMT LC-MS/MS (Supplemental Figure 13, Supplemental Figure 15). However, our TMT analyses of these samples were enlightening to the more global effects of NAMPT inhibition and KD in human muscle cells which until now has not been

explored. As previously mentioned, FK866 and NAMPT KDs have been previously performed in mice and mouse myotubes but to our knowledge this is the first reporting in human muscle cells. Previous work has shown FK866 treatment to perturb glycolysis specifically GAPDH activity which is dependent upon NAD concentration [323]. GAPDH protein was not affected in human immortalized myotubes treated with FK866 or NAMPT siRNA. However, other proteins involved in G3P biosynthesis TKT and TPI were lower in FK866 treated cells which interestingly was not rescued in cells co-treated with NR. NAMPT KD cells after 48 hours demonstrated upregulations in several proteasomal subunits and ubiquitin ligases implicating increased proteolysis (Supplemental Figure 13). Interestingly, cells treated with FK866 for 48 hours and NAMPT KD after 48 hours only shared 3 proteins that were commonly upregulated (GNPAT, UBQLN2, SLC1A5) and 3 proteins that were commonly downregulated (JCAD, GALT, PIGT) (Supplemental Figure 14). However, the common upregulation of the ubiquitin ligase UBQLN2 in both conditions coupled with the increase in proteasomal subunits in each condition strongly suggest cellular stress and potentially breakdown. The 72 hour NAMPT KD phenotype appears exacerbated with gene ontology pathways such as mitochondrial depolarization, apoptotic signaling and response to ER stress being upregulated while proteins involved in sarcomere organization and muscle contraction are being downregulated (Supplemental Figure 15). These findings are in line with mouse muscle-specific NAMPT KO models which induce muscular atrophy [324, 325]. This muscle atrophy phenotype *in vivo* results in impaired exercise capacity, and premature death of the animal. Collectively these data support the null hypothesis that NAMPT and NAD^+ do not alter GLO1 protein or activity. However, inhibition or KD of NAMPT in human muscle does appear to have

important detrimental consequences to muscle that warrant continued investigation. In addition, these data add to the mounting evidence in the literature that NR may not be a viable strategy for the prevention or treatment of aberrant metabolic phenotypes in muscle [334-337]. Future work should focus on optimizing the ability of NR or other NAD precursors to improve NAD^+ bioavailability in muscle *in vivo* and *in vitro* as a potential mitigation strategy for conditions characterized by muscle atrophy and dysfunction such as aging, in activity, and to some extent obesity and diabetes.

5.3.2 Effect of SIRT1 KD on Muscle GLO1

Our strategy to alter NAMPT and NAD was chosen not only to test their effects on GLO1, but we had hypothesized that any potential effect they exert would do so via inhibition of SIRT1 leading to hyperacetylation of GLO1. However, when we measured acetylation of P53 (a known target of SIRT1) there was no effect of FK866 treatment in our cells (Supplemental Figure 5). These data are in line with previous work in C2C12 that has shown no effect of NAMPT KD to affect SIRT1 protein, activity or total protein acetylation despite reductions in NAD concentration [392]. However, cells co-treated with NR did show significant reduction of P53 acetylation indicating that SIRT1 activity is likely to have been enhanced in response to NR co-treatment (Supplemental Figure 9). Interestingly, the co-treatment with NR also induced a significant (~50%) increase in GLO1 (Figure 4.9 A) despite the acetylation status of GLO1 not being altered (Figure 4.11). To directly test the effect of SIRT1 on GLO1 we knocked down SIRT1 in human immortalized myotubes. There was no effect of SIRT1 KD on GLO1 protein, transcripts, acetylation, or specific activity. Interestingly, during the time of collecting these data, a newly published manuscript performed mutation experiments on several lysine residues

(K157, K159, K148) that have been previously annotated in PhosphoSitePlus to be acetylated [393]. Notably, we also observed acetylation of K157 and K159 in our own hands via LC-MS/MS analysis of HEK293T cells overexpressing GLO1 and treated with NAM and TSA (Supplemental Figure 17). *In silico* analysis using Provean predicted mutation of K157 or K159 to alanine as an acetylation mimetic would be detrimental to GLO1 activity (Supplemental Figure 17). However, Cortizo et al. demonstrated that mutation of K157 and K159 to arginine residues as a deacetylation mimetic trended to decrease enzymatic activity of GLO1 in HeLa cells. Interestingly, mutation of K148 to arginine promoted loss of GLO1 protein. These data are contrary to previous work by Spanos et al. and our hypothesis of GLO1 acetylation promoting GLO1 degradation and perturbing activity. It also appears that residue specific acetylation may have independent effects on GLO1 abundance and activity. These differences in effects may be due in part to their location on the GLO1 molecule. K157 and K159 for example are both located on a beta loop adjacent to the substrate binding domain of GLO1 and indeed mutation of these residues were found to affect GLO1 activity. On the other hand, K148 is located more superficially on the enzyme which may make PTMs on it such as acetylation more readily recognized by other proteins such as ubiquitin ligases. Collectively these data suggest higher order regulation of GLO1 via acetylation which based on our findings do not appear to be regulated by SIRT1. Importantly, several works from Dr. Simon Schenk's lab have demonstrated that muscle-specific SIRT1 KO mice do not have elevations in global protein acetylation [366, 367], impairments in exercise mediated glucose uptake [367], or impairments mitochondrial biogenesis or exercise performance [366]. In addition, work from his lab has also shown that over-expression of SIRT1 in muscle does not

enhance muscle metabolism, exercise capacity, or insulin sensitivity in young mice [312-314] or protect HFD mice from developing insulin resistance [315]. These data could indicate that while SIRT1 may be important for regulating metabolism, the redundance conferred by the presence of six other Sirtuins may be able to sufficiently compensate for a loss of SIRT1 by maintaining proper acetylome regulation. Importantly, this evidence is not sufficient to suggest that regulation of protein acetylation is unimportant for muscle metabolism rather that other factors, perhaps those with less redundance may be more important. For example, recent work from Schenk's lab has demonstrated that the expression of P300 and CBP in muscle is critically important for insulin mediated glucose uptake in muscle [377].

5.3.3 Mini-Screen of Other Factors that May Regulate GLO1 via Acetylation

Therefore, to determine if other deacetylases or acetyltransferases may be regulating GLO1 protein or activity we performed a small screen in human immortalized myotubes using inhibitors against SIRT2 (AGK2), all sirtuins (NAM), all HDACs (TSA), P300 (CCM), or GCN5 (MB-3). These studies reemphasized the complexity of GLO1 regulation that was demonstrated by the mutation experiments performed by Cortizo et al. For example, inhibition of SIRT2 tended to increase GLO1 protein but decreased its specific activity. We targeted SIRT2 as opposed to other sirtuins due to its cytoplasmic location and because it had been identified to potentially deacetylate GLO1 in a large *in vitro* deacetylase screen [175]. In addition, few data exist examining the role of SIRT2 in muscle metabolism several studies have implicated SIRT2 expression in regulating muscle insulin sensitivity. However, the data are still unclear as to whether SIRT2 augments or attenuates insulin signaling and glucose uptake in muscle [394, 395].

Similar to SIRT2 inhibition, inhibition of acetyltransferases P300 or GCN5 also generated divergent responses in GLO1 protein and specific activity. For example, inhibition of P300 increased GLO1 protein and decreased GLO1 specific activity whereas GCN5 inhibition decreased GLO1 protein and increased its specific activity. We had hypothesized that inhibition of both acetyl transferases would augment both GLO1 protein and activity by preventing GLO1 acetylation. However, given recent evidence suggesting that acetylation of different residues may have independent effects on GLO1 activity and stability may explain these divergent results [393]. Regardless, the present data coupled with the data by Cortizo et al. suggest that simple *in vitro* models may not adequately recapitulate complexity of *in vivo* biology which likely induces an amalgamation of PTMs that promote an emergent phenotype.

5.4 Caveats and Limitations

Our data have several limitations and caveats that are critical to keep in mind when interpreting these data and making decisions on how these results may inform future investigations.

5.4.1 Limitations in Relation to Human Data

One of the biggest limitations to our human data is the relatively small sample size of our human cohort (total n = 18) and in particular, the OB group (n = 5). However, despite the small sample size we still reached statistical significance ($p < 0.01$, T-Test) in our main outcome, GLO1 protein abundance. Our post-hoc power analysis reveals that we achieved an effect size of 1.43 and a power (1-β) of 0.830 putting our chance of committing type II error at about 17%. *A priori* power analysis demonstrates that in order

to reach a power of 0.95, future studies should include a total sample size of 24 with 12 participants in each group.

Another limitation of the human data is that acute exercise and the timing of muscle biopsies not being conducive to realizing changes in GLO1 protein. Our data demonstrated that within 3-hours post-acute exercise, GLO1 protein did not change. While protein translation occurs rapidly (typically between 20s to several minutes [396]), exercise increases both muscle protein degradation and synthesis with a net negative balance prevailing in the fasted state [397]. This suggests that accrual of individual proteins may be more likely to occur over longer periods of time, with exercise training or both. This is corroborated by our preliminary data in a separate cohort demonstrating an increase in GLO1 skeletal muscle protein after 12 weeks of exercise training and recent animal data demonstrating similar results [389]. In addition, the paradigm of exercise adaptation is such that more rapid molecular changes such as acute transcriptional changes, or PTM changes to regulate protein activity or stability occur in the short-term post exercise period which over time manifest in more long-term changes such as changes in protein abundance, mitochondrial biogenesis, vascular remodeling etc. [398]. Therefore, future studies should employ later sampling time points (i.e. 24 hours post exercise) and explore the potential for exercise training to evoke an effect.

5.4.2 Limitations in Relation to Cell Culture Experiments

Several caveats also need to be considered while interpreting our cell culture data as well. Firstly, we performed our cell culture experiments using human immortalized myotubes. These cells provided advantages that primary cell culture models cannot including their ability to be passaged essentially indefinitely without senescing or

experiencing considerable genetic drift [369, 370]. However, these cells were immortalized by stable infection of hTERT and CDK4 in human myoblasts and telomerase has been shown to be regulated by and interact with SIRT1 [286, 399]. In fact, FK866, dose and time course studies in immortalized cells revealed that NAD concentrations were minimally affected by the FK866 treatment and by NAMPT KD (Supplemental Figure 5, and Supplemental Figure 7). To determine if hTERT could potentially explain these observations, we performed time course experiments of 50 nM FK866 treatments on the same clone of myoblasts that only possessed the CDK4 overexpression. These cells did experience a significant decrease in NAD concentration with FK866 treatment which was observed with 3 hours of treatment and was not affected with 12 hour-treatment or longer (Supplemental Figure 6). Interestingly, GLO1 protein was not altered in either model across the time course out to 48 hours. These data indicate that overexpression of telomerase may protect the cell from NAD reductions in response to NAMPT inhibition but also confirm our findings that limiting cellular NAD does not affect GLO1 protein expression. Both of the cell models increased NAMPT protein expression in response to FK866 treatment which may be a compensatory mechanism for NAMPT inhibition but is likely not the only compensatory mechanism given that NAD concentrations were only preserved in the immortalized cells.

Lastly, to prevent undue oxidative stress and mimic the *in vivo* oxygen tension in muscle, we cultured the immortalized myotubes under approximately 5% oxygen. However, oxygen tension has also been shown to activate hypoxia response mechanisms such as HIF1α to promote glycolytic metabolism [400], alter GLO1 protein and copy number [144], and NAD/NADH ratio [401]. To test the potential effect on NAD and GLO1,

immortalized myotubes were cultured under standard cell incubation conditions (20% oxygen) or under 5% oxygen. However, we observed no effect of low oxygen culture on NAD or GLO1 protein expression (Supplemental Figure 8).

5.5 Future Directions

Here we demonstrate that loss of GLO1 protein in muscle appears to occur in obesity prior to onset of impaired fasting glucose. This finding along with preclinical observations [99, 149] support the notion that loss of GLO1 protein may play a role the pathogenesis of metabolic dysfunction. Specifically, early attenuation of GLO1 protein may promote a molecular milieu whereby repeated increased flux in metabolic substrates in muscle (i.e. post-prandial) may be damaging over time due to lack of an ability to detoxify MG formed as a result of metabolism. However, future work is needed to further establish the relationship between obesity and insulin resistance development and GLO1 expression in clinical samples. Particularly, profiling of GLO1 expression and dicarbonyl stress in muscle from a larger cohort of individuals spanning the glucose tolerance continuum would be useful to substantiate our observations of progressive loss of skeletal muscle GLO1 in individuals with obesity (current observations) and T2D [35]. In addition, data already exists demonstrating increased plasma MG AUC in response to a mixed meal tolerance test and OGTT [104, 113, 114]. While the source of MG in these contexts is not known, skeletal muscle is a prime candidate due to its large mass, significant contribution of muscle to glucose uptake, and the apparent attenuation of GLO1 protein that we have observed in muscle from individuals with obesity. Clinical studies using pulse-chase tracer methodologies with parallel muscle biopsies during such metabolic challenges are warranted to address this gap.

These exacerbated excursions in MG following an OGTT or MMTT may have consequences that drive the development of metabolic dysfunction. However, our *In vitro* investigation exploring the consequences of GLO1 KD in human myotubes demonstrates important proteomic consequences of muscles lacking GLO1 including shifts in muscle metabolic enzymes, increased proteasomal proteins and attenuated proteins involved in muscle structure and function. Future work should explore the *in vivo,* whole organism consequences of muscle-specific GLO1 attenuation. While several lines of evidence have explored the consequence of whole body GLO1 attenuation [99, 148, 149], the specific consequences in muscle *in vivo* remain understudied. Therefore, profiling of muscle-specific GLO1 KO in preclinical models is warranted to determine if this molecular mileu contributes to the development of metabolic dysfunction. In addition, while causality is difficult to draw in clinical populations, utilization of GLO1 inhibitors and activators in *ex vivo* preparations of human muscle samples could be used to probe the metabolic consequences of GLO1 attenuation and activation in human tissue. However, the proteomic consequences noted in the present study are strong rationale for future work to continue investigating mechanisms regulating GLO1 and to explore potential interventions that may augment GLO1 in muscle.

Understanding the importance and regulation of GLO1 in specific tissues such as muscle are important to inform effective strategies to target GLO1 to prevent and treat disease. For example, here we found that acute exercise may be able to deacetylate GLO1 and augment GLO1 activity in muscle, but more robust exercise or repeated exercise training may be required to see similar changes in OB muscle or changes in GLO1 protein. Future work should explore the if there is an optimal exercise dose (e.g.

modality, intensity, and time) or if exercise training is necessary to influence GLO1 in muscle. Recent work in mice has demonstrated fast twitch fibers are more sensitive to increases in GLO1 in response to exercise than slow twitch fibers [389]. This may implicate prescription of exercise modalities that are likely to more robustly activate fast twitch fibers, such as HIIT or resistance exercise. Additionally, we previously observed an increase in muscle GLO1 protein following a 12-week aerobic exercise training intervention in individuals with obesity and insulin resistance (unpublished observation) although these data need to be confirmed. Should these observations hold, exercise may also be a useful tool for uncovering the apparently complex mechanisms regulating GLO1 in muscle.

Finally, while our mechanistic data have primarily retained our null hypotheses and thereby ruled out a direct influence of SIRT1 on GLO1, our data have demonstrated complex regulation of muscle GLO1 via various proteins that regulate protein acetylation. Encouragingly, some clinical data has demonstrated that a first-generation GLO1 inducer consisting of trans-resveratrol and hesperitin is able to attenuate dicarbonyl stress, promote GLO1 activity and improve glucose tolerance in individuals with overweight and obesity [153]. However, the effect size of this intervention is small and may not be sufficiently effective to promote meaningful physiologic benefit. Therefore, uncovering mechanisms of GLO1 regulation remains a priority for the development of second generation GLO1-targeting pharmaceuticals.

5.6 Conclusion

In conclusion, we demonstrated for the first time that GLO1 protein abundance is attenuated in muscle from individuals with obesity. In addition, while the NAD^+-dependent

deacetylase SIRT1 appears to be attenuated in muscle in this context, NAD^+ bioavailability and SIRT1 do not appear to be necessary or sufficient to alter GLO1 stability or activity. However, regulation of GLO1 may be regulated in part through acetylation by a multitude of other factors that may independently regulate GLO1 acetylation on specific lysine residues.

APPENDICES

Appendix A – Supplemental Figures

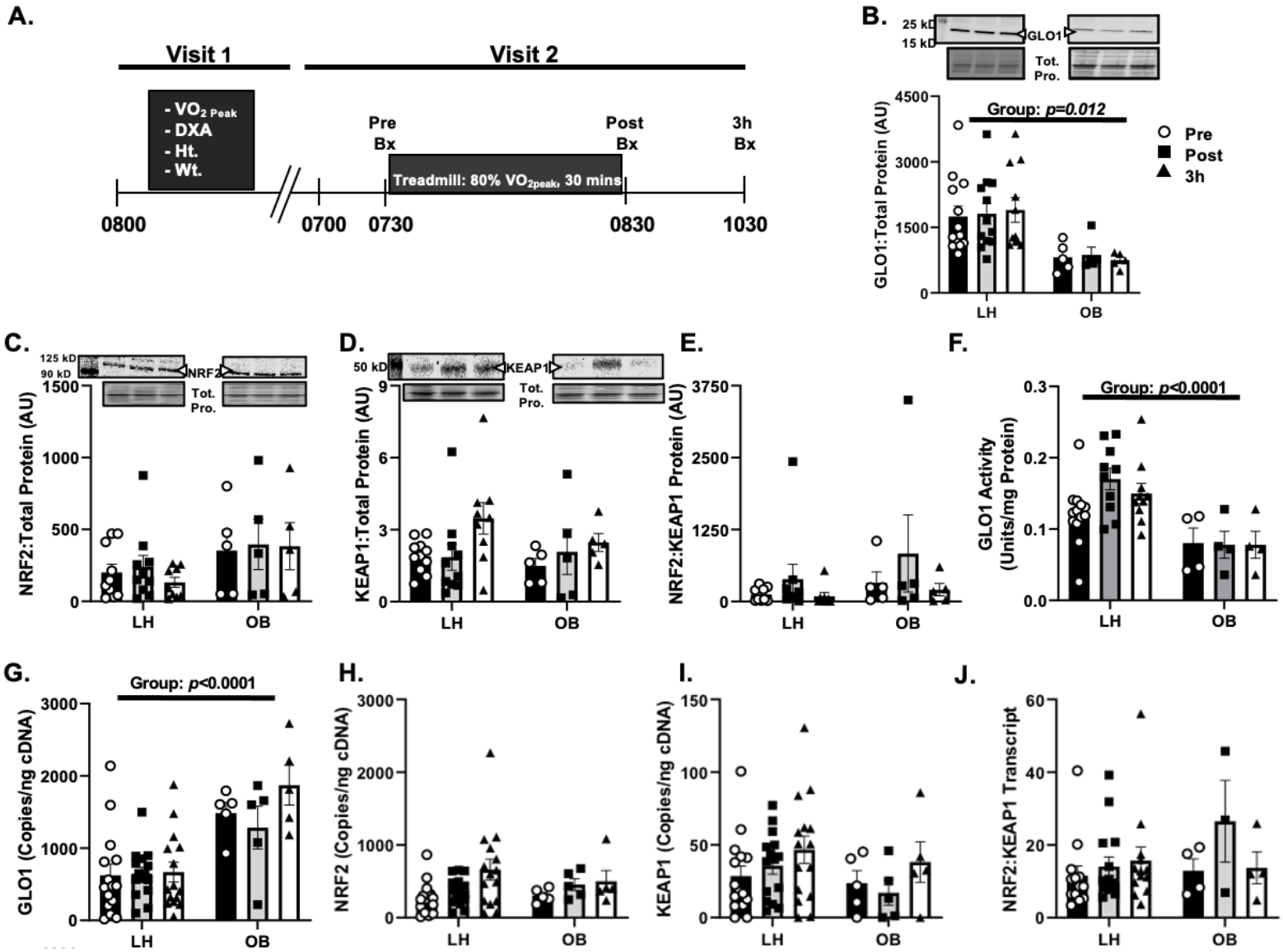

Supplemental Figure 1 Group by Time Representation of GLO1 and Canonical Regulators. A) Study schematic. B) GLO1 protein. C) NRF2 protein. D) KEAP1 protein. E) Ratio of NRF2:KEAP1 protein. F) GLO1 activity. G) GLO1 transcripts. H) NRF2 transcripts. I) KEAP1 transcripts. J) Ratio of NRF2:KEAP1 transcripts. Data are mean ± SEM. Data are analyzed by 3X2 Repeated Measures ANOVA or Mixed Model in the case of missing data.

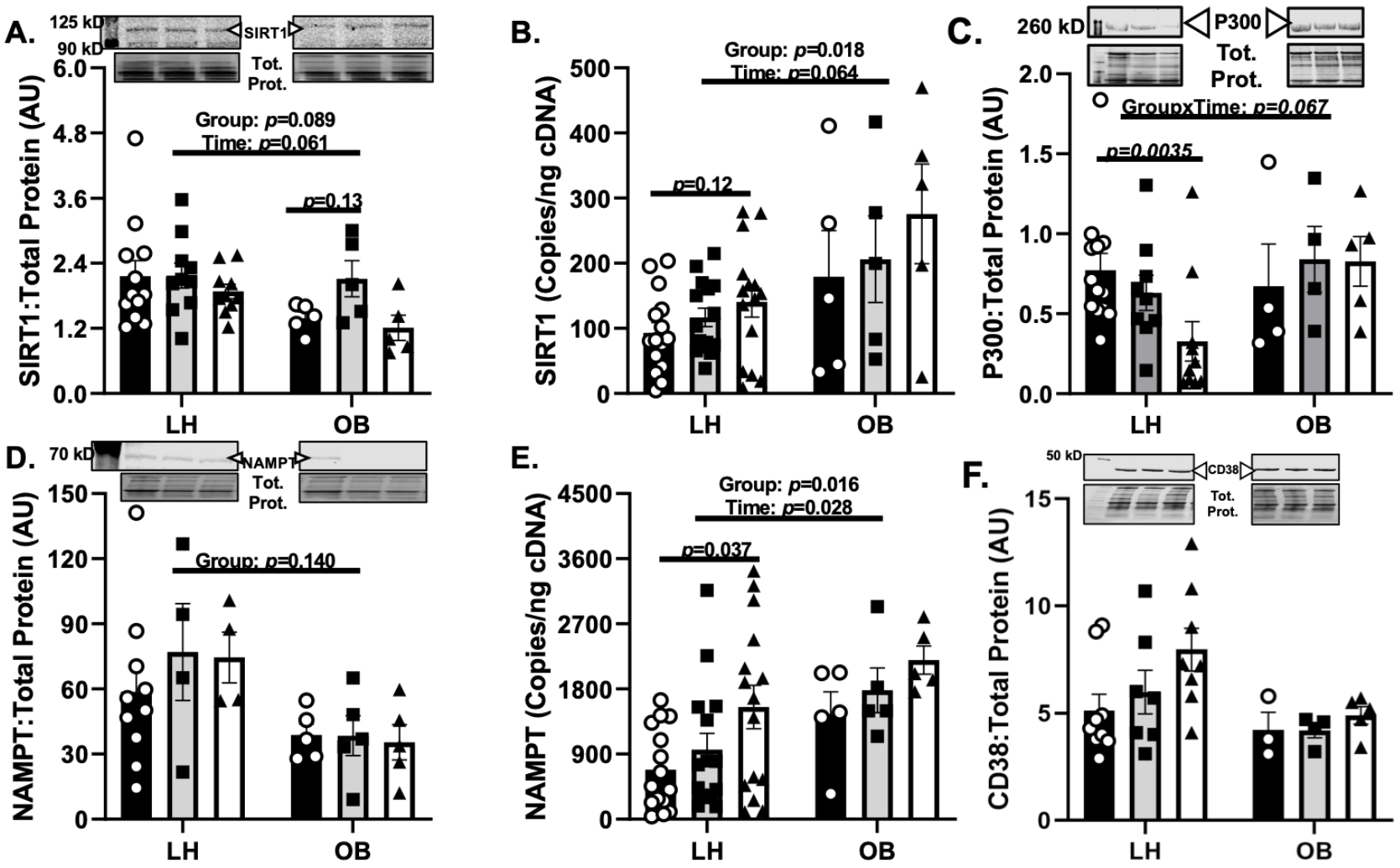

Supplemental Figure 2 Group by Time Representation of SIRT1 and Regulators of NAD and Acetylation. A) SIRT1 Protein. B) SIRT1 transcripts. C) P300 protein. D) NAMPT protein. NAMPT Transcripts. F) CD38 Protein. Data are mean ± SEM. Data are analyzed by 3X2 Repeated Measures ANOVA or Mixed Model in the case of missing data.

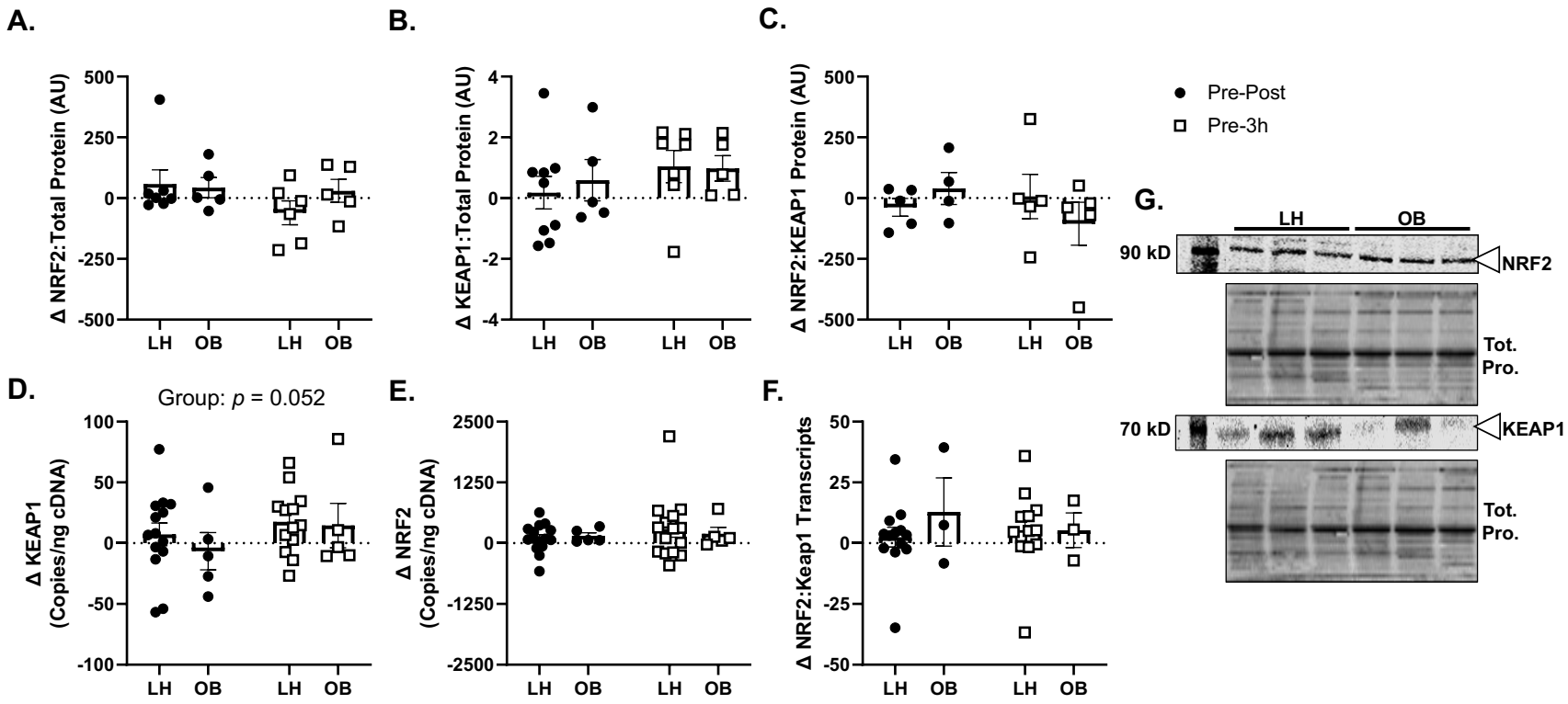

Supplemental Figure 3 Effect of Acute Exercise on NRF2/KEAP1 in LH and OB Participants. A) NRF2 protein, B) KEAP1 Protein and C) Their ratio are unaffected by acute exercise within the 3 hours following the exercise bout in both the LH and OB groups. Similarly, acute exercise had no effect on D) NRF2 transcripts, E) KEAP1 transcripts or F) Their ratio. Data are represented as mean ± SEM. Data are analyzed by 3X2 Repeated Measures ANOVA or Mixed Model in the case of missing data.

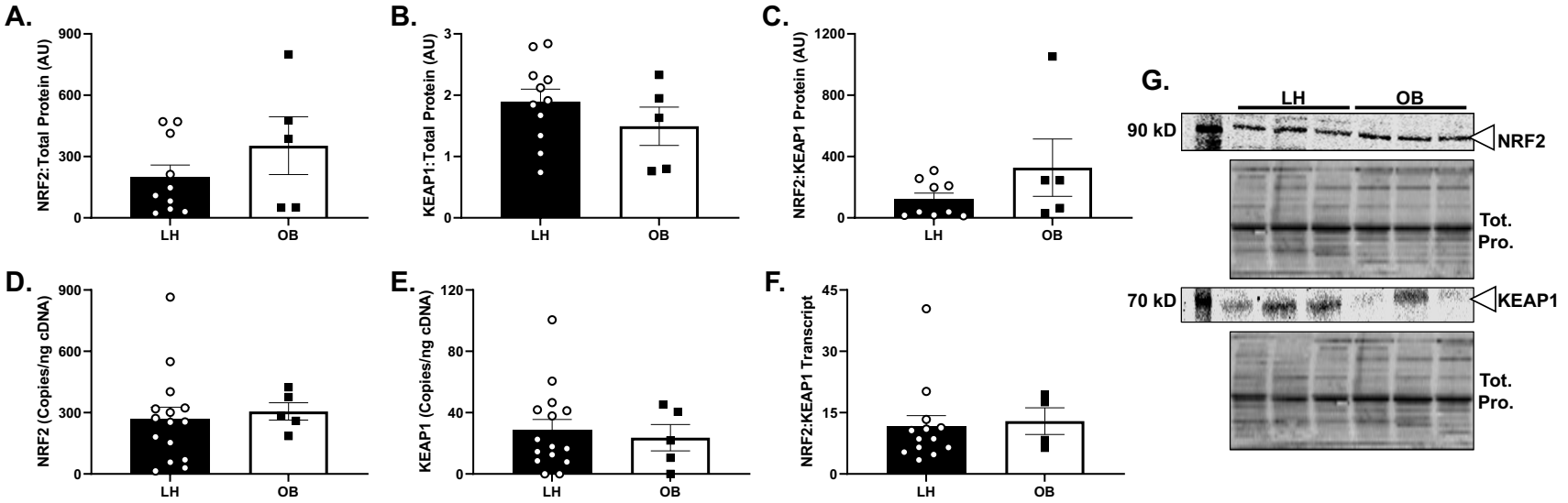

Supplemental Figure 4 Effect of Obesity on NRF2/KEAP1 Expression in Skeletal muscle. A) Expression of GLO1 transcription factor NRF2 and B) its negative regulator KEAP1 are unaltered by obesity. C) Ratio of NRF2:KEAP1 protein indicates no effect of obesity on the proportion of NRF2 and KEAP1 proteins. D) NRF2 and E) KEAP1 transcripts are also unaltered by obesity as is F) the ratio of their expression. Data are expressed as mean ± SEM and analyzed via unpaired T-Test or Wilcoxon Sign-rank test in the case of non-normally distributed data.

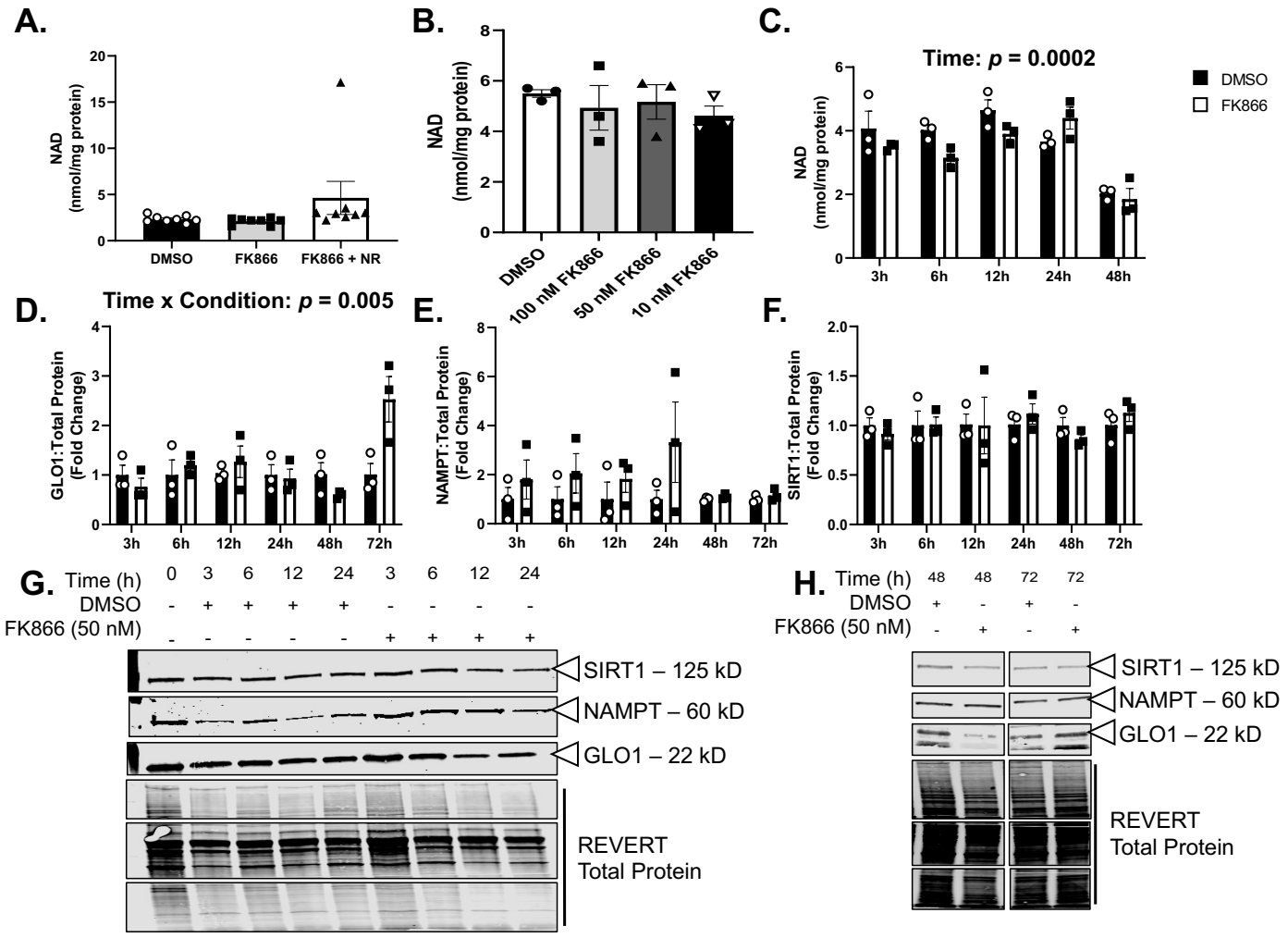

Supplemental Figure 5 Effect of FK866 Dose and Time Course on NAD, GLO1, NAMPT and SIRT1 in Human Immortalized Myotubes. A. NAD concentration following 48h treatment with 50 nM FK866 with or without co-treatment 0.5 mM NR. B. NAD concentration following 48h treatment with 100, 50 or 10 nM FK866. C. NAD concentration 3, 6, 12, 24, or 48h 50 nM FK866. D. GLO1, E. NAMPT, and SIRT1 protein expressions during time course of 50 nM FK866. G and H. Representative western blot for proteins quantified in D – F. All western blot data are expressed as average fold change from DMSO ± SEM. Data analyzed via ANOVA.

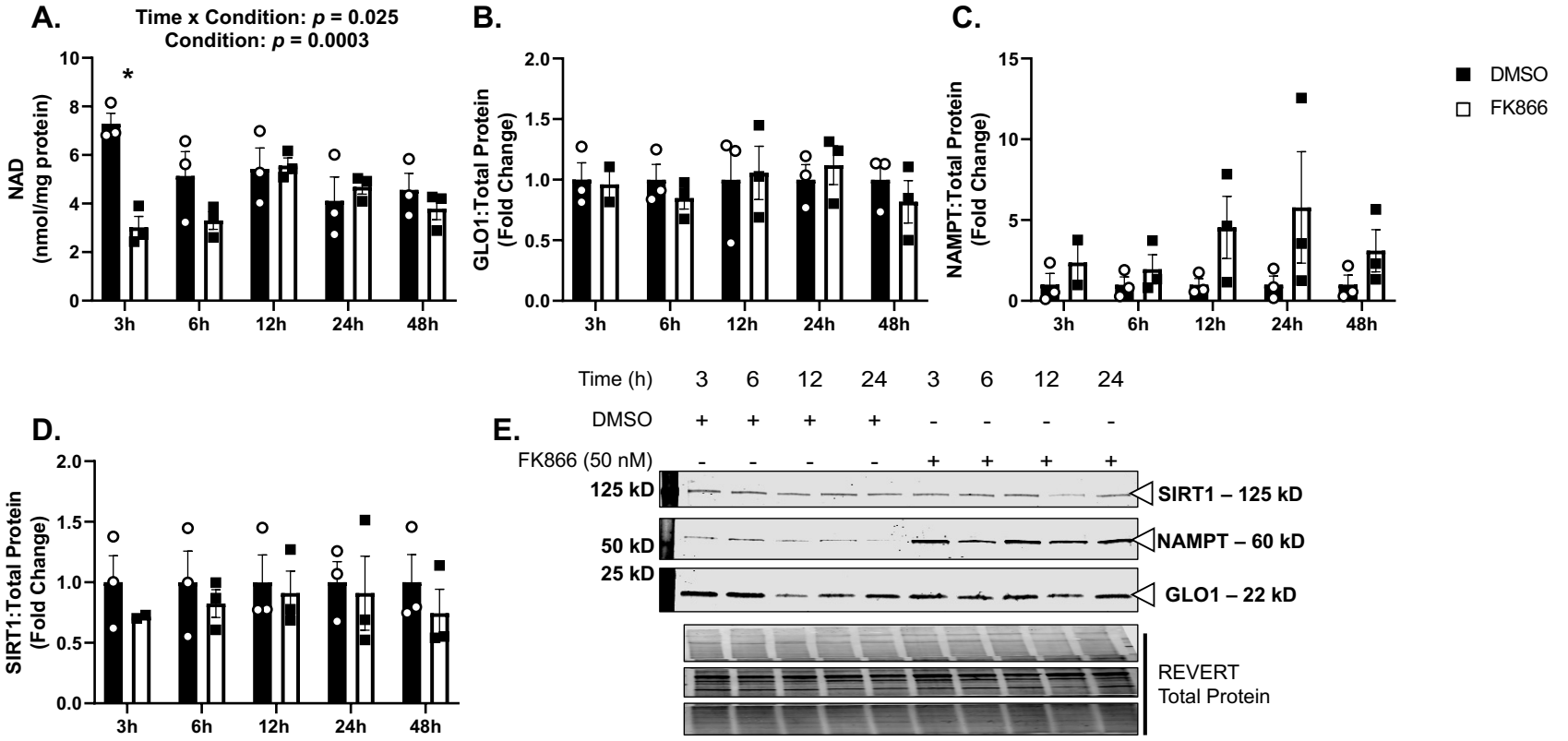

Supplemental Figure 6 Effect of FK866 Dose and Time Course on NAD, GLO1, NAMPT and SIRT1 in Human Long Telomere Myotubes. A. NAD concentration following 3, 6, 12, 24, or 48h treatment with 50 nM FK866. B. GLO1, C. NAMPT, and D. SIRT1 protein expressions during time course of 50 nM FK866. E. Representative western blot for proteins quantified in B – D. All western blot data are expressed as average fold change from DMSO ± SEM. Data analyzed via ANOVA.

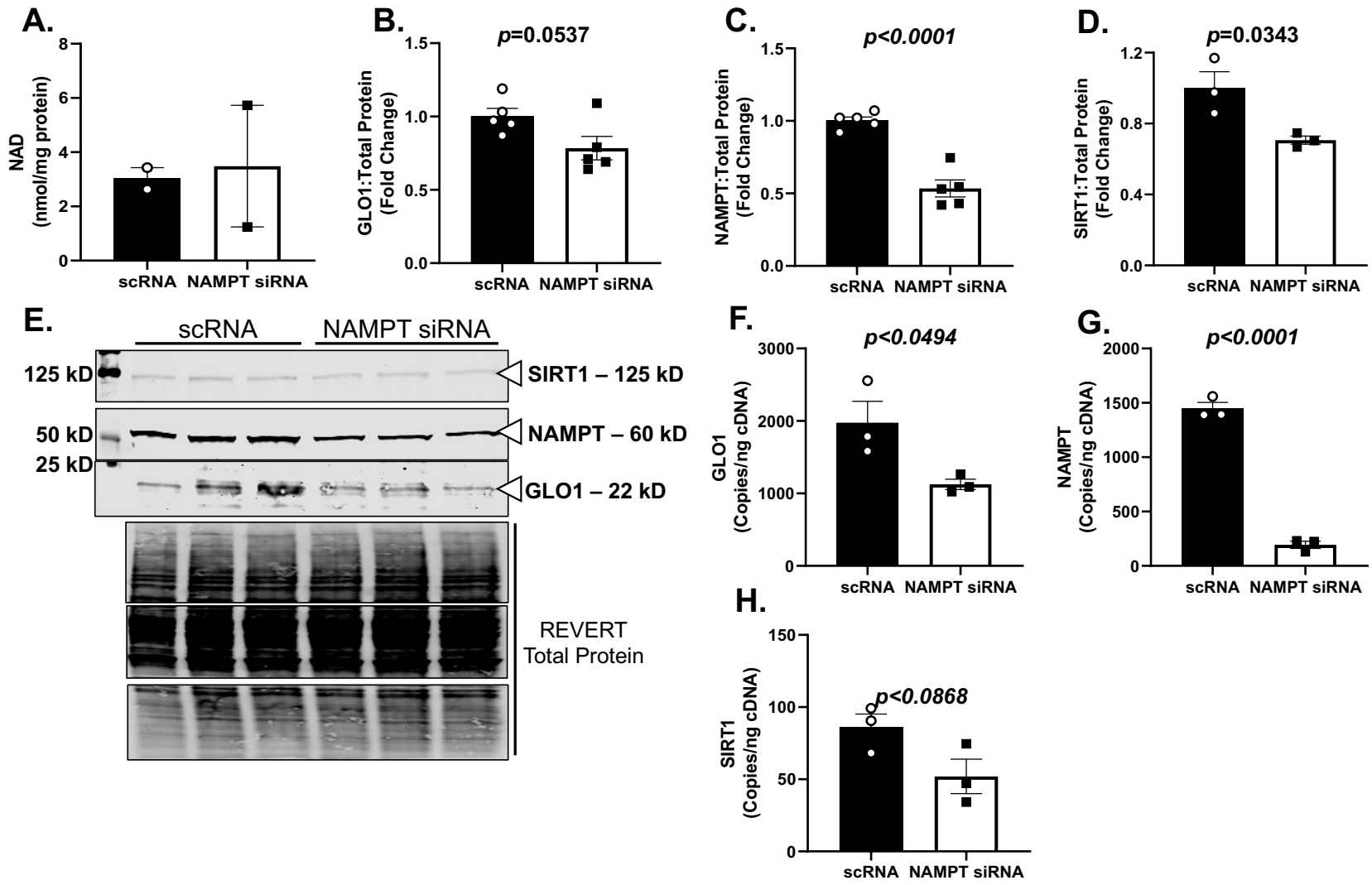

Supplemental Figure 7 Effect of NAMPT KD on NAD, GLO1, NAMPT and SIRT1 in Human Immortalized Myotubes. Human Immortalized Myotubes were transfected with scRNA or NAMPT siRNA for 48 hours. A. NAD concentration 48h NAMPT KD. B. GLO1 protein. C. NAMPT protein. D. SIRT1 protein following NAMPT KD. E. Representative western blot for proteins quantified in B – D. F. GLO1 transcripts. G. NAMPT transcripts. H. SIRT1 transcripts following NAMPT KD. All western blot data are expressed as average fold change from DMSO ± SEM. All transcript data were acquired via droplet digital PCR and expressed as copies/ng cDNA. All data analyzed via unpaired T Test.

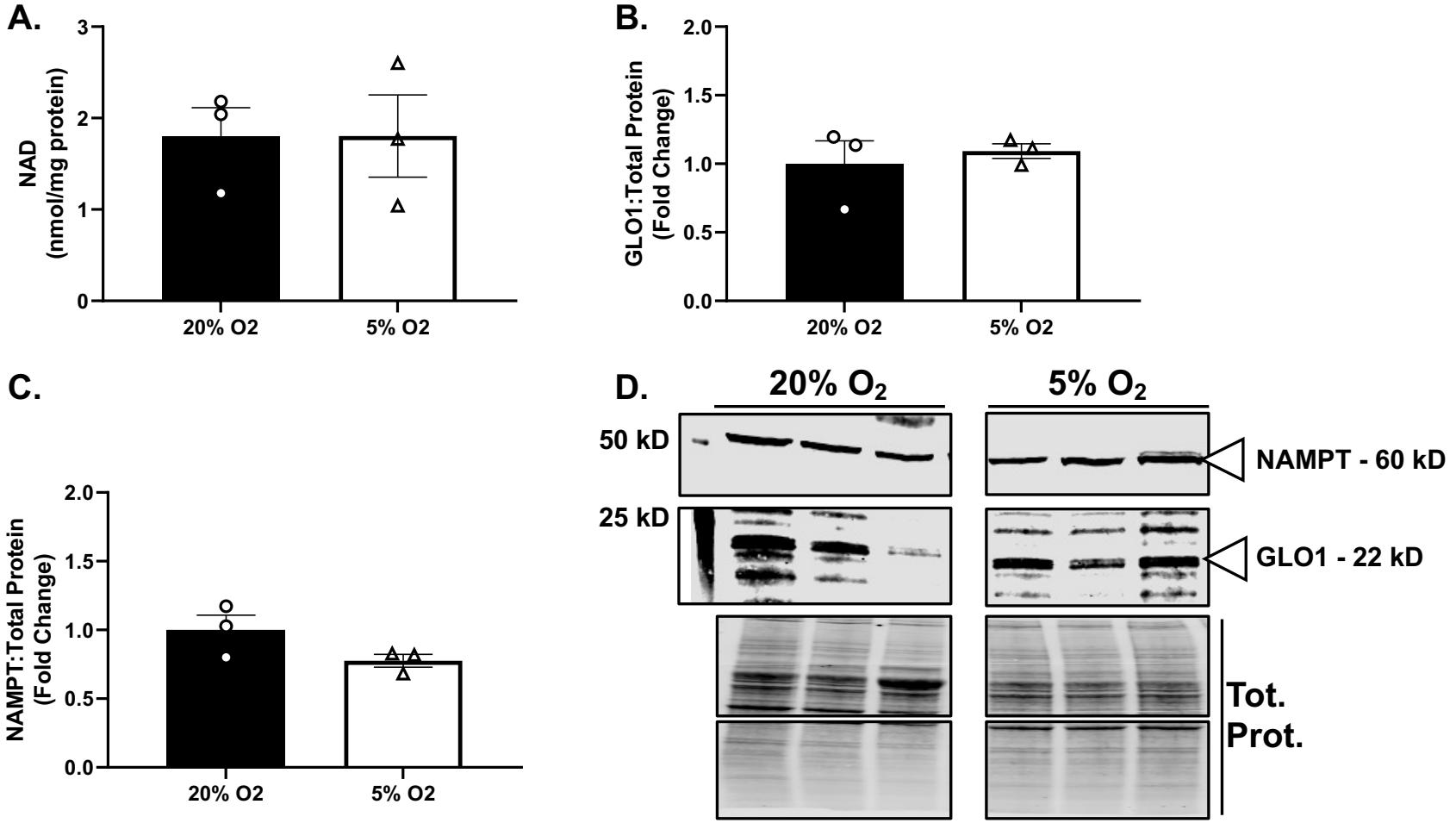

Supplemental Figure 8 Tissue Culture at Physiologic Oxygen does not Affect NAD, GLO1 or NAMPT. Human immortalized myotubes were grown and differentiated at either 20% or approximately 5% oxygen. A. NAD concentration, B. GLO1 Protein, and C. NAMPT protein are unaffected by culture at different percent oxygen. D. Western blot for NAMPT and GLO1 protein. Western blot data presented as mean ± SEM fold change from 20% O_2.

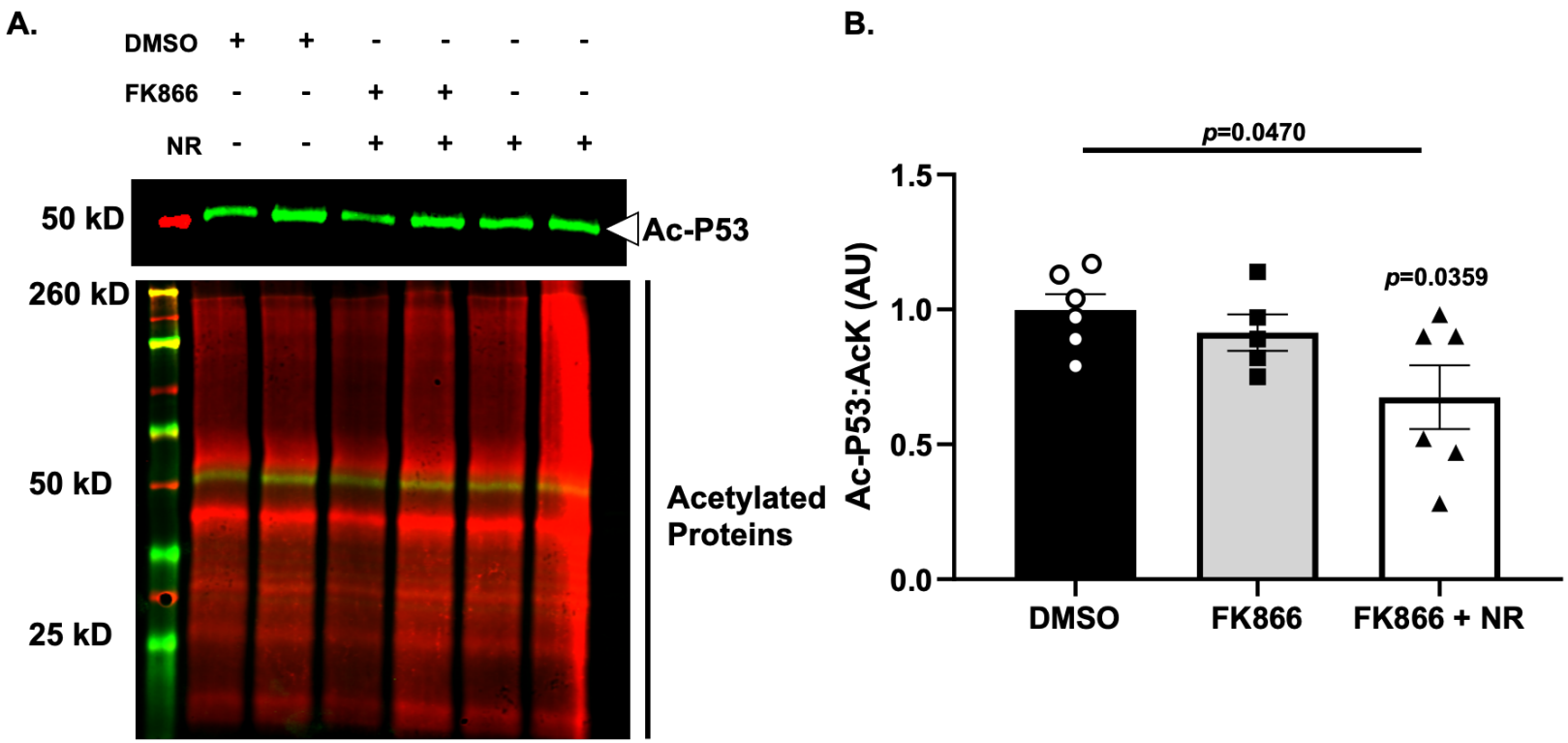

Supplemental Figure 9 Effect of FK866 and NR on Acetylated P53. Acetylated proteins were IP'ed from samples treated with FK866 or co-treated with NR. A) Representative western blot of IP eluates. B) Quantification of acetylated P53 signal normalized to acetyl lysine signal in IP eluates. Data are average fold change from DMSO ± SEM. Data analyzed via one-way ANOVA with Bonferroni Post Hoc.

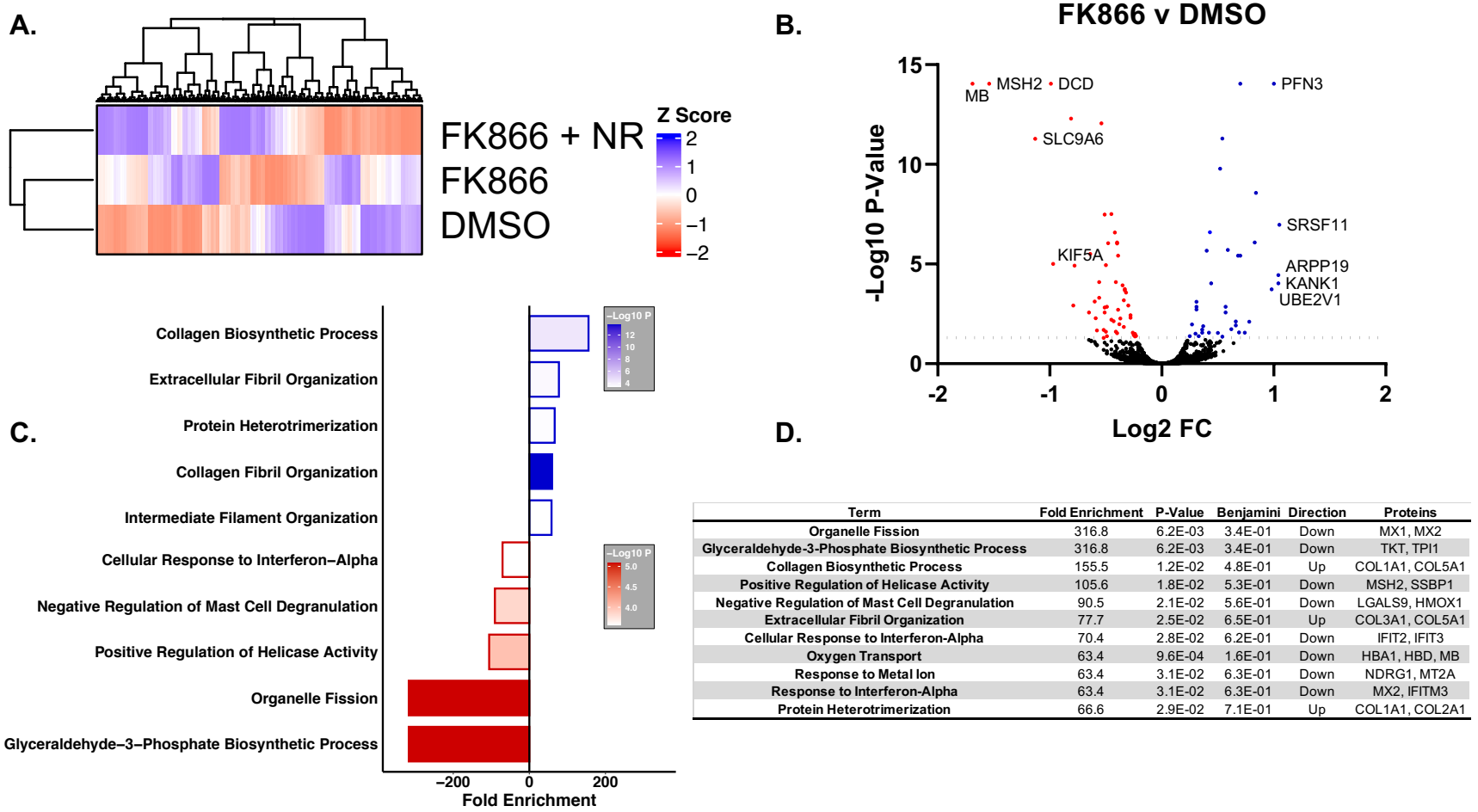

Term	Fold Enrichment	P-Value	Benjamini	Direction	Proteins
Organelle Fission	316.8	6.2E-03	3.4E-01	Down	MX1, MX2
Glyceraldehyde-3-Phosphate Biosynthetic Process	316.8	6.2E-03	3.4E-01	Down	TKT, TPI1
Collagen Biosynthetic Process	155.5	1.2E-02	4.8E-01	Up	COL1A1, COL5A1
Positive Regulation of Helicase Activity	105.6	1.8E-02	5.3E-01	Down	MSH2, SSBP1
Negative Regulation of Mast Cell Degranulation	90.5	2.1E-02	5.6E-01	Down	LGALS9, HMOX1
Extracellular Fibril Organization	77.7	2.5E-02	6.5E-01	Up	COL3A1, COL5A1
Cellular Response to Interferon-Alpha	70.4	2.8E-02	6.2E-01	Down	IFIT2, IFIT3
Oxygen Transport	63.4	9.6E-04	1.6E-01	Down	HBA1, HBD, MB
Response to Metal Ion	63.4	3.1E-02	6.3E-01	Down	NDRG1, MT2A
Response to Interferon-Alpha	63.4	3.1E-02	6.3E-01	Down	MX2, IFITM3
Protein Heterotrimerization	66.6	2.9E-02	7.1E-01	Up	COL1A1, COL2A1

Supplemental Figure 10 Proteomic Consequences of FK866 in Human Immortalized Myotubes. TMT LC-MS/MS analysis of myotubes treated with FK866 or co-treatment with NR. A) Unsupervised hierarchical clustering of identified proteins (N=2 per condition). B) Volcano plot of change in proteins in FK866-treated cells compared to DMSO-treated cells. Dotted line indicates *p* value of 0.05. C) Top 10 up and down regulated gene ontology pathways of proteins that significantly changed. D) Top 10 enriched gene ontology pathways and the proteins in that pathway that changed.

A.

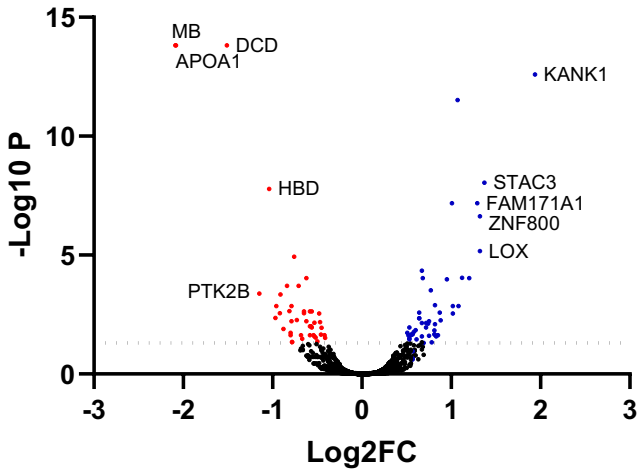

B.

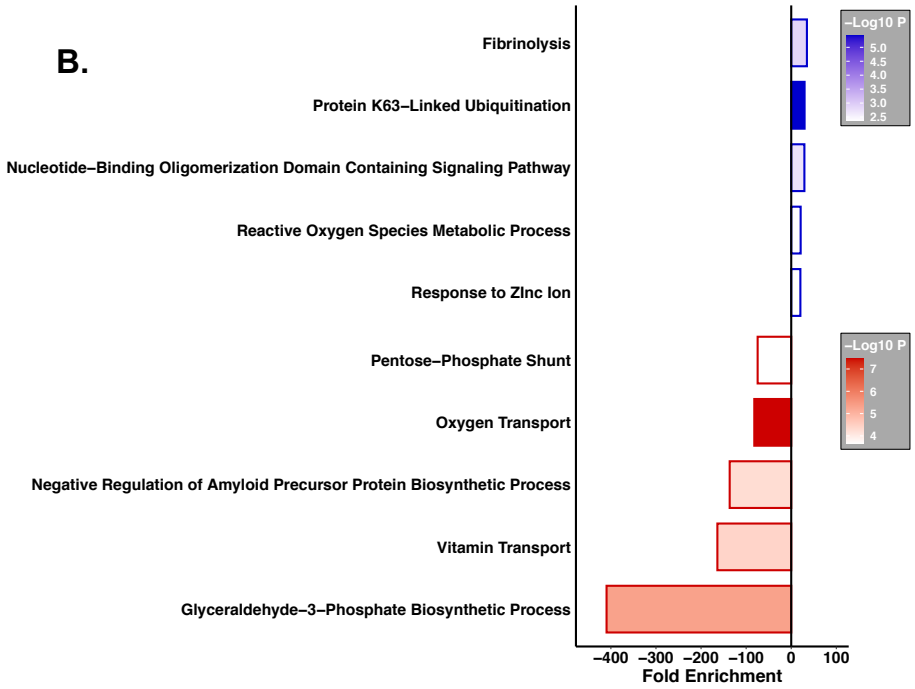

C.

Term	Fold Enrichment	P-Value	Benjamini	Direction	Proteins
Glyceraldehyde-3-Phosphate Biosynthetic Process	410	4.8E-03	4.4E-01	Down	TKT, TPI1
Vitamin Transport	164	1.2E-02	5.8E-01	Down	GC, APOA1
Negative Regulation of Amyloid Precursor Protein Biosynthetic Process	137	1.4E-02	5.9E-01	Down	ITM2B, ITM2C
Oxygen Transport	82	5.7E-04	2.1E-01	Down	HBA1, HBD, MB
Pentose-Phosphate Shunt	75	2.6E-02	8.1E-01	Down	TKT, TPI1
2-Oxoglutarate Metabolic Process	46	4.2E-02	9.2E-01	Down	DLD, GOT2
Regulation of Complement Activation	41	2.3E-03	2.9E-01	Down	CD59, C4BPA, VTN
Fibrinolysis	35	5.5E-02	1.0E+00	Up	KRT1, SERPINE1
Protein K63-Linked Ubiquitination	30	4.4E-03	8.7E-01	Up	ITCH, UBE2E3, UBE2V1
Nucleotide-Binding Oligomerization Domain Containing Signaling Pathway	29	6.5E-02	1.0E+00	Up	ITCH, UBE2V1

Supplemental Figure 11 Proteomic consequences of FK866+NR on Human Immortalized Myotubes. A) Volcano plot of change in proteins in FK866/NR co-treated cells compared to DMSO-treated cells. Dotted line indicates *p* value of 0.05. B) Top 10 up and down regulated gene ontology pathways of proteins that significantly changed. C) Top 10 enriched gene ontology pathways and the proteins in that pathway that changed.

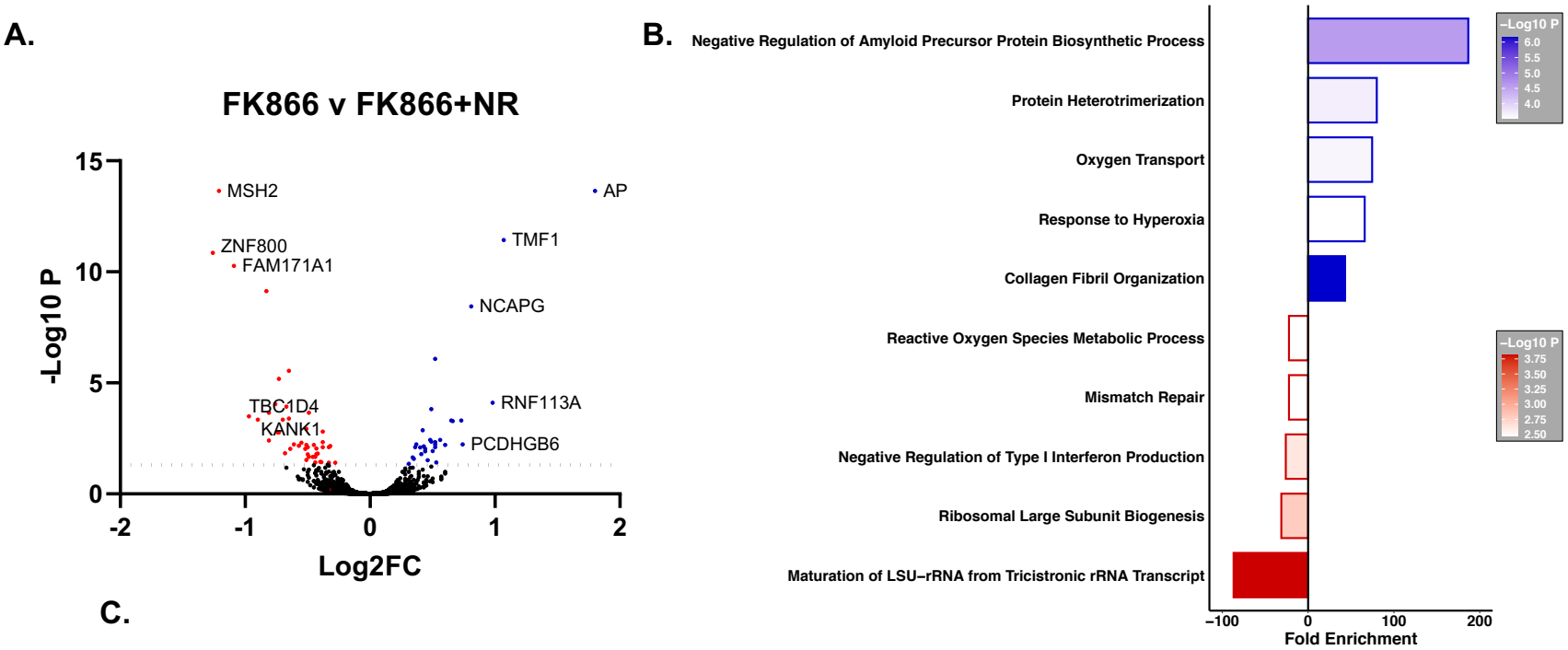

Term	Fold Enrichment	P-Value	Benjamini	Direction	Proteins
Negative Regulation of Amyloid Precursor Protein Biosynthetic Process	186.6	1.0E-02	4.1E-01	Up	ITM2B, ITM2C
Maturation of LSU-rRNA from Tricistronic rRNA Transcript	86.8	2.2E-02	1.0E+00	Down	WDR12, RPL35
Protein Heterotrimerization	80	2.4E-02	5.9E-01	Up	COL1A1, COL1A2
Oxygen Transport	74.6	2.6E-02	5.9E-01	Up	HBD, MB
Response to Hyperoxia	65.9	2.9E-02	6.2E-01	Up	COL1A1, SOD2
Collagen Fibril Organization	43.1	2.1E-03	2.1E-01	Up	COL1A1, COL1A2, COL3A1
Positive Regulation of Rho Protein Signal Transduction	43.1	4.4E-02	7.1E-01	Up	APOA1, COL3A1
Cellular Response to Amino Acid Stimulus	35.7	3.0E-03	2.1E-01	Up	COL1A1, COL1A2, COL3A1
Response to Hydrogen Peroxide	32.9	3.5E-03	2.1E-01	Up	COL1A1, MB, SOD2
Ribosomal Large Subunit Biogenesis	31.2	6.1E-02	1.0E+00	Down	WDR12, RPL26

Supplemental Figure 12 Proteomic consequences of 48h NR in Human Immortalized Myotubes. A) Volcano plot of change in proteins in FK866-treated cells compared to FK866/NR co-treated cells. Dotted line indicates *p* value of 0.05. B) Top 10 up and down regulated gene ontology pathways of proteins that significantly changed. C) Top 10 enriched gene ontology pathways and the proteins in that pathway that changed.

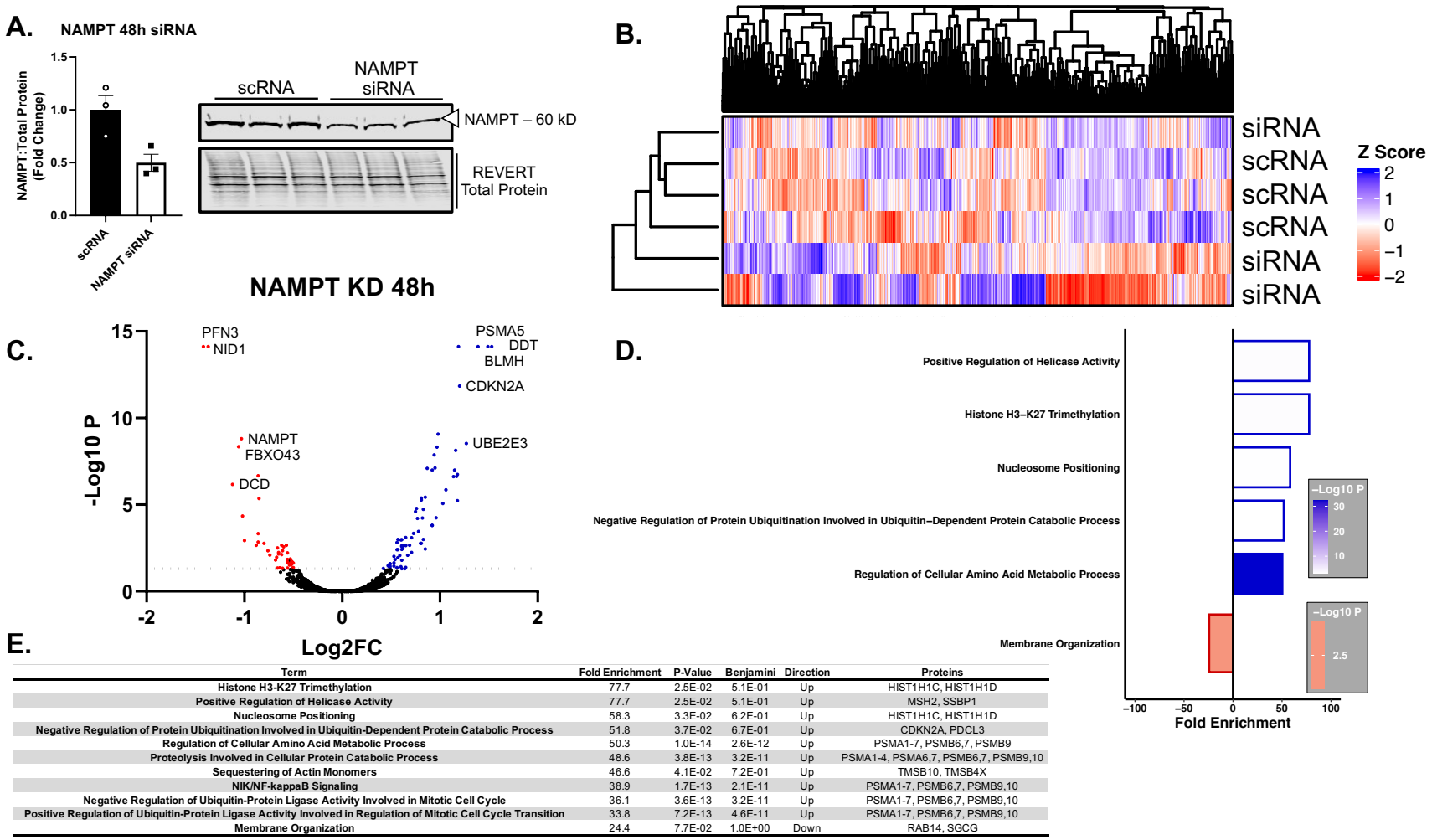

E.

Term	Fold Enrichment	P-Value	Benjamini	Direction	Proteins
Histone H3-K27 Trimethylation	77.7	2.5E-02	5.1E-01	Up	HIST1H1C, HIST1H1D
Positive Regulation of Helicase Activity	77.7	2.5E-02	5.1E-01	Up	MSH2, SSBP1
Nucleosome Positioning	58.3	3.3E-02	6.2E-01	Up	HIST1H1C, HIST1H1D
Negative Regulation of Protein Ubiquitination Involved in Ubiquitin-Dependent Protein Catabolic Process	51.8	3.7E-02	6.7E-01	Up	CDKN2A, PDCL3
Regulation of Cellular Amino Acid Metabolic Process	50.3	1.0E-14	2.6E-12	Up	PSMA1-7, PSMB6,7, PSMB9
Proteolysis Involved in Cellular Protein Catabolic Process	48.6	3.8E-13	3.2E-11	Up	PSMA1-4, PSMA6,7, PSMB6,7, PSMB9,10
Sequestering of Actin Monomers	46.6	4.1E-02	7.2E-01	Up	TMSB10, TMSB4X
NIK/NF-kappaB Signaling	38.9	1.7E-13	2.1E-11	Up	PSMA1-7, PSMB6,7, PSMB9,10
Negative Regulation of Ubiquitin-Protein Ligase Activity Involved in Mitotic Cell Cycle	36.1	3.6E-13	3.2E-11	Up	PSMA1-7, PSMB6,7, PSMB9,10
Positive Regulation of Ubiquitin-Protein Ligase Activity Involved in Regulation of Mitotic Cell Cycle Transition	33.8	7.2E-13	4.6E-11	Up	PSMA1-7, PSMB6,7, PSMB9,10
Membrane Organization	24.4	7.7E-02	1.0E+00	Down	RAB14, SGCG

Supplemental Figure 13 Proteomic Consequences of 48h NAMPT siRNA in Human Immortalized Myotubes. A) Western blotting confirmation of NAMPT protein knock down with siRNA. B) Unsupervised hierarchical clustering on all proteins identified in each experimental replicate. C) Volcano plot of proteins. Dotted line cut of set to $p = 0.05$, red dots indicate significantly changed proteins. D) Gene ontology enrichment analysis of top 10 upregulated and top 10 down regulated pathways. E) Top ten most enriched gene ontology pathways and the proteins that changed in those pathways.

A.

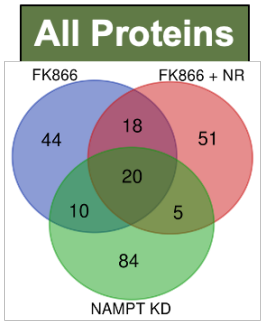

B.

Overlapping Conditions	Proteins
FK866 v NAMPT KD	JCAD, PSMA6, EFHD2, SLC9A6, GALT, PIGT, GNPAT, UBQLN2, MSH2, SLC1A5
FK866 v FK866+NR	STAC3, MB, RPL36, GSS, SDC3, KANK1, CD59, KIAA0754, CAGE1, PMPCB, OLFML3, MT2A, DLD, HBD, TKT, HBA1, GOT2, IFITM3
NAMPT KD v FK866+NR	PSMA5, CRELD1, UBE2E3, KRT10, TMSB10
All Conditions	BLMH, PSMB9, SRSF11, DCD, KRT1, TPI1, PFN3, CTTNBP2NL, SSBP1, MYO18B, WDR41, EXOSC3, FBXO43, STXBP6, SGCG, PPIF, ARPP19, UBE2V1, NID1, KRT9

C.

D.

Overlapping Conditions	Proteins
FK866 v NAMPT KD	JCAD, GALT, PIGT
FK866 v FK866+NR	CAGE1, MB, BLMH, GSS, PSMB9, OLFML3, MT2A, HBD, DLD, TPI1, TKT, CD59, HBA1, GOT2, IFITM3, KIAA0754, SSBP1
NAMPT KD v FK866+NR	NID1, KRT10
All Conditions	FBXO43, DCD, SGCG, EXOSC3

E.

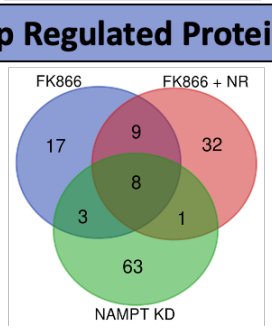

F.

Overlapping Conditions	Proteins
FK866 v NAMPT KD	GNPAT, UBQLN2, SLC1A5
FK866 v FK866+NR	STAC3, RPL36, SDC3, KRT, KANK1, PFN3, PMPCB, NID1, KRT9
NAMPT KD v FK866+NR	UBE2E3
All Conditions	SRSF11, CTTNBP2NL, MYO18B, WDR41, STXBP6, PPIF, ARPP19, UBE2V1

Supplemental Figure 14 Comparison of Proteomic Changes with NAMPT Inhibition and 48h of NAMPT KD. Significantly altered proteins from FK866/NR and 48h NAMPT KD experiments were compared using a publicly available tool at http://bioinformatics.psb.ugent.be/webtools/Venn/. Venn diagrams are presented for A) All proteins, C) Down regulated proteins, and E) Up regulated proteins and corresponding tables listing the proteins are provided in B, D and F.

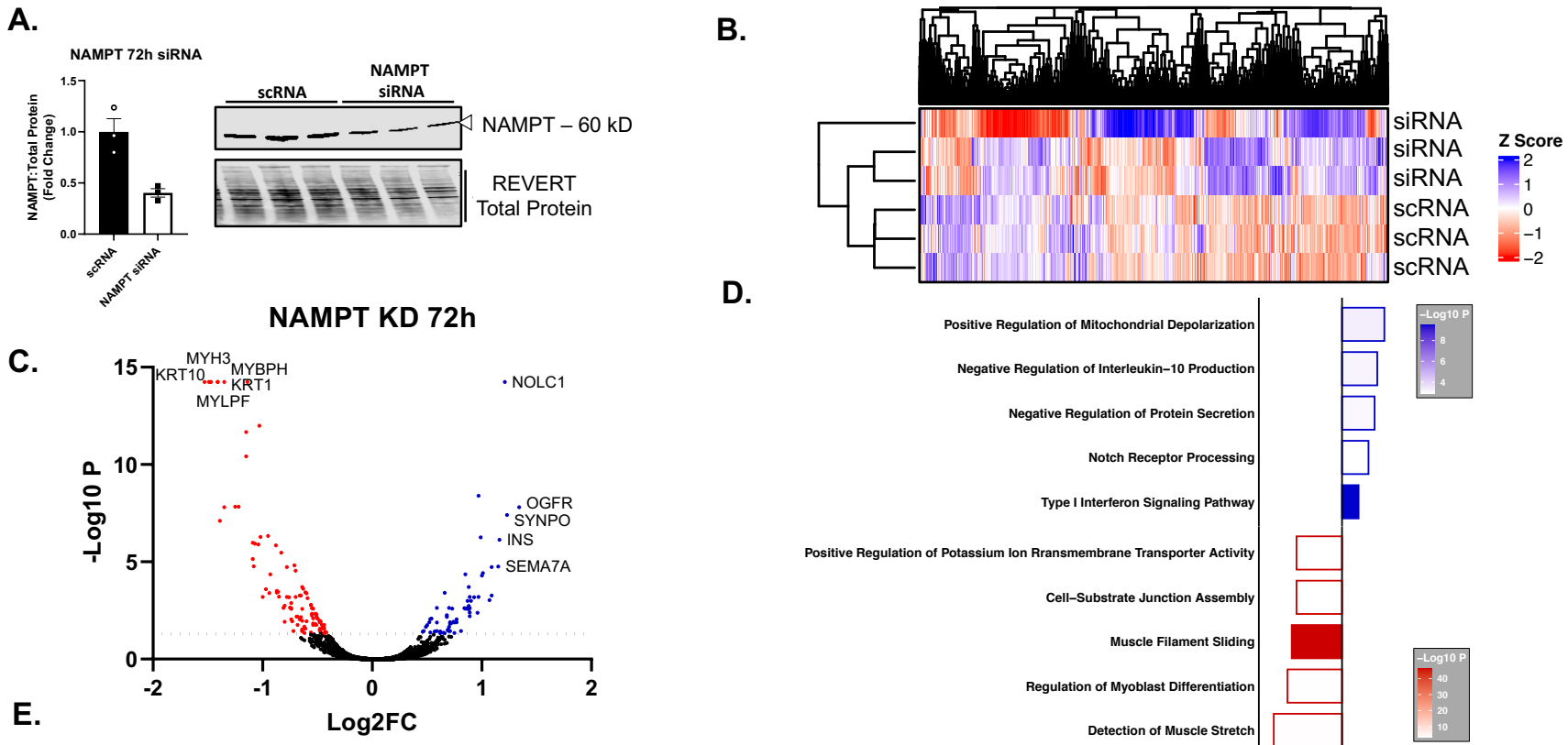

Term	Fold Enrichment	P-Value	Benjamini	Direction	Proteins
Positive Regulation of Mitochondrial Depolarization	56	3.5E-02	1.0E+00	Up	MLLT11, PARP1
Negative Regulation of Interleukin-10 Production	46.6	4.1E-02	1.0E+00	Up	CD274, DLL1
Detection of Muscle Stretch	90.3	2.2E-02	6.8E-01	Down	CSRP3, TTN
Regulation of Myoblast Differentiation	72.2	2.7E-02	8.2E-01	Down	ZFP36L1, KLHL41
Muscle Filament Sliding	66.5	8.0E-21	5.5E-18	Down	ACTN2, MYH2,3, MYH7,8, MYL1,2, MYL6B, NEB, TTN, TPM1, TPM3, TNNC2, TNNT2
Positive Regulation of Potassium Ion Rransmembrane Transporter Activity	60.2	3.2E-02	8.2E-01	Down	ATP1B1, ACTN2
Cell-Substrate Junction Assembly	60.2	3.2E-02	8.2E-01	Down	FN1, ITGA6
Striated Muscle Contraction	55.6	4.4E-05	5.1E-03	Down	CASQ2, KLHL41, MYH7, TTN
Negative Regulation of Potassium Ion Transmembrane Transporter Activity	51.6	3.8E-02	8.7E-01	Down	CASQ2, ACTN2
Sarcomere Organization	49.8	1.7E-10	3.8E-08	Down	ACTN2, ANKRD1, CASQ2, KLHL41, MYH3, OBSCN, TTN, TPM1

Supplemental Figure 15 Proteomic consequences of 72h NAMPT siRNA in Human Immortalized Myotubes. A) Western blotting confirmation of NAMPT protein knock down with siRNA. B) Unsupervised hierarchical clustering on all proteins identified in each experimental replicate. C) Volcano plot of proteins. Dotted line cut of set to $p = 0.05$, red dots indicate significantly changed proteins. D) Gene ontology enrichment analysis of top 10 upregulated and top 10 down regulated pathways. E) Top ten most enriched gene ontology pathways and the proteins that changed in those pathways.

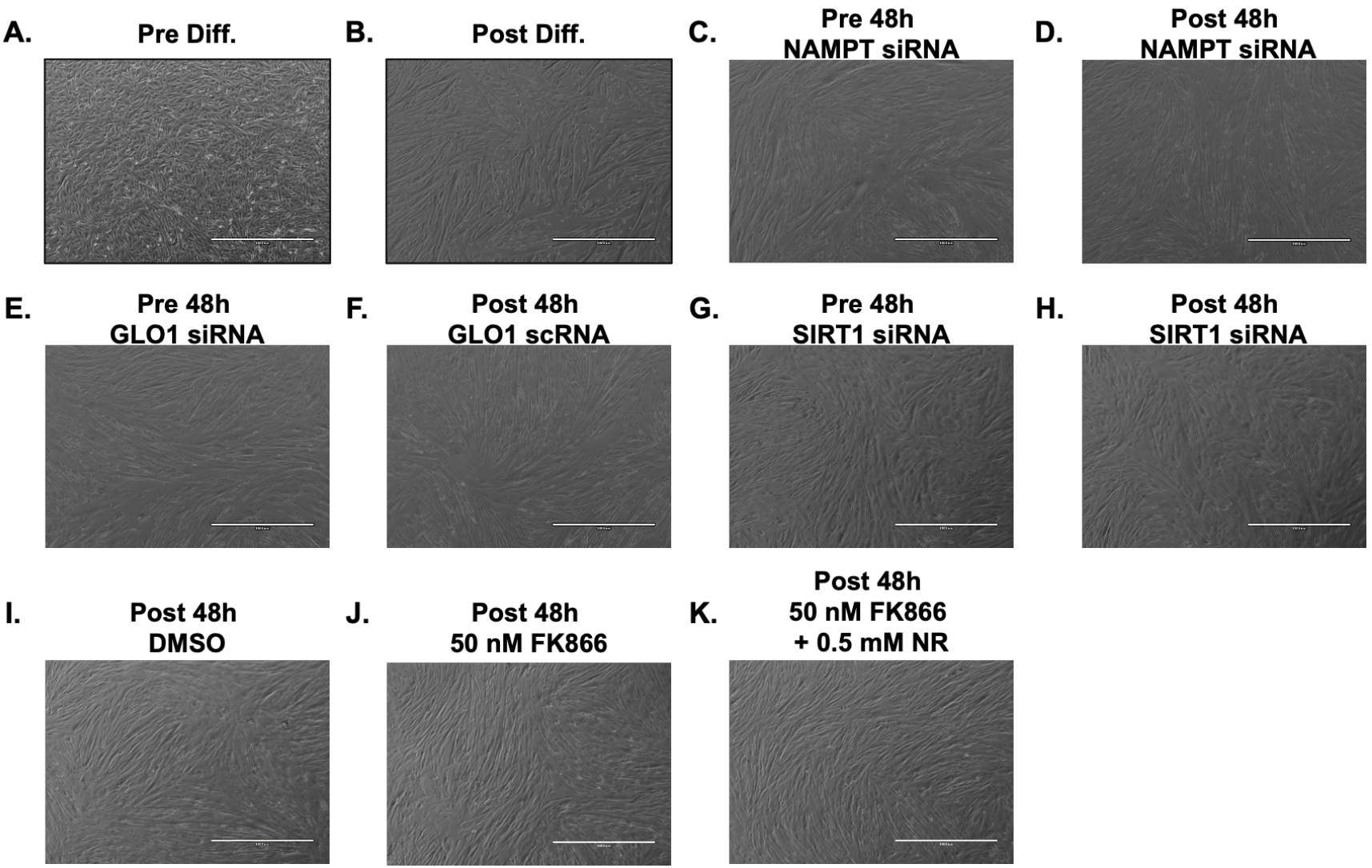

Supplemental Figure 16 Representative Images of Human Immortalized Myoblasts and Myotubes. A) Myoblasts prior to differentiation. B) Myotubes 5 dsy post differentiation. Myotubes C) Before and D) After NAMPT siRNA (48h). Myotubes E) Before and F) GLO1 siRNA (48h). Myotubes G) Before and H) After SIRT1 siRNA. Myotubes after I) DMSO, J) FK866 or FK866+NR.

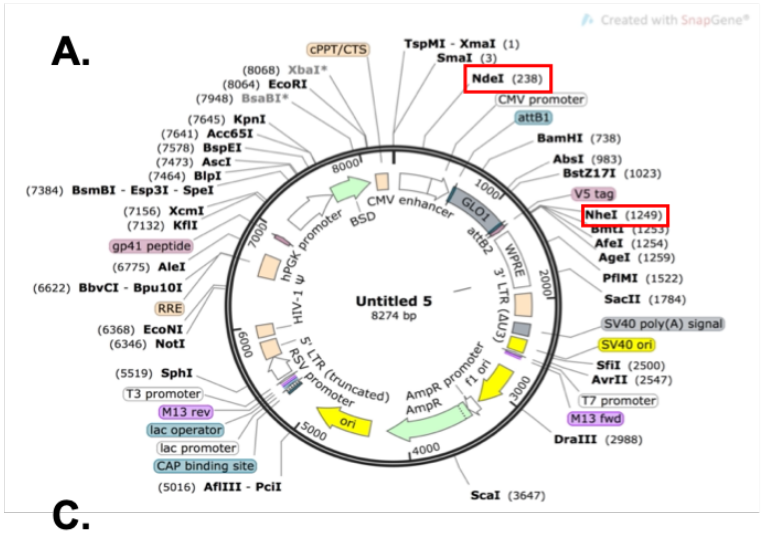

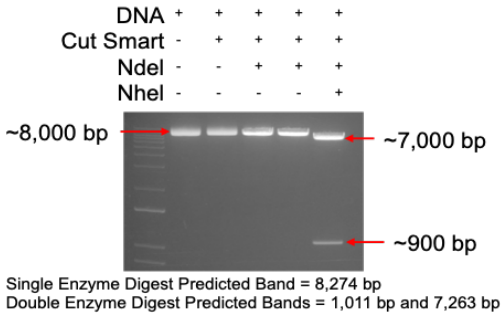

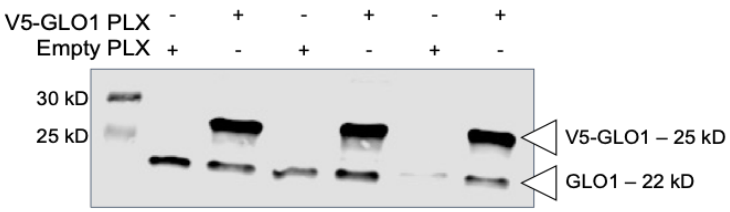

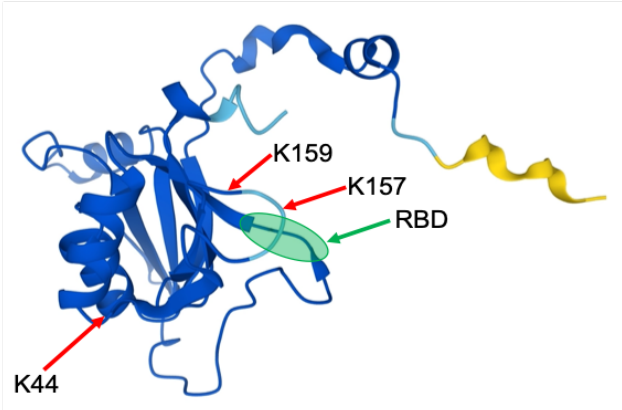

E.

Variant	PROVEAN score	Prediction (cutoff= -2.5)
K44Q	-1.928	Neutral
K157Q	-2.922	Deleterious
K159Q	-3.840	Deleterious

Supplemental Figure 17 Confirmation of GLO1 Acetylation and Identification of Lysine Acetylation Residues. A) PLX plasmid containing a V5-tagged GLO1 vector. B) Enzyme digestion to verify plasmid size. Plasmid later confirmed via sanger sequencing (not shown). C) Western blot for GLO1 and V5 in HEK293T cells transfected with an empty or V5-tagged GLO1 containing PLX plasmid. D) AlphaFold structure of GLO1 demonstrating identified acetylated lysine residues via MS/MS analysis. E) Provean *in situ* prediction of the effect of mutating identified lysine residues to glutamine to mimic acetylation.

Appendix B – List of Antibodies

Reagent /Materials	Vendor	Catalog Number	Uses	Notes
GLO1 antibody	Santa Cruz	SC133144	Immunoprecipitation of GLO1 Western blotting homogenates/lysates/AckI IP	Mouse Monoclonal Antibody
GLO1 antibody	MilliporeSigma	SAB4200193	Western blotting following GLO1 IP	Rat Monoclonal Antibody
SIRT1 antibody	Cell Signaling Tech	9475	Western blotting homogenates/lysates	Rabbit Monoclonal Antibody
NAMPT antibody	AbClonal	A0256	Western blotting homogenates/lysates	Rabbit Polyclonal Antibody
CD38 antibody	AbClonal	A1680	Western blotting homogenates/lysates	Rabbit Polyclonal Antibody
P300 antibody	Santa Cruz	SC48343	Western blotting homogenates/lysates	Mouse Monoclonal Antibody
NRF2 antibody	Abcam	Ab62352	Western blotting homogenates/lysates	Rabbit Monoclonal Antibody
KEAP1 antibody	Abclonal	A1820	Western blotting homogenates/lysates	Rabbit Polyclonal Antibody
MG-Modified proteins antibody	Cell Bio Labs	STA011	Western blotting homogenates/lysates	Mouse Monoclonal Antibody
Ubiquitin antibody	Abclonal	A0162 - 50 uL	Western blotting following GLO1 IP	Rabbit Polyclonal Antibody
P53 antibody	Santa Cruz	SC126	Western blotting following AcK IP	Mouse Monoclonal Antibody Donated by Dr. Ludlow
Pan acetyl lysine antibody	Abcam	Ab21623	Western blotting following AcK IP	Rabbit Polyclonal Antibody
Mouse IgG2a	Santa Cruz	SC3878	Negative control for GLO1 IP	Mouse IgG2a
V5 antibody	BioRad	MCA1360GA	Western blotting of cells transfected with V5-tagged GLO1	Mouse Monoclonal Antibody
Anti-Rabbit 800 CW	LiCor	926-32213	Secondary antibody for western blotting	Donkey anti-rabbit IgG
Anti-Mouse 800 CW	LiCor	926-32212	Secondary antibody for western blotting	Donkey anti-mouse IgG
Anti-Rat 680 RD	LiCor	926-68076	Secondary antibody for western blotting	Goat anti-rat IgG

Appendix Table 1 List of Antibodies.

Appendix C – List of Cells Used

Cells	Source	Catalog Number	Uses	Notes
HEK293T	ATCC	CRL-3216	GLO1 transfection experiments	Donated by Dr. Ludlow
Human immortalized myoblasts	Generated by [369]	N/A	Primary outcomes for cell culture experiments	Donated by Dr. Ludlow Stable overexpression of CDK4 and hTERT
Human myoblasts (CDK4 only)	Generated by [369]	N/A	Validation/follow up experiments	Donated by Dr. Ludlow Stable overexpression of CDK4

Appendix Table 2 List of Cells Used

Appendix D – List of Cell Culture Reagents and Materials

Reagents/Materials	Vendor/ Source	Catalog Number	Uses	Notes
DMEM	Fisher	SH30021FS	Component of Media X	Media X = 4 volumes DMEM:1 volume M199 with 10% FBS
M199	Fisher	SH3025301	Component of Media X	Media X = 4 volumes DMEM:1 volume M199 with 10% FBS
Opti-MEM	Fisher	31985062	Media used for dilution of siRNAs, scRNAs and plasmid	
FBS	Fisher	10437028	Component of Media X and growth media for myobasts	10% for treatment media, 15% for growth media
Horse serum	Fisher	26050088	Component of differentiation media for myoblasts	2% for differentitation media
Cosmic calf serum	Fisher	SH3008703	Used instead of FBS in Media X for HEK293T culture	10% for growth media
HEPEs	Invitrogen	15630-080	Components of myoblast growth media	
Zn2SO4	Fisher	S68-500	Components of myoblast growth media	
Vitamin B12	Sigma	V2786	Components of myoblast growth media	
Dexamethasone	Stem Cell Tech	72092	Components of myoblast growth media	
HGF	Chemicon Int.	GF116	Components of myoblast growth media	Added to 50 mL growth media aliquots on weekly basis
bFGF	BioPioneer	HRP-0011	Components of myoblast growth media	Added to 50 mL growth media aliquots on weekly basis
Pig skin gelatin	Sigma	G1890-500g	Components of myoblast growth media	Diluted to 1% stock with sterile water
Sterile Water	Sigma	W3500-1L	Dilution of pig skin gelatin	
100 mm plate	Fisher	877222	Cell culture	Dilution of pig skin gelatin
6-well cell culture plate	Fisher	130184	Cell culture	Coated with 0.1% pig skin gelatin prior to plating cells
Steriflip-GP 50mL Express Plus PES .22um	Sigma	SCGP00525	Filtering of media after addition of glucose or other non-sterile components	
Gibco TrypLE Select Enzyme (1X) no phenol red	Fisher	50-591-419	Lifting of cells for passaging and harvesting	100 µL per 6-well plate, 1 mL per 100 mm plate for lifting
Dextrose	Fisher	D16-500	Added to all cell culture media for myoblasts to final concentration of 25 mM	Media filtered after addition of dextrose

Low O2 gas	Cryogenic Gases	310039	Generation of low oxygen atmosphere for myoblasts	5% CO2, 2% O2, balance N2
GLO1 plasmid	Horizon Discovery	OHS6085-213573330	Transfection experiments in HEK293T cells	
Trichostatin A	Sigma	T8552-1MG	HDAC inhibitor Cell culture treatment Added to cell lysis buffer to preserve acetylation status of proteins	Sterile water as solvent
Nicotinamide riboside	Cayman Chemical	1341-23-7	Cell culture treatment to rescue NAD	Sterile water as solvent
FK866	Fisher	50-101-3518	Cell culture treatment to inhibit NAMPT	DMSO as solvent
MG132	Ubpbio	50-112-6889	Cell culture treatment to inhibit proteasome	DMSO as solvent
EX527	Tocris Bioscience	278010	Cell culture treatment to inhibit SIRT1	DMSO as solvent
AGK2	SelleckChem	S7577	Cell culture treatment to inhibit SIRT2	DMSO as solvent
Curcumin	SelleckChem	S1848	Cell culture treatment to inhibit P300	DMSO as solvent
Butyrolactone-3	Santa Cruz	SC-358657	Cell culture treatment to inhibit GCN5	DMSO as solvent
DMSO	BioTechne	3176/25mL	Solvent for cell culture treatments	
dPBS, no calcium, no magnesium	Fisher	14-190-136	Washing cells between cell changes and prior to trypsinization	
Lipofectamine RNAiMax	Fisher	13778150	Transfection of siRNAs	
Lipofectamine 3000	Fisher	L3000008	Transfection of GLO1 plasmid	

Appendix Table 3 List of Cell Culture Reagents and Materials.

Appendix E – Formulation of Human Immortalized Myoblast Growth Media

Component	Stock Concentration	Volume Needed for Stock (mL)	Weight for Stock Solution (mg)	Volume to add for 0.6059 L Media (mL)	Procedure Notes
Media X	**4:1 DMEM/Medium 199**	**N/A**	**N/A**	**500**	Prepare using sterile technique and store surplus at 4 C.
FBS	**100%**	**N/A**	**N/A**	**90.6315**	Add to media using sterile technique and store surplus at -20 C.
HEPES	**1 M**	**N/A**	**N/A**	**12.084**	Add to media using sterile technique and store surplus at -20 C.
Zn_2SO_4	**60 ug/mL**	**33.33**	**2**	**0.302**	**1)** Weigh out 2 mg of Zn_2SO_4 into 50 mL Falcon Tube. **2)** Clean Falcon tube with 70% EtOH and place in CC hood. **3)** Add 33.33 mL of **STERILE NUCLEASE-FREE WATER** to Falcon tube and mix by inverting. **4)** Filter solution through 0.22 um filter. **5)** Make 1.3 mL (enough to make 2 batches of 1.2 L of media) aliquots of stock solution into **STERILE MICROCENTRIFUGE TUBES** and store @ -20 C. **6) Add appropriate volume to complete media stock using sterile technique**

Vitamin B12	**20 mg/mL**	**5**	**100**	**0.0425**	**1)** Weight of purchased Vit. B12 is 100 mg. **2)** Clean sealed vial with 70% EtOH and place in CC hood. **3)** Add 5 mL of **STERILE NUCLEASE-FREE WATER** to vial and mix by pipetting. **4)** Make 260 uL (enough to make 3 batches of 1.2 L of media) aliquots of stock solution into **STERILE MICROCENTRIFUGE TUBES** and store @ -20 C. **5) Add appropriate volume to complete media stock using sterile technique**
Dexamethasone	**55 ug/mL**	**36.36**	**2**	**0.604**	**1)** Weigh out 2 mg of Dexamethasone into 50 mL Falcon Tube. **2)** Clean Falcon tube with 70% EtOH and place in CC hood. **3)** Add 36.36 mL of **CELL CULTURE GRADE DMSO** to Falcon tube and mix by inverting. **4)** Filter solution through 0.22 um filter. **5)** Make 2.5 mL (enough to make 2 batches of 1.2 L of media) aliquots of stock solution into **STERILE 15 mL FALCON TUBES** and store @ -20 C. **6) Add appropriate volume to complete media stock using sterile technique**

HGF	**5 ug/mL**	**2**	**0.01**	**N/A**	**1)** Weight of purchased HGF is 10 ug. **2)** Clean sealed vial with 70% EtOH and place in CC hood. **3)** Add 2 mL of **MEDIA X** to vial and mix by pipetting. **4)** Make 200 uL aliquots of stock solution into **STERILE MICROCENTRIFUGE TUBES** and store @ -20 C. **5) HGF is added weekly to complete media to a final concentration of 2.5 ng/mL**
bFGF	**20 ug/mL**	**2.5**	**0.05**	**N/A**	**1)** Weight of purchased bFGF is 50 ug. **2)** Clean sealed vial with 70% EtOH and place in CC hood. **3)** Add 2.5 mL of **MEDIA X** to vial and mix by pipetting. **4)** Make 200 uL aliquots of stock solution into **STERILE MICROCENTRIFUGE TUBES** and store @ -20 C. **5) bFGF is added weekly to complete media to a final concentration of 2.5 ng/mL**

Appendix Table 4 Formulation and Protocol for Growth Media.

Appendix F – SOP for Coating Cell Culture Plates

Component	Stock Concentration	Volume Needed for Stock (mL)	Weight for Stock Solution (g)	Working Concentration	Procedure Notes
Pig Skin Gelatin	**1%**	**100**	**1**	**0.10%**	**1)** Weigh out 1 g of pig skin gelatin into a glass vessel with screw cap. **2)** Add 100 mL of diH_2O and mix by swirling and inverting. **3)** Autoclave 1% solution **4)** Prepare CC hood **5) DO NOT PERFORM DRYING CYCLE AFTER AUTOCLAVE CYCLE, TIGHTEN CAP & MOVE DIRECTLY INTO CC HOOD** **6)** Aliquot amount needed for planned experiments and dilute 1:10 with **STERILE NUCLEASE-FREE WATER** **7)** Store remaining stock solution at 4 C **8)** Use 6 - 8 mL of 0.1% working solution to cover a 10 cm dish **9)** Let stand for 30 minutes or more at 37 C in sterile incubator **10)** Aspirate solution and use dish immediately

Appendix Table 5 Procedure for Coating Cell Culture Vessels with Pig Skin Gelatin

Appendix G – Biochemistry Kits and Reagents

Reagents /Material	Vendor/Source	Catalog Number	Uses	Notes
GLO1 ELISA	MyBioSource	MBS2021816	Quantification of GLO1 protein in cell culture samples	Quantification used to calculate specific activity in conjunction with activity assay
GLO1 activity assay	Biovision	K591-100	Determination of GLO1 activity in myotubes and human muscle tissue	Cells lysed in GLO1 activity assay buffer for activity assay and ELISA
Cell lysis buffer	Cell Signaling Tech	9803S	Homogenization of muscle and lysing of cells for western blotting and IP	
RIPA buffer	Cell Signaling Tech	9806S	Homogenization of lysing of cells for LC-MS/MS	
BCA assay reagent A and B	Fisher	0023223 and 0023224	Protein estimation in lysates and homogenates	
Protease phosphatase inhibitor cocktail	Cell Signaling Tech	5872S	Added to lysis buffer to stabilize proteins in sample	
Iodoacetamide	Sigma		Added to lysis buffer to inhibit deubiquitinases	Only added to samples marked for GLO1 Ubiquitination determination
Perchloric acid 70%	Fisher	A2296-1LB	NAD assay	
Sodium phosphate monobasic	Fisher	567545-1KG	NAD assay	Combined with dibasic to make 1M Sodium phosphate buffer, titrated to pH 8
Sodium phosphate dibasic	Fisher	567550-1KG	NAD assay	Combined with monobasic to make 1M Sodium phosphate buffer, titrated to pH 8
BSA	Roche	3117405001	NAD assay	Prepared fresh for each NAD assay
NAM	Sigma	NO636-100G	NAD assay Added to cell lysis buffer to inactivate deacetylases Cell culture treatment	Prepared fresh for each NAD assay 10mM final conc. for lysis buffer mM final conc. for cell culture treatment
Ethanol (molecular grade)	Fisher	BP2818500	NAD assay	
FMN	Sigma	F6750	NAD assay	Aliquots stored at -20 C no longer than 30 days
Resazurin	StemCell Tech	75005	NAD assay	Aliquots stored at -20 C no longer than 30 days
Alcohol dehydrogenase	Sigma	A3263	NAD assay	Aliquots stored at -80 C

Diaphorase	Sigma	5540	NAD assay	Aliquots stored at -80 C
NAD	Roche	10127965001	NAD assay	Standard curves stored at -20 C no longer than 30 days
96-well black bottom plate	Sigma	3915	NAD assay	
Acetyl lysine conjugated agarose beads	Immunechem	ICP0388-5mg	Immunoprecipitation of pan-acetylated proteins	
Catch and Release IP Kit	Sigma	17-500A	Immunoprecipitation of GLO1	Self contained agarose bead system for IP
Tris/Glycine/SDS buffer	BioRad	1610732	Running buffer for gel electrophoresis	
Nitrocellulose transfer pack	BioRad	1704159	Transblot turbo transfer system for western blotting	
10% Criterion TGX Gels	BioRad	5671033	Electrophoretic separation of proteins for western blotting	
2X Laemmeli Buffer	BioRad	1610737	Sample buffer for gel electrophoresis	
BME	BioRad	1610710XTU	Reducing reagent added to laemmeli buffer	
3-5% Criterion tris acetate gel	BioRad	3450129	Electrophoretic separation of proteins for western blotting large proteins	Used for western blotting of P300 only
XT Reducing agent	BioRad	1610792	Reducing reagent added to XT sample buffer	Used for tricine gels, P300 western blotting
XT Tricine running buffer	BioRad	1610790	Running buffer for gel electrophoresis using tricine gels	P300 western blot only
XT sample buffer	BioRad	1610791		
Ponceau	Sigma	6226-79-5	Total protein stain for western blotting	
Revert Total Protein Stain	LiCor	925-11021	Total protein stain for western blotting	
Protein-Free Blocking Buffer	LiCor	927-80003	Blocking buffer for western blotting Diluent for antibody solution	
Chameleon Protein Ladder	LiCor	928-90000	Protein molecular weigh marker for western blotting	
Tween 20	Sigma	BP337-500	Detergent added to antibody solutions for western blotting	0.1% final concentration
Control siRNA (scRNA)	Santa Cruz	SC-37007	Control for siRNA treatments	
SIRT1 siRNA	Santa Cruz	SC-40986	SIRT1 KD experiments	
GLO1 siRNA	Santa Cruz	SC-60703	GLO1 KD experiments	
NAMPT siRNA	Santa Cruz	SC-45843	NAMPT KD experiments	

RNeasy plus universal mini kit	Qiagen	1062832	RNA isolation from cell culture samples
RNeasy fibrous tissue mini kt	Qiagen	74704	RNA isolation from muscle tissue samples
Qiashredders	Qiagen	79654	Lysing cell culture pellets for RNA isolation
Qiazol	Qiagen	1023537	Lysing cell culture pellets for RNA isolation
Chloroform	Sigma	C2432-25ML	Lysing of cells for RNA isolation
RNAlater	Invitrogen	AM7020	Preservation of RNA in muscle tissue samples
iScript Advanced reverse transcription kit	BioRad	1725038	Generation of cDNA libraries from RNA
DNA midi-prep isolation kit	Macherey-Nagel	740499.250	Isolation of plasmid DNA from bacteria preps
TMT 6-plex	Fisher	PI90061	LC-MS/MS
TMT 16-plex	Fisher	PIA44521	LC-MS/MS

Appendix Table 6 List of Kits and Biochemistry Reagents.

Appendix H – Probes and Primers for PCR

Target	Vendor/Source	Catalog Number	Seqeunce 5' - 3'	Notes
GLO1 FWD Primer	IDT	N/A	GGA CCC CAG TAC CAA GGA TT	Primer pairs identified using Roche primer design for probe based PCR
GLO1 REV Primer	IDT	N/A	TGG GAA AAT CAC ATT TTT GGA T	Primer pairs identified using Roche primer design for probe based PCR
GLO1 Probe	Roche	4689089001	GCAGCAGA	UPL probe 84 (FAM)
SIRT1 FWD Primer	IDT	N/A	TGT ACG ACG AAG ACG ACG AC	Primer pairs identified using Roche primer design for probe based PCR
SIRT1 REV Primer	IDT	N/A	TTC ATC ACC GAA CAG AAG GTT	Primer pairs identified using Roche primer design for probe based PCR
SIRT1 Probe	Roche	4688627001	CTTCCTCCT	UPL probe 63 (FAM)
NAMPT FWD Primer	IDT	N/A	GCC AGC AGG GAA TTT TGT TA	Primer pairs identified using Roche primer design for probe based PCR
NAMPT REV Primer	IDT	N/A	GCC ATT CTT GAA GAC AGT ATG GA	Primer pairs identified using Roche primer design for probe based PCR
NAMPT Probe	Roche	4688643001	TCCTCCAG	UPL probe 65 (FAM)
NRF2 FWD Primer	IDT	N/A	ACA CGG TCC ACA GCT CAT C	Primer pairs identified using Roche primer design for probe based PCR
NRF2 REV Primer	IDT	N/A	TGC CTC CAA AGT ATG TCA ATC A	Primer pairs identified using Roche primer design for probe based PCR
NRF2 Probe	Roche	4685008001	CCTGGAGC	UPL probe 3 (FAM)
KEAP1 FWD Primer	IDT	N/A	GGG TCC CCT ACA GCC AAG	Primer pairs identified using Roche primer design for probe based PCR
KEAP1 REV Primer	IDT	N/A	TGG GGT TCC AGA AGA TAA GC	Primer pairs identified using Roche primer design for probe based PCR
KEAP1 Probe	Roche	4689003001	CCACCACC	UPL probe 77 (FAM)

Appendix Table 7 List of PCR Probes and Primers.

BIBLIOGRAPHY

1. WHO. *Obesity and Overweight* 2020; Available from: https://www.who.int/news-room/fact-sheets/detail/obesity-and-overweight.
2. Field, A.E., et al., *Impact of overweight on the risk of developing common chronic diseases during a 10-year period.* Arch Intern Med, 2001. **161**(13): p. 1581-6.
3. Zhao, Y., P. Wang, and S. Sang, *Dietary Genistein Inhibits Methylglyoxal-Induced Advanced Glycation End Product Formation in Mice Fed a High-Fat Diet.* The Journal of Nutrition, 2019. **149**(5): p. 776-787.
4. Maessen, D.E., et al., *Delayed Intervention With Pyridoxamine Improves Metabolic Function and Prevents Adipose Tissue Inflammation and Insulin Resistance in High-Fat Diet–Induced Obese Mice.* Diabetes, 2016. **65**(4): p. 956-966.
5. Rabbani, N. and P.J. Thornalley, *Glyoxalase 1 Modulation in Obesity and Diabetes.* Antioxid Redox Signal, 2018.
6. Ahmed, N., et al., *Degradation products of proteins damaged by glycation, oxidation and nitration in clinical type 1 diabetes.* Diabetologia, 2005. **48**(8): p. 1590-603.
7. Thornalley, P.J., *Pharmacology of methylglyoxal: formation, modification of proteins and nucleic acids, and enzymatic detoxification--a role in pathogenesis and antiproliferative chemotherapy.* Gen Pharmacol, 1996. **27**(4): p. 565-73.
8. Thornalley, P.J., *Modification of the glyoxalase system in human red blood cells by glucosein vitro.* Biochemical Journal, 1988. **254**(3): p. 751-755.
9. Rabbani, N. and P.J. Thornalley, *Glyoxalase 1 Modulation in Obesity and Diabetes.* Antioxidants & Redox Signaling, 2019. **30**(3): p. 354-374.
10. Rai, A.K., et al., *Fructose-induced AGEs-RAGE signaling in skeletal muscle contributes to impairment of glucose homeostasis.* The Journal of Nutritional Biochemistry, 2019. **71**: p. 35-44.
11. Riboulet-Chavey, A., et al., *Methylglyoxal Impairs the Insulin Signaling Pathways Independently of the Formation of Intracellular Reactive Oxygen Species.* Diabetes, 2006. **55**(5): p. 1289-1299.
12. Stratmann, B., et al., *Intracellular Accumulation of Methylglyoxal by Glyoxalase 1 Knock Down Alters Collagen Homoeostasis in L6 Myoblasts.* International Journal of Molecular Sciences, 2017. **18**(3): p. 480.
13. Spanos, C., et al., *Proteomic identification and characterization of hepatic glyoxalase 1 dysregulation in non-alcoholic fatty liver disease.* Proteome Science, 2018. **16**(1).
14. Tremmel, M., et al., *Economic Burden of Obesity: A Systematic Literature Review.* International Journal of Environmental Research and Public Health, 2017. **14**(4): p. 435.

15. Ogden, C.L., et al., *Prevalence of Childhood and Adult Obesity in the United States, 2011-2012.* JAMA, 2014. **311**(8): p. 806.
16. Földi, M., et al., *Obesity is a risk factor for developing critical condition in COVID-19 patients: A systematic review and meta-analysis.* Obesity Reviews, 2020. **21**(10).
17. Popkin, B.M., et al., *Individuals with obesity and COVID-19: A global perspective on the epidemiology and biological relationships.* Obesity Reviews, 2020. **21**(11).
18. Huang, Y., et al., *Obesity in patients with COVID-19: a systematic review and meta-analysis.* Metabolism, 2020. **113**: p. 154378.
19. Steinberg, E., E. Wright, and B. Kushner, *In Young Adults with COVID-19, Obesity Is Associated with Adverse Outcomes.* Western Journal of Emergency Medicine, 2020. **21**(4).
20. Lobstein, T., *The Cost of Not Addressing the Global Obesity Crisis*, in *COVID-19 and Obesity: The 2021 Atlas*, J. Wilding, Editor. 2021: worldobesity.org. p. 277.
21. Eckel, N., et al., *Transition from metabolic healthy to unhealthy phenotypes and association with cardiovascular disease risk across BMI categories in 90 257 women (the Nurses' Health Study): 30 year follow-up from a prospective cohort study.* The Lancet Diabetes & Endocrinology, 2018. **6**(9): p. 714-724.
22. Flegal, K.M., et al., *Association of All-Cause Mortality With Overweight and Obesity Using Standard Body Mass Index Categories.* JAMA, 2013. **309**(1): p. 71.
23. Aune, D., et al., *BMI and all cause mortality: systematic review and non-linear dose-response meta-analysis of 230 cohort studies with 3.74 million deaths among 30.3 million participants.* BMJ, 2016: p. i2156.
24. Qasim, A., et al., *On the origin of obesity: identifying the biological, environmental and cultural drivers of genetic risk among human populations.* Obesity Reviews, 2018. **19**(2): p. 121-149.
25. Chou, S.-Y., M. Grossman, and H. Saffer, *An economic analysis of adult obesity: results from the Behavioral Risk Factor Surveillance System.* Journal of Health Economics, 2004. **23**(3): p. 565-587.
26. Conway, B. and A. Rene, *Obesity as a disease: no lightweight matter.* Obesity Reviews, 2004. **5**(3): p. 145-151.
27. Bouchard, C., et al., *The Response to Long-Term Overfeeding in Identical Twins.* New England Journal of Medicine, 1990. **322**(21): p. 1477-1482.
28. Ling, C. and T. Rönn, *Epigenetics in Human Obesity and Type 2 Diabetes.* Cell Metabolism, 2019. **29**(5): p. 1028-1044.
29. Rohde, K., et al., *Genetics and epigenetics in obesity.* Metabolism, 2019. **92**: p. 37-50.
30. Defronzo, R.A., *Banting Lecture. From the triumvirate to the ominous octet: a new paradigm for the treatment of type 2 diabetes mellitus.* Diabetes, 2009. **58**(4): p. 773-95.
31. DeFronzo, R.A., et al., *Synergistic interaction between exercise and insulin on peripheral glucose uptake.* J Clin Invest, 1981. **68**(6): p. 1468-74.
32. Sibbersen, C. and M. Johannsen, *Dicarbonyl derived post-translational modifications: chemistry bridging biology and aging-related disease.* Essays Biochem, 2020. **64**(1): p. 97-110.

33. Masania, J., et al., *Dicarbonyl stress in clinical obesity.* Glycoconjugate Journal, 2016. **33**(4): p. 581-589.
34. Andersen, S.T., et al., *Risk Factors for Incident Diabetic Polyneuropathy in a Cohort With Screen-Detected Type 2 Diabetes Followed for 13 Years: ADDITION-Denmark.* Diabetes Care, 2018.
35. Mey, J.T., et al., *Dicarbonyl stress and glyoxalase enzyme system regulation in human skeletal muscle.* Am J Physiol Regul Integr Comp Physiol, 2018. **314**(2): p. R181-R190.
36. Rabbani, N., M. Xue, and P.J. Thornalley, *Methylglyoxal-induced dicarbonyl stress in aging and disease: first steps towards glyoxalase 1-based treatments.* Clin Sci (Lond), 2016. **130**(19): p. 1677-96.
37. Babizhayev, M.A., et al., *The Role of Oxidative Stress in Diabetic Neuropathy: Generation of Free Radical Species in the Glycation Reaction and Gene Polymorphisms Encoding Antioxidant Enzymes to Genetic Susceptibility to Diabetic Neuropathy in Population of Type I Diabetic Patients.* Cell Biochem Biophys, 2015. **71**(3): p. 1425-43.
38. Uribarri, J., et al., *Suppression of native defense mechanisms, SIRT1 and PPARgamma, by dietary glycoxidants precedes disease in adult humans; relevance to lifestyle-engendered chronic diseases.* Amino Acids, 2014. **46**(2): p. 301-9.
39. Wautier, M.P., et al., *Activation of NADPH oxidase by AGE links oxidant stress to altered gene expression via RAGE.* Am J Physiol Endocrinol Metab, 2001. **280**(5): p. E685-94.
40. Polykretis, P., et al., *Methylglyoxal interaction with superoxide dismutase 1.* Redox Biology, 2020. **30**: p. 101421.
41. Ishibashi, Y., et al., *Methylglyoxal-derived hydroimidazolone-1 evokes inflammatory reactions in endothelial cells via an interaction with receptor for advanced glycation end products.* Diab Vasc Dis Res, 2017. **14**(5): p. 450-453.
42. Semba, R.D., et al., *Serum carboxymethyl-lysine, an advanced glycation end product, is associated with arterial stiffness in older adults.* J Hypertens, 2015. **33**(4): p. 797-803; discussion 803.
43. Gaens, K.H., et al., *Nepsilon-(carboxymethyl)lysine-receptor for advanced glycation end product axis is a key modulator of obesity-induced dysregulation of adipokine expression and insulin resistance.* Arterioscler Thromb Vasc Biol, 2014. **34**(6): p. 1199-208.
44. Takahashi, H.K., et al., *Advanced glycation end products subspecies-selectively induce adhesion molecule expression and cytokine production in human peripheral blood mononuclear cells.* J Pharmacol Exp Ther, 2009. **330**(1): p. 89-98.
45. de la Maza, M.P., et al., *Weight increase is associated with skeletal muscle immunostaining for advanced glycation end products, receptor for advanced glycation end products, and oxidation injury.* Rejuvenation Res, 2008. **11**(6): p. 1041-8.
46. Hofmann, M.A., et al., *RAGE mediates a novel proinflammatory axis: a central cell surface receptor for S100/calgranulin polypeptides.* Cell, 1999. **97**(7): p. 889-901.

47. Yao, D. and M. Brownlee, *Hyperglycemia-induced reactive oxygen species increase expression of the receptor for advanced glycation end products (RAGE) and RAGE ligands.* Diabetes, 2010. **59**(1): p. 249-55.
48. Martens, R.J.H., et al., *Relations of advanced glycation endproducts and dicarbonyls with endothelial dysfunction and low-grade inflammation in individuals with end-stage renal disease in the transition to renal replacement therapy: A cross-sectional observational study.* PLOS ONE, 2019. **14**(8): p. e0221058.
49. Neves, C., et al., *Dietary Glycotoxins Impair Hepatic Lipidemic Profile in Diet-Induced Obese Rats Causing Hepatic Oxidative Stress and Insulin Resistance.* Oxidative Medicine and Cellular Longevity, 2019. **2019**: p. 1-14.
50. Rodrigues, T., et al., *Methylglyoxal-induced glycation changes adipose tissue vascular architecture, flow and expansion, leading to insulin resistance.* Scientific Reports, 2017. **7**(1).
51. Vlassara, H., et al., *Oral AGE restriction ameliorates insulin resistance in obese individuals with the metabolic syndrome: a randomised controlled trial.* Diabetologia, 2016. **59**(10): p. 2181-92.
52. Xu, J.X., et al., *Serum advanced glycation end products are associated with insulin resistance in male nondiabetic patients with obstructive sleep apnea.* Sleep Breath, 2015. **19**(3): p. 827-33.
53. Uribarri, J., et al., *Elevated serum advanced glycation endproducts in obese indicate risk for the metabolic syndrome: a link between healthy and unhealthy obesity?* J Clin Endocrinol Metab, 2015. **100**(5): p. 1957-66.
54. Cai, W., et al., *Oral advanced glycation endproducts (AGEs) promote insulin resistance and diabetes by depleting the antioxidant defenses AGE receptor-1 and sirtuin 1.* Proc Natl Acad Sci U S A, 2012. **109**(39): p. 15888-93.
55. Uribarri, J., et al., *Restriction of advanced glycation end products improves insulin resistance in human type 2 diabetes: potential role of AGER1 and SIRT1.* Diabetes Care, 2011. **34**(7): p. 1610-6.
56. Tan, K.C., et al., *Serum advanced glycation end products (AGEs) are associated with insulin resistance.* Diabetes Metab Res Rev, 2011. **27**(5): p. 488-92.
57. Cassese, A., et al., *In skeletal muscle advanced glycation end products (AGEs) inhibit insulin action and induce the formation of multimolecular complexes including the receptor for AGEs.* J Biol Chem, 2008. **283**(52): p. 36088-99.
58. Ng, Z.X., et al., *Soluble receptor for advanced glycation end-product (sRAGE)/pentosidine ratio: a potential risk factor determinant for type 2 diabetic retinopathy.* Int J Mol Sci, 2013. **14**(4): p. 7480-91.
59. Kerkeni, M., et al., *Elevated serum levels of AGEs, sRAGE, and pentosidine in Tunisian patients with severity of diabetic retinopathy.* Microvasc Res, 2012. **84**(3): p. 378-83.
60. Ahmed, N., *Advanced glycation endproducts--role in pathology of diabetic complications.* Diabetes Res Clin Pract, 2005. **67**(1): p. 3-21.
61. Beisswenger, P.J., et al., *Formation of immunochemical advanced glycosylation end products precedes and correlates with early manifestations of renal and retinal disease in diabetes.* Diabetes, 1995. **44**(7): p. 824-9.
62. Genuth, S., et al., *Glycation and Carboxymethyllysine Levels in Skin Collagen Predict the Risk of Future 10-Year Progression of Diabetic Retinopathy and*

Nephropathy in the Diabetes Control and Complications Trial and Epidemiology of Diabetes Interventions and Complications P. Diabetes, 2005. **54**(11): p. 3103-3111.
63. Aubert, C.E., et al., *Association of peripheral neuropathy with circulating advanced glycation end products, soluble receptor for advanced glycation end products and other risk factors in patients with type 2 diabetes.* Diabetes Metab Res Rev, 2014. **30**(8): p. 679-85.
64. Huang, K.P., et al., *AGEs-RAGE system down-regulates Sirt1 through the ubiquitin-proteasome pathway to promote FN and TGF-beta1 expression in male rat glomerular mesangial cells.* Endocrinology, 2015. **156**(1): p. 268-79.
65. Huang, K., et al., *Polydatin promotes Nrf2-ARE anti-oxidative pathway through activating Sirt1 to resist AGEs-induced upregulation of fibronetin and transforming growth factor-beta1 in rat glomerular messangial cells.* Mol Cell Endocrinol, 2015. **399**: p. 178-89.
66. Thomas, M.C., et al., *Relationship between levels of advanced glycation end products and their soluble receptor and adverse outcomes in adults with type 2 diabetes.* Diabetes Care, 2015. **38**(10): p. 1891-7.
67. Beisswenger, P.J., et al., *Detection of diabetic nephropathy from advanced glycation endproducts (AGEs) differs in plasma and urine, and is dependent on the method of preparation.* Amino Acids, 2014. **46**(2): p. 311-9.
68. Beisswenger, P.J., et al., *Early progression of diabetic nephropathy correlates with methylglyoxal-derived advanced glycation end products.* Diabetes Care, 2013. **36**(10): p. 3234-9.
69. Perkins, B.A., et al., *Serum levels of advanced glycation endproducts and other markers of protein damage in early diabetic nephropathy in type 1 diabetes.* PLoS One, 2012. **7**(4): p. e35655.
70. Coughlan, M.T., et al., *Advanced glycation urinary protein-bound biomarkers and severity of diabetic nephropathy in man.* Am J Nephrol, 2011. **34**(4): p. 347-55.
71. Coughlan, M.T. and J.M. Forbes, *Temporal increases in urinary carboxymethyllysine correlate with albuminuria development in diabetes.* Am J Nephrol, 2011. **34**(1): p. 9-17.
72. Lin, J., et al., *Inflammation and progressive nephropathy in type 1 diabetes in the diabetes control and complications trial.* Diabetes Care, 2008. **31**(12): p. 2338-43.
73. Koschinsky, T., et al., *Orally absorbed reactive glycation products (glycotoxins): an environmental risk factor in diabetic nephropathy.* Proc Natl Acad Sci U S A, 1997. **94**(12): p. 6474-9.
74. De La Cruz-Ares, S., et al., *Endothelial Dysfunction and Advanced Glycation End Products in Patients with Newly Diagnosed Versus Established Diabetes: From the CORDIOPREV Study.* Nutrients, 2020. **12**(1): p. 238.
75. Lee, J.H., et al., *Molecular mechanisms of methylglyoxal-induced aortic endothelial dysfunction in human vascular endothelial cells.* Cell Death & Disease, 2020. **11**(5).
76. Kashyap, S.R., et al., *Glycation Reduces the Stability of ApoAI and Increases HDL Dysfunction in Diet-Controlled Type 2 Diabetes.* J Clin Endocrinol Metab, 2018. **103**(2): p. 388-396.

77. Inman, C.K., et al., *The AGE-RAGE axis in an Arab population: The United Arab Emirates Healthy Futures (UAEHFS) pilot study.* J Clin Transl Endocrinol, 2017. **10**: p. 1-8.
78. Di Pino, A., et al., *High intake of dietary advanced glycation end-products is associated with increased arterial stiffness and inflammation in subjects with type 2 diabetes.* Nutr Metab Cardiovasc Dis, 2017. **27**(11): p. 978-984.
79. Schmidt, A.M., et al., *Cellular receptors for advanced glycation end products. Implications for induction of oxidant stress and cellular dysfunction in the pathogenesis of vascular lesions.* Arterioscler Thromb, 1994. **14**(10): p. 1521-8.
80. Koska, J., et al., *Advanced Glycation End Products, Oxidation Products, and Incident Cardiovascular Events in Patients With Type 2 Diabetes.* Diabetes Care, 2018. **41**(3): p. 570-576.
81. Wautier, J.L., et al., *Receptor-mediated endothelial cell dysfunction in diabetic vasculopathy. Soluble receptor for advanced glycation end products blocks hyperpermeability in diabetic rats.* J Clin Invest, 1996. **97**(1): p. 238-43.
82. Kajikawa, M., et al., *Ratio of serum levels of AGEs to soluble form of RAGE is a predictor of endothelial function.* Diabetes Care, 2015. **38**(1): p. 119-25.
83. Bollong, M.J., et al., *A metabolite-derived protein modification integrates glycolysis with KEAP1-NRF2 signalling.* Nature, 2018. **562**(7728): p. 600-604.
84. Afzal, R.K., et al., *Methylglyoxal: Antimicrobial activity against blood culture isolates of Salmonella Typhi and other Gram negative rods.* Pakistan Journal of Medical Sciences, 2019. **35**(4).
85. Abordo, E.A., H.S. Minhas, and P.J. Thornalley, *Accumulation of α-oxoaldehydes during oxidative stress: a role in cytotoxicity.* Biochemical Pharmacology, 1999. **58**(4): p. 641-648.
86. Thornalley, P.J., et al., *Imidazopurinones are markers of physiological genomic damage linked to DNA instability and glyoxalase 1-associated tumour multidrug resistance.* Nucleic Acids Res, 2010. **38**(16): p. 5432-42.
87. Rabbani, N., A. Ashour, and P.J. Thornalley, *Mass spectrometric determination of early and advanced glycation in biology.* Glycoconj J, 2016. **33**(4): p. 553-68.
88. Waris, S., et al., *Increased DNA Dicarbonyl Glycation and Oxidation Markers in Patients with Type 2 Diabetes and Link to Diabetic Nephropathy.* Journal of Diabetes Research, 2015. **2015**: p. 1-10.
89. Ahmed, N. and P.J. Thornalley, *Peptide mapping of human serum albumin modified minimally by methylglyoxal in vitro and in vivo.* Ann N Y Acad Sci, 2005. **1043**: p. 260-6.
90. Ahmed, N. and P.J. Thornalley, *Chromatographic assay of glycation adducts in human serum albumin glycated in vitro by derivatization with 6-aminoquinolyl-N-hydroxysuccinimidyl-carbamate and intrinsic fluorescence.* Biochem J, 2002. **364**(Pt 1): p. 15-24.
91. Irshad, Z., et al., *Activation of the unfolded protein response in high glucose treated endothelial cells is mediated by methylglyoxal.* Scientific Reports, 2019. **9**(1).
92. Lo, T.W., et al., *Binding and modification of proteins by methylglyoxal under physiological conditions. A kinetic and mechanistic study with N alpha-acetylarginine, N alpha-acetylcysteine, and N alpha-acetyllysine, and bovine serum albumin.* J Biol Chem, 1994. **269**(51): p. 32299-305.

93. Rabbani, N. and P.J. Thornalley, *Methylglyoxal, glyoxalase 1 and the dicarbonyl proteome.* Amino Acids, 2012. **42**(4): p. 1133-42.
94. Venkatraman, J., K. Aggarwal, and P. Balaram, *Helical peptide models for protein glycation: proximity effects in catalysis of the Amadori rearrangement.* Chem Biol, 2001. **8**(7): p. 611-25.
95. Blom, N., et al., *Prediction of post-translational glycosylation and phosphorylation of proteins from the amino acid sequence.* Proteomics, 2004. **4**(6): p. 1633-49.
96. Rabbani, N. and P.J. Thornalley, *Methylglyoxal, glyoxalase 1 and the dicarbonyl proteome.* Amino Acids, 2012. **42**(4): p. 1133-1142.
97. Rabbani, N., M. Xue, and P.J. Thornalley, *Dicarbonyl stress, protein glycation and the unfolded protein response.* Glycoconjugate Journal, 2021.
98. Bartlett, G.J., et al., *Analysis of catalytic residues in enzyme active sites.* J Mol Biol, 2002. **324**(1): p. 105-21.
99. Moraru, A., et al., *Elevated Levels of the Reactive Metabolite Methylglyoxal Recapitulate Progression of Type 2 Diabetes.* Cell Metabolism, 2018. **27**(4): p. 926-934.e8.
100. Galligan, J.J., et al., *Methylglyoxal-derived posttranslational arginine modifications are abundant histone marks.* Proc Natl Acad Sci U S A, 2018. **115**(37): p. 9228-9233.
101. Zheng, Q., et al., *Reversible histone glycation is associated with disease-related changes in chromatin architecture.* Nat Commun, 2019. **10**(1): p. 1289.
102. Agalou, S., et al., *Advanced glycation end product free adducts are cleared by dialysis.* Ann N Y Acad Sci, 2005. **1043**: p. 734-9.
103. Perkins, R.K., et al., *Experimental Hyperglycemia Alters Circulating Concentrations and Renal Clearance of Oxidative and Advanced Glycation End Products in Healthy Obese Humans.* Nutrients, 2019. **11**(3).
104. Ahmed, N., et al., *Glycated and oxidized protein degradation products are indicators of fasting and postprandial hyperglycemia in diabetes.* Diabetes Care, 2005. **28**(10): p. 2465-71.
105. Papadaki, M., et al., *Diabetes with heart failure increases methylglyoxal modifications in the sarcomere, which inhibit function.* JCI Insight, 2018. **3**(20).
106. Crisóstomo, J., et al., *Methylglyoxal chronic administration promotes diabetes-like cardiac ischaemia disease in Wistar normal rats.* Nutrition, Metabolism and Cardiovascular Diseases, 2013. **23**(12): p. 1223-1230.
107. Cusi, K., et al., *Insulin resistance differentially affects the PI 3-kinase- and MAP kinase-mediated signaling in human muscle.* J Clin Invest, 2000. **105**(3): p. 311-20.
108. Friedman, J.E., et al., *Glucose metabolism in incubated human muscle: effect of obesity and non-insulin-dependent diabetes mellitus.* Metabolism, 1994. **43**(8): p. 1047-54.
109. Broskey, N.T., et al., *The association between lactate and muscle aerobic substrate oxidation: Is lactate an early marker for metabolic disease in healthy subjects?* Physiol Rep, 2021. **9**(3): p. e14729.
110. Horowitz, J.F., et al., *Effect of short-term fasting on lipid kinetics in lean and obese women.* Am J Physiol, 1999. **276**(2): p. E278-84.

111. Shulman, G.I., *Ectopic Fat in Insulin Resistance, Dyslipidemia, and Cardiometabolic Disease.* New England Journal of Medicine, 2014. **371**(12): p. 1131-1141.
112. Rabbani, N. and P.J. Thornalley, *Measurement of methylglyoxal by stable isotopic dilution analysis LC-MS/MS with corroborative prediction in physiological samples.* Nat Protoc, 2014. **9**(8): p. 1969-79.
113. Maessen, D.E., et al., *Post-Glucose Load Plasma alpha-Dicarbonyl Concentrations Are Increased in Individuals With Impaired Glucose Metabolism and Type 2 Diabetes: The CODAM Study.* Diabetes Care, 2015. **38**(5): p. 913-920.
114. Van Den Eynde, M.D.G., et al., *Diet-induced weight loss reduces postprandial dicarbonyl stress in abdominally obese men: Secondary analysis of a randomized controlled trial.* Clinical Nutrition, 2021. **40**(5): p. 2654-2662.
115. El-Mesallamy, H.O., et al., *Levels of soluble advanced glycation end product-receptors and other soluble serum markers as indicators of diabetic neuropathy in the foot.* J Investig Med, 2011. **59**(8): p. 1233-8.
116. Li, H., et al., *Brain Senescence Caused by Elevated Levels of Reactive Metabolite Methylglyoxal on D-Galactose-Induced Aging Mice.* Frontiers in Neuroscience, 2019. **13**.
117. Markova, I., et al., *The effect of dicarbonyl stress on the development of kidney dysfunction in metabolic syndrome – a transcriptomic and proteomic approach.* Nutrition & Metabolism, 2019. **16**(1).
118. Chan, C.M., et al., *Methylglyoxal induces cell death through endoplasmic reticulum stress-associated ROS production and mitochondrial dysfunction.* J Cell Mol Med, 2016.
119. Kim, D., et al., *Methylglyoxal-Induced Dysfunction in Brain Endothelial Cells via the Suppression of Akt/HIF-1α Pathway and Activation of Mitophagy Associated with Increased Reactive Oxygen Species.* Antioxidants, 2020. **9**(9): p. 820.
120. Chu, P., et al., *Phosphocreatine protects endothelial cells from Methylglyoxal induced oxidative stress and apoptosis via the regulation of PI3K/Akt/eNOS and NF-κB pathway.* Vascular Pharmacology, 2017. **91**: p. 26-35.
121. Fiory, F., et al., *Methylglyoxal impairs insulin signalling and insulin action on glucose-induced insulin secretion in the pancreatic beta cell line INS-1E.* Diabetologia, 2011. **54**(11): p. 2941-2952.
122. Nigro, C., et al., *Methylglyoxal impairs endothelial insulin sensitivity both in vitro and in vivo.* Diabetologia, 2014. **57**(7): p. 1485-1494.
123. Barrett, E.J. and Z. Liu, *The endothelial cell: An "early responder" in the development of insulin resistance.* Reviews in Endocrine and Metabolic Disorders, 2013. **14**(1): p. 21-27.
124. Mahmoud, A.M., et al., *Hyperinsulinemia augments endothelin-1 protein expression and impairs vasodilation of human skeletal muscle arterioles.* Physiol Rep, 2016. **4**(16).
125. Matafome, P., et al., *Methylglyoxal causes structural and functional alterations in adipose tissue independently of obesity.* Archives of Physiology and Biochemistry, 2012. **118**(2): p. 58-68.
126. Vander Jagt, D.L. and L.A. Hunsaker, *Methylglyoxal metabolism and diabetic complications: roles of aldose reductase, glyoxalase-I, betaine aldehyde*

dehydrogenase and 2-oxoaldehyde dehydrogenase. Chemico-Biological Interactions, 2003. **143-144**: p. 341-351.
127. Schwanhäusser, B., et al., *Global quantification of mammalian gene expression control.* Nature, 2011. **473**(7347): p. 337-342.
128. Nishimura, C., et al., *Quantitative determination of human aldose reductase by enzyme-linked immunosorbent assay.* Biochemical Pharmacology, 1993. **46**(1): p. 21-28.
129. Larsen, K., et al., *Immunological comparison of glyoxalase I from yeast and mammals and quantitative determination of the enzyme in human tissues by radioimmunoassay.* Comparative Biochemistry and Physiology Part B: Comparative Biochemistry, 1985. **82**(4): p. 625-638.
130. Rabbani, N., M. Xue, and P.J. Thornalley, *Dicarbonyls and glyoxalase in disease mechanisms and clinical therapeutics.* Glycoconjugate Journal, 2016. **33**(4): p. 513-525.
131. Xue, M., et al., *Transcriptional control of glyoxalase 1 by Nrf2 provides a stress-responsive defence against dicarbonyl glycation.* Biochemical Journal, 2012. **443**(1): p. 213-222.
132. Suzuki, T. and M. Yamamoto, *Molecular basis of the Keap1–Nrf2 system.* Free Radical Biology and Medicine, 2015. **88**: p. 93-100.
133. Lombard, D.B., et al., *High-throughput small molecule screening reveals Nrf2-dependent and -independent pathways of cellular stress resistance.* Science Advances, 2020. **6**(40): p. eaaz7628.
134. Lewis, K.N., et al., *Regulation of Nrf2 signaling and longevity in naturally long-lived rodents.* Proceedings of the National Academy of Sciences, 2015. **112**(12): p. 3722-3727.
135. Strong, R., et al., *Longer lifespan in male mice treated with a weakly estrogenic agonist, an antioxidant, an α-glucosidase inhibitor or a Nrf2-inducer.* Aging Cell, 2016. **15**(5): p. 872-884.
136. Sykiotis, G.P. and D. Bohmann, *Keap1/Nrf2 signaling regulates oxidative stress tolerance and lifespan in Drosophila.* Dev Cell, 2008. **14**(1): p. 76-85.
137. Uruno, A., et al., *The Keap1-Nrf2 system prevents onset of diabetes mellitus.* Mol Cell Biol, 2013. **33**(15): p. 2996-3010.
138. Ogura, T., et al., *Keap1 is a forked-stem dimer structure with two large spheres enclosing the intervening, double glycine repeat, and C-terminal domains.* Proc Natl Acad Sci U S A, 2010. **107**(7): p. 2842-7.
139. Thornalley, P.J., *The glyoxalase system: new developments towards functional characterization of a metabolic pathway fundamental to biological life.* Biochemical Journal, 1990. **269**(1): p. 1-11.
140. Chakraborty, S., M. Gogoi, and D. Chakravortty, *Lactoylglutathione lyase, a critical enzyme in methylglyoxal detoxification, contributes to survival ofSalmonellain the nutrient rich environment.* Virulence, 2015. **6**(1): p. 50-65.
141. Rabbani, N., M. Al-Motawa, and P.J. Thornalley, *Protein Glycation in Plants—An Under-Researched Field with Much Still to Discover.* International Journal of Molecular Sciences, 2020. **21**(11): p. 3942.
142. Morcos, M., et al., *Glyoxalase-1 prevents mitochondrial protein modification and enhances lifespan in Caenorhabditis elegans.* Aging Cell, 2008. **7**(2): p. 260-269.

143. Stratmann, B., et al., *Glyoxalase 1-knockdown in human aortic endothelial cells - effect on the proteome and endothelial function estimates.* Sci Rep, 2016. **6**: p. 37737.
144. Shafie, A., et al., *Reappraisal of putative glyoxalase 1-deficient mouse and dicarbonyl stress on embryonic stem cells in vitro.* Biochemical Journal, 2016. **473**(22): p. 4255-4270.
145. Giacco, F., et al., *Knockdown of Glyoxalase 1 Mimics Diabetic Nephropathy in Nondiabetic Mice.* Diabetes, 2014. **63**(1): p. 291-299.
146. Wortmann, M., et al., *A Glyoxalase-1 Knockdown Does Not Have Major Short Term Effects on Energy Expenditure and Atherosclerosis in Mice.* Journal of Diabetes Research, 2016. **2016**: p. 1-8.
147. Jang, S., et al., *Generation and characterization of mouse knockout for glyoxalase 1.* Biochemical and Biophysical Research Communications, 2017. **490**(2): p. 460-465.
148. Schumacher, D., et al., *Compensatory mechanisms for methylglyoxal detoxification in experimental & clinical diabetes.* Molecular Metabolism, 2018. **18**: p. 143-152.
149. Lodd, E., et al., *The combination of loss of glyoxalase1 and obesity results in hyperglycemia.* JCI Insight, 2019. **4**(12).
150. Wang, Z., et al., *Glycine increases glyoxalase-1 function by promoting nuclear factor erythroid 2-related factor 2 translocation into the nucleus of kidney cells of streptozotocin-induced diabetic rats.* Journal of Diabetes Investigation, 2019.
151. Atkins, T.W. and P.J. Thornally, *Erythrocyte glyoxalase activity in genetically obese (ob/ob) and streptozotocin diabetic mice.* Diabetes research (Edinburgh, Scotland), 1989. **11**(3): p. 125-129.
152. Li, H., et al., *Ameliorating Methylglyoxal-Induced Progenitor Cell Dysfunction for Tissue Repair in Diabetes.* Diabetes, 2019. **68**(6): p. 1287-1302.
153. Xue, M., et al., *Improved Glycemic Control and Vascular Function in Overweight and Obese Subjects by Glyoxalase 1 Inducer Formulation.* Diabetes, 2016. **65**(8): p. 2282-94.
154. Remor, A.P., et al., *Differential effects of insulin on peripheral diabetes-related changes in mitochondrial bioenergetics: involvement of advanced glycosylated end products.* Biochim Biophys Acta, 2011. **1812**(11): p. 1460-71.
155. Hwang, H., et al., *Proteomics Analysis of Human Skeletal Muscle Reveals Novel Abnormalities in Obesity and Type 2 Diabetes.* Diabetes, 2010. **59**(1): p. 33-42.
156. Hussey, S.E., et al., *Effect of exercise on the skeletal muscle proteome in patients with type 2 diabetes.* Med Sci Sports Exerc, 2013. **45**(6): p. 1069-76.
157. El-Osta, A., et al., *Transient high glucose causes persistent epigenetic changes and altered gene expression during subsequent normoglycemia.* J Exp Med, 2008. **205**(10): p. 2409-17.
158. Brouwers, O., et al., *Glyoxalase-1 overexpression reduces endothelial dysfunction and attenuates early renal impairment in a rat model of diabetes.* Diabetologia, 2014. **57**(1): p. 224-235.
159. Brouwers, O., et al., *Glyoxalase-1 overexpression partially prevents diabetes-induced impaired arteriogenesis in a rat hindlimb ligation model.* Glycoconjugate Journal, 2016. **33**(4): p. 627-630.

160. López-Díez, R., et al., *Ager Deletion Enhances Ischemic Muscle Inflammation, Angiogenesis, and Blood Flow Recovery in Diabetic Mice.* Arteriosclerosis, Thrombosis, and Vascular Biology, 2017. **37**(8): p. 1536-1547.
161. Peng, Z., et al., *Glyoxalase-1 Overexpression Reverses Defective Proangiogenic Function of Diabetic Adipose-Derived Stem Cells in Streptozotocin-Induced Diabetic Mice Model of Critical Limb Ischemia.* STEM CELLS Translational Medicine, 2017. **6**(1): p. 261-271.
162. Angeloni, C., et al., *Neuroprotective Effect of Sulforaphane against Methylglyoxal Cytotoxicity.* Chemical Research in Toxicology, 2015. **28**(6): p. 1234-1245.
163. Subedi, L., et al., *Sulforaphane Inhibits MGO-AGE-Mediated Neuroinflammation by Suppressing NF-κB, MAPK, and AGE–RAGE Signaling Pathways in Microglial Cells.* Antioxidants, 2020. **9**(9): p. 792.
164. Angeloni, C., et al., *Novel Targets of Sulforaphane in Primary Cardiomyocytes Identified by Proteomic Analysis.* PLoS ONE, 2013. **8**(12): p. e83283.
165. Alfarano, M., et al., *The Effect of Sulforaphane on Glyoxalase I Expression and Activity in Peripheral Blood Mononuclear Cells.* Nutrients, 2018. **10**(11): p. 1773.
166. Santini, et al., *SIRT1-Dependent Upregulation of Antiglycative Defense in HUVECs Is Essential for Resveratrol Protection against High Glucose Stress.* Antioxidants, 2019. **8**(9): p. 346.
167. Huang, K., et al., *Sirt1 resists advanced glycation end products-induced expressions of fibronectin and TGF-beta1 by activating the Nrf2/ARE pathway in glomerular mesangial cells.* Free Radic Biol Med, 2013. **65**: p. 528-40.
168. Ma, F., et al., *P53/NRF2 mediates SIRT1's protective effect on diabetic nephropathy.* Biochimica et Biophysica Acta (BBA) - Molecular Cell Research, 2019. **1866**(8): p. 1272-1281.
169. Guo, M., et al., *Comprehensive analysis of circular RNA profiles in skeletal muscles of aging mice and after aerobic exercise intervention.* Aging, 2020. **12**(6): p. 5071-5090.
170. Birkenmeier, G., et al., *Posttranslational Modification of Human Glyoxalase 1 Indicates Redox-Dependent Regulation.* PLoS ONE, 2010. **5**(4): p. e10399.
171. Sankaranarayanan, S., M. Jamshed, and M.A. Samuel, *Degradation of glyoxalase I in Brassica napus stigma leads to self-incompatibility response.* Nature Plants, 2015. **1**(12): p. 15185.
172. de Hemptinne, V., et al., *Phosphorylation on Thr-106 and NO-modification of glyoxalase I suppress the TNF-induced transcriptional activity of NF-kappaB.* Mol Cell Biochem, 2009. **325**(1-2): p. 169-78.
173. Virginie, et al., *Tumour necrosis factor induces phosphorylation primarily of the nitric-oxide-responsive form of glyoxalase I.* Biochemical Journal, 2007. **407**(1): p. 121-128.
174. Morgenstern, J., et al., *Phosphorylation of T107 by CamKIIδ Regulates the Detoxification Efficiency and Proteomic Integrity of Glyoxalase 1.* Cell Reports, 2020. **32**(12): p. 108160.
175. Rauh, D., et al., *An acetylome peptide microarray reveals specificities and deacetylation substrates for all human sirtuin isoforms.* Nature Communications, 2013. **4**(1).

176. Gallogly, M.M. and J.J. Mieyal, *Mechanisms of reversible protein glutathionylation in redox signaling and oxidative stress.* Curr Opin Pharmacol, 2007. **7**(4): p. 381-91.
177. Mohr, S., et al., *Nitric oxide-induced S-glutathionylation and inactivation of glyceraldehyde-3-phosphate dehydrogenase.* J Biol Chem, 1999. **274**(14): p. 9427-30.
178. Fratelli, M., E. Gianazza, and P. Ghezzi, *Redox proteomics: identification and functional role of glutathionylated proteins.* Expert Rev Proteomics, 2004. **1**(3): p. 365-76.
179. Zaffagnini, M., et al., *The thioredoxin-independent isoform of chloroplastic glyceraldehyde-3-phosphate dehydrogenase is selectively regulated by glutathionylation.* Febs j, 2007. **274**(1): p. 212-26.
180. Michelet, L., et al., *Thioredoxins, glutaredoxins, and glutathionylation: new crosstalks to explore.* Photosynthesis Research, 2006. **89**(2-3): p. 225-245.
181. Liu, A., et al., *Metformin Delays the Development of Atherosclerosis in Type 1 Diabetes Mellitus via the Methylglyoxal Pathway.* Diabetes Therapy, 2020. **11**(3): p. 633-642.
182. Nguyen, H., et al., *A novel imidazolinone metformin-methylglyoxal metabolite promotes endothelial cell angiogenesis via the eNOS/HIF-1α pathway.* The FASEB Journal, 2021. **35**(7).
183. Oliveira, A.L., et al., *Metformin abrogates the voiding dysfunction induced by prolonged methylglyoxal intake.* European Journal of Pharmacology, 2021. **910**: p. 174502.
184. Kinsky, O.R., et al., *Metformin Scavenges Methylglyoxal To Form a Novel Imidazolinone Metabolite in Humans.* Chemical Research in Toxicology, 2016. **29**(2): p. 227-234.
185. Peters, A.S., et al., *Effect of metformin treatment in patients with type 2 diabetes with respect to glyoxalase 1 activity in atherosclerotic lesions.* Vasa, 2019. **48**(2): p. 186-192.
186. Rodrigues, T., et al., *GLP-1 improves adipose tissue glyoxalase activity and capillarization improving insulin sensitivity in type 2 diabetes.* Pharmacological Research, 2020: p. 105198.
187. Witczak, C.A., et al., *CaMKII regulates contraction- but not insulin-induced glucose uptake in mouse skeletal muscle.* Am J Physiol Endocrinol Metab, 2010. **298**(6): p. E1150-60.
188. Wright, D.C., et al., *A role for calcium/calmodulin kinase in insulin stimulated glucose transport.* Life Sci, 2004. **74**(7): p. 815-25.
189. Wright, D.C., et al., *Ca2+ and AMPK Both Mediate Stimulation of Glucose Transport by Muscle Contractions.* Diabetes, 2004. **53**(2): p. 330-335.
190. Tang, D., et al., *Pterostilbene prevents methylglyoxal-induced cytotoxicity in endothelial cells by regulating glyoxalase, oxidative stress and apoptosis.* Food and Chemical Toxicology, 2021. **153**: p. 112244.
191. Kodama, S., *Cardiorespiratory Fitness as a Quantitative Predictor of All-Cause Mortality and Cardiovascular Events in Healthy Men and Women.* JAMA, 2009. **301**(19): p. 2024.

192. Hargreaves, M. and L.L. Spriet, *Skeletal muscle energy metabolism during exercise.* Nature Metabolism, 2020. **2**(9): p. 817-828.
193. Shepherd, J.T., *Circulatory response to exercise in health.* Circulation, 1987. **76**(6 Pt 2): p. Vi3-10.
194. Joyner, M.J. and D.P. Casey, *Regulation of increased blood flow (hyperemia) to muscles during exercise: a hierarchy of competing physiological needs.* Physiological reviews, 2015. **95**(2): p. 549-601.
195. Winnick, J.J., et al., *Short-term aerobic exercise training in obese humans with type 2 diabetes mellitus improves whole-body insulin sensitivity through gains in peripheral, not hepatic insulin sensitivity.* J Clin Endocrinol Metab, 2008. **93**(3): p. 771-8.
196. Cartee, G.D., et al., *Prolonged increase in insulin-stimulated glucose transport in muscle after exercise.* Am J Physiol, 1989. **256**(4 Pt 1): p. E494-9.
197. Devlin, J.T., et al., *Enhanced peripheral and splanchnic insulin sensitivity in NIDDM men after single bout of exercise.* Diabetes, 1987. **36**(4): p. 434-9.
198. Heath, G.W., et al., *Effects of exercise and lack of exercise on glucose tolerance and insulin sensitivity.* J Appl Physiol Respir Environ Exerc Physiol, 1983. **55**(2): p. 512-7.
199. Schenk, S., et al., *Improved insulin sensitivity after weight loss and exercise training is mediated by a reduction in plasma fatty acid mobilization, not enhanced oxidative capacity.* J Physiol, 2009. **587**(Pt 20): p. 4949-61.
200. Solomon, T.P., et al., *A low-glycemic index diet combined with exercise reduces insulin resistance, postprandial hyperinsulinemia, and glucose-dependent insulinotropic polypeptide responses in obese, prediabetic humans.* Am J Clin Nutr, 2010. **92**(6): p. 1359-68.
201. Solomon, T.P., et al., *Randomized trial on the effects of a 7-d low-glycemic diet and exercise intervention on insulin resistance in older obese humans.* Am J Clin Nutr, 2009. **90**(5): p. 1222-9.
202. Toledo, F.G., et al., *Effects of physical activity and weight loss on skeletal muscle mitochondria and relationship with glucose control in type 2 diabetes.* Diabetes, 2007. **56**(8): p. 2142-7.
203. Ryan, B.J., et al., *Moderate-Intensity Exercise and High-Intensity Interval Training Affect Insulin Sensitivity Similarly in Obese Adults.* The Journal of Clinical Endocrinology & Metabolism, 2020. **105**(8): p. e2941-e2959.
204. Fealy, C.E., et al., *Functional high-intensity exercise training ameliorates insulin resistance and cardiometabolic risk factors in type 2 diabetes.* Experimental Physiology, 2018. **103**(7): p. 985-994.
205. Defronzo, R.A., R.S. Sherwin, and N. Kraemer, *Effect of Physical Training on Insulin Action in Obesity.* Diabetes, 1987. **36**(12): p. 1379-1385.
206. Roberts, C.K., J.P. Little, and J.P. Thyfault, *Modification of insulin sensitivity and glycemic control by activity and exercise.* Med Sci Sports Exerc, 2013. **45**(10): p. 1868-77.
207. Harber, M.P., et al., *Aerobic exercise training induces skeletal muscle hypertrophy and age-dependent adaptations in myofiber function in young and older men.* J Appl Physiol (1985), 2012. **113**(9): p. 1495-504.

208. Chin, E.C., et al., *Low-Frequency HIIT Improves Body Composition and Aerobic Capacity in Overweight Men.* Med Sci Sports Exerc, 2020. **52**(1): p. 56-66.
209. Chiang, T.-L., et al., *Is the goal of 12,000 steps per day sufficient for improving body composition and metabolic syndrome? The necessity of combining exercise intensity: a randomized controlled trial.* BMC Public Health, 2019. **19**(1).
210. Wewege, M., et al., *The effects of high-intensity interval training vs. moderate-intensity continuous training on body composition in overweight and obese adults: a systematic review and meta-analysis.* Obesity Reviews, 2017. **18**(6): p. 635-646.
211. Holloszy, J.O., *Biochemical adaptations in muscle. Effects of exercise on mitochondrial oxygen uptake and respiratory enzyme activity in skeletal muscle.* J Biol Chem, 1967. **242**(9): p. 2278-82.
212. Robinson, M.M., et al., *Enhanced Protein Translation Underlies Improved Metabolic and Physical Adaptations to Different Exercise Training Modes in Young and Old Humans.* Cell Metabolism, 2017. **25**(3): p. 581-592.
213. Saleem, A. and D.A. Hood, *Acute exercise induces tumour suppressor protein p53 translocation to the mitochondria and promotes a p53-Tfam-mitochondrial DNA complex in skeletal muscle.* The Journal of Physiology, 2013. **591**(14): p. 3625-3636.
214. Hood, D.A., et al., *Maintenance of Skeletal Muscle Mitochondria in Health, Exercise, and Aging.* Annual Review of Physiology, 2019. **81**(1): p. 19-41.
215. Flensted-Jensen, M., et al., *Six weeks of high intensity cycle training reduces H2O2 emission and increases antioxidant protein levels in obese adults with risk factors for type 2 diabetes.* Free Radical Biology and Medicine, 2021. **173**: p. 1-6.
216. Kim, K.S., et al., *The effect of training type on oxidative DNA damage and antioxidant capacity during three-dimensional space exercise.* Med Princ Pract, 2010. **19**(2): p. 133-41.
217. Radak, Z., et al., *Oxygen consumption and usage during physical exercise: the balance between oxidative stress and ROS-dependent adaptive signaling.* Antioxid Redox Signal, 2013. **18**(10): p. 1208-46.
218. Gounder, S.S., et al., *Impaired Transcriptional Activity of Nrf2 in Age-Related Myocardial Oxidative Stress Is Reversible by Moderate Exercise Training.* PLoS ONE, 2012. **7**(9): p. e45697.
219. Wang, P., et al., *Acute exercise stress promotes Ref1/Nrf2 signalling and increases mitochondrial antioxidant activity in skeletal muscle.* Experimental Physiology, 2016. **101**(3): p. 410-420.
220. Mallard, A.R., J.G. Spathis, and J.S. Coombes, *Nuclear factor (erythroid-derived 2)-like 2 (Nrf2) and exercise.* Free Radical Biology and Medicine, 2020. **160**: p. 471-479.
221. Lavin, K.M., et al., *Effects of aging and lifelong aerobic exercise on basal and exercise-induced inflammation.* Journal of Applied Physiology, 2020. **128**(1): p. 87-99.
222. Petersen, A.M.W. and B.K. Pedersen, *The anti-inflammatory effect of exercise.* Journal of Applied Physiology, 2005. **98**(4): p. 1154-1162.
223. Pedersen, B.K., *Anti-inflammatory effects of exercise: role in diabetes and cardiovascular disease.* European Journal of Clinical Investigation, 2017. **47**(8): p. 600-611.

224. Fiuza-Luces, C., et al., *Exercise is the real polypill.* Physiology (Bethesda), 2013. **28**(5): p. 330-58.
225. Ballmann, C., et al., *Exercise-induced oxidative stress and hypoxic exercise recovery.* Eur J Appl Physiol, 2014. **114**(4): p. 725-33.
226. Gallego-Selles, A., et al., *Regulation of Nrf2/Keap1 signalling in human skeletal muscle during exercise to exhaustion in normoxia, severe acute hypoxia and post-exercise ischaemia: Influence of metabolite accumulation and oxygenation.* Redox Biol, 2020. **36**: p. 101627.
227. Done, A.J., M.J. Newell, and T. Traustadóttir, *Effect of exercise intensity on Nrf2 signalling in young men.* Free Radical Research, 2017. **51**(6): p. 646-655.
228. Done, A.J., et al., *Exercise-induced Nrf2-signaling is impaired in aging.* Free Radical Biology and Medicine, 2016. **96**: p. 130-138.
229. Radom-Aizik, S., et al., *Effects of aerobic training on gene expression in skeletal muscle of elderly men.* Med Sci Sports Exerc, 2005. **37**(10): p. 1680-96.
230. Nolan, et al., *Global Phosphoproteomic Analysis of Human Skeletal Muscle Reveals a Network of Exercise-Regulated Kinases and AMPK Substrates.* Cell Metabolism, 2015. **22**(5): p. 922-935.
231. Hussey, S.E., et al., *Effect of Exercise on the Skeletal Muscle Proteome in Patients with Type 2 Diabetes.* Medicine & Science in Sports & Exercise, 2013. **45**(6): p. 1069-1076.
232. Polevoda, B. and F. Sherman, Genome Biology, 2002. **3**(5): p. reviews0006.1.
233. Polevoda, B. and F. Sherman, *Nα-terminal Acetylation of Eukaryotic Proteins.* Journal of Biological Chemistry, 2000. **275**(47): p. 36479-36482.
234. Allfrey, V.G., R. Faulkner, and A.E. Mirsky, *ACETYLATION AND METHYLATION OF HISTONES AND THEIR POSSIBLE ROLE IN THE REGULATION OF RNA SYNTHESIS.* Proceedings of the National Academy of Sciences, 1964. **51**(5): p. 786-794.
235. Perrone, L., et al., *Thioredoxin interacting protein (TXNIP) induces inflammation through chromatin modification in retinal capillary endothelial cells under diabetic conditions.* J Cell Physiol, 2009. **221**(1): p. 262-72.
236. L'Hernault, S.W. and J.L. Rosenbaum, *Chlamydomonas .alpha.-tubulin is posttranslationally modified by acetylation on the .epsilon.-amino group of a lysine.* Biochemistry, 1985. **24**(2): p. 473-478.
237. Gu, W. and R.G. Roeder, *Activation of p53 Sequence-Specific DNA Binding by Acetylation of the p53 C-Terminal Domain.* Cell, 1997. **90**(4): p. 595-606.
238. Ott, M., et al., *Acetylation of the HIV-1 Tat protein by p300 is important for its transcriptional activity.* Current Biology, 1999. **9**(24): p. 1489-1493.
239. Chen, Y., et al., *Quantitative Acetylome Analysis Reveals the Roles of SIRT1 in Regulating Diverse Substrates and Cellular Pathways.* Molecular & Cellular Proteomics, 2012. **11**(10): p. 1048-1062.
240. Choudhary, C., et al., *Lysine Acetylation Targets Protein Complexes and Co-Regulates Major Cellular Functions.* Science, 2009. **325**(5942): p. 834-840.
241. Verdin, E. and M. Ott, *50 years of protein acetylation: from gene regulation to epigenetics, metabolism and beyond.* Nature Reviews Molecular Cell Biology, 2015. **16**(4): p. 258-264.

242. Yucel, N., et al., *Glucose Metabolism Drives Histone Acetylation Landscape Transitions that Dictate Muscle Stem Cell Function.* Cell Rep, 2019. **27**(13): p. 3939-3955 e6.
243. Vancura, A., et al., *Reciprocal Regulation of AMPK/SNF1 and Protein Acetylation.* International Journal of Molecular Sciences, 2018. **19**(11): p. 3314.
244. Hardie, D.G., *Energy sensing by the AMP-activated protein kinase and its effects on muscle metabolism.* Proceedings of the Nutrition Society, 2011. **70**(1): p. 92-99.
245. Hallows, W.C., W. Yu, and J.M. Denu, *Regulation of Glycolytic Enzyme Phosphoglycerate Mutase-1 by Sirt1 Protein-mediated Deacetylation.* Journal of Biological Chemistry, 2012. **287**(6): p. 3850-3858.
246. Li, T., et al., *Glyceraldehyde-3-phosphate Dehydrogenase Is Activated by Lysine 254 Acetylation in Response to Glucose Signal.* Journal of Biological Chemistry, 2014. **289**(6): p. 3775-3785.
247. Xiong, Y., et al., *Regulation of Glycolysis and Gluconeogenesis by Acetylation of PKM and PEPCK.* Cold Spring Harbor Symposia on Quantitative Biology, 2011. **76**(0): p. 285-289.
248. Overmyer, K.A., et al., *Maximal oxidative capacity during exercise is associated with skeletal muscle fuel selection and dynamic changes in mitochondrial protein acetylation.* Cell Metab, 2015. **21**(3): p. 468-78.
249. Williams, A.S., et al., *Disruption of Acetyl-Lysine Turnover in Muscle Mitochondria Promotes Insulin Resistance and Redox Stress without Overt Respiratory Dysfunction.* Cell Metabolism, 2020. **31**(1): p. 131-147.e11.
250. Lombard, D.B., et al., *Mammalian Sir2 Homolog SIRT3 Regulates Global Mitochondrial Lysine Acetylation.* Molecular and Cellular Biology, 2007. **27**(24): p. 8807-8814.
251. Narita, T., B.T. Weinert, and C. Choudhary, *Functions and mechanisms of non-histone protein acetylation.* Nature Reviews Molecular Cell Biology, 2019. **20**(3): p. 156-174.
252. Rine, J., et al., *A SUPPRESSOR OF MATING-TYPE LOCUS MUTATIONS IN SACCHAROMYCES CEREVISIAE: EVIDENCE FOR AND IDENTIFICATION OF CRYPTIC MATING-TYPE LOCI.* Genetics, 1979. **93**(4): p. 877-901.
253. Rine, J. and I. Herskowitz, *Four Genes Responsible for a Position Effect on Expression From HML and HMR in Saccharomyces cerevisiae.* Genetics, 1987. **116**(1): p. 9-22.
254. Ivy, J.M., J.B. Hicks, and A.J.S. Klar, *MAP POSITIONS OF YEAST GENES SIR1, SIR3 and SIR4.* Genetics, 1985. **111**(4): p. 735-744.
255. Lin, S.-J., et al., *Calorie restriction extends Saccharomyces cerevisiae lifespan by increasing respiration.* Nature, 2002. **418**(6895): p. 344-348.
256. Lin, S.-J., P.-A. Defossez, and L. Guarente, *Requirement of NAD and SIR2 for Life-Span Extension by Calorie Restriction in Saccharomyces Cerevisiae.* Science, 2000. **289**(5487): p. 2126-2128.
257. Blander, G. and L. Guarente, *The Sir2 Family of Protein Deacetylases.* Annual Review of Biochemistry, 2004. **73**(1): p. 417-435.
258. Imai, S.-I., et al., *Transcriptional silencing and longevity protein Sir2 is an NAD-dependent histone deacetylase.* Nature, 2000. **403**(6771): p. 795-800.

259. Kaeberlein, M., M. McVey, and L. Guarente, *The SIR2/3/4 complex and SIR2 alone promote longevity in Saccharomyces cerevisiae by two different mechanisms.* Genes & Development, 1999. **13**(19): p. 2570-2580.
260. Liu, G., et al., *Loss of NAD-Dependent Protein Deacetylase Sirtuin-2 Alters Mitochondrial Protein Acetylation and Dysregulates Mitophagy.* Antioxidants & Redox Signaling, 2017. **26**(15): p. 849-863.
261. Gao, J., et al., *Deacetylation of MnSOD by PARP-regulated SIRT3 protects retinal capillary endothelial cells from hyperglycemia-induced damage.* Biochem Biophys Res Commun, 2016. **472**(3): p. 425-31.
262. Anderson, K.A., et al., *SIRT4 Is a Lysine Deacylase that Controls Leucine Metabolism and Insulin Secretion.* Cell Metabolism, 2017. **25**(4): p. 838-855.e15.
263. Kumar, S. and D.B. Lombard, *Functions of the sirtuin deacylase SIRT5 in normal physiology and pathobiology.* Critical Reviews in Biochemistry and Molecular Biology, 2018. **53**(3): p. 311-334.
264. Liu, L., et al., *Quantitative Analysis of NAD Synthesis-Breakdown Fluxes.* Cell Metabolism, 2018. **27**(5): p. 1067-1080.e5.
265. Okabe, K., et al., *Implications of altered NAD metabolism in metabolic disorders.* Journal of Biomedical Science, 2019. **26**(1).
266. Mousa, T.Y. and O.Y. Mousa, *Nicotinic Acid Deficiency*, in *StatPearls*. 2021, StatPearls Publishing

267. Luongo, T.S., et al., *SLC25A51 is a mammalian mitochondrial NAD(+) transporter.* Nature, 2020. **588**(7836): p. 174-179.
268. Williamson, D., P. Lund, and H. Krebs, *The redox state of free nicotinamide-adenine dinucleotide in the cytoplasm and mitochondria of rat liver.* Biochemical Journal, 1967. **103**(2): p. 514-527.
269. Teodoro, J.S., A.P. Rolo, and C.M. Palmeira, *The NAD ratio redox paradox: why does too much reductive power cause oxidative stress?* 2013. **23**(5): p. 297-302.
270. McReynolds, M.R., et al., *NAD+ flux is maintained in aged mice despite lower tissue concentrations.* Cell Systems, 2021.
271. Dungan, C.M., et al., *In vivo analysis of γH2AX+ cells in skeletal muscle from aged and obese humans.* The FASEB Journal, 2020. **34**(5): p. 7018-7035.
272. Park, D.R., et al., *CD38-cADPR-SERCA Signaling Axis Determines Skeletal Muscle Contractile Force in Response to β-Adrenergic Stimulation.* Cell Physiol Biochem, 2018. **46**(5): p. 2017-2030.
273. Shi, B., et al., *Targeting CD38-dependent NAD(+) metabolism to mitigate multiple organ fibrosis.* iScience, 2021. **24**(1): p. 101902.
274. Chiang, S.H., et al., *Genetic Ablation of CD38 Protects against Western Diet-Induced Exercise Intolerance and Metabolic Inflexibility.* PLoS One, 2015. **10**(8): p. e0134927.
275. Aksoy, P., et al., *Regulation of SIRT 1 mediated NAD dependent deacetylation: A novel role for the multifunctional enzyme CD38.* Biochemical and Biophysical Research Communications, 2006. **349**(1): p. 353-359.
276. Escande, C., et al., *Flavonoid Apigenin Is an Inhibitor of the NAD+ase CD38: Implications for Cellular NAD+ Metabolism, Protein Acetylation, and Treatment of Metabolic Syndrome.* Diabetes, 2013. **62**(4): p. 1084-1093.

277. Fukuhara, A., et al., *Visfatin: a protein secreted by visceral fat that mimics the effects of insulin.* Science, 2005. **307**(5708): p. 426-30.
278. Chen, M.P., et al., *Elevated plasma level of visfatin/pre-B cell colony-enhancing factor in patients with type 2 diabetes mellitus.* J Clin Endocrinol Metab, 2006. **91**(1): p. 295-9.
279. Dogru, T., et al., *Plasma visfatin levels in patients with newly diagnosed and untreated type 2 diabetes mellitus and impaired glucose tolerance.* Diabetes Res Clin Pract, 2007. **76**(1): p. 24-9.
280. Antinozzi, C., et al., *Exploratory Analysis in the Differences in Blood Serum and Seminal Plasma of Adipose-Tissue Related Peptides in Obese and Non-Obese Men and Their Correlations With Semen Parameters.* Front Endocrinol (Lausanne), 2021. **12**: p. 681939.
281. Botella-Carretero, J.I., et al., *The increase in serum visfatin after bariatric surgery in morbidly obese women is modulated by weight loss, waist circumference, and presence or absence of diabetes before surgery.* Obes Surg, 2008. **18**(8): p. 1000-6.
282. Haus, J.M., et al., *Decreased visfatin after exercise training correlates with improved glucose tolerance.* Med Sci Sports Exerc, 2009. **41**(6): p. 1255-60.
283. Myeong, et al., *SIRT1-Mediated eNAMPT Secretion from Adipose Tissue Regulates Hypothalamic NAD+ and Function in Mice.* Cell Metabolism, 2015. **21**(5): p. 706-717.
284. Bieganowski, P. and C. Brenner, *Discoveries of nicotinamide riboside as a nutrient and conserved NRK genes establish a Preiss-Handler independent route to NAD+ in fungi and humans.* Cell, 2004. **117**(4): p. 495-502.
285. Cohen, H.Y., et al., *Calorie restriction promotes mammalian cell survival by inducing the SIRT1 deacetylase.* Science, 2004. **305**(5682): p. 390-2.
286. Tanny, J.C., et al., *An enzymatic activity in the yeast Sir2 protein that is essential for gene silencing.* Cell, 1999. **99**(7): p. 735-45.
287. Vaziri, H., et al., *hSIR2(SIRT1) functions as an NAD-dependent p53 deacetylase.* Cell, 2001. **107**(2): p. 149-59.
288. Cantó, C., et al., *AMPK regulates energy expenditure by modulating NAD+ metabolism and SIRT1 activity.* Nature, 2009. **458**(7241): p. 1056-1060.
289. Yeung, F., et al., *Modulation of NF-kappaB-dependent transcription and cell survival by the SIRT1 deacetylase.* Embo j, 2004. **23**(12): p. 2369-80.
290. Gerhart-Hines, Z., et al., *Metabolic control of muscle mitochondrial function and fatty acid oxidation through SIRT1/PGC-1α.* The EMBO Journal, 2007. **26**(7): p. 1913-1923.
291. Delaney, J.R., et al., *Sir2 deletion prevents lifespan extension in 32 long-lived mutants.* Aging Cell, 2011. **10**(6): p. 1089-1091.
292. Frankel, S., T. Ziafazeli, and B. Rogina, *dSir2 and longevity in Drosophila.* Experimental Gerontology, 2011. **46**(5): p. 391-396.
293. Rogina, B. and S.L. Helfand, *Sir2 mediates longevity in the fly through a pathway related to calorie restriction.* Proceedings of the National Academy of Sciences, 2004. **101**(45): p. 15998-16003.
294. Burnett, C., et al., *Absence of effects of Sir2 overexpression on lifespan in C. elegans and Drosophila.* Nature, 2011. **477**(7365): p. 482-485.

295. Herranz, D., et al., *Sirt1 improves healthy ageing and protects from metabolic syndrome-associated cancer.* Nature Communications, 2010. **1**(1): p. 1-8.
296. Satoh, A., et al., *Sirt1 Extends Life Span and Delays Aging in Mice through the Regulation of Nk2 Homeobox 1 in the DMH and LH.* Cell Metabolism, 2013. **18**(3): p. 416-430.
297. Hubbard, B.P. and D.A. Sinclair, *Small molecule SIRT1 activators for the treatment of aging and age-related diseases.* Trends in Pharmacological Sciences, 2014. **35**(3): p. 146-154.
298. Reiten, O.K., et al., *Preclinical and clinical evidence of NAD(+) precursors in health, disease, and ageing.* Mech Ageing Dev, 2021. **199**: p. 111567.
299. Radak, Z., et al., *Redox-regulating sirtuins in aging, caloric restriction, and exercise.* Free Radical Biology and Medicine, 2013. **58**: p. 87-97.
300. Howitz, K.T., et al., *Small molecule activators of sirtuins extend Saccharomyces cerevisiae lifespan.* Nature, 2003. **425**(6954): p. 191-196.
301. Lagouge, M., et al., *Resveratrol Improves Mitochondrial Function and Protects against Metabolic Disease by Activating SIRT1 and PGC-1α.* Cell, 2006. **127**(6): p. 1109-1122.
302. Baur, J.A., et al., *Resveratrol improves health and survival of mice on a high-calorie diet.* Nature, 2006. **444**(7117): p. 337-342.
303. Timmers, S., et al., *Calorie Restriction-like Effects of 30 Days of Resveratrol Supplementation on Energy Metabolism and Metabolic Profile in Obese Humans.* Cell Metabolism, 2011. **14**(5): p. 612-622.
304. Goh, K.P., et al., *Effects of resveratrol in patients with type 2 diabetes mellitus on skeletal muscle SIRT1 expression and energy expenditure.* Int J Sport Nutr Exerc Metab, 2014. **24**(1): p. 2-13.
305. He, W., et al., *Advanced glycation end products induce endothelial-to-mesenchymal transition via downregulating Sirt 1 and upregulating TGF-beta in human endothelial cells.* Biomed Res Int, 2015. **2015**: p. 684242.
306. Joshi, M.S., et al., *Role of mitochondrial dysfunction in hyperglycaemia-induced coronary microvascular dysfunction: Protective role of resveratrol.* Diab Vasc Dis Res, 2015. **12**(3): p. 208-16.
307. Milne, J.C., et al., *Small molecule activators of SIRT1 as therapeutics for the treatment of type 2 diabetes.* Nature, 2007. **450**(7170): p. 712-716.
308. Feige, J.N., et al., *Specific SIRT1 Activation Mimics Low Energy Levels and Protects against Diet-Induced Metabolic Disorders by Enhancing Fat Oxidation.* Cell Metabolism, 2008. **8**(5): p. 347-358.
309. Beher, D., et al., *Resveratrol is Not a Direct Activator of SIRT1 Enzyme Activity.* Chemical Biology & Drug Design, 2009. **74**(6): p. 619-624.
310. Park, S.-J., et al., *Specific Sirt1 Activator-mediated Improvement in Glucose Homeostasis Requires Sirt1-Independent Activation of AMPK.* EBioMedicine, 2017. **18**: p. 128-138.
311. Pacholec, M., et al., *SRT1720, SRT2183, SRT1460, and Resveratrol Are Not Direct Activators of SIRT1.* Journal of Biological Chemistry, 2010. **285**(11): p. 8340-8351.
312. Svensson, K., et al., *Combined overexpression of SIRT1 and knockout of GCN5 in adult skeletal muscle does not affect glucose homeostasis or exercise*

performance in mice. American Journal of Physiology-Endocrinology and Metabolism, 2020. **318**(2): p. E145-E151.
313. Svensson, K., et al., *Temporal overexpression of SIRT1 in skeletal muscle of adult mice does not improve insulin sensitivity or markers of mitochondrial biogenesis.* Acta Physiologica, 2017. **221**(3): p. 193-203.
314. White, A.T., et al., *Skeletal muscle-specific overexpression of SIRT1 does not enhance whole-body energy expenditure or insulin sensitivity in young mice.* Diabetologia, 2013. **56**(7): p. 1629-1637.
315. White, A.T., et al., *High-fat diet-induced impairment of skeletal muscle insulin sensitivity is not prevented by SIRT1 overexpression.* American Journal of Physiology-Endocrinology and Metabolism, 2014. **307**(9): p. E764-E772.
316. Vil, L., et al., *AAV-mediated Sirt1 overexpression in skeletal muscle activates oxidative capacity but does not prevent insulin resistance.* Molecular Therapy - Methods & Clinical Development, 2016. **3**: p. 16072.
317. Covarrubias, A.J., et al., *Senescent cells promote tissue NAD(+) decline during ageing via the activation of CD38(+) macrophages.* Nat Metab, 2020. **2**(11): p. 1265-1283.
318. Frederick, D.W., et al., *Increasing NAD Synthesis in Muscle via Nicotinamide Phosphoribosyltransferase Is Not Sufficient to Promote Oxidative Metabolism.* Journal of Biological Chemistry, 2015. **290**(3): p. 1546-1558.
319. Trammell, S.A.J., et al., *Nicotinamide Riboside Opposes Type 2 Diabetes and Neuropathy in Mice.* Scientific Reports, 2016. **6**(1): p. 26933.
320. Costford, S.R., et al., *Skeletal muscle NAMPT is induced by exercise in humans.* Am J Physiol Endocrinol Metab, 2010. **298**(1): p. E117-26.
321. De Guia, R.M., et al., *Aerobic and resistance exercise training reverses age-dependent decline in NAD+ salvage capacity in human skeletal muscle.* Physiological Reports, 2019. **7**(12): p. e14139.
322. Lamb, D.A., et al., *Resistance training increases muscle NAD+ and NADH concentrations as well as NAMPT protein levels and global sirtuin activity in middle-aged, overweight, untrained individuals.* Aging, 2020. **12**(10): p. 9447-9460.
323. Oakey, L.A., et al., *Metabolic tracing reveals novel adaptations to skeletal muscle cell energy production pathways in response to NAD (+) depletion.* Wellcome Open Res, 2018. **3**: p. 147.
324. David, et al., *Loss of NAD Homeostasis Leads to Progressive and Reversible Degeneration of Skeletal Muscle.* Cell Metabolism, 2016. **24**(2): p. 269-282.
325. Basse, A.L., et al., *Nampt controls skeletal muscle development by maintaining Ca2+ homeostasis and mitochondrial integrity.* Molecular Metabolism, 2021. **53**: p. 101271.
326. Fletcher, R.S., et al., *Nicotinamide riboside kinases display redundancy in mediating nicotinamide mononucleotide and nicotinamide riboside metabolism in skeletal muscle cells.* Mol Metab, 2017. **6**(8): p. 819-832.
327. Ratajczak, J., et al., *NRK1 controls nicotinamide mononucleotide and nicotinamide riboside metabolism in mammalian cells.* Nature Communications, 2016. **7**(1): p. 13103.

328. Yoshino, J., et al., *Nicotinamide Mononucleotide, a Key NAD+ Intermediate, Treats the Pathophysiology of Diet- and Age-Induced Diabetes in Mice.* Cell Metabolism, 2011. **14**(4): p. 528-536.
329. Cantó, C., et al., *The NAD+ Precursor Nicotinamide Riboside Enhances Oxidative Metabolism and Protects against High-Fat Diet-Induced Obesity.* Cell Metabolism, 2012. **15**(6): p. 838-847.
330. Cartwright, D.M., et al., *Nicotinamide riboside has minimal impact on energy metabolism in mouse models of mild obesity.* Journal of Endocrinology, 2021. **251**(1): p. 111-123.
331. Williams, A.S., et al., *Nicotinamide riboside supplementation confers marginal metabolic benefits in obese mice without remodeling the muscle acetyl-proteome.* iScience, 2022. **25**(1): p. 103635.
332. Damgaard, M.V., et al., *Intravenous nicotinamide riboside elevates mouse skeletal muscle NAD+ without impacting respiratory capacity or insulin sensitivity.* iScience, 2022: p. 103863.
333. Trammell, S.A.J., et al., *Nicotinamide riboside is uniquely and orally bioavailable in mice and humans.* Nature Communications, 2016. **7**(1): p. 12948.
334. Conze, D., C. Brenner, and C.L. Kruger, *Safety and Metabolism of Long-term Administration of NIAGEN (Nicotinamide Riboside Chloride) in a Randomized, Double-Blind, Placebo-controlled Clinical Trial of Healthy Overweight Adults.* Scientific Reports, 2019. **9**(1).
335. Elhassan, Y.S., et al., *Nicotinamide Riboside Augments the Aged Human Skeletal Muscle NAD+ Metabolome and Induces Transcriptomic and Anti-inflammatory Signatures.* Cell Reports, 2019. **28**(7): p. 1717-1728.e6.
336. Dollerup, O.L., et al., *A randomized placebo-controlled clinical trial of nicotinamide riboside in obese men: safety, insulin-sensitivity, and lipid-mobilizing effects.* The American Journal of Clinical Nutrition, 2018. **108**(2): p. 343-353.
337. Dollerup, O.L., et al., *Nicotinamide riboside does not alter mitochondrial respiration, content or morphology in skeletal muscle from obese and insulin-resistant men.* The Journal of Physiology, 2020. **598**(4): p. 731-754.
338. Remie, C.M.E., et al., *Nicotinamide riboside supplementation alters body composition and skeletal muscle acetylcarnitine concentrations in healthy obese humans.* The American Journal of Clinical Nutrition, 2020. **112**(2): p. 413-426.
339. Yoshino, M., et al., *Nicotinamide mononucleotide increases muscle insulin sensitivity in prediabetic women.* Science, 2021. **372**(6547): p. 1224-1229.
340. Brenner, C., *Comment on "Nicotinamide mononucleotide increases muscle insulin sensitivity in prediabetic women".* Science, 2021. **373**(6554).
341. Yang, S.J., et al., *Nicotinamide improves glucose metabolism and affects the hepatic NAD-sirtuin pathway in a rodent model of obesity and type 2 diabetes.* The Journal of Nutritional Biochemistry, 2014. **25**(1): p. 66-72.
342. Mitchell, S.J., et al., *Nicotinamide Improves Aspects of Healthspan, but Not Lifespan, in Mice.* Cell Metabolism, 2018. **27**(3): p. 667-676.e4.
343. Qi, Z., et al., *Long-term treatment with nicotinamide induces glucose intolerance and skeletal muscle lipotoxicity in normal chow-fed mice: compared to diet-induced obesity.* J Nutr Biochem, 2016. **36**: p. 31-41.

344. Akiu, M., et al., *Discovery of DS68702229 as a Potent, Orally Available NAMPT (Nicotinamide Phosphoribosyltransferase) Activator.* Chemical and Pharmaceutical Bulletin, 2021. **69**(11): p. 1110-1122.
345. Civitarese, A.E., et al., *Calorie Restriction Increases Muscle Mitochondrial Biogenesis in Healthy Humans.* PLoS Medicine, 2007. **4**(3): p. e76.
346. Cantó, C., et al., *Interdependence of AMPK and SIRT1 for Metabolic Adaptation to Fasting and Exercise in Skeletal Muscle.* Cell Metabolism, 2010. **11**(3): p. 213-219.
347. Koltai, E., et al., *Exercise alters SIRT1, SIRT6, NAD and NAMPT levels in skeletal muscle of aged rats.* Mech Ageing Dev, 2010. **131**(1): p. 21-8.
348. Pardo, P.S., et al., *Induction of Sirt1 by Mechanical Stretch of Skeletal Muscle through the Early Response Factor EGR1 Triggers an Antioxidative Response.* Journal of Biological Chemistry, 2011. **286**(4): p. 2559-2566.
349. Koltai, E., et al., *Master athletes have higher miR-7, SIRT3 and SOD2 expression in skeletal muscle than age-matched sedentary controls.* Redox Biol, 2018. **19**: p. 46-51.
350. Liao, Z.Y., et al., *The effect of exercise, resveratrol or their combination on Sarcopenia in aged rats via regulation of AMPK/Sirt1 pathway.* Exp Gerontol, 2017. **98**: p. 177-183.
351. Quinn, L.S., et al., *IL-15 Is Required for Postexercise Induction of the Pro-Oxidative Mediators PPARδ and SIRT1 in Male Mice.* Endocrinology, 2014. **155**(1): p. 143-155.
352. Li, L., et al., *Mitochondrial biogenesis and PGC-1α deacetylation by chronic treadmill exercise: differential response in cardiac and skeletal muscle.* Basic Research in Cardiology, 2011. **106**(6): p. 1221-1234.
353. Suwa, M., et al., *Endurance exercise increases the SIRT1 and peroxisome proliferator-activated receptor gamma coactivator-1alpha protein expressions in rat skeletal muscle.* Metabolism, 2008. **57**(7): p. 986-98.
354. Gurd, B.J., et al., *Nuclear SIRT1 activity, but not protein content, regulates mitochondrial biogenesis in rat and human skeletal muscle.* Am J Physiol Regul Integr Comp Physiol, 2011. **301**(1): p. R67-75.
355. Edgett, B.A., et al., *Dissociation of Increases in PGC-1α and Its Regulators from Exercise Intensity and Muscle Activation Following Acute Exercise.* PLoS ONE, 2013. **8**(8): p. e71623.
356. Guerra, B., et al., *SIRT1, AMP-activated protein kinase phosphorylation and downstream kinases in response to a single bout of sprint exercise: influence of glucose ingestion.* Eur J Appl Physiol, 2010. **109**(4): p. 731-43.
357. Radak, Z., et al., *Age-dependent changes in 8-oxoguanine-DNA glycosylase activity are modulated by adaptive responses to physical exercise in human skeletal muscle.* Free Radical Biology and Medicine, 2011. **51**(2): p. 417-423.
358. Little, J.P., et al., *A practical model of low-volume high-intensity interval training induces mitochondrial biogenesis in human skeletal muscle: potential mechanisms.* The Journal of Physiology, 2010. **588**(6): p. 1011-1022.
359. Gurd, B.J., et al., *High-intensity interval training increases SIRT1 activity in human skeletal muscle.* Appl Physiol Nutr Metab, 2010. **35**(3): p. 350-7.

360. Bae, J.Y., et al., *Effects of detraining and retraining on muscle energy-sensing network and meteorin-like levels in obese mice.* Lipids in Health and Disease, 2018. **17**(1).
361. Vogt, É.L., et al., *Metabolic and Molecular Subacute Effects of a Single Moderate-Intensity Exercise Bout, Performed in the Fasted State, in Obese Male Rats.* International Journal of Environmental Research and Public Health, 2021. **18**(14): p. 7543.
362. You, B., et al., *The Treatment of Rhodiola Mimics Exercise to Resist High-Fat Diet-Induced Muscle Dysfunction via Sirtuin1-Dependent Mechanisms.* Frontiers in Pharmacology, 2021. **12**: p. 750.
363. Skleryk, J.R., et al., *Two weeks of reduced-volume sprint interval or traditional exercise training does not improve metabolic functioning in sedentary obese men.* Diabetes, Obesity and Metabolism, 2013. **15**(12): p. 1146-1153.
364. Liu, H.W. and S.J. Chang, *Moderate Exercise Suppresses NF-κB Signaling and Activates the SIRT1-AMPK-PGC1α Axis to Attenuate Muscle Loss in Diabetic db/db Mice.* Front Physiol, 2018. **9**: p. 636.
365. Little, J.P., et al., *Low-volume high-intensity interval training reduces hyperglycemia and increases muscle mitochondrial capacity in patients with type 2 diabetes.* J Appl Physiol (1985), 2011. **111**(6): p. 1554-60.
366. Philp, A., et al., *Sirtuin 1 (SIRT1) deacetylase activity is not required for mitochondrial biogenesis or peroxisome proliferator-activated receptor-gamma coactivator-1alpha (PGC-1alpha) deacetylation following endurance exercise.* (1083-351X (Electronic)).
367. Kang, J.H., et al., *Sirtuin 1 is not required for contraction-stimulated glucose uptake in mouse skeletal muscle.* J Appl Physiol (1985), 2021. **130**(6): p. 1893-1902.
368. Chaves, A.B., et al., *Exercise reduces the protein abundance of TXNIP and its interacting partner REDD1 in skeletal muscle: potential role for a PKA-mediated mechanism.* J Appl Physiol (1985), 2022. **132**(2): p. 357-366.
369. Stadler, G., et al., *Establishment of clonal myogenic cell lines from severely affected dystrophic muscles - CDK4 maintains the myogenic population.* Skeletal Muscle, 2011. **1**(1): p. 12.
370. Thorley, M., et al., *Skeletal muscle characteristics are preserved in hTERT/cdk4 human myogenic cell lines.* Skeletal Muscle, 2016. **6**(1).
371. Wright, W.E. and J.W. Shay, *Inexpensive low-oxygen incubators.* Nat Protoc, 2006. **1**(4): p. 2088-90.
372. McAlister, G.C., et al., *MultiNotch MS3 enables accurate, sensitive, and multiplexed detection of differential expression across cancer cell line proteomes.* Anal Chem, 2014. **86**(14): p. 7150-8.
373. Nahimana, A., et al., *The NAD biosynthesis inhibitor APO866 has potent antitumor activity against hematologic malignancies.* Blood, 2009. **113**(14): p. 3276-3286.
374. Sayed, M.E., et al., *Catalysis-dependent inactivation of human telomerase and its reactivation by intracellular telomerase-activating factors (iTAFs).* Journal of Biological Chemistry, 2019. **294**(30): p. 11579-11596.
375. Huang, C.-C., et al., *Effect of Exercise Training on Skeletal Muscle SIRT1 and PGC-1α Expression Levels in Rats of Different Age.* International Journal of Medical Sciences, 2016. **13**(4): p. 260-270.

376. Fritzen, A.M., et al., *5'-AMP activated protein kinase alpha2 controls substrate metabolism during post-exercise recovery via regulation of pyruvate dehydrogenase kinase 4.* J Physiol, 2015. **593**(21): p. 4765-80.
377. Martins, V.F., et al., *p300 or CBP is required for insulin-stimulated glucose uptake in skeletal muscle and adipocytes.* JCI Insight, 2022. **7**(1).
378. Wang, T.J., et al., *2-Aminoadipic acid is a biomarker for diabetes risk.* J Clin Invest, 2013. **123**(10): p. 4309-17.
379. Lee, H.J., et al., *2-Aminoadipic acid (2-AAA) as a potential biomarker for insulin resistance in childhood obesity.* Scientific Reports, 2019. **9**(1).
380. Choi, S.-E., et al., *Elevated microRNA-34a in obesity reduces NAD+levels and SIRT1 activity by directly targeting NAMPT.* Aging Cell, 2013. **12**(6): p. 1062-1072.
381. Ward, Z.J., et al., *Projected U.S. State-Level Prevalence of Adult Obesity and Severe Obesity.* New England Journal of Medicine, 2019. **381**(25): p. 2440-2450.
382. Twig, G., et al., *Diabetes Risk Among Overweight and Obese Metabolically Healthy Young Adults.* Diabetes Care, 2014. **37**(11): p. 2989-2995.
383. DeFronzo, R.A., J.D. Tobin, and R. Andres, *Glucose clamp technique: a method for quantifying insulin secretion and resistance.* Am J Physiol, 1979. **237**(3): p. E214-23.
384. Egan, B. and J.R. Zierath, *Exercise metabolism and the molecular regulation of skeletal muscle adaptation.* Cell Metab, 2013. **17**(2): p. 162-84.
385. Zhou, W.Y., et al., *Circular RNA: metabolism, functions and interactions with proteins.* Mol Cancer, 2020. **19**(1): p. 172.
386. Lang, X., et al., *Treadmill exercise mitigates neuroinflammation and increases BDNF via activation of SIRT1 signaling in a mouse model of T2DM.* Brain Research Bulletin, 2020. **165**: p. 30-39.
387. Kelly, K.R., et al., *Lifestyle-induced decrease in fat mass improves adiponectin secretion in obese adults.* Med Sci Sports Exerc, 2014. **46**(5): p. 920-6.
388. Nelson, R.K., et al., *Daily physical activity predicts degree of insulin resistance: a cross-sectional observational study using the 2003–2004 National Health and Nutrition Examination Survey.* International Journal of Behavioral Nutrition and Physical Activity, 2013. **10**(1): p. 10.
389. Egawa, T., et al., *Methylglyoxal reduces molecular responsiveness to 4 weeks of endurance exercise in mouse plantaris muscle.* J Appl Physiol (1985), 2022.
390. Gouzi, F., et al., *Reference values for vastus lateralis fiber size and type in healthy subjects over 40 years old: a systematic review and metaanalysis.* Journal of Applied Physiology, 2013. **115**(3): p. 346-354.
391. MacDonald, T.L., et al., *Hyperglycaemia is associated with impaired muscle signalling and aerobic adaptation to exercise.* Nat Metab, 2020. **2**(9): p. 902-917.
392. Agerholm, M., et al., *Perturbations of NAD+ salvage systems impact mitochondrial function and energy homeostasis in mouse myoblasts and intact skeletal muscle.* American Journal of Physiology-Endocrinology and Metabolism, 2018. **314**(4): p. E377-E395.
393. Cortizo, F.G., et al., *The activity of glyoxylase 1 is regulated by glucose-responsive phosphorylation on Tyr136.* Mol Metab, 2022. **55**: p. 101406.

394. Arora, A. and C.S. Dey, *SIRT2 negatively regulates insulin resistance in C2C12 skeletal muscle cells.* Biochimica et Biophysica Acta (BBA) - Molecular Basis of Disease, 2014. **1842**(9): p. 1372-1378.
395. Lantier, L., et al., *SIRT2 knockout exacerbates insulin resistance in high fat-fed mice.* PLOS ONE, 2018. **13**(12): p. e0208634.
396. Alberts, B., et al., *Molecular Biology of the Cell. 4th edition*. 4 ed. From mRNA to Protein. 2002, https://www.ncbi.nlm.nih.gov/books/NBK26829/: New York: Garland Science.
397. Kumar, V., et al., *Human muscle protein synthesis and breakdown during and after exercise.* J Appl Physiol (1985), 2009. **106**(6): p. 2026-39.
398. Neufer, P.D., et al., *Understanding the Cellular and Molecular Mechanisms of Physical Activity-Induced Health Benefits.* Cell Metab, 2015. **22**(1): p. 4-11.
399. Amano, H., et al., *Telomere Dysfunction Induces Sirtuin Repression that Drives Telomere-Dependent Disease.* Cell Metabolism, 2019. **29**(6): p. 1274-1290.e9.
400. Favier, F.B., et al., *HIF-1-driven skeletal muscle adaptations to chronic hypoxia: molecular insights into muscle physiology.* Cellular and Molecular Life Sciences, 2015. **72**(24): p. 4681-4696.
401. Xiao, W., et al., *NAD(H) and NADP(H) Redox Couples and Cellular Energy Metabolism.* Antioxidants & Redox Signaling, 2018. **28**(3): p. 251-272.